

Characterization of the Chanzyme TRPM7 in Macrophages

Michael S. Schappe

M.S. Biological & Physical Sciences, University of Virginia  
B.S. Biochemistry & Molecular Biology, The Pennsylvania State University

A Dissertation Presented to the Faculty of the University of Virginia in Candidacy for the Degree  
of Doctor of Philosophy

Department of Pharmacology  
University of Virginia

January 2019

Bimal N. Desai, Ph.D.  
Douglas Bayliss, Ph.D.  
Alison Criss, Ph.D.  
Sarah Ewald, Ph.D.  
Norbert Leitinger, Ph.D.

## **Abstract**

The innate immune system forms the foundation of immunity through pathogen recognition and maintenance of tissue homeostasis. In particular, myeloid phagocytes are specialized in recognizing host- and microbe-derived molecules to direct cytokine production, phagocytosis, and antigen presentation. The receptors for immunomodulatory molecules require signals from secondary messengers, such as  $\text{Ca}^{2+}$  ions, to modulate signal transduction and drive pro- and anti-inflammatory cellular programs. Electrical signals have long been associated with core functions of innate immunity, and recent discoveries have begun to define the ion channels associated with inflammatory signal transduction and phagocytosis. In this dissertation, I describe the role of ion channels in innate immunity. TRP-family ion channels are essential cellular sensors that transduce sensory inputs into electrical signals, predominantly through  $\text{Ca}^{2+}$  signals, to control cellular function. In particular, my research focuses on characterization of TRPM7 in macrophages. We discovered that TRPM7 is required for activation of macrophages by LPS and regulates macrophage phagocytosis of apoptotic cells.

## Acknowledgements

The University of Virginia has been a special community to be a part of during my doctoral training. The fantastic faculty, students, and staff of the Department of Pharmacology have helped develop my skills as a professional scientist beyond what I ever expected starting graduate school. The academic community at UVA, including Graduate Biosciences Society and the many interest groups, provided exciting opportunities, incredible support, and unforgettable experiences, and there is no better place to live during graduate school than Charlottesville.

Joining the lab of my advisor Bimal Desai has been the most fortuitous decision of graduate school. Despite my initial ignorance of immunology and ion channels, your unwavering support has helped me reach goals and milestones I never thought possible. You have been paramount to my development as a scientist and growth as a person. Your dedication to encouraging me to achieve my best at all times, constantly challenging expectations, and desire for us to cultivate skills beyond the bench has made my doctoral training more than I ever could have asked for from my Ph.D. I am incredibly grateful for everything that you have taught me.

The support from the Desai Lab members has been instrumental to my pursuit of the work in this dissertation. Your scientific expertise, lab organizational skills, and enthusiasm made every day in lab exciting and enjoyable. To Marta, Eric, Phil, and Taylor: it has truly been an honor to work alongside you and you have been the best friends to have in the lab over these last five+ years. To Suresh and Kalina, you always inspired me to work hard and aspire for more. To Michelle, Julia, and Jason, I hope to emulate your kindness (and patience) to all new lab members in my future. And to Zach, Sumeet, and Syra, thank you for your enthusiasm to learn new things, patience with me, and for the opportunity for us to learn from each other.

Thank you to my committee for your always insightful comments and feedback. I could not have asked for better mentorship from Drs. Doug Bayliss, Alison Criss, Sarah Ewald, and Norbert Leitinger during my dissertation research. They constantly refined my critical thinking, expanded

my intellectual horizons, and provided encouraging words of advice at all of the critical stages of my training. You have all gone above what can be expected to make yourself available for discussion and questions, and I cannot thank you enough for your support. In addition, I would like to thank Drs. Paula Barrett, Amy Bouton, David Castle, and Janet Cross for their sincere words of advice, patience with my occasional requests, and perspective on research, mentorship, and leadership.

Charlottesville has been a special community to be a part of for graduate school, and I cannot thank my friends enough for their resolute support through these past few years. I am so fortunate that there have been so many incredible people that I cannot name everyone individually. From classmates to roommates, Friendsgivings to happy hours, and late study nights to late lab nights, you will certainly be lifelong friends. I am also so grateful to the friends who have been there before graduate school, “vacationed” in Charlottesville when they could, and provided fantastic hospitality for me over the years.

Thank you to my family for your love and encouragement. To my fiancée Caroline, you inspire me every day with your own work and actions, make me a better version of myself, and I cannot wait to enjoy life’s adventures together. To my fantastic brothers, David and John, I am always appreciative of your words of encouragement and I am so proud of everything that you do. And to my loving parents, Julie and Steve, you have been my steady support through these years, and thank you for sharing your experience, love, and wisdom with me throughout my life.

## Table of Contents

Abstract	2
Acknowledgements	3
Table of Contents	5
List of Figures	8
List of Tables	9
List of Abbreviations	10
<u>Chapter 1: Ion Channels in Innate Immune Cells</u>	<u>11</u>
Overview of Innate Immunity	11
Electrophysiology for Immunologists	13
Brief review of signal transduction and implications for ion channels	15
Channels regulating membrane potential	17
<i>K<sup>+</sup> Channels</i>	18
<i>TRPM4</i>	19
Ca <sup>2+</sup> -permeable channels	19
Store-operated calcium entry	20
Purinergic (P2X) channels	22
Mitochondrial and mechanosensitive Ca <sup>2+</sup> -permeable channels	23
TRP Channels	24
Focus: TRPM7	30
FIGURES: Chapter 1	32
<u>Chapter 2: Chanzyme TRPM7 mediates the Ca<sup>2+</sup>-influx essential for lipopolysaccharide-induced toll-like receptor 4 endocytosis and macrophage activation</u>	<u>38</u>
ABSTRACT	39
Graphical Abstract	40
INTRODUCTION	41
RESULTS	44
<i>Trpm7</i> -deficient macrophages from <i>Trpm7<sup>fl/fl</sup> (LysM Cre)</i> mice develop normally.	44
TRPM7 is required for LPS-induced inflammatory gene expression in macrophages.	45
TRPM7 controls TLR4 receptor endocytosis.	47
LPS-induced phosphorylation of NFκB and IRF3 is regulated by TRPM7.	48
LPS-induced nuclear translocation of NFκB p65 and IRF3 is dependent on TRPM7.	49
Clamping intracellular Ca <sup>2+</sup> mimics the defects in LPS response seen in the absence of TRPM7.	51
The influx of extracellular Ca <sup>2+</sup> is essential for TLR4 endocytosis.	52
LPS-induced TLR4 endocytosis requires local elevations in cytosolic Ca <sup>2+</sup> .	53
LPS-induced Ca <sup>2+</sup> entry is mediated by TRPM7.	53
Blocking TRPM7 channel activity using FTY720 also diminishes LPS-induced cytosolic Ca <sup>2+</sup> -elevations, TLR4 endocytosis, and downstream signaling.	55
CD14, not TLR4, mediates LPS-induced Ca <sup>2+</sup> entry in primary macrophages	56

<i>Trpm7<sup>fl/fl</sup></i> ( <i>LysM Cre</i> ) mice are resistant to LPS-induced peritonitis.	57
DISCUSSION	58
FIGURES: Chapter 2	62
TABLES: Chapter 2	90
METHODS	92
Mice	92
Genotyping and Characterization of Mice	92
BMDM characterization via <i>Trpm7</i> Exon 17	93
RNA Interference	93
Cell Culture	93
Patch Clamp Electrophysiology	94
Inflammasome Activation	94
Gene Expression Analysis	95
Quantitative Real-time PCR	95
Receptor Endocytosis via Flow Cytometry	96
Protein Immunoblots	97
Immunofluorescence Microscopy	97
Nuclear Translocation via ImageStream	98
Ca <sup>2+</sup> Imaging	98
<i>In vivo</i> LPS Challenge	99
Statistics	100

Chapter 3: TRPM7-mediated electrical activity and calcium signaling regulate phagosome maturation during macrophage efferocytosis 101

ABSTRACT	102
Graphical Abstract	103
INTRODUCTION	104
RESULTS	108
Rapid, localized cytosolic Ca <sup>2+</sup> elevations are required for phagosome acidification during efferocytosis	108
Identification of novel Ca <sup>2+</sup> channel regulators of phagosome acidification	110
TRPM7 regulates phagosomal acidification during macrophage efferocytosis	111
Myeloid cells require TRPM7 for phagosome maturation of apoptotic cells in an <i>in vivo</i> model of efferocytosis.	112
TRPM7 regulates the fusion of phagosome and lysosomes.	113
TRPM7 associates with the nascent phagosome	114
TRPM7 channel activity is essential for phagosome maturation	115
TRPM7 mediates peri-phagosomal elevations in cytosolic Ca <sup>2+</sup> during efferocytosis.	117
DISCUSSION	118
FIGURES: Chapter 3	124
TABLES: Chapter 3	146
METHODS	149
Mouse Strains	149
Cell Culture	149
Preparation of apoptotic cells	149

Measurement of Phagocytosis by Flow Cytometry	150
Ca <sup>2+</sup> Channel Screen using siRNA	151
Perforated-Patch Clamp Electrophysiology	152
Immunocytochemistry	152
Ca <sup>2+</sup> Imaging during Phagocytosis	153
Expression of TRPM7 Constructs	153
In vivo measurement of phagocytosis	154
Generation of DQ Green BSA Reporter Beads	155
Ca <sup>2+</sup> Imaging with ATP stimulation	155
Statistics	155
<u>Chapter 4: Discussion and Future Directions</u>	<u>157</u>
<u>Appendix A: Measurement of TLR4 and CD14 Receptor Endocytosis Using Flow Cytometry</u>	<u>166</u>
Abstract	167
Background	168
Materials and Reagents	169
Equipment	170
Software	171
Procedure	171
Data analysis	173
Notes	174
Recipes	175
Acknowledgments	177
FIGURES: Appendix A	178
<u>Resulting Publications</u>	<u>183</u>
<u>References</u>	<u>184</u>

## List of Figures

Figure 1. Ion channels expressed in innate immune cells	32
Figure 2. Regulation of membrane potential in innate immune cells	34
Figure 3. Cryo-EM Structure of TRPM7 with EDTA (adapted PDB: 5ZX5)	36
Figure 4. Schematic of regulation of LPS signal transduction by TRPM7	40
Figure 5. Characterization of <i>Trpm7<sup>fl/fl</sup></i> (LysM Cre) mice and <i>Trpm7</i> -deficient macrophages	62
Figure 6. Characterization of <i>Trpm7</i> gene deletion in macrophages	64
Figure 7. Effect of anti- <i>Trpm7</i> siRNA and FTY720 on pro-inflammatory gene expression	66
Figure 8. TRPM7 regulates TLR4 endocytosis and downstream NF $\kappa$ B and IRF3 phosphorylation.	68
Figure 9. TLR4 signal transduction is regulated by TRPM7	70
Figure 10. LPS-induced nuclear translocation of NF $\kappa$ B p65 and IRF3 is defective in <i>Trpm7</i> -deficient BMDMs.	72
Figure 11. TLR4 receptor endocytosis is required for normal signal transduction	74
Figure 12. LPS signaling and NF $\kappa$ B translocation are abrogated by clamping intracellular Ca <sup>2+</sup> but there is no further decrease in <i>Trpm7</i> -deficient macrophages.	76
Figure 13. TLR4 signal transduction is largely, but not completely, dependent on Ca <sup>2+</sup> signaling.	78
Figure 14. LPS-induced Ca <sup>2+</sup> elevations are highly compromised in <i>Trpm7</i> -deficient macrophages.	80
Figure 15. Blocking TRPM7 channel activity abrogates LPS-induced Ca <sup>2+</sup> entry and TLR4 endocytosis.	82
Figure 16. LPS-induced signal transduction is inhibited by FTY720 treatment	84
Figure 17. <i>Trpm7<sup>fl/fl</sup></i> (LysM Cre) mice are resistant to LPS-induced peritonitis	86
Figure 18. Flow cytometry gating strategy for LPS-induced peritonitis model	88
Figure 19. Schematic of regulation of efferocytosis by TRPM7	103
Figure 20. Ca <sup>2+</sup> signaling requirements of phagosome acidification and identification of the ion channel TRPM7 as a regulator of phagosome acidification.	124
Figure 21. Validation of flow cytometry-based assay for phagocytosis.	126
Figure 22. Experimental controls and validation of siRNA channel screen.	128
Figure 23. TRPM7 is required for acidification of apoptotic cells during efferocytosis	130
Figure 24. Degradation of apoptotic cell cargo by peritoneal macrophages requires TRPM7	132
Figure 25. Experimental controls for in vivo peritoneal cell clearance	134
Figure 26. TRPM7 regulates phago-lysosome fusion in macrophages	136
Figure 27. TRPM7 associates with the nascent phagosome and is activated by acidic pH.	138
Figure 28. Flow cytometry gating strategy for phagocytosis by FTY720-treated BMDMs	140
Figure 29. Phagocytosis of apoptotic cells triggers phagosome-proximal elevations in Ca <sup>2+</sup> that are dependent on TRPM7	142
Figure 30. Analysis of phagosome-proximal Ca <sup>2+</sup> measurements	144
Figure 31. Schematic of TLR4 and CD14 endocytosis protocol	178
Figure 32. TLR4 and CD14 receptor endocytosis data analysis and suggested presentation.	180

## List of Tables

<i>Table 1. Clinical scoring guidelines</i>	90
<i>Table 2. Key Resources Table – Chapter 2</i>	90
<i>Table 3. Key Resources Table – Chapter 3</i>	146
<i>Table 4. Primer Sequences for Ca<sup>2+</sup> Channel Gene Expression Analysis</i>	147
<i>Table 5. siRNA Sequences from Ca<sup>2+</sup> Channel Screen (SMARTpool siRNA – Dharmacon)</i>	148
<i>Table 6. Antibodies used for measuring TLR4 and CD14 endocytosis</i>	182

## List of Abbreviations

2-APB	Aminoethoxydiphenylborane, 52
BMDM	Bone marrow-derived macrophage, 51
CLP	cecal ligation puncture, 19
DAG	diacylglycerol, 16
DAMP	danger-associated molecular pattern, 11
DC	dendritic cell, 19
GPCR	G-protein coupled receptor, 15
GPI	Glycosylphosphatidylinositol, 42
IP3	inositol trisphosphate, 16
IP3R	inositol trisphosphate receptor, 16
IRF3	Interferon regulatory transcription factor 3, 41
ITAM	immunoreceptor tyrosine-based activation motif, 15
$\text{I}\kappa\text{B}\alpha$	Nuclear factor of kappa light polypeptide gene enhancer in B-cells inhibitor, alpha, 49
LPS	lipopolysaccharide, 16 Lipopolysaccharide, 39
MyD88	Myeloid differentiation factor 88, 41
NF $\kappa$ B	Nuclear factor kappa B, 41
NLRP3	NACHT, LRR, and PYD domains-containing protein 3, 42
PAMP	pathogen associated molecular pattern, 11
PAMPs	Pathogen-associated molecular patterns, 41
PIP2	phosphatidylinositol 4,5-bisphosphate, 15
PKC	protein kinase c, 16
PLC	phospholipase C, 16 Phospholipase C, 42
PMA	phorbol 12-myristate 13-acetate, 17
PRR	pattern recognition receptor, 15
ROS	reactive oxygen species, 17
RTK	receptor tyrosine kinase, 15
RyR	ryanodine receptor, 20
SOCE	Store-operated calcium entry, 42
TCR	T-cell receptor, 51
TLR	toll-like receptor, 15
TLRs	Toll-like receptors, 39
TRAM	Translocation associated membrane protein 1, 41
TREMs	triggering receptor expressed on myeloid cells, 15
TRIF	TIR-domain containing adapter-inducing interferon-beta, 41
TRP	Transient receptor potential channel, 42
TRP channel	Transient receptor channel, 14
TRPM7	Transient receptor potential melastatin-like 7, 39
$V_m$	membrane potential, 13

## **CHAPTER 1: ION CHANNELS IN INNATE IMMUNE CELLS**

The innate immune system is our first defense against pathogens and vital to tissue homeostasis. The 'sensory' ability of the innate immune system to detect microbe and danger-associated signals initiates carefully modulated cellular programs for pro- and anti-inflammatory responses. Ongoing research and drug development strive to exploit the cellular mechanisms that underlie critical immunological processes, such as cytokine production, phagocytosis of microbes and apoptotic cells, and antigen presentation. All cells, including immune cells, express ion channels to regulate membrane potential and flux of signaling ions, such as  $\text{Ca}^{2+}$ , to control cellular function, such as proliferation, development, migration, gene expression, and programmed cell death<sup>1</sup>. Here, I will discuss the essential role of ion channels in the innate immune system, with a focus on studies supported by genetic evidence (i.e. mutations in human patients, interfering RNA, or "knockout" mice).

### **Overview of Innate Immunity**

All living organisms serve as hosts for other species, from symbiotic relationships to deleterious ones. Host organisms have evolved strategies to detect and, if necessary, destroy foreign pathogens, which include microbes (bacteria, fungi, viruses) and other parasites. The innate immune system orchestrates the initial defense against pathogens, discriminating between self and non-self molecules using germline-encoded receptors to detect pathogen and danger-associated molecular patterns (PAMPs and DAMPs). In vertebrates, the innate immune responses are essential to activation of the adaptive immune system, which is a long-lasting immunological response mediated by T and B lymphocytes.

The innate immune system carefully balances pro- and anti-inflammatory cellular programs to support tissue development, organ homeostasis, and host defense, and these

responses must be rapid, specific, and tightly regulated to permit the appropriate immunological activation. For instance, destruction of a single *E. coli* bacterium requires distinct cellular programs from clearance of dying cells. The innate immune system can be broadly defined to include any cells involved in host intrinsic defense, such as epithelial cells that comprise barrier surfaces in addition to conventional immune cells. Although non-immunological cells can play a vital role in host defense, most of our understanding is derived from studies of myeloid phagocytes, which will largely be the focus of this introduction.

Myeloid phagocytes include neutrophils, monocytes, dendritic cells, and macrophages<sup>2</sup>. These cells use a combination of reactive oxygen species, degradative enzymes, and other factors to facilitate engulfment and destruction of phagocytic cargo. Neutrophils, the most abundant leukocyte in human blood (~65% of cells), patrol the circulatory system to mediate pathogen clearance. These short-lived cells (~12 hours) rapidly migrate into tissues in response to chemotactic cues via extravasation, but are not normally found in healthy tissues nor do they efficiently clear apoptotic cells. Monocytes circulate in the vasculature, extravasating into tissues in response to chemokines or 'danger' signals. Monocytes can differentiate into dendritic cells and macrophages, and evidence from transcriptomic and lineage-tracing studies indicate that monocyte-derived cells are of distinct origin from tissue-resident phagocytes<sup>3</sup>. Dendritic cells are professional antigen presenting cells, serving as a direct interface between the innate and adaptive immune system. Upon uptake of "immunologically interesting" cargo, dendritic cells migrate to lymph tissue to present antigen-derived peptides on their cell surface to T cells - with appropriate co-stimulation, the activated T cell can migrate and proliferate to initiate an adaptive immune response. Macrophages are the quintessential phagocyte, residing in nearly all bodily tissues to clear dead cells, debris, and pathogens via phagocytosis. Although also capable of antigen presentation, macrophage responses to phagocytic cargo, both through clearance and cytokine production, define their immunological footprint. Together, these cells form the backbone of innate immunity.

. All cells express ion channels, which are fundamental to migration, cell development, proliferation, and apoptosis. The core functions of innate immunity, which include cytokine production, phagocytosis, and antigen presentation, are highly sensitive to intracellular ion concentrations. Ion channels control the entry of  $\text{Ca}^{2+}$  ions, and the 'opening and closing' of channels is sensitive to signaling initiated by immunological receptors. Together, ion channels and  $\text{Ca}^{2+}$  dynamics rapidly shape signal transduction, which can also shape long-term immunological signaling through indirect regulation of metabolic and transcriptional networks.

## Electrophysiology for Immunologists

Expression of ion channels and transporters endows cells with the ability to control the passage of ions across membrane barriers, converting electrical signals into a nonelectrical response (most often translated by  $\text{Ca}^{2+}$ -permeable channels). Cells employ this ionic gradient as an energy source to produce electrical signals, take up nutrients, manage the balance of tissue electrolytes, regulate cell volume, and secrete proteins<sup>4</sup>. A schematic of major ion channels expressed in innate immune cells is illustrated in

Figure 1. The electrical polarization of the plasma membrane – or **membrane potential ( $V_m$ )** – depends on transporters and ion channels to maintain concentration gradients across biological membranes. The diffusion of ions is dependent on three major factors: the ionic concentration gradient, permeability of the ion (i.e. channel opening), and membrane potential. Generally, the balance of  $\text{Na}^+$ ,  $\text{K}^+$ ,  $\text{Cl}^-$  ions (~20-fold concentration gradient) establishes resting  $V_m$ , while ions with large gradients (10,000-fold for  $\text{Ca}^{2+}$  and  $\text{Zn}^{2+}$ ) are used for signaling. Upon opening, ion channels allow ions to freely diffuse 'down' their electrochemical gradient, which influences  $V_m$  (discussed later). In contrast to ion channels, pores remain open to allow free diffusion of molecules (or proteins) through membranes, and active transporter proteins require ATP to move charged molecules; these are discussed in other helpful reviews<sup>5-7</sup>.

Ion channels act as “switches” to release energy stored by electrochemical gradients. All channels contain a *pore domain*, which allows ions to pass through the membrane, and a *sensor domain* which allow the channel to respond to cues that determine an open or closed state. Small conformational changes “open” an ion channel to permit specific ion(s) to be conducted through the channel pore (often more than  $10^6$  ions per second). As described by Roderick MacKinnon (2003 Nobel Prize in Chemistry), ion channels create a “proteinaceous passageway” that extends through the membrane bilayer, allowing a channel to “feel” an ion, and if it is a favorable energetic interaction, the pore domain allows the ion to pass through (known as *ionic selectivity*)<sup>4</sup>. To modify electrical (and nonelectrical) signaling, only very small changes in ionic flux must occur. Cells have evolved channels of varying cationic selectivity, ranging from permeability for one ion ( $P_{Ca}/P_{Na} > 1000$  for Orai channels<sup>8</sup>) to ‘cation non-selective’ channels (most TRP channels), which may be permeable to both monovalent ( $Na^+$ ,  $K^+$ ) and divalent ( $Ca^{2+}$ ,  $Mg^{2+}$ ,  $Zn^{2+}$ ) cations<sup>9</sup>. Chloride is the only halogen-group element abundantly found in biology, thus channels and transporters need only select  $Cl^-$  over phosphate, sulfate, bicarbonate, and anionic proteins (which are significantly larger, molecularly)<sup>4</sup>. Together, the interplay amongst these channels influences changes in membrane potential (largely driven by levels of  $Na^+$ ,  $K^+$ , and  $Cl^-$ ) and the flux of ionic signals as second messengers (such as  $Ca^{2+}$  and  $Zn^{2+}$ ).

The cell surface contains thousands of channels to establish the cell’s  $V_m$  and dictate the precise timing and localization of the entry of charged ions, particularly  $Ca^{2+}$ , to influence cellular signaling. Likewise, immune cells only express a subset of the over 300 mammalian genes that encode ion channels (ImmGen). Early investigations of immune cells’ electrical properties discovered that many immunomodulatory molecules (including endotoxin, serum complement proteins, and formyl-methionyl peptides<sup>10</sup>) stimulated changes in membrane potential in immune cells and kindled immunologists’ interest in ion channels. These studies observed patterns of both transient and sustained changes in membrane potential in response to antigens, immunocomplexes, and during phagocytosis. In the nearly 40 years since these seminal studies,

advances in molecular tools and genetically-encoded  $\text{Ca}^{2+}$  indicators have permitted a recent renaissance in understanding the role of ion channels in the immune system.

## **Brief review of signal transduction and implications for ion channels**

Innate immune responses are defined by the ability to detect foreign (and danger-associated) molecular patterns, which drive both pro- and anti-inflammatory cellular programs. These responses are modulated by the mosaic of immunological receptors that recognize host-derived chemokines, growth factors, immunoglobulins, and nucleotides. Many of these signaling responses activate, or are influenced by, ion channels and  $\text{Ca}^{2+}$  signaling. How innate immune cells *detect* these signaling molecules and *decipher* transduction of heterologous stimuli remains an area of intense research interest<sup>11-13</sup>. Ion channels help translate rapid ionic and biochemical signals into rapid cellular responses, and in collaboration with immunological receptors, drive robust, long-term immunological programs. Thus, coordination of this coincidence detection by both receptors and channels must be modulated to drive immunological responses.

Upon detection of an immunomodulatory signal, receptors lead to production or release of second messengers (including  $\text{Ca}^{2+}$ , bioactive lipids, cyclic-nucleotides, and NO) that are localized to a specific protein activity (e.g. opening of an ion channel) and allow precise spatiotemporal control of receptor signaling and regulation of immunity<sup>14-16</sup>. Activation of Gq-coupled GPCRs (G protein-coupled receptors; certain nucleotide, eicosanoid, hormone, complement receptors, and others), RTKs (Receptor tyrosine kinase; TAM-family, growth factors), PRRs (Pattern recognition receptors; TLR1/2 and TLR4-CD14 complex; see below), and receptors with ITAM-domains (Immunoreceptor tyrosine-based activation motif;  $\text{FcR}\gamma$ , Dectin-1,  $\beta$ -2 integrins, TREMs) activate phosphatidylinositol-specific lipases, commonly by a Src-family kinase-dependent mechanism. These immunological receptors cluster around membrane domains rich in phosphatidylinositol 4,5-bisphosphate (“PIP2”), a favorite target for phospholipase

C enzymes (PLCs). Mammalian PLCs hydrolyze membrane PIP and PIP<sub>2</sub> to generate two second messengers: diacylglycerol (DAG) and inositol trisphosphate (IP<sub>3</sub>). IP<sub>3</sub> mediates release of Ca<sup>2+</sup> from intracellular stores through IP<sub>3</sub> receptors (IP<sub>3</sub>R; discussed later), and multiple enzymes generate new membrane lipids or modify others (such as DAG lipase converting DAG into arachidonic acid, a pivotal parent lipid for production of eicosanoids<sup>17</sup>). Membrane phospholipids differentially modulate ion channel activity, and G-proteins can directly regulate some TRP and K<sup>+</sup> channels<sup>18,19</sup>. Opening and closing ion channels in response to immunological signals is essential for regulating cytosolic Ca<sup>2+</sup> levels and oscillations, which tunes signal transduction<sup>20,21</sup>, and membrane potential. These signals also activate protein kinase C (PKC), a central regulator of signal transduction in the immune cells<sup>22</sup>, thereby incorporating PKC substrates into Ca<sup>2+</sup>-sensitive signaling pathways. Thus, through modulation of V<sub>m</sub> and Ca<sup>2+</sup> signaling, second messengers and ion channels, endow immune cells with the ability to respond to an array of stimuli by integrating short-term, receptor-initiated signals into long-term transcriptional responses to drive well-defined cellular programs.

For instance, our recent study shows that recognition of LPS by the TLR4-CD14 receptor complex activates the ion channel TRPM7, leading to elevations in cytosolic Ca<sup>2+</sup> in bone marrow-derived macrophages<sup>23</sup>. Optimal LPS-induced transcriptional responses require TLR4, which localizes to PIP<sub>2</sub>-rich plasma membrane domains to initiate signaling<sup>24</sup>, and CD14, which initiates LPS-induced Ca<sup>2+</sup> elevations<sup>23</sup> and activates Syk and PLC $\gamma$ <sup>25,26</sup>. Together these activities are required to promote endocytosis of TLR4 and complete activation of NF $\kappa$ B and Type I IFN gene transcription. However, as a GPI-anchored protein, it is unknown how CD14 facilitates Syk activation, and how rapid pulses or oscillations in cytosolic Ca<sup>2+</sup> shape well-defined LPS transcriptional responses over time. Regulation of LPS-signal transduction by Ca<sup>2+</sup> signaling and TRPM7 in macrophages is discussed in detail in Chapter 2.

## Channels regulating membrane potential

Beginning in 1975<sup>27</sup>, seminal studies observed that macrophages and granulocytes exhibited changes in membrane potential (within sec to min) in response to ligands that triggered superoxide production<sup>28</sup> and during phagocytosis<sup>29</sup>. Innate immune cells typically maintain a resting membrane potential of between -70 and -35 mV, depending on the cell type and measurement method<sup>28,30,31</sup>. In response to PMA or zymosan, the amount of stimulus-induced reactive oxygen species (ROS) production correlated with the magnitude of membrane depolarization and could be modulated by artificially inducing depolarization with high extracellular K<sup>+</sup> (5 to 150 mM)<sup>28</sup>. Notably, peritoneal macrophages and J774 cells (a human macrophage cell line) can depolarize (rate of ~1mV/ms up to 0 mV) in response to extracellular ATP and repolarize within seconds after ATP removal<sup>31</sup>. Likewise, acidification of lysosomes and phagosomes builds up substantial positive charge in the endosomal space, which requires relief by anions or cation efflux for sustainable acidification<sup>32,33</sup> – this phenomena is explored in detail in Chapter 3. Thus, there is a close relationship between membrane depolarization and the functional activity of innate immune cells, although this subject is grossly understudied in the immune system.

$V_m$  is largely maintained in innate immune cells by K<sup>+</sup> channels, transient receptor potential melastatin-like 4 (TRPM4), and Cl<sup>-</sup>-conducting channels (with the support of ATP-driven pumps). It should be noted that ion channels regulate  $V_m$  by causing small imbalances in charge ('carried' by ions) at the membrane, not by modulating the bulk concentration of ions in solution. Changes in membrane potential modulate the activity of voltage-gated (e.g. K<sup>+</sup> channels) and voltage-sensitive (e.g. TRP channels) channels. This distinction refers to channel properties where "sensitive" channels are constitutively active and modulated the magnitude of channel conductance with  $V_m$ , but "gated" channels are only open when a certain  $V_m$  is reached. Coupled with elevated  $[Ca^{2+}]_{cyt}$ , depolarization of the membrane limits subsequent Ca<sup>2+</sup> elevations through a diminished electrochemical gradient. K<sup>+</sup> channels allow diffusion of K<sup>+</sup> out of the cytoplasm and

promote membrane hyperpolarization ( $V_m$  further from 0 mV), whereas opening of  $\text{Na}^+$  channels (such as TRPM4, which is highly selective for  $\text{Na}^+$  ions) depolarizes the plasma membrane (see Figure 2).

While voltage-gated  $\text{Na}^+$  and  $\text{Ca}^{2+}$  channels are critical to restoring resting  $V_m$  in many cell types, innate immune cells only exhibit a voltage-gated  $\text{K}^+$  channel, but not  $\text{Na}^+$  or  $\text{Ca}^{2+}$  conductance (for macrophages, see Ref<sup>30</sup>). Although there is pharmacological evidence of immune cell-sensitivity to common  $\text{Na}^+$ -channel blockers<sup>34</sup>, future studies must use genetic and electrophysiological approaches to adequately characterize  $\text{Na}^+$ -selective channels in innate immunity. Likewise,  $\text{Cl}^-$  contributes to resting  $V_m$ , but the channels responsible for anionic conductances in immune cells have remained largely elusive until recently (i.e. the volume-regulated anion channel current ( $I_{\text{VRAC}}$ )). In peripheral blood mononuclear cells, anion conductance results in mild depolarization due to the relationship between measured resting membrane potential ( $V_m = -53$  mV) and Nerst potential for  $\text{Cl}^-$  ( $E_{\text{Cl}} = -33$  mV;  $[\text{Cl}^-]_{\text{cyt}} = 38$  mM, assuming no compartmentalization)<sup>35</sup>, which is in contrast to its hyperpolarizing effect on neurons. Recently, LRRC8 was identified as a channel component for  $I_{\text{VRAC}}$ <sup>36,37</sup>, and in humans, mutations in *LRRC8A* show it is essential for B cell development<sup>38</sup>. However, the role of LRRC8 and identity of major  $\text{Cl}^-$  channels in innate immunity remain unclear<sup>39</sup>.

### *K<sup>+</sup> Channels*

Since the observations of voltage-gated  $\text{K}^+$  channel activity in the 1980s, multiple  $\text{K}^+$  channels have been identified in innate immune cells, including voltage-gated (Kv1.3 and Kv1.5),  $\text{Ca}^{2+}$ -activated (KCa1.1 and KCa3.1), and inward rectifying  $\text{K}^+$  channels (Kir2.1)<sup>40-42</sup>. These channels work in concert to hyperpolarize the cell in response to elevations in cytosolic  $\text{Ca}^{2+}$  or depolarization caused by non-selective cation channels. Voltage-gated and  $\text{Ca}^{2+}$ -activated  $\text{K}^+$  channels outwardly efflux  $\text{K}^+$  ions from the cytosol to repolarize the cell membrane. Inward rectifying  $\text{K}^+$  channel 1 (Kir2.1) was originally cloned as *lrk1* from murine macrophages<sup>40</sup>. This

channel is expressed in the myeloid cells, but not in NK, T, or B cells (ImmGen). The unique electrophysiological properties of the Kir2.1 channel allow cells to maintain a depolarization state (due to lack of outward current at positive membrane potentials) and, in the absence of depolarizing signals, promote a resting membrane potential near the equilibrium potential of K<sup>+</sup> ( $E_K = -90$  mV). Although the studies cited here provide strong evidence for a functional role of these channels in macrophages, few recent studies (or genetic approaches<sup>43</sup>) have characterized K<sup>+</sup> channels in innate immunity.

### ***TRPM4***

TRPM4 is a monovalent cation-selective channel, and channel opening would depolarize the cellular membrane by permitting the influx of Na<sup>+</sup>. TRPM4 is activated in response to elevations in cytosolic Ca<sup>2+</sup> ( $EC_{50}=3.5$  μM in absence of PIP2)<sup>44</sup>. In a model of sepsis (cecal ligation puncture; CLP), loss of *Trpm4* enhanced susceptibility to septicemia in mice, dramatically increasing inflammatory cytokine production in myeloid-specific and global deletions of *Trpm4*<sup>45</sup>. Likewise, TRPM4 was required for phagocytosis of *E. coli* in peritoneal macrophages, but no defects in Ca<sup>2+</sup> responses or phagocytosis were observed in *Trpm4*-deficient neutrophils. In a separate study<sup>46</sup>, TRPM4-deficient DCs had enhanced Ca<sup>2+</sup> responses to *E. coli* supernatants (i.e. LPS), likely due to lack of tonic depolarization by TRPM4. Deletion of *Trpm4* impaired DC migration to lymph nodes *in vivo*. However, this did not impact DC differentiation *ex vivo*. Thus, TRPM4 normally restricts PAMP-induced Ca<sup>2+</sup> responses in monocytes, BMDMs, and DCs through modulation of  $V_m$ .

### **Ca<sup>2+</sup>-permeable channels**

Since the experiments of Sidney Ringer in the 1880s to reanimate frog hearts, Ca<sup>2+</sup> has been appreciated as a key signaling ion of biology (a brief history and context can be found here<sup>47</sup>). Along with phosphate ions, Ca<sup>2+</sup> provides precise regulation of hundreds (if not, thousands) of

proteins by altering protein conformation and charge. Extracellular tissue fluid and blood have  $\text{Ca}^{2+}$  levels of  $\sim 2.4$  mM, but in resting cells, free, cytoplasmic  $\text{Ca}^{2+}$  is maintained at only 10-100 nM. Ion channels, transporters, and exchangers carefully control the entry, storage, and release of  $\text{Ca}^{2+}$  within the cell, with a substantial portion of cellular ATP production dedicated to the extrusion and sequestration of  $\text{Ca}^{2+}$  ions. This 10,000+-fold gradient provides cells with an immense reservoir of potential energy to call upon as needed.  $\text{Ca}^{2+}$  levels are elevated in the cytosol through 1) the extracellular space by plasma membrane channels, 2) release from ER stores, and although largely mysterious, 3) release from other intracellular stores, such as lysosomes, mitochondria, or specialized endosomes.

$\text{Ca}^{2+}$  intrinsically acts as a rapid, highly localized second messenger as free  $\text{Ca}^{2+}$  is rapidly bound by a variety of proteins, extruded from the cell, or taken up into the mitochondria or the ER (which store  $\mu\text{M}$  to mM levels of  $\text{Ca}^{2+}$ ). These aspects of  $\text{Ca}^{2+}$  signaling, as well as a brief review of the protein domains that bind  $\text{Ca}^{2+}$  and the pumps that establish resting  $\text{Ca}^{2+}$  levels, have been excellently discussed elsewhere<sup>48,49</sup>.

## **Store-operated calcium entry**

As discussed above, a multitude of cellular receptors activate PLCs to cleave PIP<sub>2</sub> into DAG and IP<sub>3</sub>. Cytosolic IP<sub>3</sub> is rapidly detected by the IP<sub>3</sub> receptor (IP<sub>3</sub>R), which is a tetrameric, ligand-gated ion channel. IP<sub>3</sub>R (*Iptr1* to *3*) are non-selective cation channels that open upon binding of IP<sub>3</sub> to allow  $\text{Ca}^{2+}$  to diffuse from the ER into the cytoplasm. At least one IP<sub>3</sub>R type is expressed in almost all cells. Likewise, ryanodine receptors (RyRs; *Ryr1* to *3*) are intracellular membrane-resident ion channels that are activated by  $\mu\text{M}$  levels of cytoplasmic  $\text{Ca}^{2+}$ . Although modest expression of these channels is reported in expression databases (ImmGen), functional validation of RyRs in immunity is poorly defined. Opening allows release of intracellular  $\text{Ca}^{2+}$  stores, and RyRs are predominantly expressed in the sarcoplasmic reticulum of skeletal muscle, myocardium, and neurons<sup>50</sup>. Likewise, limited genetic studies of IP<sub>3</sub>R and RyR indicate that genetic

disruption of these channels does not generate any gross defects in immune cells<sup>51,52</sup>, suggesting that there is likely compensatory function amongst these channels. Despite being downstream of many key immunological receptors, these channels represent a relatively overlooked area of immunology.

Seconds after receptor-mediated release of  $\text{Ca}^{2+}$  from the ER, cells activate plasma membrane  $\text{Ca}^{2+}$  channels, termed “store-operated  $\text{Ca}^{2+}$  entry.” As ER  $\text{Ca}^{2+}$  is depleted, a small, highly  $\text{Ca}^{2+}$ -selective current is conducted by Orai channels ( $\text{Ca}^{2+}$  release activated current;  $I_{\text{CRAC}}$ )<sup>53</sup>. STIM proteins, along with support of adaptors<sup>54</sup>, sense depletion of ER  $\text{Ca}^{2+}$  using EF-hand motifs, which triggers clustering of STIM proteins in the ER membrane. Aggregates of STIMs then associate with Orai channels at the plasma membrane to promote opening of the Orai channel<sup>55</sup> which conducts  $\text{Ca}^{2+}$  into the cytoplasm.

Mutations in ORAI1 and STIM1 in human patients suggest that SOCE is essential for activation of the adaptive immune system, but interestingly, no defects in the development or function of myeloid cells was observed<sup>56</sup>. Deletion of *Stim1* and *Stim2* completely ablates SOCE, as deletion of single Orai channels (*Orai1*, 2, or 3) or Stim proteins may be insufficient to disrupt SOCE<sup>57</sup>, and innate immune cells appear to express all Stim and Orai proteins to some degree. Likewise in the innate immune system, both BMDMs and BMDCs with knockout of both *Stim1* and *Stim2* did not exhibit any developmental or functional defects in response to PAMPs, phagocytosis, and inflammasome activation, despite the lack of a characteristic SOCE response<sup>57</sup>.  $\text{Ca}^{2+}$  signaling was required for all tested myeloid cell functions, but the results demonstrate that STIM-proteins, and thereby SOCE, do not play a significant role in activation of macrophages or dendritic cells<sup>57</sup>.

Given the fundamental nature of SOCE, this process may contribute to context specific signaling in innate immunity. *Stim1*-deficient macrophages exhibit decreased  $\text{Ca}^{2+}$  responses to FcR-crosslinking<sup>58</sup> and during FcR-mediated phagocytosis<sup>59</sup>. In dendritic cells, STIM1 regulates migration and antigen presentation of IgG-opsonized cargo, but is dispensable for phagosome

acidification<sup>60</sup>, a hallmark of phagosome maturation<sup>61</sup>. In summary, STIM-family proteins, and thereby SOCE, may be utilized in specialized circumstances, such as FcR signaling or perhaps ER-mitochondrial contacts<sup>62</sup>, but are largely dispensable for innate immunity<sup>63</sup>.

Consequently, the unclear significance of SOCE in innate immunity indicates that other  $\text{Ca}^{2+}$  permeable channels serve as central regulators of immunity. These channels include P2X-family and TRP channels, while emerging roles for mechanosensitive and mitochondrial  $\text{Ca}^{2+}$  channels are still being identified. I will discuss these channel groups in detail below, concluding with a focus on TRPM7 – the subject of this dissertation.

## **Purinergic (P2X) channels**

### **P2X4**

Despite evidence of high expression in innate immune cells (ImmGen), few studies have examined P2X4 in the immune system. P2X4 is reported to be localized in lysosomes by immunocytochemistry using a knockout-validated antibody<sup>64</sup>. However, lysosomal abnormalities are not reported from the global *P2rx4* knockout mice, and its expression was observed on the cell surface and intracellularly<sup>65</sup>. P2X4, but not P2X7, mediates bacterial killing by macrophages in response to 100  $\mu\text{M}$  ATP, and global *P2rx4* knockout mice are more susceptible to CLP-induced sepsis, exhibiting increased systemic inflammatory cytokine production<sup>66</sup>. Although adoptive transfer experiments demonstrated the phenotype was largely driven by myeloid cells<sup>66</sup>, development of a floxed-mouse for conditional deletion of *P2rx4* would greatly aid future studies examining the role of P2X4 in the immune system.

### **P2X7**

P2X7 channel is central for inflammatory activation of myeloid cells, especially during NLRP3 inflammasome activation<sup>67</sup>. Requiring concentrations greater than 500  $\mu\text{M}$  ATP for activation, P2X7 channel forms a large, non-selective pore permeable to a variety of cations, dyes, and

organic solutes<sup>68-70</sup>. Activation of the channel is associated with a K<sup>+</sup> ion efflux that is thought to be critical to NLRP3 inflammasome activation, and *P2rx7*-deficient macrophages and neutrophils have severely compromised IL-1 $\beta$  release during inflammasome activation<sup>71,72</sup>. Although macrophages from P2X7 global knockout mice have normal production of COX-2 and LPS-induced cytokine transcription, they are defective in ATP-mediated IL-1 $\beta$  release *in vivo*<sup>73</sup>. However, opening P2X7 would also allow an influx of Na<sup>+</sup> and Ca<sup>2+</sup>, likely causing a dramatic disruption of cellular electrochemical gradients in myeloid cells. Innate immune cells are unlikely to typically utilize P2X7 during all instances of IL-1 $\beta$  release and may only do so during pyroptosis.

## **Mitochondrial and mechanosensitive Ca<sup>2+</sup>-permeable channels**

An emerging mechanism of Ca<sup>2+</sup> regulation is derived from the discovery of *bona fide* mechanosensitive Piezo channels and the mitochondrial proteins Letm1 and MCU. Piezo1 and Piezo2 are mechanically-activated cation channels<sup>74,75</sup> that transduce a variety of mechanosensory inputs in physiology<sup>76</sup>. Although these channels appear to be expressed in innate immune cells (ImmGen) and would be predicted to be important for motility or pseudopod formation, characterization of their role in immunity awaits investigation.

In the mitochondria, Letm1, a Ca<sup>2+</sup>-H<sup>+</sup> antiporter<sup>77</sup>, and MCU, a Ca<sup>2+</sup> selective ion channel<sup>78,79</sup>, facilitate uptake of Ca<sup>2+</sup> into the mitochondrial matrix. The outer mitochondrial membrane contains large pores which allow free diffusion of cytosolic ions, but the inner mitochondrial membrane controls ionic permeability through pumps and transporters, maintaining a resting cytoplasm-to-mitochondrial membrane potential of nearly -200 mV. Mitochondrial dehydrogenases for cellular metabolism are Ca<sup>2+</sup>-sensitive<sup>80</sup>, and mitochondrial Ca<sup>2+</sup> uptake likely plays a major role in modulating metabolic activity of all cells. Although the precise immunological role for Letm1 and MCU is unknown, the regulation of mitochondrial Ca<sup>2+</sup> likely serves as a

fundamental mechanism to modulate production of reactive oxygen species and cellular metabolism to mount effective immunological responses<sup>81</sup>.

## TRP Channels

TRP channels are a superfamily of cation-selective, Ca<sup>2+</sup> permeable ion channels with polymodal activation mechanisms<sup>18,82</sup>. The 28 mammalian TRP channels form six-transmembrane domain proteins, which form homo- and heterotetrameric channels, have been grouped into six families based on homology: TRPA, TRPC, TRPP, TRPV, TRPML, and TRPM. TRP channels are responsive to multiple molecular and chemical stimuli (in the form of direct ligands and second messengers) and capable of modulating cellular signaling through changes in membrane potential and Ca<sup>2+</sup> signaling. In general, opening of TRP channels permits flow of ions extracellular Na<sup>+</sup> and Ca<sup>2+</sup> into the cytosol, thereby causing a charge imbalance that depolarizes the cell membrane. Consequently, TRP channels are well-positioned to serve as major cellular sensors and integrate signaling from a variety of receptors.

Direct activation (or inhibition) of channel function can be induced by exogenous small molecules and inorganic ions, such as Ca<sup>2+</sup> and Mg<sup>2+</sup>. Direct activation can also occur through detection of temperatures changes and pH, which occurs within physiological range for TRPV4 (active above 23°C) and TRPM7 (EC<sub>50</sub> at pH 5), respectively<sup>83</sup>. Although natural ligands for some TRP channels have been identified (for instance, cold and menthol for TRPM8<sup>84</sup>, which is not expressed in the immune system), the physiological ligands for most TRP channels remain to be discovered. It should be noted that reports of direct channel regulation, particularly by mechanosensation or phosphorylation, should be interpreted with caution. Activation of *bona fide* biological sensory transducers, as in the case of membrane stretch, may indirectly regulate channel activity through production of second messengers. Likewise, there is no evidence for phosphorylation alone to directly activate ion channel activity, although it may facilitate association

with modulatory accessory proteins. Generally, only sensory stimuli applied in physiologically-meaningful range should be considered. Biological signaling fundamentally depends on changes in protein conformation or charge to signal, and eventually all proteins will respond to energetic changes invoked by sufficiently strong alterations in mechanical force, high or low pH, and temperature.

TRP channels are regulated indirectly by 'coincidence detection' of other receptor signaling events, such as levels of PIP<sub>2</sub>, other bioactive lipids, changes in  $V_m$ , or detection of second messengers. Indirect regulation of TRP channels may also be achieved by controlling the number of channels present in the membrane (a mechanism shared by some GPCRs<sup>85</sup>). Multiple TRP channel members (such as the TRPMLs) are localized to endosomes, and insertion and removal of TRP channels into the plasma membrane by these endosomes has been proposed as a potential regulatory mechanism<sup>18,82</sup>. As described below, some TRP channels are crucial regulators of cytokine secretion and membrane fusion events, particularly TRPMLs, TRPM2, and TRPM7. Although it is likely that this mode of regulation occurs in innate immunity and other cell types, direct evidence of this hypothesis as a major regulatory mechanism for TRP channels has not been demonstrated.

Overall, TRP channels are active at resting  $V_m$ , prudently trickling  $Ca^{2+}$  and other cations into the cytosol, but only a subset of TRP channels are expressed in the innate immune system. These channels are expressed at relatively low density, with only a few hundred channels at the plasma membrane in innate immune cells, and most are effectively self-inactivated by high cytosolic concentrations (>0.1 mM) of divalent cations. The polymodal activation, localization to specific organellular domains, and ability to link enzymatic activity to conduction of millions of ion per second suggests that TRP channels are well-suited to serve as cellular amplifiers of signal transduction<sup>18</sup>.

### ***TRPC, TRPA1, and TRPP***

Gene expression data indicate that TRPPs (also known as PKDs) may be expressed in the innate immune system (ImmGen). To date, no studies on TRPP channels in innate immune cells, including validation of their expression, have been conducted. In contrast, TRPC-group and TRPA1 are not expressed in the immune system. In our review of the literature, there is no genetically validated experimental evidence demonstrating expression of functional TRPA1 or TRPC channels in the immune system.

### ***TRPV***

#### **TRPV2**

TRPV2 is gated by noxious heat (>52°C) and  $\Delta^9$ -tetrahydrocannabinol (THC)<sup>86</sup>, but other physiological ligands remain to be discovered. siRNA-knockdown of *Trpv2* in dendritic cells suggests that TRPV2 may be important for cellular responses to heat (43°C)<sup>87</sup>, which would be highly relevant in fever-responses during infection; however, the cellular consequence for this response is unresolved. *Trpv2*-deficient macrophages are defective in migration and phagocytosis, but not production of TNF $\alpha$  in response to LPS<sup>88</sup>. Phagocytosis of IgG-coated beads, complement-opsonized beads, or zymosan particles by peritoneal macrophages and BMDMs required TRPV2, which localized to phagosomes of IgG-opsonized cargo. Accordingly, TRPV2 global KO mice were more susceptible to infection with *L. monocytogenes*. TRPV2 was necessary for phagocytosis-associated membrane depolarization and synthesis of PIP2 (which could also be produced by membrane depolarization with high extracellular K<sup>+</sup>) at cargo contact sites. Diminished PIP2 resulted in decreased clustering of FcRs, which decreased cargo binding and phagocytosis<sup>88</sup>. Recent studies have examined the influence of  $V_m$  on PIP2 clustering and signal transduction<sup>89</sup>, and this mechanism may extend beyond TRPV2 and be a common consequence of inhibition of TRP channels.

## *TRPV4*

Localized at the plasma membrane, TRPV4 is activated by arachidonic acid and temperatures above 24°C<sup>90</sup>. TRPV4-mediated Ca<sup>2+</sup> signaling in macrophages is proposed to mediate production of prostaglandins in the gut, which are detected by gut smooth muscle cells to regulate homeostatic gut motility<sup>91</sup>. *Trpv4* global KO mice had decreased PGE2 production in response to TRPV4 agonists; however, PGE2 production was not measured in response to physiological stimuli, nor is a gating mechanism for the channel identified. Although TRPV4-eGFP reporter mice were used to interrogate key cells types *in vivo*, ~25% of TRPV4-expressing cells were not immune cells (likely enteric endothelial cells) and could account for the effects of global *Trpv4*-deletion<sup>91</sup>. To understand the role of TRPV4 in innate immunity, future studies require use of tissue specific deletion of *Trpv4*.

## **TRPML**

### *TRPML1*

TRPML1 is endogenously activated by membrane PI(3,5)P2<sup>92</sup> and sphingosine<sup>93</sup>, and this channel is localized to lysosomes<sup>82</sup>. Human mutations in the TRPML1-encoding gene *Mcoln1* result in Type IV Mucopolysaccharidosis, a severe disorder caused by dysregulation of cellular lipid storage<sup>94</sup>. During phagocytosis of IgG-opsonized cargo, TRPML1 is activated by accumulation of PI(3,5)P2 on Lamp1+ endosomes, a marker of lysosomes and late endosomes/phagosomes, which promotes lysosomal Ca<sup>2+</sup> release<sup>95,96</sup>. During phagocytosis of IgG-opsonized red blood cells by BMDMs, TRPML1 promotes lysosomal exocytosis, which drives recruitment of new membrane to promote phagocytosis<sup>95</sup>. TRPML1 is localized to phagolysosomes, and whole-phagosome electrophysiology verified the presence of the channel. TRPML1 currents were not observed in basal phagosome recordings, requiring induction by synthetic agonists. Correspondingly, using an siRNA knockdown approach, TRPML1 was found to mediate phagolysosomal fusion during phagosome maturation of IgG-opsonized beads, and this effect could be increased by TRPML1 overexpression<sup>96</sup>. Experiments to resolve the spatiotemporal lysosomal

Ca<sup>2+</sup> dynamics during phagocytosis are difficult to interpret, as the authors used fluorescent Ca<sup>2+</sup>-indicator dyes that were sequestered into endosomal compartments<sup>96</sup> or relied on overexpression of GCaMP3-channel fusion constructs<sup>95</sup>, which measure lysosome-proximal Ca<sup>2+</sup>, not direct release of Ca<sup>2+</sup> from lysosomes. In dendritic cells, TRPML1 promotes migration through nanotubes, which is proposed to be via Ca<sup>2+</sup>-mediated regulation of actinomyosin cellular machinery<sup>97</sup>. Although this is proposed to occur via lysosomal Ca<sup>2+</sup> release, neither direct observations of lysosomal Ca<sup>2+</sup>, nor an activation mechanism for TRPML1 are shown. However, measurement of cytosolic Ca<sup>2+</sup> levels in response to a TRPML1 agonist and thapsigargin, which blocks pumps that sequester Ca<sup>2+</sup> in the ER, indicate that TRPML1-deficient DCs have decreased basal cytosolic Ca<sup>2+</sup> levels<sup>97</sup>. *In vivo*, excessive accumulation of red blood cells (which require clearance by phagocytes) was observed in the spleen, as well as neurons during brain development *in vivo* in TRPML1 global knockout mice<sup>95</sup>. TRPML1 likely plays a major role in regulation of lysosomal biogenesis and maintenance; thus, disruption of TRPML1 may have secondary effects on immune cell processes, such as migration.

### *TRPML2*

TRPML2 is expressed at relatively low levels in resting BMDMs, but robustly upregulated (10-fold) in response to LPS<sup>98</sup>, a substantial transcriptional increase (albeit, unusual) for an ion channel. TLR ligand-induced production of chemokines, notably CCL2, was dependent on TRPML2 expression, leading to defects in macrophage recruitment in a models of peritonitis *in vivo*<sup>98</sup>. *In vitro*, LPS-induced production of CCL2 can be augmented with a novel TRPML2 agonist (ML2-SA1), which was validated with genetic knockout controls<sup>99</sup>. Using ML2-SA1 to probe endosomal subtypes, TRPML2 localizes to recycling endosomes, presumably to mediate CCL2 secretion. Although the immunological significance of specialized endosomes, particularly the granules of neutrophils, is clear, the role of endosomal sorting in innate immune cells is underexplored. Through modulation by PI(3,5)P2 in specialized endosomes, TRPMLs provide a direct link between channels and innate immune responses.

## **TRPM**

### *TRPM2*

TRPM2 channel is activated by oxidative stress and the metabolite adenosine 5'-diphosphoribose (ADPR)<sup>100</sup>. TRPM2, along with TRPM7 (and TRPM6, which is not expressed in immune cells), is known as a “chanzyme”, as it contains a C-terminal domain with enzymatic activity. TRPM2 contains a NUDT9 homology domain, which is a putative pyrophosphatase<sup>101</sup>; however, whether this domain is functional has recently been contested<sup>102</sup>. Deletion or inhibition of *Trpm2* is protective in multiple murine inflammatory models, including lung infection with *P. aeruginosa* or endotoxin, CLP-induced sepsis, DSS-induced colitis, and intravenous inoculation with *L. monocytogenes*<sup>103-105</sup>. Independently of NADPH oxidase activity<sup>104</sup>, TRPM2 is activated by ROS to mediate Ca<sup>2+</sup> entry required for transcription of inflammatory cytokines and chemokines, and this has been observed in THP1<sup>106</sup> and U937 cells<sup>103</sup> (human monocyte cell lines), monocytes, BMDMs<sup>104</sup>, and alveolar macrophages<sup>107</sup>. In the context of microbial infection, TRPM2 was required for killing of *P. aeruginosa*, and whole-phagosome electrophysiology recordings indicated that ADPR and H<sub>2</sub>O<sub>2</sub>-inducible currents (indicative of TRPM2) were present on red blood cell-containing phagosomes<sup>104</sup>. However, only ~50% of induced current was attributable to TRPM2, and TRPM2 did not mediate phagolysosomal fusion or killing of *S. aureus* by BMDMs.

*Trpm2*-deficient mice are highly susceptible to intravenous infection with *L. monocytogenes*, with immunodeficiencies as severe as IFN $\gamma$ R-deficient mice due to lack of iNOS upregulation and IFN $\gamma$  production in *Trpm2*-null mice. However, the most striking defects in IFN $\gamma$  production were seen in NK cells<sup>105</sup>. In NK cells, cytolytic activity during anti-tumoral immunity requires TRPM2 for degranulation, due to decreased release of granzyme B<sup>108</sup>. CD38-dependent (an ADPR expressed on most immune cells) Ca<sup>2+</sup> signaling was required for degranulation of NK cells, suggesting that TRPM2 may be a central regulator of ROS-stimulated granule release in other innate immune cells, such as neutrophils<sup>109</sup>, although this model has not been investigated.

## Focus: TRPM7

TRPM7 is a tetrameric ion channel, with each large protein subunit (~241 kDa) containing six transmembrane domains – the structure has been recently solved using Cryo-EM<sup>110</sup> (see Figure 3). Global deletion of *Trpm7* is embryonic lethal, and TRPM7 is expressed at low levels in all cells, but its expression is highest in the brain, heart, and hematopoietic cells<sup>111</sup>. As evidenced by patch-clamp electrophysiology, TRPM7 is expressed at the plasma membrane, but it is also expressed on intracellular vesicles<sup>112</sup>.

In addition to the non-selective cation pore domain, TRPM7 contains a serine-threonine kinase domain, which can be cleaved by caspases to free the kinase domain during Fas-induced apoptosis<sup>113</sup>. Additional contexts of TRPM7 cleavage remain to be discovered, but liberation of the kinase domain increases channel current<sup>113</sup>, suggesting that the kinase domain may regulate TRPM7 channel activity (or recruitment of TRPM7 to the plasma membrane). The TRPM7 kinase can phosphorylate PLCs<sup>114,115</sup>, annexin A1<sup>116</sup>, myosin II light chain kinase<sup>117</sup>, and histones<sup>118</sup>, but the cell biological significance of these events is unclear. TRPM7 kinase-dead mice develop normally, and functional TRPM7 currents are present in peritoneal macrophages<sup>119</sup>. Using these same mice, mast cells with defective TRPM7 kinase show decreased histamine release<sup>120</sup>, although the precise mechanism was unresolved. Future studies on TRPM7 kinase require genetic approaches in kinase-dead mice (or new, gene-edited mice) to interrogate the role of TRPM7 kinase in innate immunity.

TRPM7 channel (single-channel conductance of 41 pS) is activated by acidic extracellular pH<sup>121</sup>, modulated by local levels of PIP2<sup>122,123</sup>, and inhibited by intracellular Mg<sup>2+</sup><sup>124</sup>, although other physiological ligands remain to be discovered. In neurons, TRPM7 regulates vesicular fusion, and TRPM7-deficient neurons are protected from Ca<sup>2+</sup> overload during ROS-induced cell

death<sup>125</sup>. In the immune system, TRPM7 is required for normal development of T cells<sup>111</sup>, but until now, no studies have investigated the role of TRPM7 in innate immunity.

Herein this dissertation, I describe the first mouse strain with a genetic deletion of *Trpm7* in the innate immune system (*Trpm7<sup>fl/fl</sup>LysMCre*), with a focus on the role of TRPM7 in macrophages. This research characterizes TRPM7 during two major macrophage functions: inflammatory cytokine production and phagocytosis. In Chapter 2, I discuss the role of TRPM7 in LPS signal transduction, which was recently published in *Immunity*<sup>23</sup>. Chapter 3 describes the regulation of macrophage efferocytosis, or the phagocytosis of apoptotic cells, by TRPM7 during phagosome maturation (at the time of writing, this work has been submitted for peer review). Finally, Chapter 4 discusses outstanding questions and future directions for studies regarding the role of TRPM7 in innate immunity.

# FIGURES: Chapter 1

Figure 1. Ion channels expressed in innate immune cells

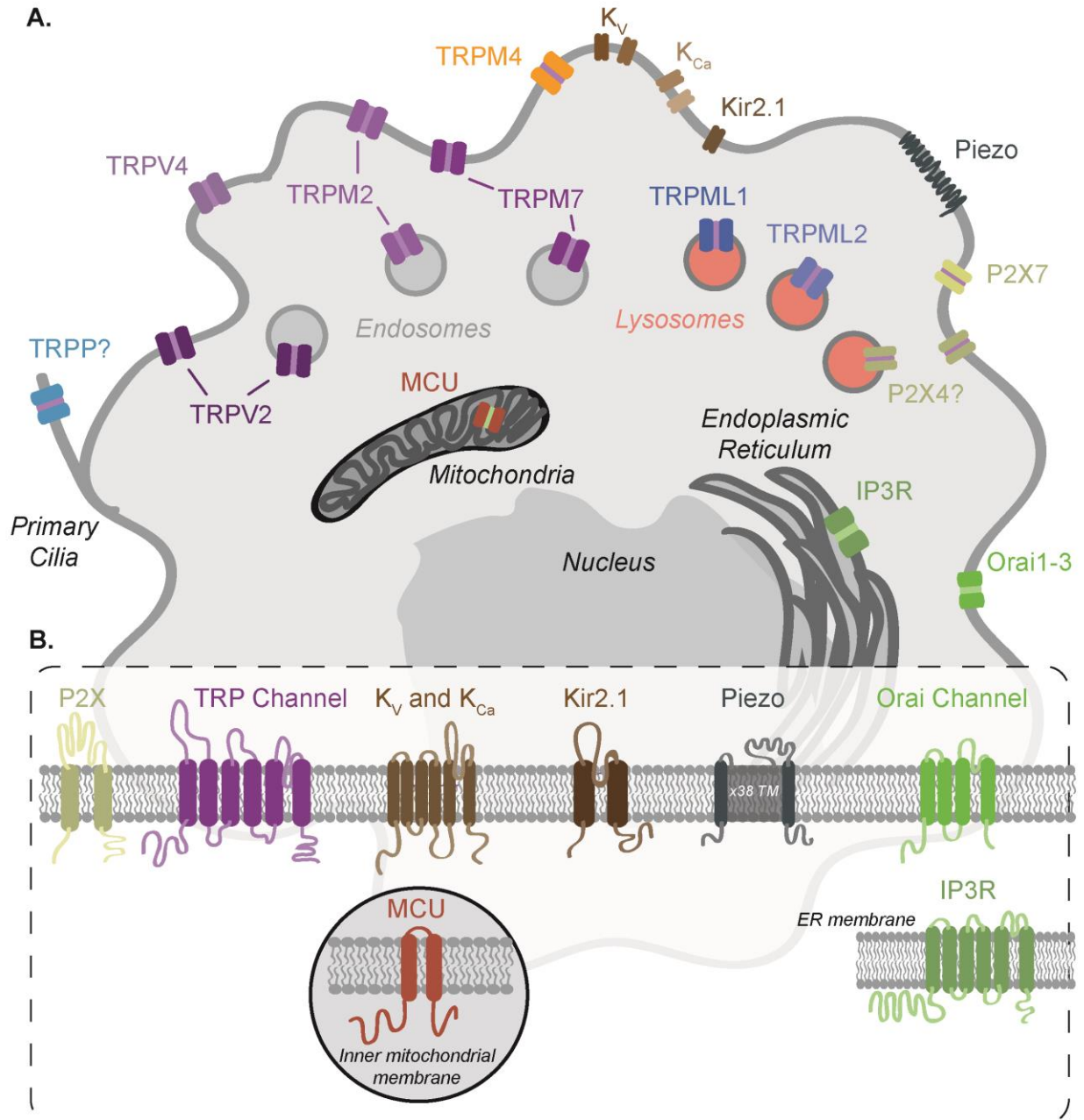


**Figure 1. Ion channels expressed in innate immune cells**

**A.** Schematic of ion channels expressed in macrophages. Characterization of ion channel expression in innate immunity is best characterized in macrophages. Subcellular localization is portrayed as described from studies in resting cells.

**B.** Cartoon of the general architecture of ion channel families in innate immunity. Monomeric subunits and transmembrane domains are illustrated. Proteins are not shown to scale.

**Figure 2. Regulation of membrane potential in innate immune cells**

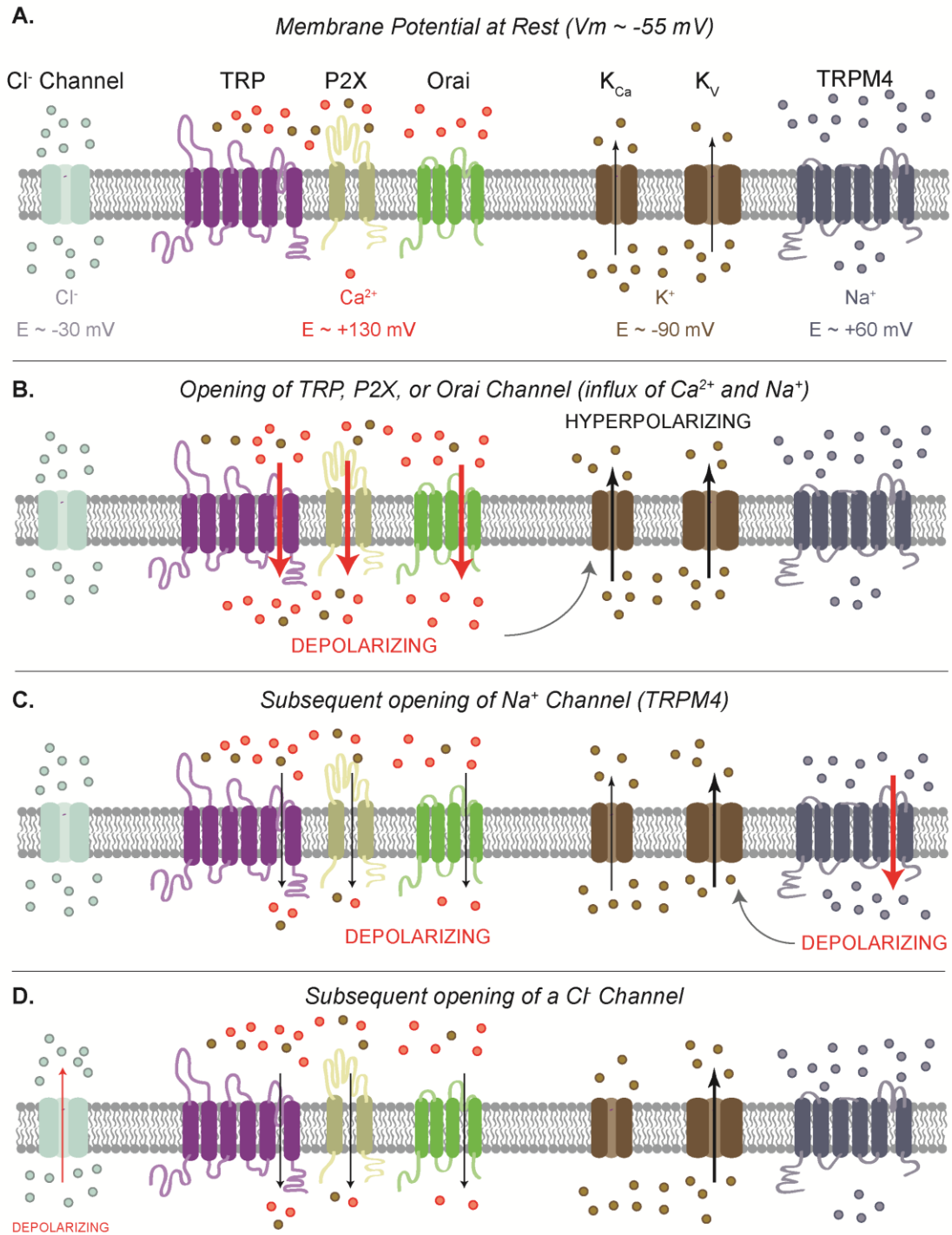


## Figure 2. Regulation of membrane potential in innate immune cells

**A.** Schematic of major ion channel families that maintain resting membrane potential in innate immune cells. Although many channels are expressed on intracellular membranes, ion channels and movement of ions at the plasma membrane are shown. Estimated equilibrium potential ( $E$ ) for given ions is listed. Black arrow indicates generally hyperpolarizing direction and movement of ions; red arrow, depolarizing.

**B.** Opening of a non-selective cation channel (TRP, P2X) or  $\text{Ca}^{2+}$ -selective channel (Orai) results in membrane depolarization ( $V_m$  closer to 0 mV). Depolarizing  $V_m$  and/or increased cytosolic  $\text{Ca}^{2+}$  activates  $K_V$  and  $K_{Ca}$  channels, which allow  $K^+$  efflux to promote membrane hyperpolarization ( $V_m$  further from 0 mV; here, closer to resting  $V_m$ ).

**C.** Opening of a  $\text{Na}^+$  channel (e.g. TRPM4) depolarizes the cell, which decreases the driving force for  $\text{Ca}^{2+}$  entry and activates  $K_V$  channels.

**D.** Activation of  $\text{Cl}^-$  channels causes a mild depolarization of  $V_m$ , which would decrease  $\text{Ca}^{2+}$  entry through other channels (as in *Panel C*) and activate  $K_V$  channels. Measurement of intracellular  $\text{Cl}^-$  levels (~ 38 mM) relative to the resting  $V_m$  of a typical myeloid cell and calculated  $E_{\text{Cl}}$  suggest that opening of a  $\text{Cl}^-$  should cause depolarization; however, characterization of  $\text{Cl}^-$  channels and regulation of  $\text{Cl}^-$  levels in immune cells is poorly defined.

**Figure 3. Cryo-EM Structure of TRPM7 with EDTA (adapted PDB: 5ZX5)**

**A.** Mouse TRPM7 with EDTA (3.3 Angstroms) (PDB: 5ZX5)  
Structure from Duan et al. *PNAS* 2018 using 3D Viewer from RCSB Protein Data Bank

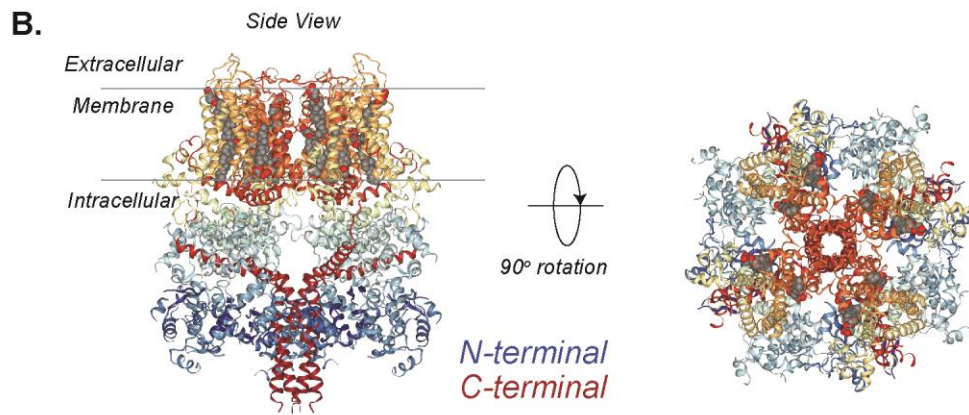
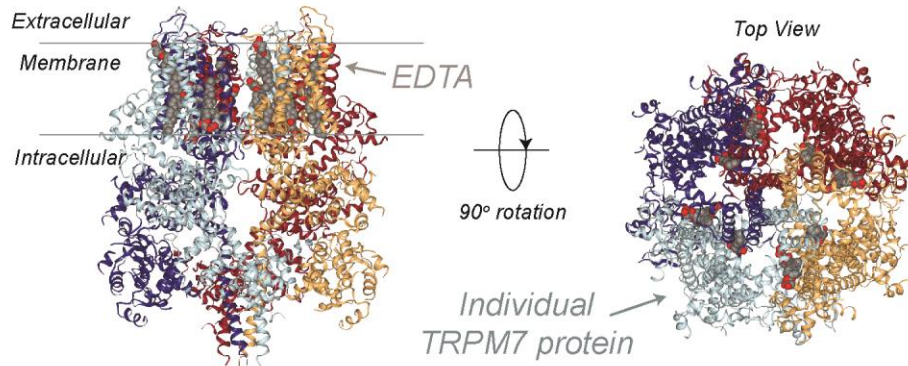


**Figure 3. Cryo-EM Structure of TRPM7 with EDTA (adapted PDB: 5ZX5)**

**A.** 3.3 Å cryo-EM structure of full-length, tetrameric TRPM7 (EDTA in grey; ball-and-stick model). Four individual TRPM7 proteins are shown in distinct colors. Side view is shown at left; top view, right.

**B.** Same structure shown in *Panel A* with N-terminal and C-terminal ends pseudocolored (“Rainbow” pseudocoloring). N-terminal end is shown in blue; C-terminal end is shown in red.

“Cartoon” models were generated using the 3D Viewer tool from Research Collaboratory for Structural Bioinformatics Protein Data Bank (RCSB PDB). Reference structure: 5ZX5. Structure was deposited by Clapham and colleagues<sup>110</sup>.

# CHAPTER 2: CHANZYME TRPM7 MEDIATES THE $Ca^{2+}$ -INFLUX ESSENTIAL FOR LIPOPOLYSACCHARIDE-INDUCED TOLL-LIKE RECEPTOR 4 ENDOCYTOSIS AND MACROPHAGE ACTIVATION

## Disclaimer:

The contents of this chapter (text and figures) appear as published in *Immunity*. Minor modifications to the manuscript contents have been made for increased clarity, such as titles for supplemental figures and expanded explanations as necessary in the text indicated by [brackets]. This work was published with the following citation: Schappe, M., Szteyn, K., Stremaska, M., Mendu, S., Downs, T., Seegren, P. Mahoney, M., Dixit, S., Krupa, J., Stipes, E., Rogers, J., Adamson, S., Leitinger, N., Desai, B. "Chanzyne TRPM7 mediates  $Ca^{2+}$  influx necessary for LPS-induced TLR4 endocytosis and macrophage activation." *Immunity*, 48(1):59-74e5, Jan 2018. DOI:10.1016/j.immuni.2017.11.026. All figures were prepared by MSS. All experiments were performed by MSS unless otherwise indicated in the figure legends.

## ABSTRACT

Toll like receptors (TLRs) sense pathogen-associated molecular patterns to activate the production of inflammatory mediators. TLR4 recognizes lipopolysaccharide (LPS) and drives the secretion of inflammatory cytokines, often contributing to sepsis. We report that Transient receptor potential melastatin-like 7 (TRPM7), a non-selective but Ca<sup>2+</sup>-conducting ion channel, mediates the cytosolic Ca<sup>2+</sup> elevations essential for LPS-induced macrophage activation. LPS triggered TRPM7-dependent Ca<sup>2+</sup> elevations essential for TLR4 endocytosis and the subsequent activation of the transcription factor IRF3. In a parallel pathway, the Ca<sup>2+</sup>-signaling initiated by TRPM7 was also essential for the nuclear translocation of NFκB. Consequently, TRPM7-deficient macrophages exhibited major deficits in the LPS-induced transcriptional programs, failing to produce IL-1β and other key pro-inflammatory cytokines. In accord with these defects, mice with myeloid-specific deletion of *Trpm7* are protected from LPS-induced peritonitis. Our study highlights the importance of Ca<sup>2+</sup>-signaling in macrophage activation and identifies the ion channel TRPM7 as a central component of TLR4 signaling.

## Graphical Abstract

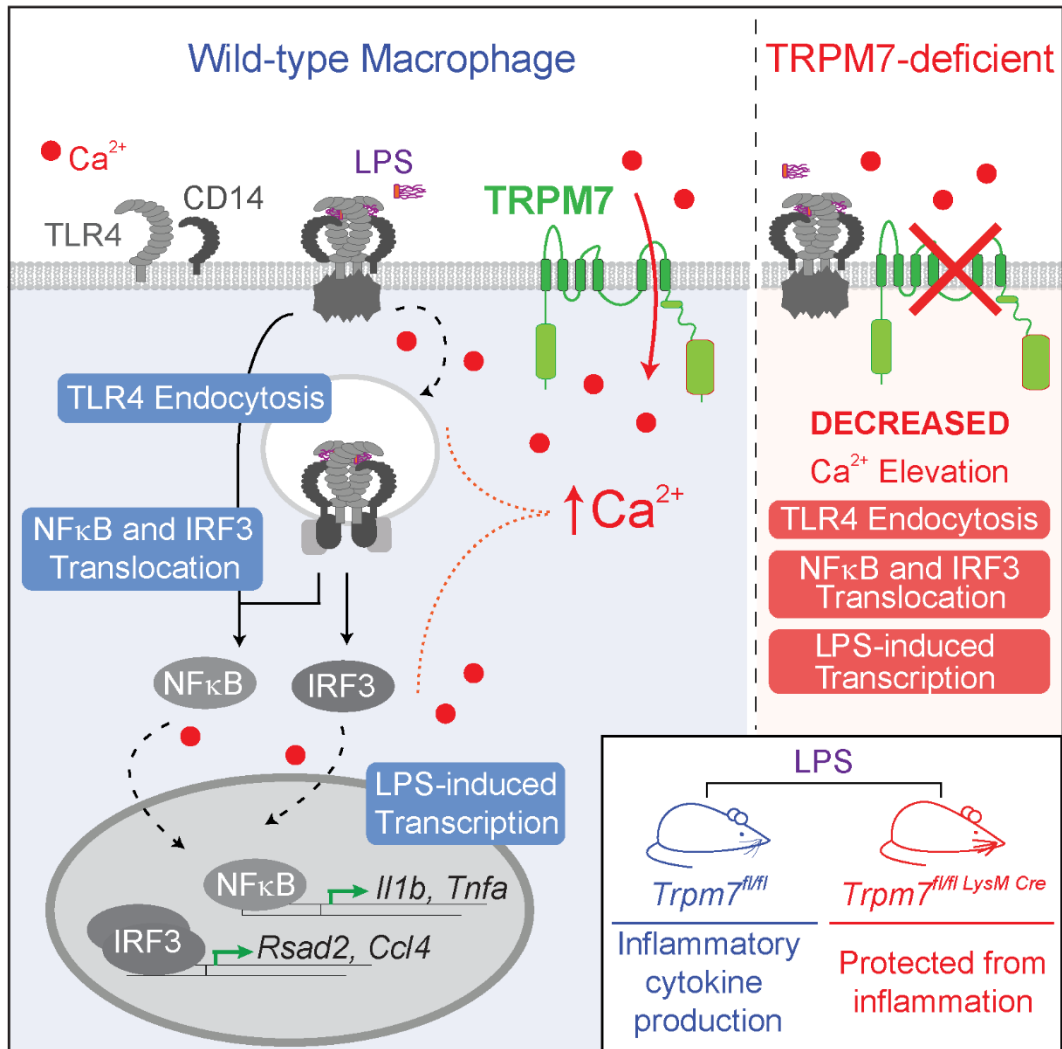


**Figure 4. Schematic of regulation of LPS signal transduction by TRPM7**

## INTRODUCTION

Cells of the innate immune system trigger finely-tuned cellular responses for host defense, while minimizing collateral damage to the host<sup>126</sup>. An array of pattern-recognition receptors (PRRs) sense pathogen-associated molecular patterns (PAMPs) to activate the downstream intracellular signaling machinery necessary for mediating host defense<sup>127</sup>. A family of membrane-resident PRRs called the Toll-like receptors (TLRs) are of central importance because their ectodomains sense the presence of PAMPs, eliciting cellular responses that fit the pattern of infection<sup>128</sup>. According to an emerging framework, the subcellular location of activated TLRs plays a pivotal role in the choice of specific adaptors protein, linked signaling pathways, and elaboration of suitable transcriptional programs<sup>129,130</sup>. This paradigm is clearly evident in the case of TLR4, a major sensor of bacterial lipopolysaccharide (LPS)<sup>131</sup>. Using different adaptors, TLR4 signals distinctly from the cell membrane and early endosomes, expanding the repertoire of transcribed genes and refining the cellular processes for a potent immunological response.

LPS triggers dimerization of TLR4 at the cell membrane and promotes the assembly of “Myddosome”, the myeloid-differentiation factor 88 (MyD88)-containing adaptor complex, to initiate the activation of NF $\kappa$ B. The interaction of TLR4 with co-receptors, such as CD14 and MD2<sup>25,132</sup>, also promotes the endocytosis of LPS-bound TLR4 receptor complex. The formation of TLR4-containing *signaling endosomes* triggers the association of TLR4 to TRIF (and its coadaptor TRAM). Although both MyD88 and TRIF drive the activation and nuclear translocation of NF $\kappa$ B, TRIF uniquely promotes the activation of transcription factor IRF3, resulting in the expression of Type I interferon response genes<sup>133</sup>. Thus, TLR4 endocytosis serves as a pivotal regulatory event to amplify NF $\kappa$ B activation and modulate the cellular response through the additional activation of IRF3. The mechanisms that regulate the initiation and rate of TLR4 endocytosis during LPS stimulation are therefore of paramount importance to understanding the full spectrum of TLR4 signaling in inflammatory conditions. In addition to illuminating the

underlying role of membrane traffic in inflammatory signaling, defining the mechanisms of TLR4 endocytosis may reveal novel pharmacological targets for the treatment of sepsis.

The LPS-induced endocytosis of TLR4 and the subsequent TRIF-mediated IRF3 activation are highly dependent on CD14, a GPI-linked cell surface protein. CD14 has been proposed to promote the activation of Syk and phospholipase C (PLC)- $\gamma$ 2 (PLC- $\gamma$ 2), which are necessary for the Ca<sup>2+</sup>-dependent endocytosis of TLR4<sup>25,26</sup>. This model suggested a role for store-operated Ca<sup>2+</sup> entry (SOCE) in the regulation of TLR4 signaling. Similarly, in addition to the essential role in TLR4 endocytosis, intracellular Ca<sup>2+</sup> elevations regulate NF $\kappa$ B activity<sup>21,134</sup> and NLRP3 inflammasome activation<sup>135,136</sup>. Interestingly, although the requirement for Ca<sup>2+</sup> signaling in inflammatory signaling is abundantly clear, complete loss of SOCE in macrophages deficient in *Stim1* and *Stim2* does not affect their response to LPS<sup>57</sup>. This indicates that Orai channels, the molecular conduits of SOCE, are dispensable for LPS-induced cytokine production and NLRP3 inflammasome activation in macrophages. The real identity of the ion channel(s) responsible for LPS-triggered Ca<sup>2+</sup>-signaling and TLR4 endocytosis, therefore, emerges as a mystery of biological and pharmacological significance.

Transient Receptor Potential (TRP) channels constitute a large family of cation-selective ion channels<sup>83</sup>. Despite the expression of many TRP channels in hematopoietic cells, their functions in the immune system remain largely undefined. The *chanzyme* TRPM7, a TRP channel that also contains an enzymatic kinase domain, is highly expressed in macrophages, but whether it has a role in processes pertinent to innate immunity is not known. TRPM7 is permeable to Na<sup>+</sup>, Ca<sup>2+</sup>, Mg<sup>2+</sup> and Zn<sup>2+</sup>, and previously, it has been implicated in the endocytosis of Fas receptor<sup>113</sup> – a death receptor that, similar to TLR4, requires the generation of signaling endosomes for full activation during apoptosis. TRPM7 channel is regulated by various signals pertinent to inflammation, including caspase-dependent cleavage<sup>113</sup> and extracellular pH<sup>137</sup>. Furthermore, TRPM7 channel activity is highly sensitive to membrane PIP<sub>2</sub> levels<sup>123</sup>, which implies regulatory

inputs through PLC activation. Based on these observations, we hypothesized that TRPM7 may have an important function in macrophage activation by PAMPs. Using a novel mouse line *Trpm7<sup>fl/fl</sup>* (*LysM Cre*) mice, wherein TRPM7 is selectively deleted in myeloid cells including macrophages, we have discovered that LPS-mediated macrophage activation is highly dependent on TRPM7. Mice with *Trpm7* deleted selectively in macrophages are resistant to LPS-induced peritonitis. We show that TRPM7 mediates the LPS-induced  $\text{Ca}^{2+}$ -elevations that are essential for TLR4 endocytosis (and therefore, IRF3 activation) and for  $\text{NF}\kappa\text{B}$  nuclear translocation. Since TRP channels are highly attractive drug targets<sup>138</sup>, these discoveries may stimulate novel pharmacological strategies for the treatment of chronic infections, septic shock, and autoinflammatory diseases.

## RESULTS

### ***Trpm7*-deficient macrophages from *Trpm7<sup>fl/fl</sup>* (*LysM Cre*) mice develop normally.**

To study TRPM7 function in macrophages, we deleted *Trpm7* selectively in myeloid cells by generating *Trpm7<sup>fl/fl</sup>* (*LysM Cre*) mice in a mixed background of sv129 and C57BL/6J (schematized in **Fig. 5A**). Through PCR-based genotyping, we confirmed that the LoxP-flanked exon 17 of *Trpm7* was deleted in the bone marrow-derived macrophages (BMDMs) from *Trpm7<sup>fl/fl</sup>* (*LysM Cre*) (herein, ***Trpm7<sup>-/-</sup>*** or **KO**) mice, but not in the BMDMs derived from *Trpm7<sup>fl/fl</sup>* (herein, ***Trpm7<sup>+/+</sup>*** or **WT**) or *Trpm7<sup>fl/fl</sup>* (*Lck Cre*) mice, which deletes *Trpm7* in thymocytes (**Fig. 6A**). The qRT-PCR-based analysis of TRPM7 mRNA expression levels, using exon 17-directed primers, showed substantially decreased levels of TRPM7 mRNA in *Trpm7<sup>-/-</sup>* BMDMs, relative to WT BMDMs (**Fig. 6B**). We also confirmed that the deletion was not detectable in lymphoid cells derived from *Trpm7<sup>fl/fl</sup>* (*LysM Cre*) mice (data not shown). The deletion of exon 17 generates a frameshift in protein translation, resulting in a null mutant<sup>111</sup>. To confirm the loss of TRPM7 channel activity in *Trpm7<sup>-/-</sup>* macrophages, we used whole-cell patch clamp electrophysiology to record Mg<sup>2+</sup>-inhibitable TRPM7 currents ( $I_{\text{TRPM7}}$ ) in *Trpm7<sup>+/+</sup>* and *Trpm7<sup>-/-</sup>* peritoneal macrophages. The configuration and parameters used for these recordings are shown in *Figure 6C*. As shown in the current-voltage relationship (**Fig. 5B, left**), the *Trpm7<sup>+/+</sup>* macrophages elicit robust outwardly rectifying (blue trace) and Mg<sup>2+</sup>-inhibitable (orange trace)  $I_{\text{TRPM7}}$ , but this current is absent in *Trpm7<sup>-/-</sup>* macrophages (red trace). In *Trpm7<sup>-/-</sup>* macrophages, the mean current density for  $I_{\text{TRPM7}}$  was severely abrogated (WT, 38.9 pA/pF; KO, 9.8 pA/pF; n=5), and the residual current was not inhibitable by Mg<sup>2+</sup> (**Fig. 5B, right**). Deletion of *Trpm7* did not affect the cellularity of bone marrow; both *Trpm7<sup>fl/fl</sup>* and *Trpm7<sup>fl/fl</sup>* (*LysM Cre*) mice yielded equal numbers of isolated bone marrow cells (**Fig 6D**). The ability of bone marrow cells to differentiate *ex vivo* into macrophages, in the absence of TRPM7, was also normal based on flow cytometric analysis of differentiated cells. Expression of the characteristic macrophage surface markers CD11b and F4/80<sup>139</sup> was comparable between

*Trpm7*<sup>+/+</sup> and *Trpm7*<sup>-/-</sup> BMDMs (**Fig. 6E**) when immunophenotyped at day 4 (d4) and d7 in culture (**Fig. 6F**). The cultured *Trpm7*<sup>-/-</sup> BMDMs did not show any significant deficits in their proliferation (**Fig. 6G**). [However, this characterization did not investigate whether development of myeloid cell subsets, including egress out of the bone marrow. Although flow cytometry studies have not revealed any gross defects myeloid cell development, additional studies should be conducted to explore this possibility, especially given that TRPM7 is reported to regulate T cell<sup>111</sup> and B cell<sup>140</sup> development.] Collectively, these results demonstrate that *Trpm7* is efficiently deleted in macrophages obtained from *Trpm7*<sup>fl/fl</sup>(*LysM Cre*) mice without causing any deficits in macrophage development and proliferation. These results, therefore, enable a systematic ‘loss of function’ analysis of TRPM7 in macrophage-mediated innate immunity.

### **TRPM7 is required for LPS-induced inflammatory gene expression in macrophages.**

Activation of macrophages by PAMPs induces a program of inflammatory gene expression and the eventual secretion of inflammatory cytokines<sup>141</sup>. The secretion of potent inflammatory cytokines IL-1 $\beta$  and IL-18 however, also requires additional regulatory inputs from the inflammasome machinery<sup>142</sup>. The “activating ligands” of various inflammasome complexes trigger the caspase-mediated maturation and unconventional secretion of IL-1 $\beta$  and IL-18<sup>143</sup>. Interestingly, both the LPS-induced priming of *Il1b* gene and the inflammasome-mediated secretion of IL-1 $\beta$  are dependent on Ca<sup>2+</sup>-signaling<sup>144,145</sup>, but the identity of the pertinent ion channels is not known. To test the hypothesis that TRPM7 controls inflammasome-dependent IL-1 $\beta$  secretion, we primed *Trpm7*<sup>+/+</sup> and *Trpm7*<sup>-/-</sup> BMDMs with LPS (100ng/mL, 3h) and then stimulated the BMDMs with various inflammasome activating ligands<sup>143,146</sup> (*schematized in Fig. 5C*). *Trpm7*<sup>-/-</sup> BMDMs displayed a drastic reduction (~75% decrease) in IL-1 $\beta$  secretion, relative to *Trpm7*<sup>+/+</sup> BMDMs, across all activation conditions (**Fig. 5D**). Concomitantly, we also tested the

hypothesis that TRPM7 regulates LPS-induced inflammatory gene expression in macrophages. After LPS treatment (100 ng/mL, 3h), we observed substantially reduced upregulation of genes involved in the inflammatory response, with striking reductions in *Il1b*, *Nlrp3*, *Il6*, *Tnfa*, *Nos2*, *Ccl4*, and *Rsad2* (**Fig. 5E** and **Fig. 6J**). Treatment of *Trpm7<sup>+/+</sup>* or *Trpm7<sup>-/-</sup>* macrophages with LPS did not alter *Trpm7* mRNA expression (**Fig. 6H**), nor did expression of *LysM Cre* in mixed-background mice with normal *Trpm7* alleles (*Trpm7<sup>+/+</sup>*) decrease LPS responsiveness in BMDMs (**Fig. 6I**).

Next, we reasoned that if TRPM7 was directly regulating TLR4 signaling, acute siRNA-mediated knockdown of *Trpm7* mRNA should also result in defective LPS response. We successfully knocked down *Trpm7* mRNA with siRNA (30 nM) in RAW 264.7 cells, a murine macrophage line (**Fig. 6A**). RAW 264.7 cells transfected with anti-TRPM7 siRNA, but not control siRNA, exhibited significant reductions in *Nos2*, *Tnfa*, and *Il6* mRNA expression after LPS treatment (**Fig. 6A**). Similarly, treatment of BMDMs with a potent TRPM7 channel inhibitor FTY720<sup>147</sup> reduced LPS-induced expression of *Il6* and *Il1b* mRNA by over 80% relative to LPS alone (**Fig. 6B**). Interestingly, in RAW 264.7 cells, FTY720 reduced LPS-induced TNF $\alpha$  transcription only modestly (**Fig. 6C**), suggesting that TRPM7 may exert additional effects through its kinase domain, independent of I<sub>TRPM7</sub>. Use of FTY720 at concentrations sufficient to activate sphingosine-1-phosphate receptors<sup>148</sup> did not recapitulate these effects (**Fig. 6D**), indicating that FTY720 suppresses the LPS response predominantly through the inhibition of TRPM7 channel.

To examine whether TRPM7 was required for signaling through other TLRs, we stimulated *Trpm7<sup>+/+</sup>* and *Trpm7<sup>-/-</sup>* BMDMs with LPS (a TLR4 ligand), Pam3CSK4 (TLR 1/2 ligand), PolyI:C (TLR3 ligand), and ODN 1826 (TLR9 ligand, also “CpG DNA”) (**Fig. 5F**). We observed a robust decrease in ligand-induced transcription *Il1b* mRNA by LPS and Pam3CSK4 in *Trpm7<sup>-/-</sup>* BMDMs, but not in response to ODN 1826. Moreover, PolyI:C was able to induce robust *Rsad2* expression, a readout of TRIF-dependent signaling, in *Trpm7<sup>-/-</sup>*. As expected, PolyI:C did not induce robust *Il1b* gene expression, nor did Pam3CSK4 and ODN 1826 strongly induce *Rsad2* mRNA (**Fig 5F** and **Fig. 6K**) These results indicate that TRPM7 is essential for LPS-induced macrophage

activation, but *Trpm7*<sup>-/-</sup> macrophages do not have a general defect in inflammatory signaling. Thus, the drastically reduced gene expression of *Il1b*, amongst many other inflammatory genes, underlies the defect in the secretion of IL-1 $\beta$  in *Trpm7*<sup>-/-</sup> macrophages.

### **TRPM7 controls TLR4 receptor endocytosis.**

Internalization of the TLR4-CD14 receptor complex is a pivotal signaling checkpoint during LPS-signaling<sup>149</sup>. Endosomal TLR4-TRIF complexes are required to initiate the transcription of IRF3-regulated genes in response to LPS<sup>133</sup>. Moreover, TLR4 association with TRAM-TRIF-dependent signaling amplifies the activation of NF $\kappa$ B upon LPS stimulation<sup>150,151</sup>. Expression of TRIF-dependent gene transcripts (i.e. *Ccl4* and *Rsad2*) was decreased in *Trpm7*<sup>-/-</sup> macrophages (**Fig. 5E**). Since TRPM7 has been previously shown to regulate Fas receptor endocytosis<sup>113</sup>, we hypothesized that TRPM7 regulates LPS signal transduction through the control of TLR4 endocytosis. [The methodology to measure receptor endocytosis was published in detail in a separate paper stemming from this work<sup>152</sup>.] A monoclonal anti-TLR4 antibody (clone: MTS510) binds to TLR4-MD2 dimers only in the absence of LPS-induced assembly of TLR4-signaling complex (which includes dimerization of TLR4/MD2 dimers)<sup>153</sup>. The earliest events in LPS-induced TLR4 signaling can, therefore, be inferred and quantified from the loss of MTS510 signal in flow cytometry. Both *Trpm7*<sup>+/+</sup> and *Trpm7*<sup>-/-</sup> BMDMs rapidly initiated the assembly of TLR4 signaling complex after LPS treatment (**Fig. 8A**), indicating that the initial assembly of LPS-induced TLR4-signaling complex occurs independently of TRPM7. The monoclonal antibody clone SA15-21 binds to TLR4 regardless of LPS-induced allosteric changes and can be used to track the loss of TLR4 at the cell surface<sup>154</sup> and thus, infer and quantify TLR4 endocytosis through flow cytometry. Using this method, we measured the LPS-induced internalization of TLR4 over time. As shown (**Fig. 8B**), *Trpm7*<sup>-/-</sup> macrophages showed significantly reduced internalization of TLR4 after LPS stimulation, displaying nearly 2-fold higher surface TLR4 levels compared to

*Trpm7<sup>+/+</sup>* BMDMs (*Trpm7<sup>+/+</sup>*, 37%; *Trpm7<sup>-/-</sup>*, 66%, n=4). We then measured the internalization of CD14, which controls LPS-TLR4 endocytosis and formation of LPS-TLR4 signaling endosomes<sup>25</sup>. After 30m of LPS treatment, *Trpm7<sup>+/+</sup>* BMDMs displayed rapid endocytosis of CD14 (37% of CD14 remaining at the cell surface) and then, CD14 levels recovered over time, presumably due to receptor recycling. In striking contrast, CD14 internalization was severely abated in *Trpm7<sup>-/-</sup>* macrophages (81% of surface CD14 remaining, 30m post-LPS) and there was no observable recovery of surface CD14 levels (**Fig. 8C**). Prior to LPS treatment, there were no differences in the total levels of CD14 or TLR4 at the cell surface in *Trpm7<sup>+/+</sup>* and *Trpm7<sup>-/-</sup>* BMDMs (**Fig. 9A and 9B**). These results indicate that TRPM7 is not required for the initial assembly of LPS-TLR4-signaling complex at the plasma membrane but it is essential for the endocytosis of the LPS-TLR4-CD14 signaling complex.

### **LPS-induced phosphorylation of NFκB and IRF3 is regulated by TRPM7.**

LPS-initiated signaling triggers multiple post-translational modifications in the p65 subunit of NFκB (NFκB p65) prior to nuclear translocation<sup>155</sup>. The phosphorylation of NFκB p65 at S276 and S536 (in mice, S534) is associated with nuclear translocation<sup>156</sup> and transcriptional transactivation<sup>157</sup>, respectively. Likewise, phosphorylation at IRF3 S396 (in mice, S388) is crucial for the induction of Type I IFNs<sup>158</sup>. We examined if LPS-induced phosphorylation of either NFκB p65 or IRF3 was impaired in *Trpm7<sup>-/-</sup>* BMDMs. LPS treatment (100 ng/ml) induced the phosphorylation of NFκB p65 in *Trpm7<sup>+/+</sup>* BMDMs, and this effect was significantly increased compared to *Trpm7<sup>-/-</sup>* BMDMs at both S276 (*Trpm7<sup>+/+</sup>*, 6.5-fold increase; *Trpm7<sup>-/-</sup>*, 3.4-fold increase) (**Fig. 9C**) and at S534 (*Trpm7<sup>+/+</sup>*, 4.5-fold; *Trpm7<sup>-/-</sup>* 1.8-fold increase). Similarly, LPS-induced phosphorylation of IRF3 (S388) increased (7.0-fold) after LPS treatment in *Trpm7<sup>+/+</sup>* BMDMs, relative to 0 min, but *Trpm7<sup>-/-</sup>* BMDMs showed delayed kinetics of phosphorylation and lower levels of P-IRF3 after LPS stimulation in (**Fig. 8D, 8E, and 9D**). We also measured P-IRF3

levels by flow cytometry (using a different anti-P-IRF3 antibody clone validated for flow cytometry). This analysis revealed that LPS treatment for up to 3h did not increase P-IRF3 levels in *Trpm7*<sup>-/-</sup> BMDMs, while it increased P-IRF3 (S388) levels significantly in *Trpm7*<sup>+/+</sup> BMDMs (**Fig. 9E** and **9F**). As a proximal readout, degradation of I $\kappa$ B $\alpha$  may indicate the degree of signal transduction upstream of NF $\kappa$ B p65. Despite clear signaling defects at the level of NF $\kappa$ B and IRF3 in *Trpm7*<sup>-/-</sup> BMDMs, we did not observe defects in I $\kappa$ B $\alpha$  degradation, suggesting that TRPM7 regulates LPS signaling downstream of I $\kappa$ B $\alpha$  (**Fig. 8D** and **8E**). Thus, in the absence of TRPM7, LPS-induced phosphorylation of the key transcription factors, NF $\kappa$ B and IRF3, are significantly compromised.

### **LPS-induced nuclear translocation of NF $\kappa$ B p65 and IRF3 is dependent on TRPM7.**

Next, we tested whether *Trpm7*<sup>-/-</sup> macrophages are deficient in nuclear translocation of NF $\kappa$ B p65 and IRF3. Deletion of TLR4 signaling adaptors delays the kinetics of NF $\kappa$ B translocation resulting in reduced cytokine production<sup>159</sup>. Pre-treatment with the dynamin inhibitor Dynasore (80  $\mu$ M)<sup>160,161</sup> inhibits TLR4 endocytosis, and we examined if this had effects on LPS signaling in *Trpm7*<sup>+/+</sup> and *Trpm7*<sup>-/-</sup> BMDMs (**Fig. 11A**). With Dynasore treatment, we observed significantly decreased LPS-induced transcription of *Il1b*, *Il6*, and *Rsad2* in *Trpm7*<sup>+/+</sup> macrophages. However, there was no additional effect of Dynasore treatment on *Trpm7*<sup>-/-</sup> macrophages, further suggesting that TLR4 endocytosis and downstream signaling in response to LPS is dependent on TRPM7. It has been previously established that Dynasore treatment blocks TRIF-dependent signaling through IRF3<sup>133</sup>. However, in Dynasore-treated *WT* BMDMs, the nuclear translocation of NF $\kappa$ B p65 and phosphorylation of NF $\kappa$ B p65 are both reduced by ~50% after LPS treatment (**Fig. 11B** and **11C**). We then examined the role of TRPM7 in NF $\kappa$ B translocation in response to LPS directly through ImageStream flow cytometric imaging, which permits highly quantitative measurements of nuclear localization on large cell populations<sup>162</sup> (**Fig. 10A**). Indeed, *Trpm7*<sup>-/-</sup> BMDMs exhibit reduced (33%

of *Trpm7*<sup>+/+</sup> BMDMs) nuclear translocation of NFκB p65, 30m after LPS treatment (**Fig. 10B** and **10C**). We also examined the subcellular distribution of NFκB p65 using confocal microscopy. Without stimulation, NFκB p65 was diffuse throughout the cytosol in *Trpm7*<sup>+/+</sup> and *Trpm7*<sup>-/-</sup> BMDMs. Upon LPS treatment (100ng/mL), nearly 60% of cellular NFκB was localized to the nucleus within 30 min of stimulation in *Trpm7*<sup>+/+</sup> macrophages. However, NFκB p65 remained diffusely distributed in *Trpm7*<sup>-/-</sup> BMDMs after 30m of LPS stimulation (**Fig. 10D**). The observed differences were not due to expression levels of NFκB p65, which was unaffected (mRNA) by the deletion of TRPM7 (**Fig. 11D**). We then examined the subcellular distribution of IRF3 using confocal microscopy. Similar to NFκB p65, IRF3 was diffuse throughout the cytosol in unstimulated BMDMs. Upon LPS treatment (100ng/mL), low levels of IRF3 were observed 30 min after LPS in *Trpm7*<sup>+/+</sup> BMDMs, while nearly 50% of cellular IRF3 was localized to the nucleus within 60 min of stimulation in *Trpm7*<sup>+/+</sup> macrophages (**Fig. 10E**). However, IRF3 remained excluded from the nucleus in *Trpm7*<sup>-/-</sup> BMDMs 60 min after LPS treatment, as evaluated by intensity analysis of IRF3 localization (**Fig. 10G** and **Fig. 11G**). To further confirm these findings, we examined total protein distribution using subcellular fractionation (**Fig. 11E**). NFκB p65 was observed in the nuclear fraction within 15 min of LPS stimulation in *Trpm7*<sup>+/+</sup> BMDMs, with peak translocation at 30m post-LPS stimulation. However, NFκB p65 translocation was strikingly diminished in *Trpm7*<sup>-/-</sup> BMDMs, with very low levels of nuclear NFκB p65, up to 60 min after LPS treatment (**Fig. 10F**). Likewise, IRF3 nuclear translocation was significantly reduced in *Trpm7*<sup>-/-</sup> BMDMs (33% decrease from *Trpm7*<sup>+/+</sup> by densitometry) after LPS treatment (**Fig. 11F**). Further, in response to ODN 1826 (TLR9 ligand), NFκB p65 translocation was not impaired in *Trpm7*<sup>-/-</sup> BMDMs, indicating that TRPM7 does not broadly regulate NFκB p65 nuclear translocation (**Fig. 11H**). Together, these complementary approaches demonstrate that TRPM7 regulates the nuclear translocation of LPS-induced transcription factors, downstream of TLR4 endocytosis. The transcriptional defects in *Trpm7*<sup>-/-</sup> macrophages are therefore attributable primarily to the role of

TRPM7 in the early phases of TLR4 signaling and subsequently decreased nuclear translocation of LPS-inducible transcription factors.

### **Clamping intracellular Ca<sup>2+</sup> mimics the defects in LPS response seen in the absence of TRPM7.**

Stimulation of the T cell receptor (TCR), but not tumor necrosis factor receptor (TNFR), induces a Ca<sup>2+</sup>-dependent phosphorylation of NFκB p65 at S536<sup>163</sup>. It is, however, unknown if LPS-induced phosphorylation of NFκB p65 at S536 (S534 in mice) requires intracellular Ca<sup>2+</sup> or [Ca<sup>2+</sup>]<sub>i</sub> elevations. We depleted and clamped [Ca<sup>2+</sup>]<sub>i</sub> by loading the macrophages with the high affinity Ca<sup>2+</sup>-chelator BAPTA-AM and then stimulated them with LPS. Preventing [Ca<sup>2+</sup>]<sub>i</sub> elevations during LPS stimulation decreased the phosphorylation of NFκB p65 at S534 (**Fig. 12A** and **Fig. 13A**). We then measured LPS-induced NFκB p65 nuclear translocation in BAPTA-AM loaded BMDMs using ImageStream flow cytometry. In *Trpm7*<sup>+/+</sup> macrophages, NFκB translocation was significantly decreased (~60% of control) after LPS treatment (**Fig. 12B** and **12C**). As shown previously (**Fig. 10B**), nuclear translocation of NFκB was greatly reduced in *Trpm7*<sup>-/-</sup> BMDMs, but notably, clamping [Ca<sup>2+</sup>]<sub>i</sub> did not further depress NFκB translocation. Gene expression analysis also demonstrated that BAPTA-AM severely inhibited LPS-induced transcription in *Trpm7*<sup>+/+</sup> BMDMs, but had little additional effect in *Trpm7*<sup>-/-</sup> BMDMs (**Fig. 12D**). We then sought to “rescue” Ca<sup>2+</sup>-dependent transcriptional defects by mobilizing [Ca<sup>2+</sup>]<sub>i</sub> using the Ca<sup>2+</sup> ionophore Ionomycin during LPS stimulation. Ionomycin provided no additional induction of gene expression in *Trpm7*<sup>+/+</sup> BMDMs compared to LPS alone, suggesting that the LPS-induced [Ca<sup>2+</sup>]<sub>i</sub> elevations were functionally maximal. Ionomycin alone did not induce inflammatory gene expression either (data not shown). However, Ionomycin clearly rescued the LPS-induced gene expression in *Trpm7*<sup>-/-</sup> macrophages. This was the case for the upregulation of *I11b* and *Rsad2*, downstream transcriptional targets of MyD88- and TRIF-signaling, respectively (**Fig 12E**). Interestingly, with

the exception of *Il18*, not all LPS-induced genes regulated by TRPM7 were  $\text{Ca}^{2+}$  sensitive (**Fig. 13B**). However, *Il1b* mRNA expression induced by ODN 1826 was sensitive to  $\text{Ca}^{2+}$  depletion by BAPTA-AM (**Fig. 13C**), indicating that CpG DNA-induced gene transcription is intrinsically  $\text{Ca}^{2+}$  sensitive (although this  $\text{Ca}^{2+}$ -influx is not mediated by TRPM7). Overall, these results argue that although the predominant function of TRPM7 during TLR4 signaling is to mediate  $[\text{Ca}^{2+}]_i$  elevation, it may also influence TLR4 signaling via other means (discussed later).

### **The influx of extracellular $\text{Ca}^{2+}$ is essential for TLR4 endocytosis.**

In macrophages, LPS initiates a rapid rise in  $[\text{Ca}^{2+}]_i$ <sup>164</sup>. Based on the use of 100  $\mu\text{M}$  1-Aminoethoxydiphenylborane (2-APB), it was proposed that the release of  $\text{Ca}^{2+}$  from intracellular stores is necessary for TLR4 endocytosis<sup>26</sup>. However, 2-APB is a highly non-specific ion channel inhibitor, and it blocks TRPM7<sup>165</sup> amongst many other ion channels<sup>166-168</sup>. To better understand the nature of LPS-induced  $[\text{Ca}^{2+}]_i$  mobilization, we readdressed whether  $[\text{Ca}^{2+}]_i$  elevations are necessary for TLR4 endocytosis and also identified the source of that  $\text{Ca}^{2+}$  more definitively. To prevent cytosolic  $[\text{Ca}^{2+}]_i$  elevations, regardless of the source, RAW 264.7 cells were loaded with BAPTA-AM and then stimulated with LPS prior to the measurement of TLR4 endocytosis by flow cytometry. BAPTA-AM-loaded cells showed a drastic reduction in TLR4 endocytosis (96% and 86% of surface TLR4 remaining 30m and 60m, respectively), confirming the previous report that  $\text{Ca}^{2+}$ -signaling is essential for TLR4 endocytosis (**Fig. 12F**). We also measured TLR4 endocytosis after acutely replacing the extracellular solution with a  $\text{Ca}^{2+}$ -free solution. In this condition,  $\text{Ca}^{2+}$  in the intracellular stores would remain available for mobilization but there would be no influx of extracellular  $\text{Ca}^{2+}$ . Strikingly, removal of extracellular  $\text{Ca}^{2+}$  also greatly diminished the endocytosis of TLR4, with over 70% of surface TLR4 remaining 60m after LPS treatment (compared to 30% in *WT*) (**Fig. 12F**). These results indicate that the influx of extracellular  $\text{Ca}^{2+}$  is essential for TLR4 endocytosis.

### **LPS-induced TLR4 endocytosis requires local elevations in cytosolic Ca<sup>2+</sup>.**

To further define the control of TLR4 endocytosis by Ca<sup>2+</sup>, we loaded the cells with either BAPTA-AM (fast-acting Ca<sup>2+</sup> chelator) or the slow-acting EGTA-AM (both 10μM) prior to LPS treatment. This experimental design takes advantage of the kinetics of Ca<sup>2+</sup>-chelation to determine whether a local influx of Ca<sup>2+</sup> controls TLR4 endocytosis. BAPTA-AM loaded RAW 264.7 cells were unable to internalize TLR4 after LPS treatment, displaying 86% (at 30 min) and 75% (at 60 min) of TLR4 at the plasma membrane after LPS treatment. Vehicle (DMSO) treated cells displayed 25% (at 30 min) and 20% (at 60 min) of surface TLR4 after LPS (**Fig. 12G**). This indicates that the rapid chelation of Ca<sup>2+</sup> by BAPTA-AM, which clamps global as well as local Ca<sup>2+</sup> elevations, abrogates TLR4 endocytosis almost entirely. In contrast, EGTA-AM loaded RAW 264.7 cells exhibited a moderately impaired rate of TLR4 endocytosis, but successfully internalized TLR4 60 min post-LPS (**Fig. 12G**). These results argue that the slow chelation of Ca<sup>2+</sup> by EGTA-AM, which fails to prevent rapid, local Ca<sup>2+</sup>-elevations (likely Ca<sup>2+</sup> in proximity to TLR4), permits the Ca<sup>2+</sup>-signaling necessary for TLR4 endocytosis. Overall, these results suggest that TLR4 endocytosis is controlled by a local rise in [Ca<sup>2+</sup>]<sub>i</sub> at the plasma membrane.

### **LPS-induced Ca<sup>2+</sup> entry is mediated by TRPM7.**

The involvement of PLC-γ2 for the endocytosis of TLR4<sup>25,26</sup> had suggested a Ca<sup>2+</sup> entry mechanism involving store-operated Ca<sup>2+</sup> entry (SOCE). Surprisingly, the disruption of SOCE by the deletion of *Stim1* and *Stim2* does not affect TLR-ligand induced cytokine production in macrophages<sup>57</sup>. These results indicate that Orai channels, the molecular conduits of SOCE, are not critical for LPS-induced macrophage activation, and the ion channels that mediate LPS-induced Ca<sup>2+</sup> signaling for TLR endocytosis and downstream signaling remain elusive.

Considering that TRPM7 is permeable to  $\text{Ca}^{2+}$  and is critical for TLR4 signaling, but not all TLRs, we hypothesized that TRPM7 directly mediates LPS-induced  $\text{Ca}^{2+}$  entry. Using BMDMs loaded with  $\text{Ca}^{2+}$ -sensitive ratiometric fluorescent dye Fura2-AM, we measured  $[\text{Ca}^{2+}]_i$  elevations in response to TLR ligands. A robust rise in cytosolic  $[\text{Ca}^{2+}]_i$  was observed after stimulation with LPS (100 ng/ml) and Pam3CSK4 (100 ng/ml), with LPS yielding a 44.5% larger  $[\text{Ca}^{2+}]_i$  elevation than Pam3CSK4 (**Fig. 14A**). Stimulation with ODN 1826 (1  $\mu\text{M}$ ), also induced  $[\text{Ca}^{2+}]_i$  elevations, although to a significantly lower degree than LPS and Pam3CSK4 (down to 29% of LPS and 53% of Pam3CSK4).

To examine the role of TRPM7 in LPS-induced  $\text{Ca}^{2+}$  entry, we performed live cell imaging *Trpm7<sup>+/+</sup>* and *Trpm7<sup>-/-</sup>* BMDMs. *Trpm7<sup>+/+</sup>* BMDMs display a rapid rise in  $[\text{Ca}^{2+}]_i$ , peaking less than 2 min after LPS stimulation (**Fig. 14B**). In contrast, *Trpm7<sup>-/-</sup>* BMDMs displayed a severely blunted rise in LPS-induced  $[\text{Ca}^{2+}]_i$ , which was decreased in both peak intensity and duration. However, both *Trpm7<sup>+/+</sup>* and *Trpm7<sup>-/-</sup>* BMDMs responded normally to ionomycin. We made similar observations using both Fura-2-AM and Fluo-4-AM  $\text{Ca}^{2+}$  imaging dyes (data not shown). We also investigated the  $[\text{Ca}^{2+}]_i$  elevations in response to both sustained (15 min) (**Fig. 14C-E**) and a short pulse (60 sec) of LPS stimulation, after which, the extracellular bath solution was replaced by the LPS-free solution (**Fig. 14F-H**). In both stimulation conditions, *Trpm7<sup>-/-</sup>* BMDMs exhibited a significantly diminished  $[\text{Ca}^{2+}]_i$  elevations compared to *Trpm7<sup>+/+</sup>* BMDMs (**Fig. 14E** and **14H**) – the mean peak  $[\text{Ca}^{2+}]_i$  level was down to ~43% of that in *WT* or *Trpm7<sup>+/+</sup>* BMDMs. With the caveat that LPS bound to TLR4 may not be easily washed out, it is interesting that a 60s stimulation with LPS results in a robust  $[\text{Ca}^{2+}]_i$  rise. We then measured whether Pam3CSK4 and ODN 1826 induced  $\text{Ca}^{2+}$  entry was dependent on TRPM7. Consistent with the observations from gene expression analysis (**Fig. 14F**), *Trpm7<sup>-/-</sup>* BMDMs displayed a significant reduction in Pam3CSK4-induced cytosolic  $[\text{Ca}^{2+}]_i$  entry, relative to *Trpm7<sup>+/+</sup>* BMDMs. However, ODN 1826-induced  $\text{Ca}^{2+}$  entry occurred independently of TRPM7. Overall, these results clearly demonstrate that TRPM7

controls the Ca<sup>2+</sup>-entry triggered by LPS and Pam3CSK3, but not the Ca<sup>2+</sup>-entry triggered by ODN 1826.

### **Blocking TRPM7 channel activity using FTY720 also diminishes LPS-induced cytosolic Ca<sup>2+</sup>-elevations, TLR4 endocytosis, and downstream signaling.**

While TRPM7 is required for LPS-induced Ca<sup>2+</sup> elevations, TRPM7 could contribute to Ca<sup>2+</sup> entry in an indirect manner, for instance by regulating another channel through its kinase domain. In *Figure 7B*, we used FTY720, a TRPM7 channel blocker<sup>147</sup>, to demonstrate that TRPM7 channel activity played a critical role in LPS-induced gene expression. Here, we demonstrate that FTY720 can block LPS-induced Ca<sup>2+</sup>-influx. Treatment of BMDMs with FTY720 (5 μM) decreased LPS-induced Ca<sup>2+</sup>-influx 6-fold, relative to untreated cells (**Fig. 15A** and **15B**). In BMDMs, FTY720 (5 μM) also decreased the rate of TLR4 endocytosis (**Fig. 15C** and **16E**), with nearly 80% of surface TLR4 remaining 60 min after LPS treatment; BAPTA-AM pre-treatment completely ablated TLR4 endocytosis. FTY720 treatment also mimicked the effects of BAPTA-AM on the phosphorylation of NFκB p65 (**Fig. 16A** and **16B**). Both FTY720 and BAPTA-AM decreased the phosphorylation of NFκB (S534) to ~50% of untreated cells. We also examined RAW 264.7 cells, a murine BALB/c macrophage cell line, in response to TRPM7 blockade by FTY720. In these cells, FTY720 treatment decreased LPS-induced Ca<sup>2+</sup> influx to ~45% of untreated cells (**Fig. 16C** and **16D**). FTY720 also drastically reduced the phosphorylation of NFκB p65 at S534 (**Fig. 16F**). Transcriptionally, the reduction in LPS-induced *I11b* mRNA by FTY720 was comparable to clamping of [Ca<sup>2+</sup>]; with BAPTA-AM (**Fig. 16G**). Using cell fractionation, we determined that the nuclear translocation of NFκB p65 is greatly delayed in FTY720-treated RAW 264.7 cells, 15 min after LPS treatment (**Fig. 16H**). Some translocation was detectable at 30 min, but it was significantly less when compared to vehicle treated controls. The inhibition of NFκB p65 nuclear translocation by FTY720 was also evident using immunofluorescence confocal microscopy (**Fig.**

**16I)** and ImageStream flow cytometry (data not shown). Furthermore, we tested the effect of FTY720 on LPS-induced transcription in human THP-1 monocytes. In response to LPS, FTY720 (5 $\mu$ M) pre-treatment decreased the transcription of both *Ccl4* (down to 51% of untreated), *Ii6* (to 14% of untreated), and *Ii1b* (to 16% of untreated) (**Fig. 15D**), suggesting both MyD88 and TRIF-dependent signaling are compromised in human monocytes. Thus, blocking TRPM7 channel activity acutely inhibits LPS-induced Ca<sup>2+</sup> entry, TLR4 endocytosis, and gene transcription, similar to *Trpm7*<sup>-/-</sup> macrophages. Together, these results indicate that TRPM7 channel directly conducts Ca<sup>2+</sup> to mediate LPS-induced signaling.

### **CD14, not TLR4, mediates LPS-induced Ca<sup>2+</sup> entry in primary macrophages**

Given that TRPM7 channel mediates LPS-induced Ca<sup>2+</sup> entry, the molecular identity of the LPS receptor responsible for modulating TRPM7, and thereby Ca<sup>2+</sup> entry, is unknown. To address this question, we performed live cell Ca<sup>2+</sup> imaging on BMDMs from C57BL/6J (herein, "WT"), *Tlr4*<sup>-/-</sup>, and *Cd14*<sup>-/-</sup> mice. Upon stimulation with LPS (100 ng/ml), WT BMDMs responded with a rapid rise in [Ca<sup>2+</sup>]<sub>i</sub> over 5 min of stimulation (**Fig 15E**). Surprisingly, *Tlr4*<sup>-/-</sup> BMDMs exhibited only a modest decrease in LPS-induced [Ca<sup>2+</sup>]<sub>i</sub> elevation (down to ~76% of WT response at *t* = 140s). In striking contrast, *Cd14*<sup>-/-</sup> BMDMs failed to elevate [Ca<sup>2+</sup>]<sub>i</sub> in response to LPS (down to ~15% of WT) (**Fig 15F**). Thus, these results indicate that CD14 functions as the predominant trigger for LPS-induced Ca<sup>2+</sup> influx.

### ***Trpm7<sup>fl/fl</sup>* (LysM Cre) mice are resistant to LPS-induced peritonitis.**

We evaluated the significance of macrophage-resident TRPM7 *in vivo* by challenging the mice with an intraperitoneal injection of LPS (0.2 mg/kg) (**Fig. 17A**). *In vivo* administration of LPS elicits a rapid cytokine response, and the increased serum levels of TNF $\alpha$ , IFN- $\gamma$ , and IL-6 promote pathological inflammation in less than 6 hours after LPS administration<sup>169</sup>. After LPS challenge, mice were observed for pathological symptoms using a composite clinical score<sup>170</sup> (**Table 1**), recorded in a double-blinded manner. *Trpm7<sup>fl/fl</sup>* (LysM Cre) mice displayed decreased sensitivity to LPS challenge over the course of 24h when compared to *Trpm7<sup>fl/fl</sup>* mice (**Fig. 17B**). Resistance to LPS challenge was also clearly evident at 4h after LPS administration, with a 4-fold increase in composite clinical score in *Trpm7<sup>fl/fl</sup>* mice compared to *Trpm7<sup>fl/fl</sup>*(LysM Cre) mice (**Fig. 17C**). Importantly, serum cytokine levels of TNF $\alpha$ , IFN- $\gamma$ , and IL-6 were significantly decreased (to ~50%) in *Trpm7<sup>fl/fl</sup>* (LysM Cre) mice relative to LPS-treated *Trpm7<sup>fl/fl</sup>* mice (**Fig. 17D**). Likewise, we observed decreased transcription of *Tnfa* and *Il1b* mRNA levels in immune cells isolated via peritoneal lavage 4h after LPS administration (**Fig. 17E**). We then used flow cytometry to examine the differences, if any, in the infiltration of macrophages from LPS-treated *Trpm7<sup>fl/fl</sup>* and *Trpm7<sup>fl/fl</sup>*(LysM Cre) mice (**Fig. 18A and 18B**). There were no differences in the proportion of peritoneal macrophages (CD45+ CD11b+ F4/80+) between *Trpm7<sup>fl/fl</sup>* and *Trpm7<sup>fl/fl</sup>* (LysM Cre) mice, 24h after LPS challenge (**Fig. 17F and 17G**). However, the gross recruitment of immune cells was greatly reduced in LPS-treated *Trpm7<sup>fl/fl</sup>* (LysM Cre) mice. *Trpm7<sup>fl/fl</sup>* mice had a 2-fold increase in the number of CD45+ immune cells and macrophages into the peritoneum (24h post-LPS). In contrast, *Trpm7<sup>fl/fl</sup>*(LysM Cre) mice did not show a significant increase in CD45+ cells or macrophages (CD45+ CD11b+ F4/80+) (**Fig. 17H**). Overall, in comparison to *Trpm7<sup>fl/fl</sup>* mice, the *Trpm7<sup>fl/fl</sup>*(LysM Cre) mice are protected from LPS-induced pathology. We observed decreased

cytokine production and reduced recruitment of immune cells in the peritoneum – rendering *Trpm7<sup>fl/fl</sup>(LysM Cre)* mice significantly resistant to LPS-induced peritonitis.

## DISCUSSION

We have uncovered a novel TRPM7-mediated  $\text{Ca}^{2+}$ -signaling pathway that is essential for LPS-induced macrophage activation and is, therefore, central to innate immunity. TRPM7 channel mediates cytosolic  $\text{Ca}^{2+}$  elevations in response to LPS, and this  $\text{Ca}^{2+}$  influx is necessary for TLR4 receptor endocytosis and IRF3 activation. Similarly, in a presumably parallel arm of LPS-signaling, the  $\text{Ca}^{2+}$ -influx also regulates the activation and nuclear translocation of  $\text{NF}\kappa\text{B}$ . Thus, TRPM7 controls the transcriptional programs mediated by the two key transcription factors,  $\text{NF}\kappa\text{B}$  and IRF3, during LPS-induced macrophage activation. In accord with these findings, the selective deletion of *Trpm7* in myeloid cells renders the mice resistant to LPS-induced peritonitis, revealing TRPM7 as a major controller of pro-inflammatory cytokine production by myeloid cells *in vivo*. These discoveries are highly significant because TRPM7 now emerges as a pharmacologically tractable molecular target for developing novel therapeutic strategies directed against sepsis and auto-inflammatory diseases.

LPS has long been known to trigger a rapid elevation in cytosolic  $\text{Ca}^{2+}$ <sup>164</sup>, but the identity of the ion channel responsible for initiating this  $\text{Ca}^{2+}$ -signaling pathway has remained elusive. Likewise, the endocytosis of the TLR4 signaling complex is a crucial early event in cellular LPS response, and this process was known to be  $\text{Ca}^{2+}$ -dependent<sup>26</sup>. However, due to the non-specific properties of pharmacological inhibitors, it was previously concluded that the release of  $\text{Ca}^{2+}$  from intracellular stores and through IP3 receptors, is the key process necessary for TLR4 endocytosis. In that model, the activation of  $\text{PLC}\gamma 2$  (and the generation of IP3) during LPS signaling leads to the release of ER  $\text{Ca}^{2+}$  through the IP3 receptors and subsequently results in store-operated  $\text{Ca}^{2+}$ -entry (SOCE) through the Orai channels. Surprisingly, macrophages that are completely deficient

in *Stim1-Stim2* and SOCE show no defects in LPS-induced production of inflammatory cytokines, indicating that SOCE is not a major determinant of TLR4-signaling<sup>57</sup>. The release of intracellular Ca<sup>2+</sup> (and subsequent SOCE) may occur concomitantly with TRPM7 activity, but these processes are not the salient regulators of TLR4 signaling. This is also supported by the observation that although Ca<sup>2+</sup>-elevations are severely diminished in *Trpm7*<sup>-/-</sup> macrophages, they are not entirely absent. [The release of ER Ca<sup>2+</sup> stores, such as during stimulation with ATP, results in an acute, peaking within ms of ligand stimulation, with the slower refilling filling in behind the initial release. Topologically, LPS-induced Ca<sup>2+</sup> responses are consistent with a slower activation of channel activity, suggest an ER-Ca<sup>2+</sup> independent mechanism.] We emphasize that our findings do not negate a role for other ion channels in regulating various aspects of macrophage activation<sup>1,103,171-173</sup>. While pharmacological approaches have suggested a vague role for TRPM7 in macrophages<sup>174</sup>, our study is the first to define the function of TRPM7 in a mechanistic manner using mice with a targeted genetic deletion of TRPM7 in macrophages.

Given our observations that CD14, not TLR4, is vital to LPS-induced Ca<sup>2+</sup> entry, we propose that the activation of TRPM7 through a CD14-mediated event, likely located in close proximity to TLR4, is the essential Ca<sup>2+</sup>-signaling component of this pathway. The resulting local Ca<sup>2+</sup>-influx promotes the endocytosis of TLR4 at rates that are physiologically meaningful for downstream signaling, including IRF3 activation. Similarly, TRPM7-mediated Ca<sup>2+</sup>-signaling also regulates the parallel activation of NFκB, but this process is likely influenced by additional inputs from the TLR4 signaling endosomes. This idea is supported by our observation that the inhibition of TLR4 endocytosis by the dynamin inhibitor Dynasore substantially reduces LPS-induced NFκB translocation. However, given the multitude of dynamin-family GTPases in the cell, Dynasore will likely abrogate multiple cellular processes, and thus, we are cautious in our conclusions from Dynasore-treated cells. Interestingly, IκBα degradation appears to be intact in *Trpm7*<sup>-/-</sup> macrophages, but NFκB p65 phosphorylation is decreased. This observation suggests that as-

yet unidentified  $\text{Ca}^{2+}$ -triggered kinase likely modulates  $\text{NF}\kappa\text{B}$  p65 activity during LPS signaling. Recent evidence suggests that phosphorylation at S534  $\text{NF}\kappa\text{B}$  p65 is crucial for the stability of p65 signaling. We observed a striking  $\text{Ca}^{2+}$  sensitivity of this phospho-site, suggesting that the spatiotemporal aspects of  $\text{Ca}^{2+}$ -signaling can greatly modify  $\text{NF}\kappa\text{B}$  signaling. Thus,  $\text{Ca}^{2+}$  likely plays a dual role – a rapid role in “jump starting” TLR4 endocytosis and possibly a slower role in tailoring an appropriate inflammatory response by modifying the activity of  $\text{NF}\kappa\text{B}$ . This study defines the function of TRPM7 channel activity in macrophage activation, but the role of the TRPM7 kinase activity in inflammatory signaling remains unexplored. Our experiments with the TRPM7 channel blocker FTY720 reveal that TRPM7 channel activity does not account for the entire spectrum of defects seen in *Trpm7*<sup>-/-</sup> macrophages. [Likewise, CD14-deficient BMDMs do not exhibit defects in Myd88-dependent signal transduction, and if anything, have increased pro-inflammatory cytokine transcription<sup>25</sup>. Given that *Trpm7*-deficient macrophages have decreased Myd88-dependent transcription as well, this indicates that TRPM7 kinase may regulate this aspect of TLR4 signaling independently of TLR4 endocytosis and  $\text{Ca}^{2+}$  entry. Alternatively,] in embryonic stem cells, the cleaved TRPM7 kinase domain has been shown to translocate to the nucleus and modify the chromatin landscape through the phosphorylation of histones<sup>118</sup>. Since TRPM7 is cleaved by multiple proteases (including caspases), a similar function of the cleaved kinase domain may be of salience to inflammatory gene expression in macrophages.

In addition to the role of the kinase domain, a number of other important questions emerge from this study and are the focus of our ongoing and future studies. The molecular mechanism by which TRPM7 is activated during LPS-signaling is not yet clear [ - this is discussed in further detail in Chapter 4]. Previously, we have shown that the TRPM7 channel is activated by a caspase-mediated proteolytic event that also dissociates the kinase domain from the membrane resident channel<sup>113</sup>. The function of TRPM7 kinase activity in the regulation of inflammatory gene expression is thus a major topic of interest. Intracellular LPS has been shown to activate caspase-

11<sup>175</sup>, but LPS-induced, TRPM7-mediated Ca<sup>2+</sup>-influx is relatively rapid, and it is highly unlikely that a brief pulse of LPS can activate caspase-11 in less than a minute. Other possibilities include direct activation of TRPM7 by LPS or activation by the local depletion of PIP<sub>2</sub><sup>123</sup> in close proximity to TLR4. Lastly, once the Ca<sup>2+</sup>-influx is triggered in close proximity to TLR4, the identity of the Ca<sup>2+</sup>-sensitive molecular switch in the endocytic machinery is not yet known.

## FIGURES: Chapter 2

Figure 5. Characterization of *Trpm7<sup>f/f</sup>* (*LysM Cre*) mice and *Trpm7*-deficient macrophages

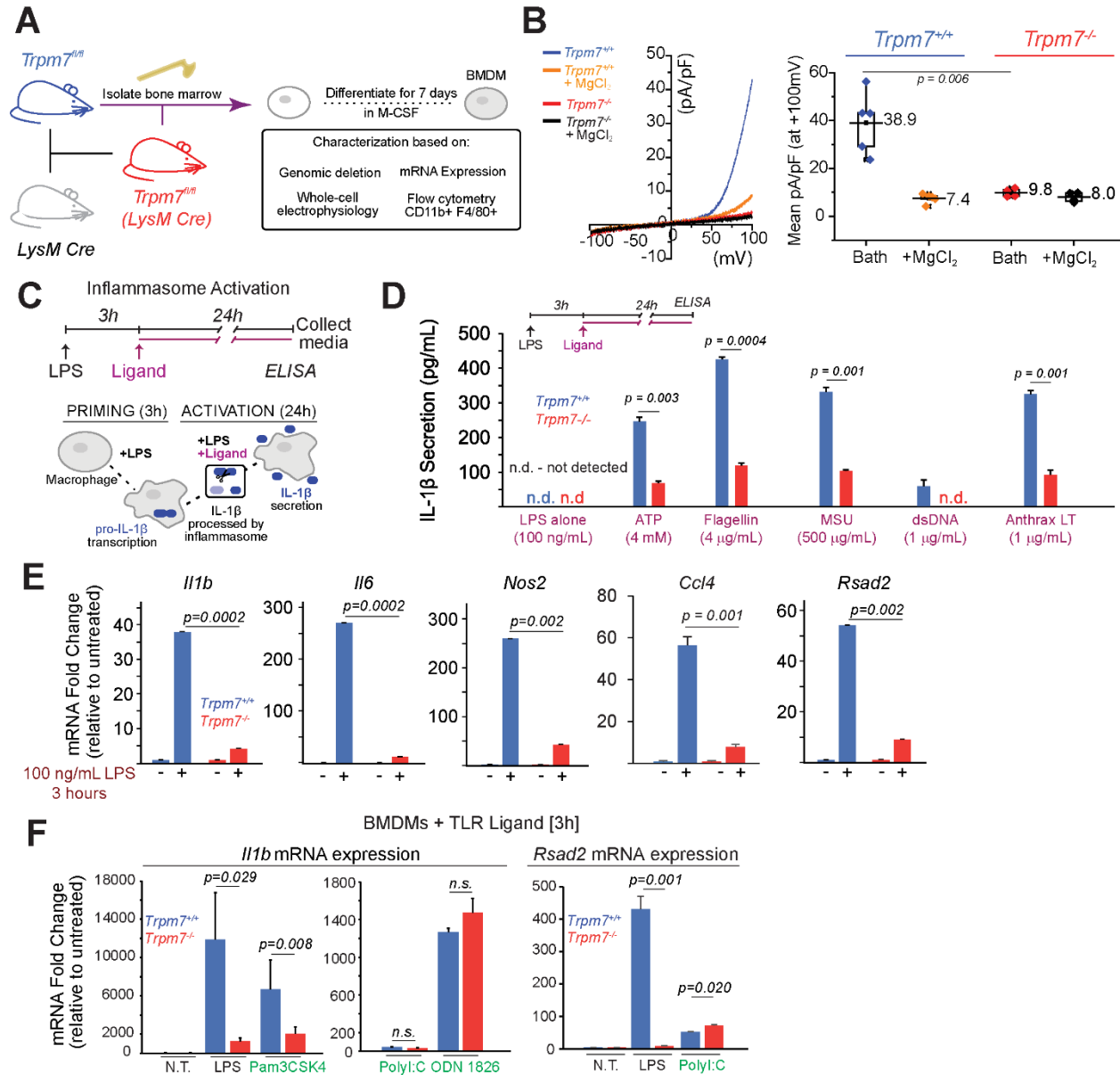


**Figure 5. Characterization of *Trpm7<sup>fl/fl</sup>* (*LysM Cre*) mice and *Trpm7*-deficient macrophages**

(A) Schematic showing generation of *Trpm7<sup>fl/fl</sup>* (*LysM Cre*) mice and bone-marrow-derived macrophage (BMDM) culture.

(B) A representative I-V relationship of whole-cell Mg<sup>2+</sup>-inhibitable I<sub>TRPM7</sub> in freshly isolated *Trpm7<sup>fl/fl</sup>* [*Trpm7<sup>+/+</sup>*] and *Trpm7<sup>fl/fl</sup>* (*LysM Cre*) [*Trpm7<sup>-/-</sup>*] peritoneal macrophages (left panel). The statistics of TRPM7 current densities (n=5) are shown as box charts (right panel). Experiment by SKM.

(C) Schematic of inflammasome activation assay used for results shown in *panel D*. The inflammasome activating ligands were added after 3h of LPS priming (100 ng/mL). The secreted IL-1 $\beta$  in the culture supernatants (collected at 24h) was quantified by ELISA. Experiments by MM.

(D) Quantification of secreted IL-1 $\beta$  in the supernatants of *Trpm7<sup>+/+</sup>* and *Trpm7<sup>-/-</sup>* BMDMs, stimulated with indicated inflammasome activating ligands, as depicted in *panel C*. Error bars represent SEM, n=4.

(E) Gene expression analysis (qRT-PCR) of *Trpm7<sup>+/+</sup>* and *Trpm7<sup>-/-</sup>* BMDMs after stimulation with 100 ng/mL LPS (3h). Changes in mRNA levels, relative to untreated BMDMs are shown. Error bars represent SD (Means representative of n=3 independent experiments).

(F) Gene expression analysis (qRT-PCR) of *Trpm7<sup>+/+</sup>* and *Trpm7<sup>-/-</sup>* BMDMs after stimulation with indicated ligand (3h). BMDMs treated with LPS (100 ng/ml), Pam3CSK4 (100 ng/mL), PolyI:C (25  $\mu$ g/mL), or ODN 1826 (1  $\mu$ M). Changes in mRNA levels, relative to untreated BMDMs are shown. Error bars represent SD (Means representative of n=3 independent experiments). Experiment by TKD.

**Figure 6. Characterization of *Trpm7* gene deletion in macrophages**

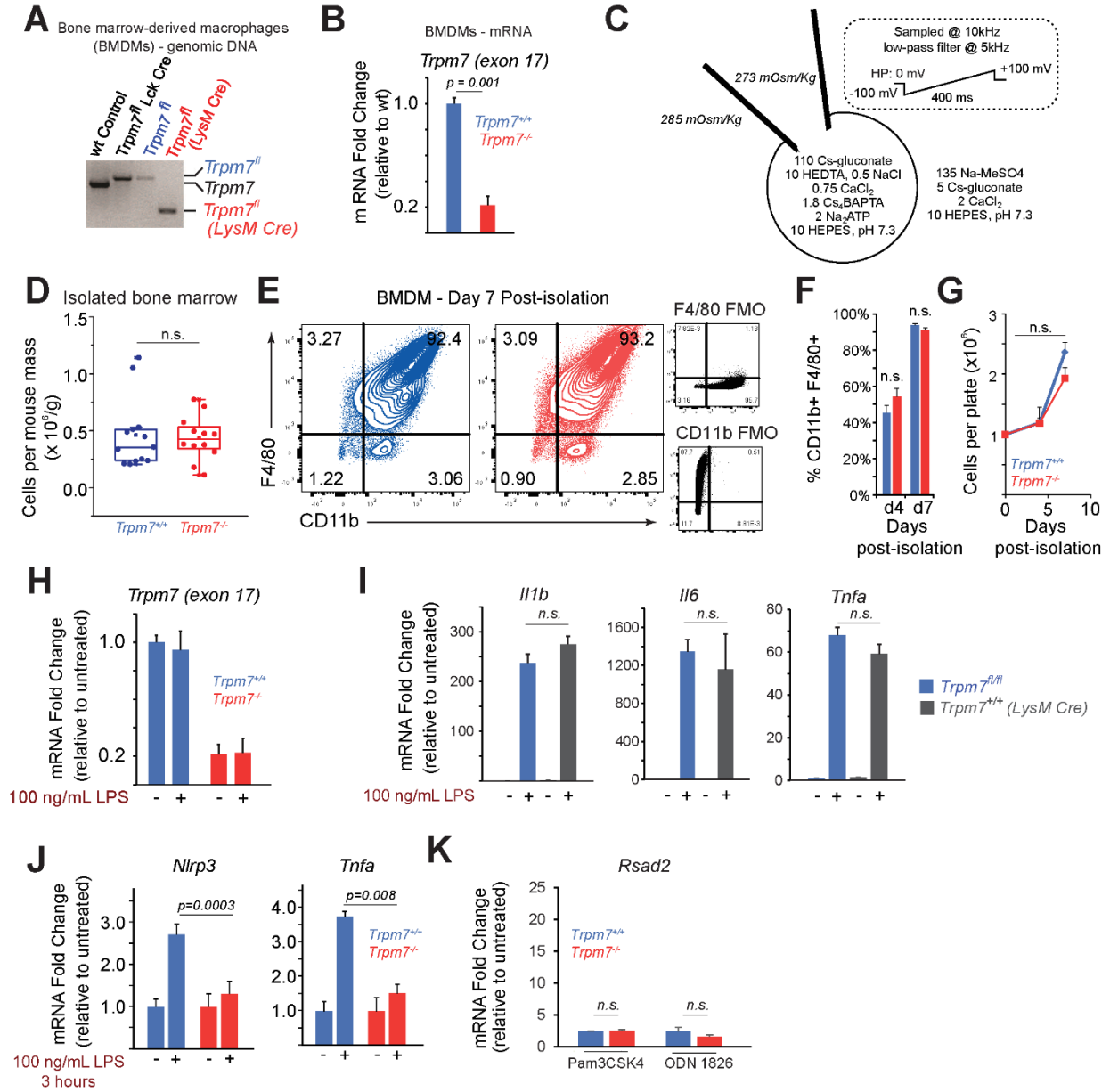


## Figure 6. Characterization of *Trpm7* gene deletion in macrophages

(A) Genotyping of the targeted *Trpm7* genomic locus amplified via PCR from indicated BMDMs. Increased amplicon size reflects the insertion of *loxP* sites in macrophages obtained from *Trpm7<sup>fl/fl</sup>* mice. Decreased size reflects Cre-mediated excision of *loxP*-flanked *exon 17* of *Trpm7* in macrophages obtained from *Trpm7<sup>fl/fl</sup> (LysM Cre)* mice but not in macrophages isolated from *Trpm7<sup>fl/fl</sup> (Lck Cre)* mice, used as controls. Experiment by MM.

(B) qRT-PCR analysis using primers directed against *loxP*-flanked *exon 17* shows the relative difference in the TRPM7 mRNA in BMDMs from *Trpm7<sup>fl/fl</sup> (LysM Cre)* (*Trpm7<sup>-/-</sup>*) mice and *Trpm7<sup>fl/fl</sup> (Trpm7<sup>+/+</sup>)* with intact *exon 17*. Means representative of n=5 measurements. Error bars represent SD.

(C) Schematic of electrophysiology conditions used for whole-cell patch clamp recordings shown in *Figure 5B*.

(D) Live cell counts from freshly isolated bone marrow (day 0) shown as statistical box charts. Trypan blue-excluded cell counting was carried out using an automated cell counter.

(E) Flow cytometry-based phenotypic characterization of BMDMs on day 7 after *ex vivo* differentiation. Representative bivariate cytographs are shown (n=4).

(F) Quantification of measurements depicted in *panel E*, error bars represent SEM (n=4).

(G) Live cell counts of BMDMs in culture during differentiation. After isolation, BMDMs were plated at a density of  $1 \times 10^6$  cells per plate and collected for counting at indicated time points. Cell counts were determined via trypan blue exclusion. Error bars represent SEM (n=4). Experiment by TKD.

(H) qRT-PCR analysis of LPS-induced changes in TRPM7 mRNA expression. BMDMs were treated with LPS (100 ng/mL, 3h) prior to RNA isolation. Error bars represent SD (n=3).

(I) qRT-PCR analysis of LPS-induced inflammatory gene expression in *Trpm7<sup>fl/fl</sup>* and *Trpm7<sup>+/+</sup> (LysM Cre)* BMDMs. Error bars represent SD. Means represent n=2 independent experiments.

(J) Additional mRNA expression analysis from genes as shown in *Fig. 5E*.

(K) Additional mRNA expression analysis of *Rsad2* as shown in *Fig. 5F*.

**Figure 7. Effect of anti-*Trpm7* siRNA and FTY720 on pro-inflammatory gene expression**

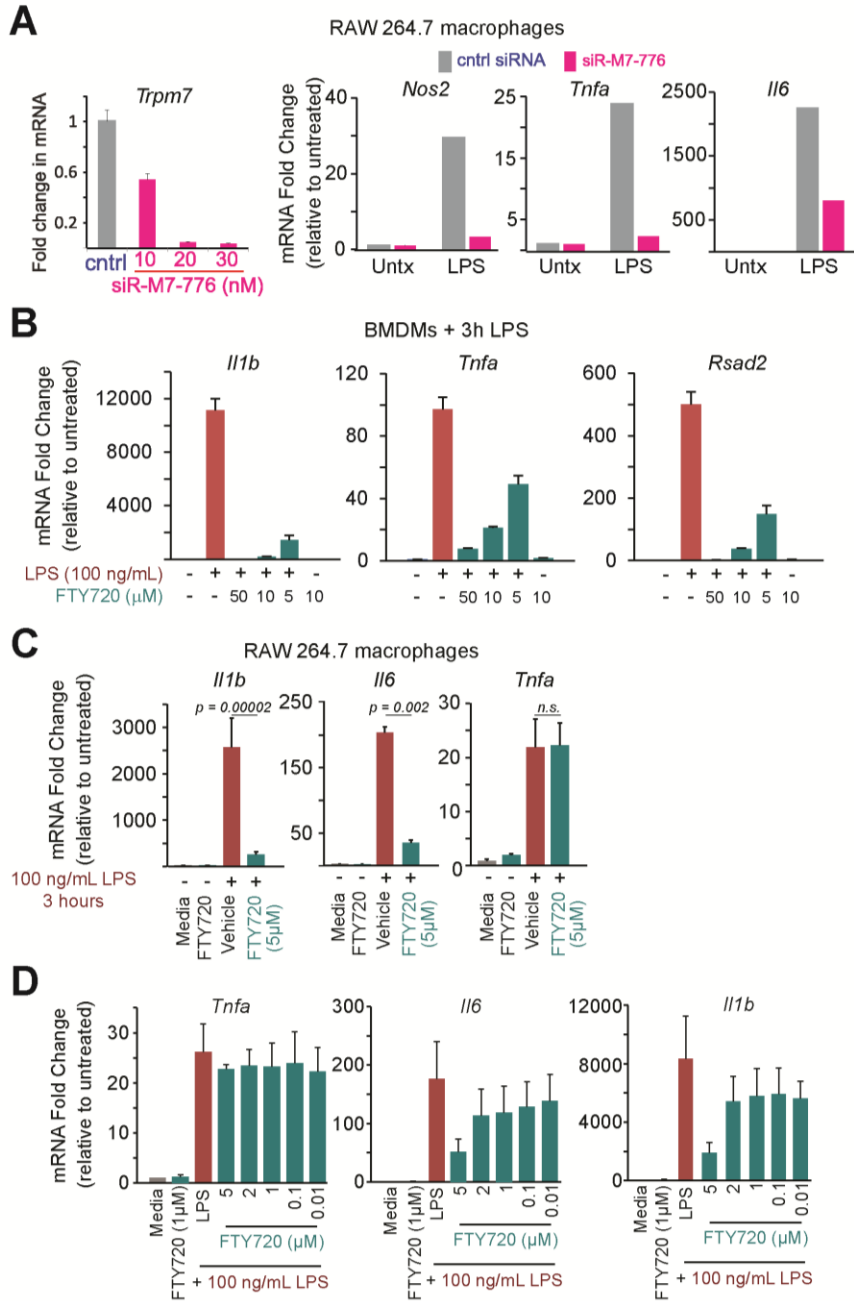


## Figure 7. Effect of anti-*Trpm7* siRNA and FTY720 on pro-inflammatory gene expression

(A) Gene expression analysis (qRT-PCR) of indicated inflammatory genes in RAW 264.7 cells. Left panel is dose-dependent effect of TRPM7-directed siRNA (siR-M7-776) on TRPM7 mRNA levels. Right panels are RAW 264.7 cells treated with LPS (500 ng/mL, 12h). The cells were treated with 20 nM siR-M7-776 (TRPM7-directed) or control (scrambled) siRNA prior to LPS treatment. Experiment by JK.

(B) qRT-PCR analysis of indicated inflammatory genes in BMDMs after 15 min pre-treatment with FTY720, at indicated concentrations, for 3h. Error bars reflect SD of independent experiments (n=3). Changes in mRNA levels, relative to untreated macrophages are shown. Error bars represent SD (Means representative of n=3 independent experiments).

(C) Inflammatory gene expression analysis (qRT-PCR) from RAW 264.7 cells after treatment with 100 ng/mL LPS (3h). Cells were treated with FTY720 or vehicle (EtOH) in media prior to LPS treatment. Experiment by SD.

(D) qRT-PCR analysis of indicated inflammatory genes in RAW 264.7 cells after treatment with FTY720, at indicated concentrations, for 3h. Error bars reflect SD of independent experiments (n=3). Experiment by SD.

**Figure 8. TRPM7 regulates TLR4 endocytosis and downstream NF $\kappa$ B and IRF3 phosphorylation.**

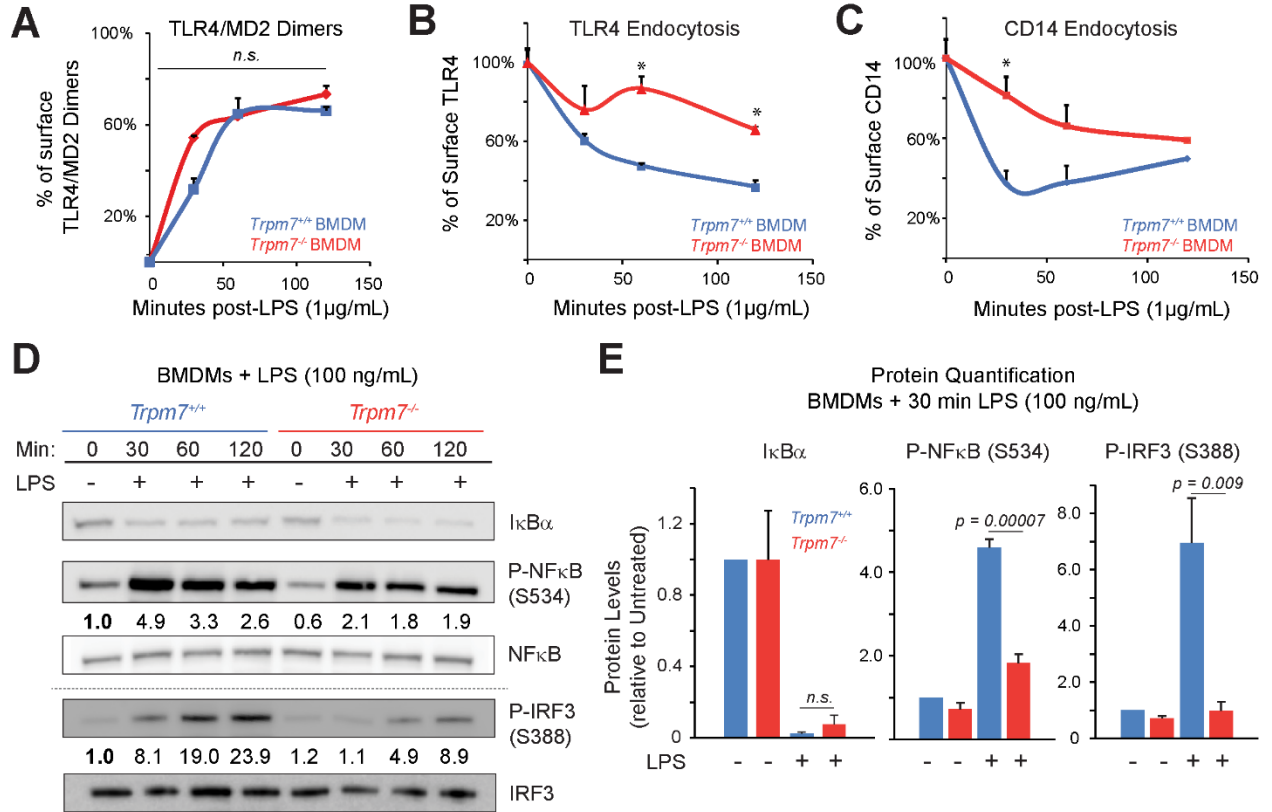


**Figure 8. TRPM7 regulates TLR4 endocytosis and downstream NF $\kappa$ B and IRF3 phosphorylation.**

(A) Flow cytometry-based quantification of TLR4/MD2 dimers on the BMDM cell surface at indicated times after LPS (1  $\mu$ g/mL) treatment. The change in percentage of cell surface TLR4/MD2 dimers was derived by staining the cells with an antibody specific for TLR4/MD2 dimers and calculations were based on the Mean fluorescence intensities (MFI). Error bars represent SEM (n=3). Experiment by MES.

(B) Flow cytometry-based quantification of TLR4 on the BMDM cell surface at indicated times after LPS (1  $\mu$ g/mL) treatment. An anti-TLR4 antibody was used for staining. The error bars represent SEM (n=4).

(C) Flow cytometry-based quantification of CD14 on the BMDM cell surface at indicated times after LPS (1  $\mu$ g/mL) treatment using an anti-CD14 antibody. Analysis was similar to *panel B*. Error bars represent SEM (n=5).

(D) Immunoblot analysis of NF $\kappa$ B p65 phosphorylation at S276 and S534 (in humans S536), P-IRF3 at S388, and I $\kappa$ B $\alpha$  protein levels from whole cells lysates of indicated BMDMs. Cells were stimulated with LPS (100 ng/mL) as indicated. Blots are representative of at least three independent experiments (n>3). Densitometry values indicate phospho-protein levels relative to total protein (ratios) which were then normalized to *Trpm7*<sup>+/+</sup> at 0 min. Grey-dotted line denotes that the bottom gels were obtained from independent samples obtained using identical conditions.

(E) Quantification of immunoblots shown in *Panel D*. The densitometric values were calculated by taking the ratios of phospho-protein levels relative to total protein and then normalizing the ratios to *Trpm7*<sup>+/+</sup> at 0 min. Bar charts represent means from at least three independent experiments (n= 4 for P-IRF3, n = 3 for others). Error bars are SEM. See also *Fig. 9D*.

**Figure 9. TLR4 signal transduction is regulated by TRPM7**

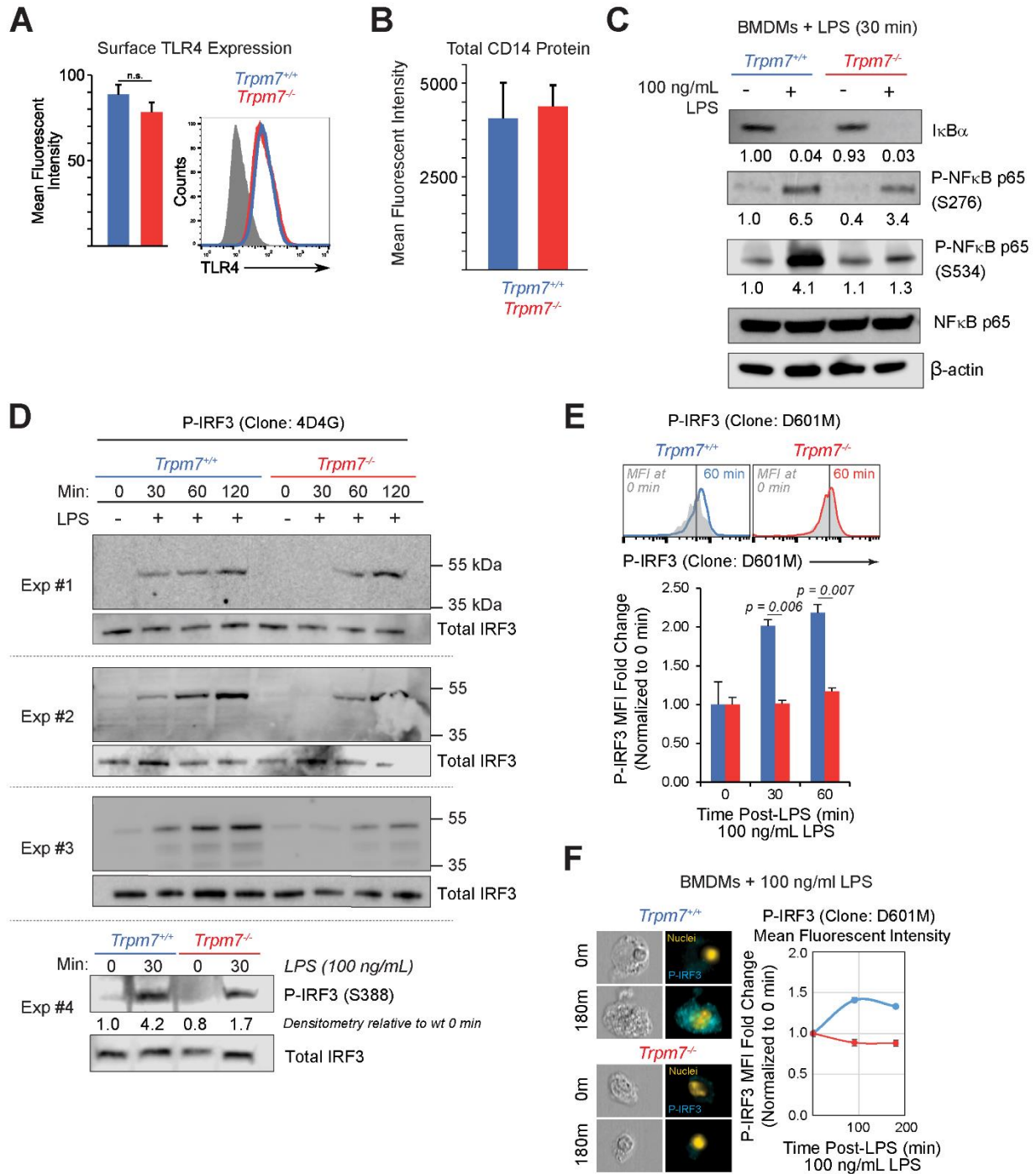


## Figure 9. TLR4 signal transduction is regulated by TRPM7

(A) Flow cytometry-derived mean fluorescence intensities (MFI) of TLR4 staining in *Trpm7*<sup>+/+</sup> and *Trpm7*<sup>-/-</sup> BMDMs, reflecting cell surface TLR4 levels (left panel). Error bars reflect SEM (n=4). Representative overlays of TLR4 histograms are shown in the right panel. The control histogram derived from unstained cells is depicted in gray.

(B) Flow cytometry-derived MFI of CD14 staining in *Trpm7*<sup>+/+</sup> and *Trpm7*<sup>-/-</sup> BMDMs, reflecting cell CD14 levels. Error bars represent SEM (n=3).

(C) Immunoblot analysis of NF $\kappa$ B/p65 phosphorylation at S276 and S534 (in humans S536) and I $\kappa$ B $\alpha$  protein levels from whole cells lysates of *Trpm7*<sup>+/+</sup> and *Trpm7*<sup>-/-</sup> BMDMs stimulated with LPS (100 ng/ml; 30 min). Values for signal intensity are normalized to  $\beta$ -actin and total protein relative to untreated sample. Representative of n=3 independent experiments.

(D) Immunoblot analysis of P-IRF3 (S388) and total IRF3 protein levels from whole cells lysates of *Trpm7*<sup>+/+</sup> and *Trpm7*<sup>-/-</sup> BMDMs stimulated with LPS (100 ng/ml), as indicated. Blots for P-IRF3 and total IRF3 are shown from individual experiments. The densitometric values for P-IRF3 were calculated by taking the ratios of phospho-protein levels relative to total protein and then normalizing the ratios to *Trpm7*<sup>+/+</sup> at 0 min. The statistics are shown in *Figure 8E*.

(E) Analysis of IRF3 phosphorylation at S388 in BMDMs by flow cytometry. *Trpm7*<sup>+/+</sup> and *Trpm7*<sup>-/-</sup> BMDMs were stimulated with LPS (100 ng/ml) for indicated times, stained for viability (Live/Dead stain), and fixed prior to analysis. Later, the cells were stained with anti-P-IRF3 (Clone D601M). (*Top*) Representative histograms of P-IRF3 MFI; grey-filled histograms indicate P-IRF3 protein levels at 0 min (untreated). (*Bottom*) Quantification of P-IRF3 protein levels. Fold change is normalized to P-IRF3 MFI at 0 min. Error bars are SEM (n=3).

(F) Representative images (n> 5000 cells) taken from ImageStream flow cytometry analysis of indicated BMDMs, stimulated with LPS (100 ng/mL for indicated time) and stained with anti-P-IRF3 antibody (Clone: D601M) and DRAQ-5 (nuclei) (*left panels*). Levels of P-IRF3 at indicated time points after LPS treatment were quantified based on MFI at 0 min (*right panel*). Error bars represent SEM (n>5000 cells).

**Figure 10. LPS-induced nuclear translocation of NFκB p65 and IRF3 is defective in *Trpm7*-deficient BMDMs.**

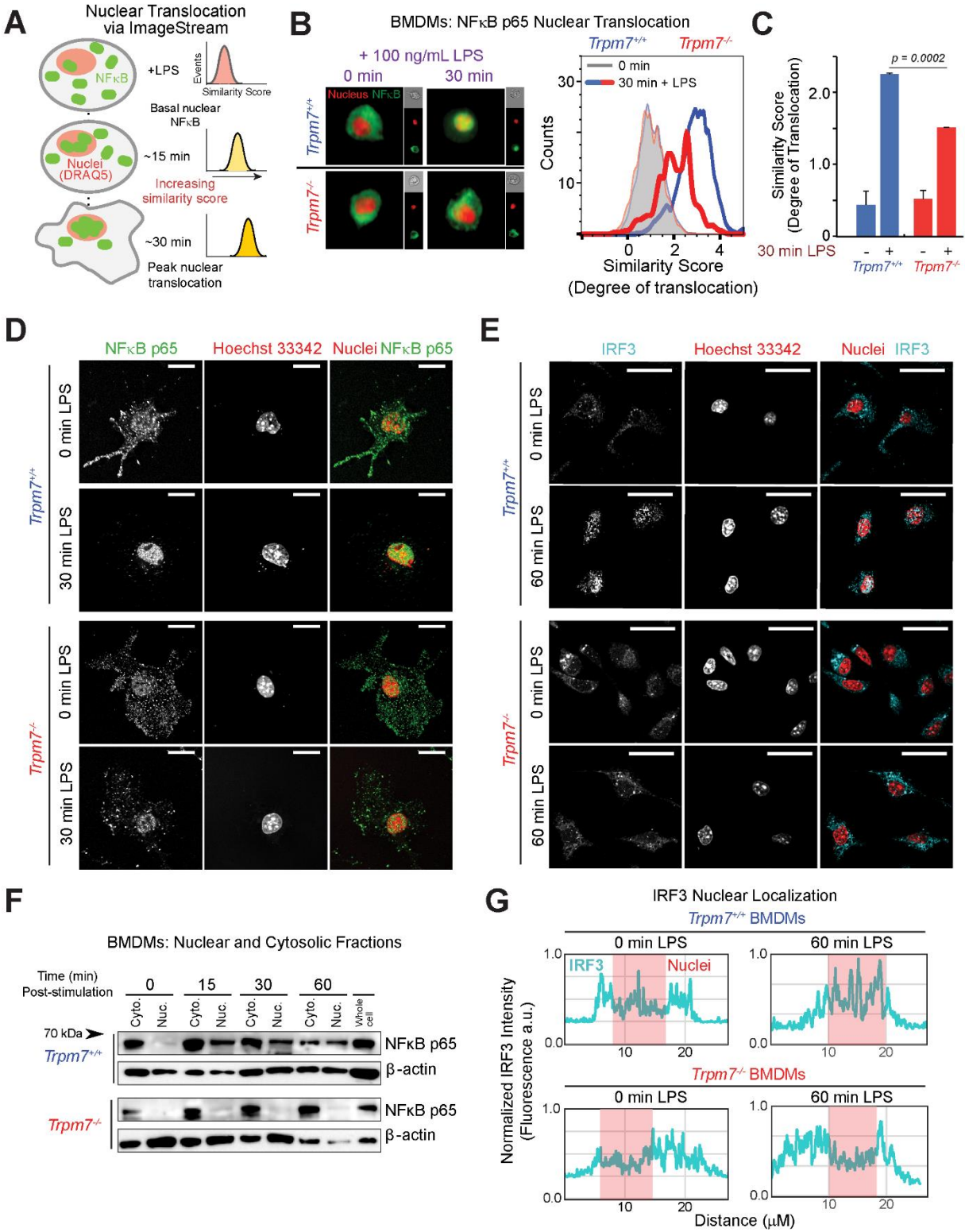


**Figure 10. LPS-induced nuclear translocation of NF $\kappa$ B p65 and IRF3 is defective in *Trpm7*-deficient BMDMs.**

(A) Schematic of ImageStream analysis of LPS-induced NF $\kappa$ B translocation. Quantification of nuclear translocation is reflected by and directly proportional to the similarity scores of NF $\kappa$ B and nuclear staining. Similarity scores of individual cells are displayed together as a histogram.

(B) Representative images ( $n > 2000$  cells) taken from ImageStream flow cytometry analysis of indicated BMDMs, stimulated with LPS (100 ng/mL, 30m) and stained with anti-NF $\kappa$ B p65 antibody and DRAQ5 (nuclear stain) (*left panels*). An overlaid image of NF $\kappa$ B p65 staining (green) and DRAQ5 (red) is shown and the single channel images of that cell are shown on the right in smaller sizes. The overlay of histograms depicts the representative similarity scores derived for each condition (*right panel*), quantified in *Panel C* ( $n=4$ ).

(C) Quantification of ImageStream flow cytometry results depicted in *Panel B*. Error bars are SEM ( $n=4$ ).

(D) Confocal immunofluorescence microscopy images of fixed BMDMs, treated or untreated with LPS (100 ng/ml, 30m) as indicated, and stained with anti-NF $\kappa$ B p65 and Hoechst nuclear stain. Images shown are a single optical section (0.25  $\mu$ m). Scale bar = 15  $\mu$ m. Typical results of  $n=3$  experiments.

(E) Confocal immunofluorescence microscopy images of fixed BMDMs, treated or untreated with LPS (100 ng/ml, 60m) and stained with anti-IRF3 and Hoechst nuclear stain. Images shown are a single optical section (0.25  $\mu$ m). Scale bar = 25  $\mu$ m.

(F) Immunoblot analysis of NF $\kappa$ B p65 present in cytosolic and nuclear fractions obtained from indicated BMDMs at various time points after LPS (100 ng/ml) treatment. Immunoblots of  $\beta$ -actin in each fraction is also shown. These are representative results of independent experiments ( $n=3$ ).

(G) Linear intensity analysis of IRF3 nuclear localization. Fluorescent intensity of IRF3 signal (cyan) was measured with a single x-y plane line trace; location of nuclei is overlaid (red). Line traces depict typical cells from *panel E* and are illustrated in *Fig. 11H*.

**Figure 11. TLR4 receptor endocytosis is required for normal signal transduction**

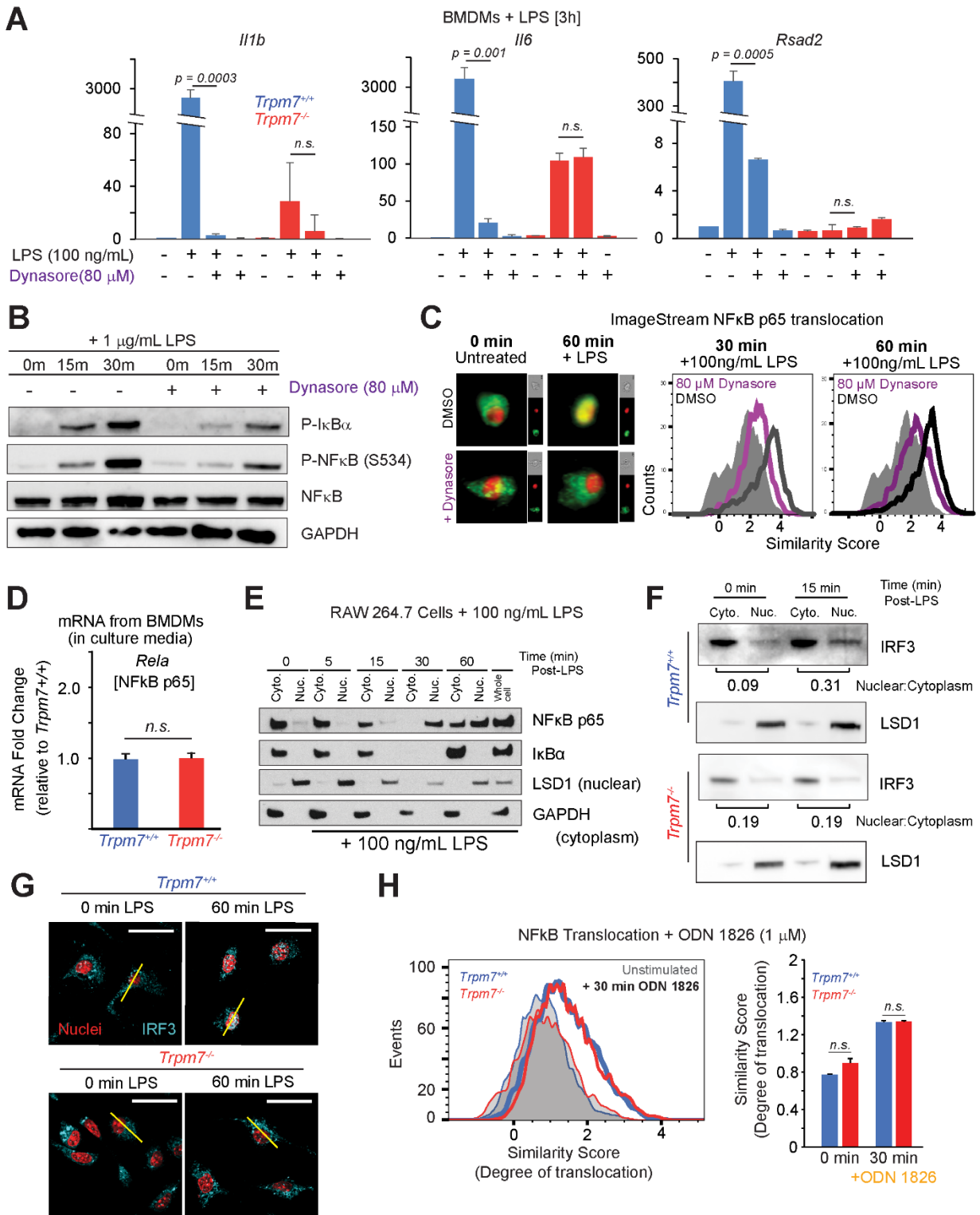


### Figure 11. TLR4 receptor endocytosis is required for normal signal transduction

(A) Gene expression analysis (qRT-PCR) of *Trpm7*<sup>+/+</sup> and *Trpm7*<sup>-/-</sup> BMDMs stimulated as indicated. BMDMs were pre-treated in serum-free media with or without dynasore (80  $\mu$ M; 30 min) prior to LPS stimulation (100 ng/ml; 3h). Error bars represent SD (n=3)

(B) Immunoblot analysis of whole cell lysates from BMDMs treated as indicated. BMDMs were pre-treated in serum-free media with or without dynasore (80  $\mu$ M; 30 min) prior to LPS stimulation.

(C) Representative images (n> 5000 cells) taken from ImageStream flow cytometry analysis of untreated and Dynasore treated WT BMDMs, stimulated with LPS (100 ng/mL, 60m) and stained with anti-NF $\kappa$ B/p65 antibody and DRAQ5 (a nuclear stain) are shown (*left panels*). An overlaid image of NF $\kappa$ B/p65 staining (green) and DRAQ5 (red) is shown and the single channel images of that cell are shown on the right of that image in smaller sizes. The right panel shows an overlay of histograms depicting the similarity scores derived for each condition, 30m and 60m after LPS treatment. The filled histogram represents untreated cells.

(D) qRT-PCR analysis of NF $\kappa$ B/p65 gene expression in indicated BMDMs. Error bars reflect SD (n=3).

(E) Immunoblot analysis of NF $\kappa$ B/p65 and I $\kappa$ B $\alpha$  present in cytosolic and nuclear fractions obtained from RAW 264.7 cells at various time points after LPS (100 ng/ml) treatment. Immunoblots of LSD1 (a nuclear protein) and GAPDH (a cytosolic protein) are also shown.

(F) Immunoblot analysis of IRF3 present in cytosolic and nuclear fractions from indicated BMDMs, untreated and treated with LPS (100 ng/ml, 15m). Immunoblots of LSD1, a nuclear marker are also shown. These are representative results of independent experiments (n=3).

(G) Representation of linear intensity analysis in *Fig 10F*. Images are relabeled from *Fig 10D* with region of interest annotated (yellow).

(H) Representative histograms taken from ImageStream flow cytometry (n> 7000 cells) analysis of *Trpm7*<sup>+/+</sup> and *Trpm7*<sup>-/-</sup> BMDMs, stimulated with ODN 1826 (1  $\mu$ M, 30m). Histograms depict similarity scores after staining with anti-NF $\kappa$ B/p65 antibody and DRAQ5 (a nuclear stain) are shown (*left panels*); the filled histogram represents untreated cells. The right panel depicts quantification of similarity scores. Error bars are SEM (n=4).

**Figure 12. LPS signaling and NFκB translocation are abrogated by clamping intracellular Ca<sup>2+</sup> but there is no further decrease in *Trpm7*-deficient macrophages.**

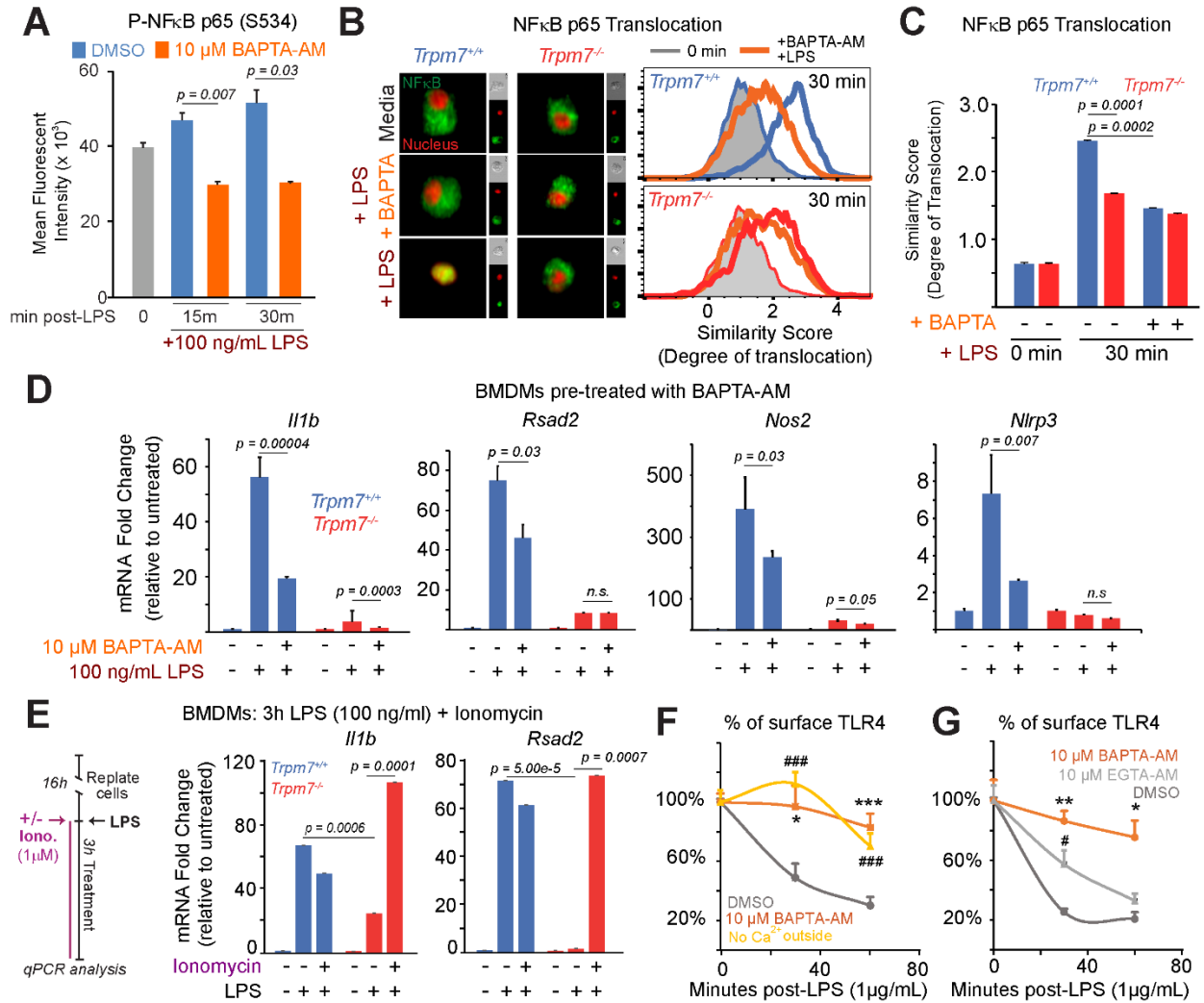


**Figure 12. LPS signaling and NFκB translocation are abrogated by clamping intracellular Ca<sup>2+</sup> but there is no further decrease in *Trpm7*-deficient macrophages.**

(A) Flow cytometry-based quantification of phospho-NFκB p65, as indicated by MFI, in DMSO (vehicle control) and BAPTA-AM loaded BMDMs in response to LPS (100 ng/mL, indicated time points). The error bars represent SEM (n=3).

(B) Representative images (n>5000 cells) from ImageStream analysis of DMSO and BAPTA-AM loaded cells are shown (*left panel*). Cells were stimulated with LPS (100 ng/ml, 30m) and then stained with anti-NFκB p65 antibody and DRAQ5 (a nuclear stain), prior to ImageStream analysis. To the right of the merged image of NFκB p65 (green) and DRAQ5 (red), single channel images of that cell are shown in smaller sizes. Overlaid histograms of similarity scores derived from each condition are shown (*right panels*); unstimulated (grey-filled), BAPTA-AM pre-treated (orange), and LPS treated (blue-*wt*; red-*KO*) are shown. The data are representative and typical of independent experiments (n=2).

(C) Quantification of similarity scores from *panel B*, reflecting the degree of NFκB p65 translocation in indicated conditions. Error bars represent SEM (n=3).

(D) qRT-PCR analysis of indicated inflammatory genes in *Trpm7*<sup>+/+</sup> and *Trpm7*<sup>-/-</sup> BMDMs treated as depicted. Prior to LPS treatment (100 ng/mL, 3h), BMDMs were pre-treated with DMSO or BAPTA-AM for 30 min in serum-free media. Error bars represent SD (n=3).

(E) qRT-PCR analysis of indicated inflammatory genes in *Trpm7*<sup>+/+</sup> and *Trpm7*<sup>-/-</sup> BMDMs treated as indicated in the schematic of the experimental design (*left panel*). Mean expression relative to untreated condition (*right panel*). Ionomycin is added with LPS to induce Ca<sup>2+</sup> influx. Error bars represent SD (n=3).

(F) Flow cytometry-based quantification of cell surface TLR4 in RAW 264.7 cells at indicated times after LPS (1 μg/mL) treatment. Cells were treated with BAPTA-AM or DMSO as indicated prior to LPS treatment. Extracellular Ca<sup>2+</sup>-free conditions supplemented 10 mM EGTA. The error bars reflect SEM (n=3). \* is BAPTA-AM treatment and # is low Ca<sup>2+</sup> outside relative to *wt*. \* indicates p<0.05, \*\*\* or ### indicates p<0.001.

(G) Flow cytometry-based quantification of cell surface TLR4 in RAW 264.7 cells at indicated times after LPS (1 μg/mL) treatment. Cells were treated with BAPTA-AM, EGTA-AM, or DMSO as indicated prior to LPS treatment. The error bars reflect SEM (n=3). \* is BAPTA-AM treatment and # is EGTA-AM relative to *wt*. \* or # indicates p<0.05, \*\* or ## indicates p<0.01.

**Figure 13. TLR4 signal transduction is largely, but not completely, dependent on Ca<sup>2+</sup> signaling.**

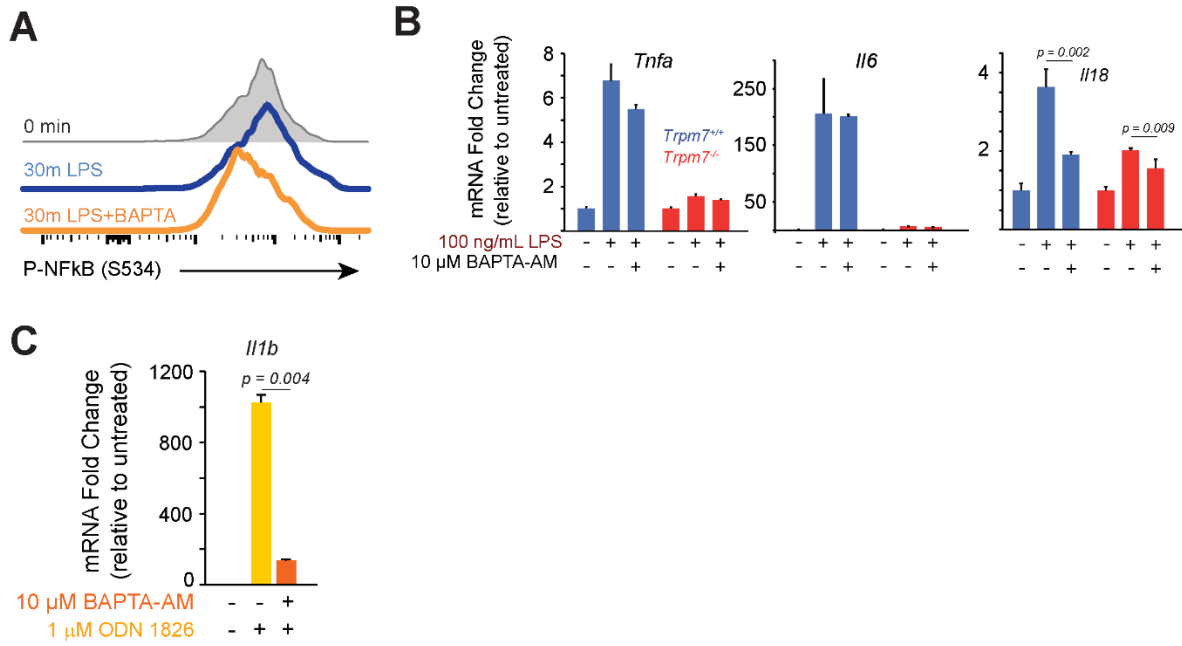


**Figure 13. TLR4 signal transduction is largely, but not completely, dependent on Ca<sup>2+</sup> signaling.**

(A) An extension of *Fig. 12A*, representative histograms of phospho-NFκB p65 (S534) staining in indicated BMDMs.

(B) Expression of indicated inflammatory genes (qRT-PCR) in *Trpm7*<sup>+/+</sup> and *Trpm7*<sup>-/-</sup> BMDMs, treated as indicated in *Fig. 12D*. Prior to LPS treatment (100 ng/mL, 3h), BMDMs were loaded with vehicle or BAPTA-AM for 30m in serum-free media. Error bars represent SD (n=3).

(C) qRT-PCR analysis of *I11b* mRNA expression in WT BMDMs. Prior to ODN 1826 treatment (1 μM, 3h), BMDMs were loaded with vehicle (DMSO) or BAPTA-AM for 30m in serum-free media. Error bars represent SD (n=3).

**Figure 14. LPS-induced  $\text{Ca}^{2+}$  elevations are highly compromised in *Trpm7*-deficient macrophages.**

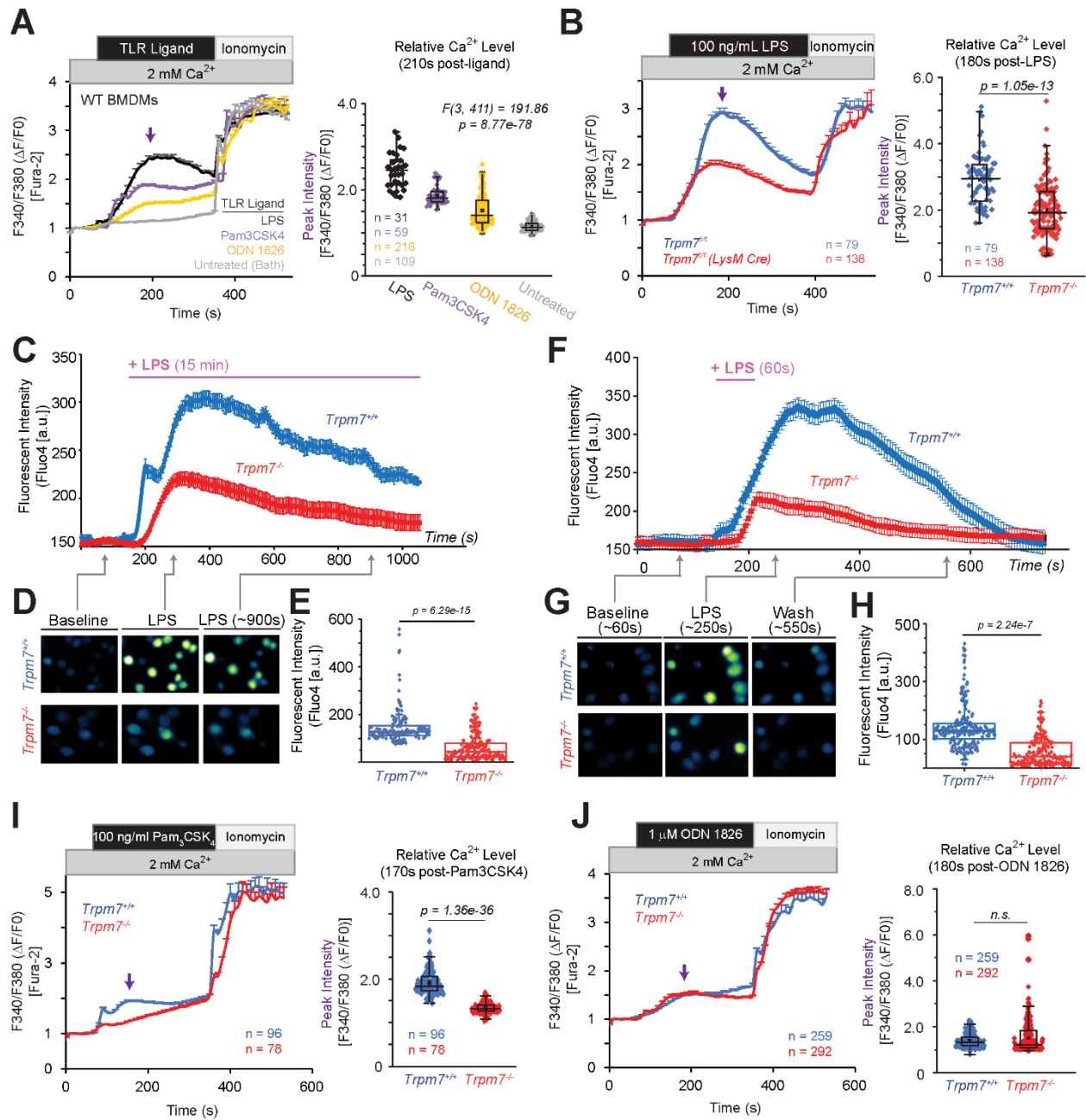


**Figure 14. LPS-induced  $\text{Ca}^{2+}$  elevations are highly compromised in *Trpm7*-deficient macrophages.**

(A) Relative changes in  $[\text{Ca}^{2+}]_i$  over time in WT BMDMs treated with indicated TLR ligands for 5 min. Cells were treated with either LPS (100 ng/ml), Pam3CSK4 (100 ng/ml), ODN 1826 (1  $\mu\text{M}$ ), or bath solution (untreated). *Left panel:* trace represents mean  $\Delta\text{F340/F380}$  ratio from all samples and error bars are SEM; ionomycin (1  $\mu\text{M}$ ) was perfused as a positive control. The arrow indicates the time point of peak  $[\text{Ca}^{2+}]_i$ , these values were used for statistical analysis. *Right panel:* Quantification of peak  $[\text{Ca}^{2+}]_i$  after LPS stimulation; box-whisker plot is overlaid on individual measurements. One-way ANOVA statistical analysis and *n* values (number of cells) are indicated in the figure. Results are a compilation of three independent experiments.

(B) Relative changes in  $[\text{Ca}^{2+}]_i$  over time in *Trpm7*<sup>+/+</sup> and *Trpm7*<sup>-/-</sup> BMDMs treated with LPS (100 ng/ml) for 5 min. *Left panel:* trace represents mean  $\Delta\text{F340/F380}$  ratio from all samples (*n*=79 and *n*=138 for *Trpm7*<sup>+/+</sup> and *Trpm7*<sup>-/-</sup>, respectively) and error bars are SEM. Ionomycin (1  $\mu\text{M}$ ) was perfused as a positive control. *Right panel:* Quantification of peak  $[\text{Ca}^{2+}]_i$  after LPS stimulation; box-whisker plot is overlaid on individual measurements; *n* values (number of cells analyzed) indicated in figure. Results are a compilation of three independent experiments.

(C) Relative changes in the fluorescence of Fluo-4AM-loaded BMDMs, reflecting changes in intracellular  $\text{Ca}^{2+}$  concentration  $[\text{Ca}^{2+}]_i$  BMDMs after LPS (1  $\mu\text{g/mL}$ ) treatment for 15 min. Error bars reflect SEM (*n*=146 and *n*=179 for *Trpm7*<sup>+/+</sup> and *Trpm7*<sup>-/-</sup>, respectively). These represent typical results from four independent experiments. Experiment by KS.

(D) Representative fluorescence images from indicated time points in the experiments shown in *panel C*.

(E) Statistical representation of mean peak intensities of Fluo-4 fluorescence after LPS treatment from *panel C*.

(F) Relative changes in  $[\text{Ca}^{2+}]_i$  over time in *Trpm7*<sup>+/+</sup> and *Trpm7*<sup>-/-</sup> BMDMs treated with LPS (1  $\mu\text{g/mL}$ ) for 60s. Error bars are SEM (*n*=217 and *n*=190 for *Trpm7*<sup>+/+</sup> and *Trpm7*<sup>-/-</sup>, respectively). These represent typical results from four independent experiments. Experiment by KS.

(G) Representative images from indicated time points in *panel F*.

(H) Statistical representation of mean peak intensities after LPS treatment from *panel F*.

(I) Relative changes in  $[\text{Ca}^{2+}]_i$  over time in *Trpm7*<sup>+/+</sup> and *Trpm7*<sup>-/-</sup> BMDMs treated with Pam3CSK4 (100 ng/ml) for 5 min. *Left and Right panels* depicted as in *Fig. 14B*.

(J) Relative changes in  $[\text{Ca}^{2+}]_i$  over time in *Trpm7*<sup>+/+</sup> and *Trpm7*<sup>-/-</sup> BMDMs treated with ODN 1826 (1  $\mu\text{M}$ ) for 5 min. *Left and Right panels* depicted as in *Fig. 14B*.

**Figure 15. Blocking TRPM7 channel activity abrogates LPS-induced Ca<sup>2+</sup> entry and TLR4 endocytosis.**

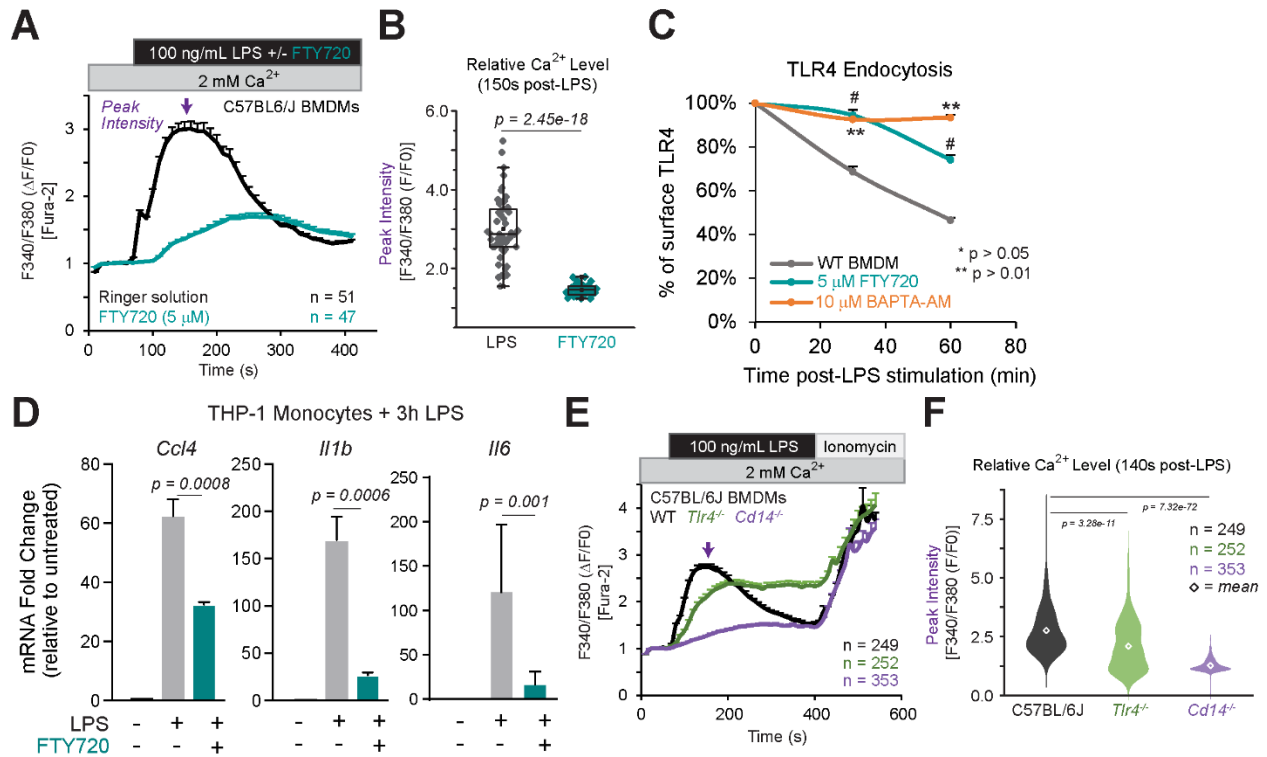


**Figure 15. Blocking TRPM7 channel activity abrogates LPS-induced Ca<sup>2+</sup> entry and TLR4 endocytosis.**

(A) Relative changes in [Ca<sup>2+</sup>]<sub>i</sub> over time in C57BL/6 BMDMs treated with LPS (100 ng/ml) or LPS+FTY720 (5 μM) for 5 min. Trace represents mean ΔF340/F380 ratio from all samples and error bars are SEM. Ionomycin (1 μM) was perfused as a positive control. Results are from n=3 independent experiments; *n* value indicated in figure.

(B) Quantification of peak [Ca<sup>2+</sup>]<sub>i</sub> after LPS stimulation from *Fig 6A*. Box-whisker plot is overlaid on individual measurements.

(C) Flow cytometry based measurement of cell surface TLR4 levels in BMDMs, pre-treated with either vehicle (DMSO), FTY720, or BAPTA-AM for 15 min, and then stimulated with LPS as indicated. The relative change in the percentage of cell surface TLR4 levels was inferred based on mean MFI values. Error bars represent SEM (n=3; \* indicates p < 0.05, \*\* p < 0.01). \* indicates significance from WT relative to BAPTA-AM; #, FTY720 group. These results represent typical results obtained in n=2 independent experiments.

(D) Gene expression analysis (qRT-PCR) of human THP-1 monocytes stimulated with LPS (100 ng/ml; 3h) with FTY720 pre-treatment as indicated. Bar charts represent mean of n=3 independent experiments. Error bars are SEM (n=3). Experiment by PVS.

(E) Relative changes in [Ca<sup>2+</sup>]<sub>i</sub> over time in BMDMs treated with LPS (100 ng/ml) for 5 min. Ionomycin (1 μM) was perfused as a positive control. Traces represent mean ΔF340/F380 ratio from all samples measured and error bars are SEM. Results are representative from n=5 independent experiments.

(F) Quantification of peak [Ca<sup>2+</sup>]<sub>i</sub> after LPS stimulation from *Fig 6E*. Violin plot is shown to illustrate range and distribution of data points; diamond indicates mean value for group. One-way ANOVA (F[2,851] = 266.23) indicates p = 1.6e-90. T-test used to compare groups with C57BL/6J BMDMs.

**Figure 16. LPS-induced signal transduction is inhibited by FTY720 treatment**

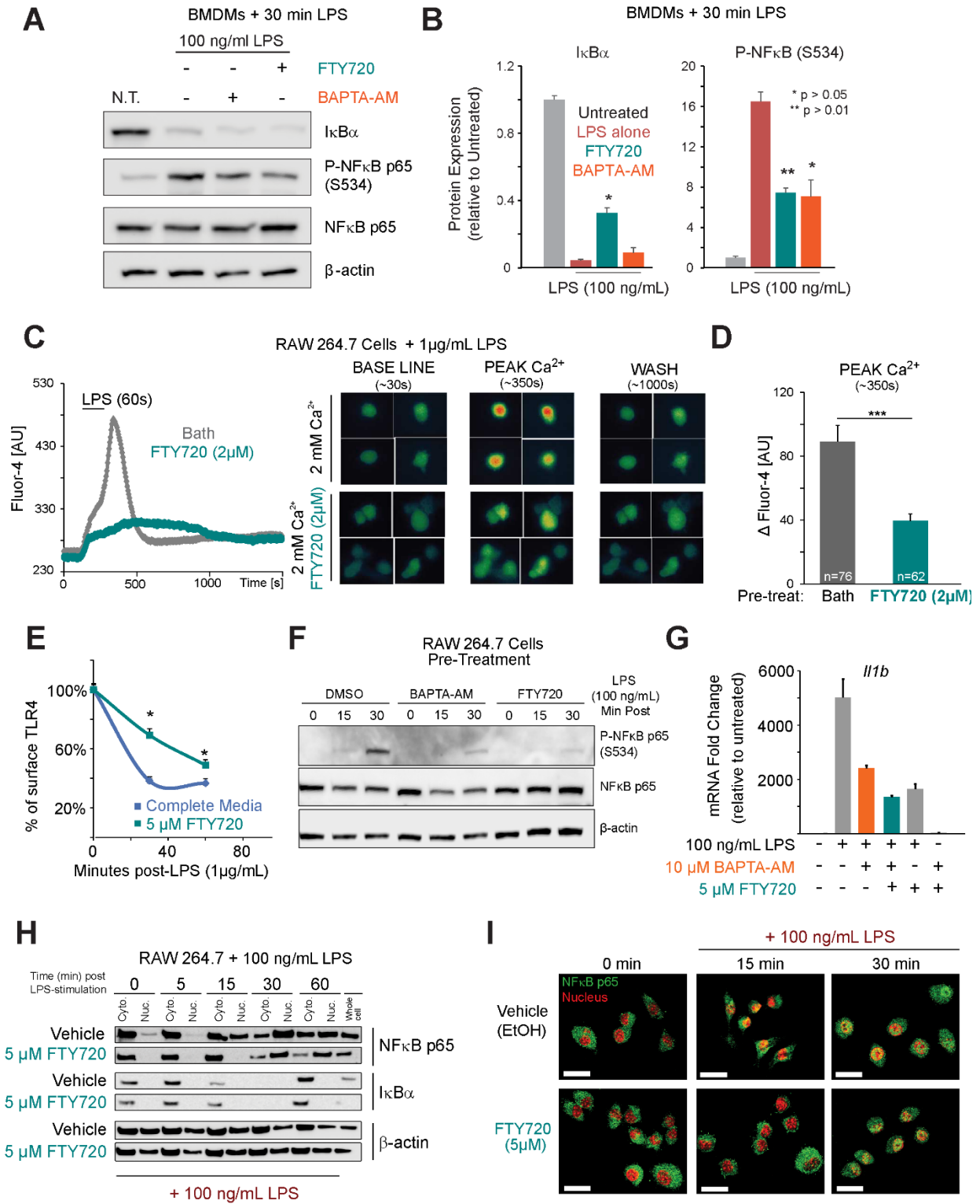


## Figure 16. LPS-induced signal transduction is inhibited by FTY720 treatment

(A) Immunoblot analysis of LPS-induced NF $\kappa$ B phosphorylation at S534 and I $\kappa$ B $\alpha$  protein in the whole cell lysates of BMDMs pre-treated as follows: BAPTA-AM (10  $\mu$ M, 30m), FTY720 (5  $\mu$ M, 15m), DMSO as vehicle control. These data are representative of n=3 independent experiments. Experiment supported by TKD.

(B) Quantification of immunoblots as shown in *Fig 13A*. Relative protein expression is normalized to corresponding total protein and then 0 min treatment. Bar charts represent means from n = 3 independent experiments. Error bars are SEM (n=3). T-test for significance compared to LPS alone.

(C) Relative changes in LPS-induced intracellular Ca<sup>2+</sup> concentration [Ca<sup>2+</sup>]<sub>i</sub> in untreated or FTY720-treated RAW 264.7 cells (*left panel*). Representative images of Fluo-4 fluorescence are shown on the right. Experiment by KS.

(D) Quantification of LPS-induced peak fluorescent intensities in indicated conditions, relative to untreated cells (\*\*\*) indicates p < 0.001).

(E) Flow cytometry based measurement of cell surface TLR4 levels in BMDMs, pre-treated with either vehicle or FTY720 for 15 min, and then stimulated with LPS as indicated. The relative change in the percentage of cell surface TLR4 levels was inferred based on MFI values. Error bars represent SEM (n=3; \* indicates p < 0.05).

(F) Immunoblot analysis of LPS-induced NF $\kappa$ B phosphorylation at S534 in the whole cell lysates of RAW 264.7 cells pre-treated as follows: BAPTA-AM (10  $\mu$ M, 30m), FTY720 (5  $\mu$ M, 15m), DMSO as vehicle control. These data are representative of n=3 independent experiments. Experiment by MES.

(G) Expression analysis (qRT-PCR) of *I11b* in RAW 264.7 cells pre-treated as indicated prior to LPS (100 ng/ml, 3h). Error bars represent SD (n=3).

(H) Immunoblot analysis of NF $\kappa$ B/p65 and I $\kappa$ B $\alpha$  in cytosolic and nuclear fractions of RAW 264.7 cells pre-treated with FTY720 or Vehicle (EtOH), and then stimulated with LPS (100 ng/ml) for indicated times. The results represent typical results seen in n=3 independent experiments.

(I) Immunofluorescence confocal microscopy images showing NF $\kappa$ B/p65 nuclear translocation in RAW 264.7 cells, pre-treated with FTY720 or Vehicle (EtOH) prior to LPS stimulation for indicated times. Scale bar = 10  $\mu$ m. These are representative images from n=2 independent experiments.

**Figure 17. *Trpm7<sup>fl/fl</sup>* (*LysM Cre*) mice are resistant to LPS-induced peritonitis**

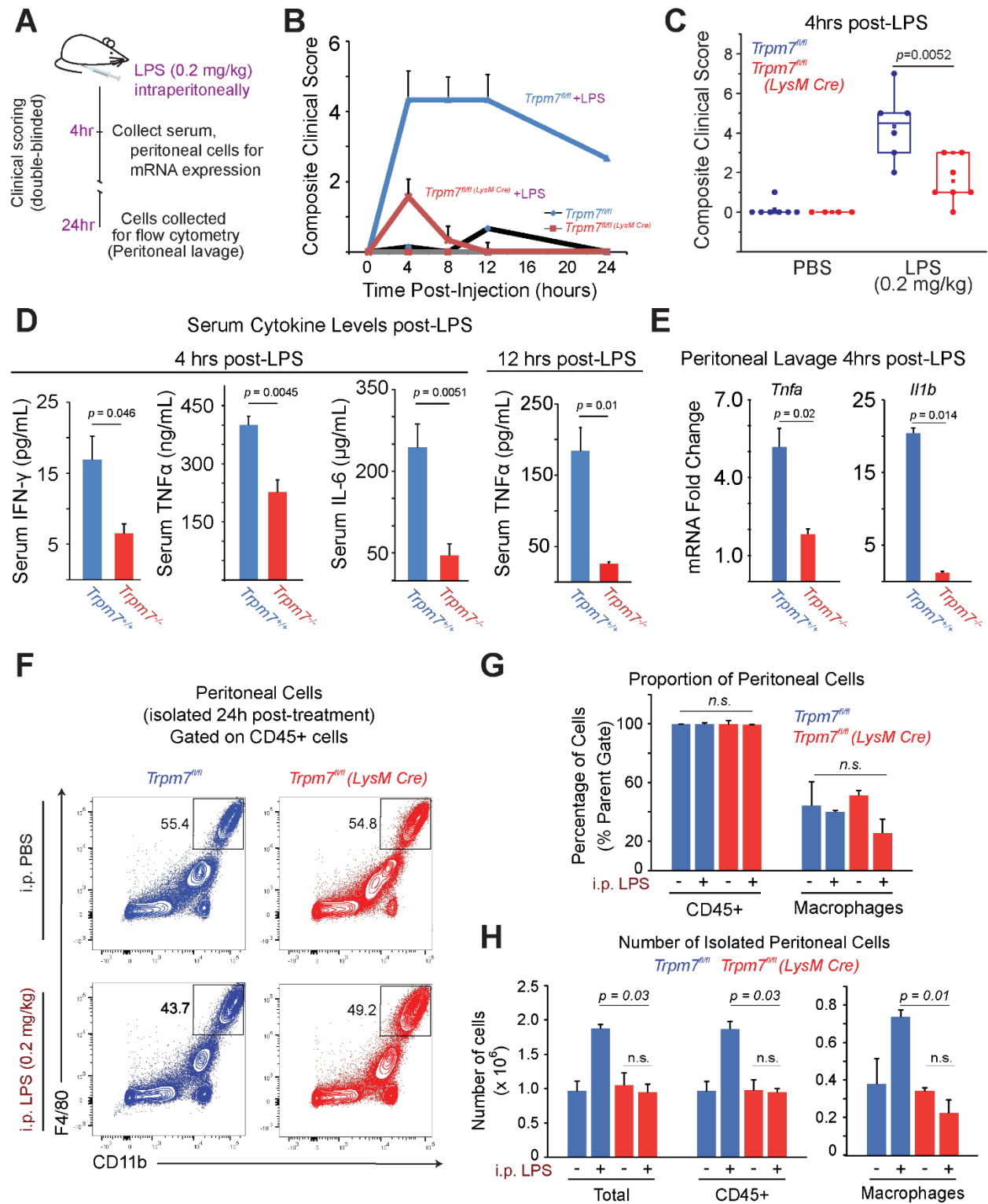


**Figure 17. *Trpm7<sup>f/f</sup>* (*LysM Cre*) mice are resistant to LPS-induced peritonitis**

(A) Schematic of LPS-induced peritonitis mouse model and analysis. Experiments were supported by MES, JSR, and SAA.

(B) After a sub-lethal dose of LPS (0.2 mg/kg, i.p), the mice were observed for 24 hrs by a double-blinded experimenter to record clinical scores in accord with an index described in *Table S1*. Error bars represent SEM (n>5).

(C) Statistical box charts showing composite clinical scores from individual mice, at 4h of observation with indicated treatments (see panel A for details). Data were compiled from three independent cohorts of mice. Box chart parameters are described in methods.

(D) ELISA measurements of indicated cytokines in the serum collected after LPS (0.2 mg/kg) injections at indicated time points. Error bars represent SEM (n>6 compiled from three independent cohorts).

(E) Gene expression analysis (qRT-PCR) of cells collected via a peritoneal lavage, after LPS (0.2 mg/kg, 4h) injections. Quantification is relative to PBS-injected controls (not shown). Error bars represent SEM (n=4 mice).

(F) Flow cytometry-based immunophenotypic analysis of peritoneal macrophages for the indicated cell surface markers, after gating on CD45+ cells. The legacy of gates is shown in *Figure 13*. Cells were isolated from peritoneal lavage after LPS (0.2 mg/kg, 24h). The data represent typical results from independent experiments (n=3 mice).

(G) The mean percentage of peritoneal hematopoietic (CD45+) and macrophages (CD45+ CD11b+ F4/80+) determined by flow cytometry analysis shown in *Figure 13*. Error bars represent SEM (n=3 mice).

(H) Mean numbers of total cells, hematopoietic (CD45+) and macrophages (CD45+ CD11b+ F4/80+) in peritoneal lavages, as determined by flow cytometry analysis shown in *Panel F*. Cell counts were calculated by accounting for the number of cells analyzed, percentages of cells in legacy gates, and recovery volume of peritoneal lavage. Error bars represent SEM (n=3 mice). See also *Figure 18* and *Table 1*.

Figure 18. Flow cytometry gating strategy for LPS-induced peritonitis model

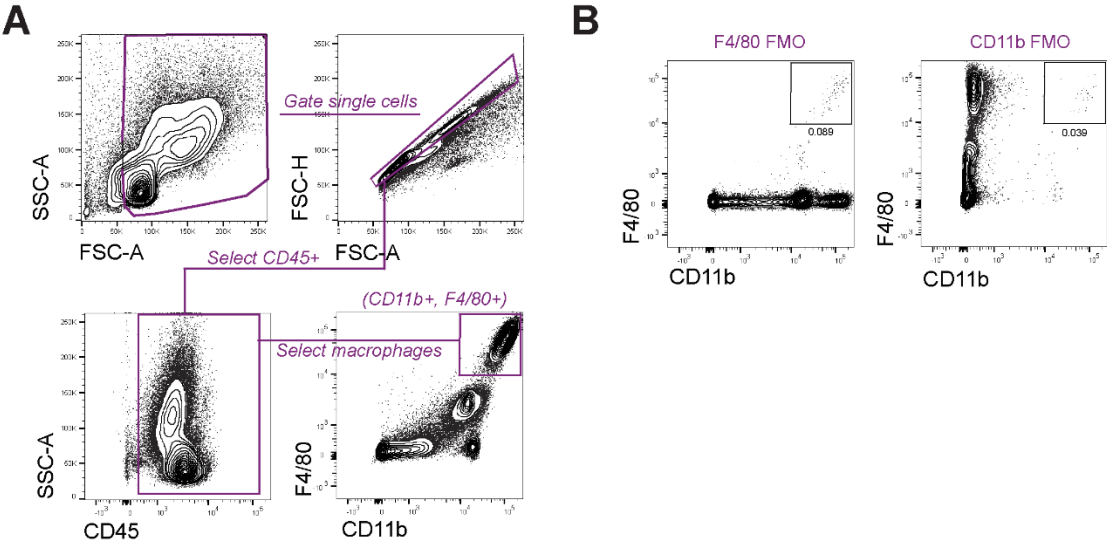


**Figure 18. Flow cytometry gating strategy for LPS-induced peritonitis model**

(A) Flow cytometry gating strategy used in Fig. 17F-H

(B) Fluorescence minus one (FMO) gating controls for flow cytometry analysis.

## TABLES: Chapter 2

**Table 1.** Clinical scoring guidelines

All clinical scores were determined by double-blind observation.

Scoring Parameter	0	1	2
Conjunctivitis	Normal	Single eye open with visible discharge	Eyes closed with discharge and swelling
Lethargy	Normal locomotion and reaction, >3 steps	Inactive, <3 steps after moderate stimulation	Only lifting of head after moderate stimulation, <1 step
Hair coat	Well groomed with smooth coat	Rough coat, minor ruffling	Unkempt fur, dull coat
Grimace pain scale	Normal	Moderate orbital tightening or nose bulge	Severe orbital tightening, nose bulge, and collapsed ear position

**Table 2.** Key Resources Table – Chapter 2

REAGENT	SOURCE	IDENTIFIER
<b>Inflammatory Ligands</b>		
LPS (LPS-EB Ultrapure; E. coli strain 0111:B4)	Invivogen	tlrl-3pelps
ATP	Invivogen	tlrl-atp
Flagellin from S. typhimurium	Invivogen	tlrl-epstfla-5
MSU Crystals	Invivogen	tlrl-msu
dsDNA [Poly(dA:dT)]	Invivogen	tlrl-patn
Anthrax LT	Gift of Dr. Molly Hughes (UVA)	n/a
Pam3CSK4	Invivogen	tlrl-pms
PolyI:C	Enzo	ALX-746-021
ODN 1826	Invivogen	tlrl-1826
<b>Antibodies for Western Blot</b>		
Rabbit polyclonal P-NF $\kappa$ B p65 (S276) (#3037)	Cell Signaling Technologies	3037
Rabbit monoclonal P-NF $\kappa$ B p65 (S536) (clone: 93H1)	Cell Signaling Technologies	3033
Rabbit monoclonal NF $\kappa$ B p65 (clone: C22B4)	Cell Signaling Technologies	4764
Rabbit monoclonal NF $\kappa$ B p65 XP (clone: D14E12)	Cell Signaling Technologies	8242
Mouse monoclonal $\beta$ -actin (clone: BA3R)	Thermo Fisher	MA515739
Rabbit monoclonal P-IRF3 (S396) (clone: 4D4G)	Cell Signaling Technologies	4947
Rabbit monoclonal IRF3 (clone: D83B9)	Cell Signaling Technologies	4302
Anti-mouse HRP secondary	JacksonImmuno	111035144 (Ms)
Anti-rabbit HRP secondary	JacksonImmuno	111035144 (Rb)
Mouse monoclonal I $\kappa$ B $\alpha$ (clone: L35A5)	Cell Signaling Technologies	4814
Rabbit monoclonal LSD1 (C69G12)	Cell Signaling Technologies	2184

Rabbit monoclonal GAPDH XP (clone: D16H11)	Cell Signaling Technologies	5174
<b>Antibodies for Flow Cytometry</b>		
Rabbit monoclonal P-IRF3 (S396) (clone: D6O1M)	Cell Signaling Technologies	29047
F4/80 (PE-Cy7) (clone: BM8)	eBioscience	25480182
CD11b (Alexa Fluor 488) (clone: M1/70)	eBioscience	53011282
TLR4/MD-2 (PE-Cy7) (clone: MTS510)	eBioscience	25992482
TLR4 (PE) (clone: SA15-21)	Biolegend	145404
CD14 (APC) (clone: Sa2-8)	eBioscience	17014181
CD45 (APC-eFluor 780) (clone: 30-F11)	eBioscience	47045182
TruStain FcX (anti-CD16/32)	Biolegend	101320
<b>Antibodies for Immunocytochemistry</b>		
NF $\kappa$ B p65 (clone: C22B4)	Cell Signaling Technologies	4764
Anti-rabbit Alexa Fluor 488 secondary	JacksonImmuno	711545152
<b>Chemical Reagents</b>		
Hoechst 33342	Invitrogen	H3570
DRAQ-5	Molecular Probes	62254
FTY720	Cayman Chemical	162359560
Ionomycin	Thermo Fisher	I24222
BAPTA-AM	Thermo Fisher	B6769
Fura-2-AM	Thermo Fisher	F1221
Fluo-4-AM	Thermo Fisher	F14201
Dynasore	ApexBio	A1605
EGTA-AM	Thermo Fisher	E1219
<b>ELISA Kits</b>		
Mouse IL-6 ELISA MAX Deluxe	Biolegend	431306
Mouse IL-1 $\beta$ ELISA MAX Deluxe	Biolegend	432606
Mouse TNF $\alpha$ ELISA MAX Deluxe	Biolegend	430906
<b>Gene Expression Analysis Kits</b>		
SensiMix SYBR NO-ROX Kit	Bioline	BIO-98020
ISOLATE II RNA Mini Kit	Bioline	BIO-52073
GoScript Reverse Transcriptase System	Promega	A5001

## METHODS

### Mice

Male and female mice between 6 and 12 weeks of age were used for all experiments. *Trpm7<sup>fl/fl</sup>* and *Trpm7<sup>fl/fl</sup> (Lck Cre)* mice were described previously<sup>111</sup>. To generate *Trpm7<sup>fl/fl</sup> (LysM Cre)* mice, *Trpm7<sup>fl/fl</sup>* mice were crossed with *Lyz2<sup>tm1(cre)lfo</sup>* (“LysM Cre”) mice<sup>176</sup> (Jackson Laboratories, Bar Harbor, ME) expressing Cre under the *Lyz2* gene promoter/enhancer elements, which selectively deletes *Trpm7*-exon 17 in myeloid cell-specific manner. Male C57BL/6J [#000664], *Tlr4*<sup>-/-</sup> [B6.B10ScN-*Tlr4*<sup>ps-del</sup>/JthJ; #007227], and *CD14*<sup>-/-</sup> [B6.129S4-*Cd14*<sup>tm1Frm</sup>/J; #003726] mice were purchased from Jackson Laboratories; all mice were 6 to 8 weeks of age. Mice were housed and bred in accordance with policies and procedures of the University of Virginia Institutional Animal Care and Use Committee (IACUC).

### Genotyping and Characterization of Mice

Tail samples were dissolved in 75 µl of digestion buffer (25 mM NaOH, 0.2 mM EDTA) for 30 min at 85°C, and digestion was stopped with 75 µl of 40 mM Tris-HCl. 1 µl of the reaction was used as a template for PCR using MyTaq Hot Start Polymerase and 5X MyTaq Red Reaction Buffer (Bioline; #BIO-21112 and #BIO-37112, respectively). PCR products were electrophoretically separated on a 1% agarose gel and visualized with ethidium bromide. Genotype was determined using the following primers:

Expression of Cre recombinase in *Trpm7<sup>fl/fl</sup> (LysM Cre)* mice. Primer sequences and method for analysis were as previously described<sup>176</sup>:

LysM Cre Primer: 5'-CCCAGAAATGCCAGATTACG-3'

Common Primer: 5'-CTTGGGCTGCCAGAATTTCTC-3'

Wild-type Primer: 5'-TTACAGTCGGCCAGGCTGAC-3'

Expression of Cre recombinase in *Trpm7<sup>fl/fl</sup>* (*Lck Cre*) mice

Forward Primer: 5'-GATTTTCGACCAGGTTTCGTTC-3'

Reverse Primer: 5'-GCTAACCAGCGTTTCGTTC-3'

The presence of absence of LoxP sites flanking *Trpm7* exon 17:

Forward Primer: 5'-CAGAGGTACTGGCAATTGTG-3'

Reverse Primer: 5'-ACGAGGACTCAGCATATAGC -3'

### **BMDM characterization via *Trpm7* Exon 17**

DNA was isolated from 5 x 10<sup>6</sup> BMDMs according to protocols for "Genotyping" described above.

PCR products were amplified via primers flanking *Trpm7* exon 17.

### **RNA Interference**

RAW 264.7 cells incubated as described in text with either anti-TRPM7 (siR-M7-776) or scrambled siRNA (Integrated DNA Technologies). siRNA were designed with the following sequences:

Sense: CAACUAAUUCUGUUCGUCUGAUGUU

Antisense: AACAUCAAGACGAACAGAAUUAGUUG

### **Cell Culture**

Primary murine BMDMs were isolated from bone marrow and differentiated in RPMI 1640 (Gibco) with 10% fetal bovine serum (FBS) and 20% L929-conditioned media and used between 7 and 10 days after isolation. RAW 264.7 cells (ATCC) were cultured in DMEM (Gibco) with 10% FBS. BMDMs and RAW 264.7 cells were gently scraped for detachment as needed. THP-1 cells

(ATCC) were cultured in RPMI 1640 supplemented with 0.05 mM 2-mercaptoethanol and 10% FBS. All cells were cultured at 37°C and 5% CO<sub>2</sub>.

### **Patch Clamp Electrophysiology**

TRPM7 currents ( $I_{TRPM7}$ ) were measured in whole cell configuration as illustrated (**Fig. 6C**). The standard external solution contained (in mM): 135 Na-methanesulfonate, 5 Cs-gluconate, 2.5 CaCl<sub>2</sub>, 10 HEPES, pH 7.3 (adjusted with NaOH), and osmolality 280-290 mOsm/Kg. The standard pipette solution contained (in mM): 110 Cs-gluconate, 0.5 NaCl, 0.75 CaCl<sub>2</sub>, 10 HEPES, 10 HEDTA, 1.8 Cs<sub>4</sub>-BAPTA, 2 Na<sub>2</sub>ATP, pH 7.3 (adjusted with CsOH), and osmolality 273 mOsm/Kg. Free [Ca<sup>2+</sup>] = ~100nM and was calculated via the Maxchelator algorithm (<http://maxchelator.stanford.edu/webmaxc/webmaxcS.htm>). Peritoneal macrophages were freshly-isolated prior to analysis by peritoneal lavage. MgCl<sub>2</sub> (10 mM) was added to the external solution to inhibit TRPM7 currents. The recording protocol used 400 ms ramps from -100 mV to +100 mV and a holding potential (HP) of 0 mV. Signals were low-pass filtered at 5 kHz and sampled at 10 kHz. All electrophysiology experiments were conducted at RT (~23°C) using an Axopatch 200B amplifier (Molecular Devices, Sunnyvale, CA).

### **Inflammasome Activation**

BMDMs were cultured at a density of 0.75 x 10<sup>6</sup> cells/mL in 6 or 24-well plates. Cells were washed with PBS prior to addition of culture media containing LPS (100 ng/mL) for 3 hrs. Media was removed and replaced with XVIVO 15 media (Lonza; #04744Q) containing LPS (100 ng/mL) and indicated concentrations of ligands. Cell media was collected, centrifuged at 13000g to remove dead cells and debris, and analyzed for IL-1β secretion via sandwich ELISA (Biolegend).

## Gene Expression Analysis

Cells were cultured on 24 well plates at a density of  $0.5 \times 10^6$ /ml in a culture volume of 500  $\mu$ L/well and stimulated as indicated. For pharmacological studies, BMDMs were pre-treated with the following compounds prior to addition of LPS: FTY720 for 15 min in culture media; Dynasore for 30 min in RPMI 1640; BAPTA-AM for 30 min in  $Ca^{2+}$ -free Hanks' buffered saline solution with 0.02% pluronic acid. Quantitative real-time PCR analysis of gene expression is described in below.

### Quantitative Real-time PCR

Total RNA was isolated using the ISOLATE II RNA Mini Kit (Bioline). RNA concentrations were measured using NanoDrop 2000c (Thermo Scientific) and normalized amongst the experimental sample set. cDNA was reverse transcribed using the GoScript Reverse Transcription System (Promega Corporation) according to the manufacturer's instructions. qPCR measurements were setup in triplicate using the SensiMix SYBR NO-ROX Kit (Bioline) and amplified in CFX connect Real-Time system (Bio-Rad, USA) according to the manufacturer's instructions. Data were analyzed using the CFX manager 3.1 software (Bio-Rad, USA) according to the  $\Delta\Delta C_t$  method<sup>177</sup>. B-2-microglobulin was used to normalize for cDNA input error.

Gene Name	Primer Sequence (forward) 5' – 3'	Primer Sequence (reverse) 5' – 3'
<i>Il1b</i>	GCAACTGTTTCCTGAACTCAACT	ATCTTTTGGGGTCCGTCAACT
<i>Nlrp3</i>	CTCTCCCGCATCTCCATTTGT	GCTTGGATGCTCCTTGACCA
<i>Il6</i>	TAGTCCTTCCTACCCCAATTTCC	TTGGTCCTTAGCCACTCCTTC
<i>Tnfa</i>	CCCTCACACTCAGATCATCTTCT	GCTACGACGTGGGCTACAG
<i>Nos2</i>	GTTCTCAGCCCAACAATACAAGA	GTGGACGGGTTCGATGTCAC
<i>Rsad2</i>	AACAGGCTGGTTTGGAGAAGA	AGCAAGAATGTCCAATACTCCC
<i>Trpm7</i>	AGCAGTATTCCAATGATTTTGGC	TCATAGCCATCGTTTCATCCTGT
<i>Rela</i>	AGGCTTCTGGGCCTTATGTG	TGCTTCTCTCGCCAGGAATAC
<i>Il18</i>	AAGAAAGCCGCCTCAAACCT	AGTGAAGTCGGCCAAAGTTGT
<i>Ccl4</i>	TCTGTGCAAACCTAACCCCG	GAGGGTCAGAGCCATTGGT
<i>B2m</i>	GGCCTGTATGCTATCCAGAA	GAAAGACCAGTCCTTGCTGA

## Receptor Endocytosis via Flow Cytometry

[Development of this method resulted in an additional publication from this work, which describes the approach in greater detail<sup>152</sup>. In brief,] BMDMs ( $0.5 \times 10^6$ ) were treated as indicated at 37°C. For experiments depicted in *Figure 14*, cells were pre-treated in HBSS and treated in Ca<sup>2+</sup>-free HBSS with 2% FBS and other reagents as indicated. Cells were washed with cold PBS and collected at 4°C in FACS Buffer (0.5% BSA, 2 mM EDTA in PBS). Cells were stained on ice with TruStain FcX (Biolegend) according to the manufacturer's recommendations for 10 min and then for 20 to 30 min using the appropriate antibodies. Stained cells were washed in cold FACS Buffer, resuspended in 200 µl of FACS Buffer, and placed on ice for immediate analysis. Cell surface staining was measured on the BD FACSCanto II flow cytometer.

The efficiency of surface receptor endocytosis was determined as previously described<sup>132</sup>. For measurement of CD14 and TLR4 endocytosis, cells were stained on ice with TruStain FcX (as recommended by the manufacturer) and then stained for 20 min on ice with fluorescently conjugated anti-TLR4 (0.2 µg/mL; clone: SA15-21) or anti-CD14 (0.4 µg/mL; clone: Sa2-8) antibodies in FACS buffer. Cells were washed in cold FACS buffer prior to analysis via flow cytometry. Mean fluorescence intensity (MFI) of CD14 and TLR4 was measured from unstimulated stained and unstained cells on the BD FACSCanto II. The percentage of surface receptor expression is the ratio of MFI from stimulated cells to unstimulated cells at indicated time points. Ratios are plotted to express receptor endocytosis over time. For measuring the formation of TLR4/MD-2 dimers, the percent of TLR4/MD-2 dimers were determined by calculating the fraction of 100% of the inverse of TLR4/MD-2 monomers, as measured by MFI values (via anti-TLR4 clone: MTS510 staining). TLR4/MD-2 monomers were determined by the ratio of MFI stimulated to unstimulated cells.

## **Protein Immunoblots**

Biochemical fractions were prepared with modification as described by Rockland, Inc. (<http://www.rockland-inc.com/NuclearExtract.aspx>). In brief, macrophages ( $5 \times 10^6$  cells) were treated as indicated and collected at 4°C. Cells were washed with 1 mL of cold PBS and resuspended in 6X pellet volumes (PV) of cytoplasmic buffer ([in mM] 10 HEPES, 60 KCl, 1 EDTA, and 0.075% NP40) for 5 min on ice. The suspension was centrifuged for 5 min at 1500 rpm at 4°C. Supernatant (cytoplasmic extract) was removed to a new tube. Pellet was washed in 12X PV in cytoplasmic buffer without NP40. Nuclei were collected by centrifugation and supernatants were discarded. The pellet was lysed in 1X PV with nuclear buffer ([in mM] 20 Tris-Cl, 420 NaCl, 1.5 MgCl<sub>2</sub>, 0.2 EDTA) for 10 min on ice. Both cytoplasmic extracts and nuclei mixture were centrifuged at maximum speed for 10 min to remove debris. Supernatants were collected for immunoblot analysis.

Whole cell lysates were prepared by collecting cells in Lysis Buffer (150 NaCl, 50 Tris-HCl pH 7.4, 2 EDTA, 0.5% TritonX-100) and lysis cells for 30 min on ice. Lysates were cleared of debris by centrifugation at 14000rpm for 10 min. Supernatants were collected, mixed with 5X Laemmli Sample Buffer (0.3M Tris-HCl pH 6.8, 10% SDS, 50% glycerol, 25% beta-mercaptoethanol, 0.05% bromophenol blue), and boiled at 95°C prior to SDS-PAGE analysis. Using cleared lysates, protein content was determined via BCA Assay (ThermoFisher; #23225) according to the manufacturer's instructions. Samples were loaded into 4-20% or 12% ExpressPlus PAGE gels (GenScript; #M42012 and #M01210, respectively) and electrophoretically separated according to the manufacturer's instructions (150 V for 60 min in MES Running Buffer).

## **Immunofluorescence Microscopy**

BMDMs were seeded on plates seeded with coverslips overnights. BMDMs were then treated as indicated at 37°C. Cells were washed in cold PBS and fixed in cold PFA (4% PFA in PBS) for 15

min at RT. Coverslips were washed 3 times with wash buffer (0.05% tween-20 in PBS) to removed residual PFA. Coverslips were permeabilized for 5 min in 0.1% Triton X-100 in PBS and blocked for 1h at RT in blocking buffer (1% BSA, 0.1% fish gelatin, 0.1% Triton-X-100, 0.05% Tween-20, and 5% donkey serum in PBS). Coverslips were stained with the anti-NFκB or anti-IRF3 antibody (1:250 dilution in blocking buffer) (Cell Signaling; #4764 and #4302), respectively) for 2h at RT. Cells were washed 3X with wash buffer and stained with anti-rabbit-Alexa Fluor 488 conjugated antibody (1 μg/mL) (JacksonImmuno) for 1h at RT. After washing 3X in wash buffer, coverslips were stained with Hoechst 33342 (1:2000) for 10 min at RT. Coverslips were washed 2X in wash buffer prior to mounting with VectaMount medium (Vector Laboratories, CA; #H5000). Mounted samples were cured overnight at RT and imaged within 24h. Images were collected using an Olympus FluoView 1000 under 40X or 60X objective lens. Images were analyzed with ImageJ software.

### **Nuclear Translocation via ImageStream**

Cells were treated as described at 37°C. Cells were then transferred to 4°C for 5 min, washed 2X with PBS, and collected by gentle scraping. Cells were fixed with cold paraformaldehyde (4%) for 15 min at RT. Cells were permeabilized with Perm Buffer (2 mM EDTA, 0.5% BSA, 0.1% triton X-100 in PBS) for 5 min and stained with primary antibody and anti-rabbit secondary antibody as recommended in Perm Buffer. Cells were resuspended in FACS Buffer (2 mM EDTA, 0.5% BSA in PBS) with DRAQ5 prior to analysis via ImageStream.

### **Ca<sup>2+</sup> Imaging**

Cells were allowed to adhere to #1 thickness coverslips overnight (~16h) prior to analysis. For ratiometric Ca<sup>2+</sup> imaging, cell were incubated for 30 min with agitation at RT with 5 μM of Fura-2-AM in presence of 0.02% of pluronic acid (BIOTIUM) and 500 μM probenecid (Enzo; ALX-430113G005) in Ringer solution ([in mM] 155 NaCl, 4.5 KCl, 2 CaCl<sub>2</sub>, 1 MgCl<sub>2</sub>, 5 HEPES, 10

glucose, pH 7.4). Fura-2-AM emissions were collected at 510 nm and with 340/380 nm excitation. Ratio of 340/380 was calculated by the  $\Delta F/F_0$  method<sup>178</sup>. For Fluo-4-AM imaging, cells were incubated for 2h at 37°C with 5  $\mu$ M of Fluo-4-AM in presence of 0.02% of pluronic acid and 2.5 mM probenecid in standard extracellular solution (SES; [in mM] 145 NaCl, 5 KCl, 2 CaCl<sub>2</sub>, 2 MgCl<sub>2</sub>, 10 HEPES, 10 glucose, pH 7.4). For Fluo-4 imaging, cells were excited at 488 nm and emissions were measured at 530 nm. In all cases, fluorescent excitation was performed using a DG4 Illuminator (Sutter Instruments, Canada) and fluorescence was detected using an ORCA-Flash 4.0 V2 CMOS camera (Hamamatsu) using SlideBook 6 software. Measurements were performed with continuous perfusion of bath solution with a gravity feed system and ionomycin (1  $\mu$ M) was perfused as a positive control for cellular responsiveness. Experiments were performed in Ringer solution or SES with addition of TLR ligands as indicated in figures and legends.

### ***In vivo* LPS Challenge**

*Trpm7<sup>fl/fl</sup>* and *Trpm7<sup>fl/fl</sup> (LysM Cre)* mice were injected intraperitoneally with 0.2 mg/kg LPS (200 $\mu$ l) or PBS. Mice were weighed less than 1 hr prior to injection to determine dosage. Mice were randomly assigned to treatment groups and all observations were performed by a double-blinded experimenter (blind to treatment and genotype). Mice were observed for up to 24h. Mice were euthanized at 4 hours to collect blood serum and peritoneal immune cells. Serum was collected after centrifugation of whole blood at 4°C for 10 min at 2500g. Serum concentrations of IL-6 and TNF $\alpha$  were measured via ELISA (Biolegend). IFN $\gamma$  was measured via Luminex analysis conducted by the UVA Flow Cytometry Core Facility.

Peritoneal cells were isolated by injection of 8 mL of cold PBS into the peritoneal cavity. The peritoneal lavage fluid was collected, and cells were centrifuged at 4°C for 6 min at 350g. The pellet was resuspended in ACK lysis buffer for 5 min to lyse red blood cells. Cells were collected and subjected to staining for flow cytometry. Cells were stained on ice with TruStain FcX

(Biolegend, #101320) for 10 min and then for 30 min with anti-F4/80 (clone: BM8), CD11b (clone: M1/70), and CD45 (clone: 30-F11) antibodies at the manufacturer recommended concentrations. Stained cells were washed with 1 mL of cold FACS Buffer, resuspended in 200  $\mu$ l of FACS Buffer, and placed on ice for immediate analysis. Cell surface staining was measured on the BD FACSCanto II. Gating strategy is described in **Fig. 18**.

## **Statistics**

All data were analyzed using Origin Pro 9.1.0 (Origin Lab) or Excel (Microsoft) software. Data are presented as means with error bars, which reflect standard deviation (SD) or standard error of the mean (SEM) as indicated in figure legends. Bar charts were plotted with Excel, dot plots and box charts were plotted using Origin Pro, and Violin plots were plotted in R studio (R package 'ggplot2'). Statistical box charts are shown as a box (range of 25-75 percentile) and whisker bars (1-99 percentile) with data points overlaid; the median is represented by a horizontal line and mean is shown as an empty square. Violin plots represent distribution of individual sample values and the diamond represents the mean value for the group. Normality and variance for data sets were tested graphically. The sample size is indicated in figures and legends. Statistical significance was determined using paired t-test (two-tailed), unless indicated otherwise in legend. A *p* value less than 0.05 was considered statistically significant.

# **CHAPTER 3: TRPM7-MEDIATED ELECTRICAL ACTIVITY AND CALCIUM SIGNALING REGULATE PHAGOSOME MATURATION DURING MACROPHAGE EFFEROCYTOSIS**

## **Disclaimer:**

The contents of this chapter (text and figures) appear as prepared for publication. At the time of writing, this work has been submitted for publication and is currently under consideration at *ELife* with the following co-authors and title: Schappe, MS, Downs, TK, Mendu SK, Flegal, Z., Stipes, EJ, Stremaska, ME, Seegren, PV, Desai, BN. "Efferocytosis requires periphagosomal Ca<sup>2+</sup> elevations and TRPM7-mediated electrical activity." All figures were prepared by MSS. All experiments were performed by MSS unless indicated otherwise in the figure legends.

## ABSTRACT

Efficient and non-inflammatory clearance of apoptotic cells, also known as efferocytosis, is a fundamental biological process of major significance to developmental biology, organ physiology, and immunology. Much progress has been made in understanding the mechanisms through which macrophages find and engulf apoptotic cells, but the signals that regulate the digestion of the apoptotic cell cargo are not well-understood. Here, we show that rapid and local  $\text{Ca}^{2+}$ -signals are required for phagosome maturation during efferocytosis. Using an siRNA screen, we identified TRPM7 as a  $\text{Ca}^{2+}$ -conducting ion channel that is essential for phagosome maturation. With *Trpm7*-targeted mouse lines, we demonstrate that in the absence of TRPM7, macrophages fail to fully acidify their phagosomes or digest the cargo. In *Trpm7*<sup>-/-</sup> macrophages, the local, peri-phagosomal  $\text{Ca}^{2+}$ -signals are abrogated, and there is a striking failure to form large phagolysosomes. Lastly, we provide evidence that TRPM7 can mediate a pH-activated cationic discharge necessary to sustain the activity of the phagosomal V-ATPase pumps. Overall, we reveal TRPM7 as a novel and crucial controller of phagosome maturation during efferocytosis.

**Graphical Abstract**

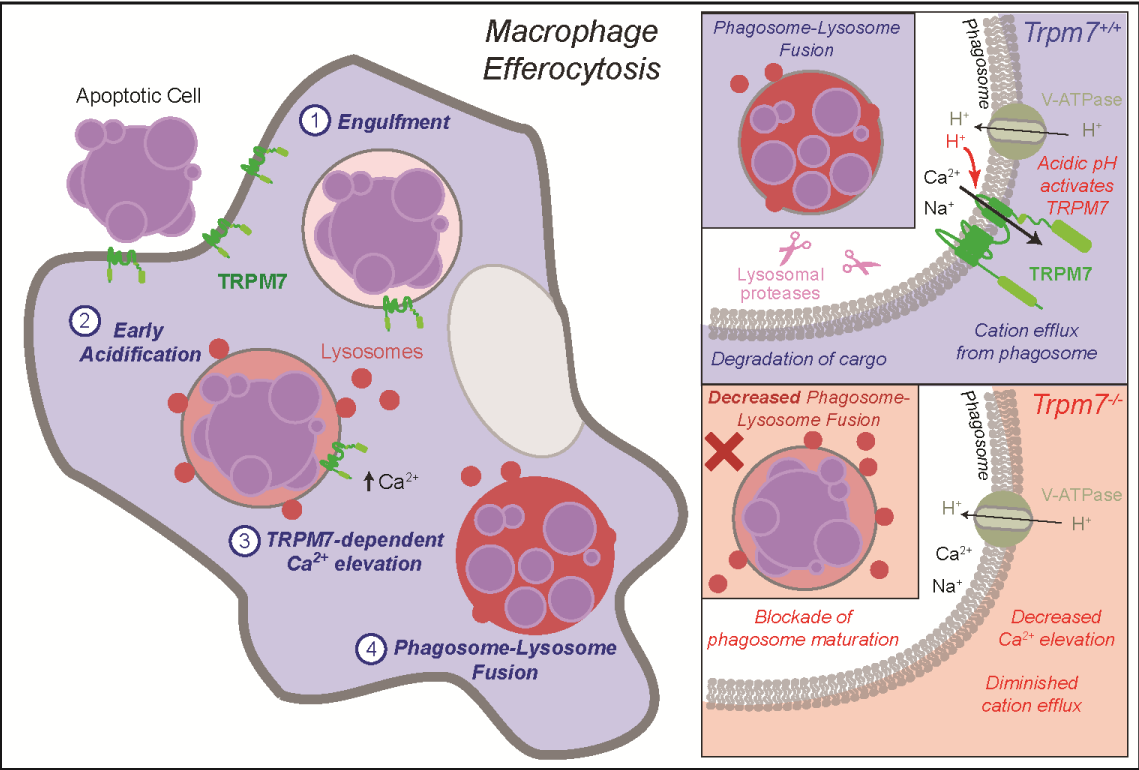


**Figure 19. Schematic of regulation of efferocytosis by TRPM7**

## INTRODUCTION

Efferocytosis encompasses the cellular processes through which apoptotic cells are recognized, engulfed and digested by other cells. The efficient removal of cellular corpses by the innate immune system shapes tissue development, organ homeostasis and wound repair<sup>179</sup>. Dysfunctional efferocytosis may therefore underlie the inflammatory pathology of chronic age-related diseases afflicting a wide variety of organ systems. In a healthy human body, billions of cells die every day<sup>180</sup>, and many of these are cleared by macrophages, the quintessential phagocytes resident in most tissues. For normal tissue homeostasis, the macrophages sense, recognize, and engulf apoptotic cells in an immunologically silent manner – this promotes regenerative processes without the inflammatory and self-destructive activation of the immune system<sup>12,181</sup>. Phagocytes employ a variety of cell surface receptors to recognize and engulf non-opsonized apoptotic cells. The mechanisms that control the early stages of engulfment, and the formation of a nascent phagosome, have been well-characterized<sup>182</sup>. However, the machinery and signals that regulate *phagosome maturation*, the intracellular process that leads to digestion of the engulfed apoptotic cell without inflammatory fallout, remain substantially more enigmatic<sup>183</sup>. Defining the cell biology of phagosome maturation, in terms of novel molecular components and signaling mechanisms, is therefore crucial for a clear understanding of tissue homeostasis, inflammation and wound repair.

The nascent phagosome is not intrinsically destructive and undergoes an extensive transformation during phagosome maturation<sup>184</sup>. Cytoskeletal rearrangements guide the sequential transition and subcellular location of a phagosome from an ‘early’ to ‘late’ stage, culminating with the fusion of phagosome with lysosomes<sup>185</sup>. During the early stages of maturation, and in preparation for fusion with lysosomes, the phagosomal membrane modifies its phospholipid composition<sup>182,186</sup> and through vesicular fusion, recruits a specialized proteome to become an increasingly acidic vacuolar compartment. The phagosome rapidly acquires the

vacuolar ATP-ase (V-ATPase) complex, which pumps protons into the phagosome via ATP hydrolysis and drives the initial phagosome acidification<sup>187</sup>. Notably, since injection of H<sup>+</sup> has a hyper-polarizing effect on the phagosome membrane, the efficiency of V-ATPase pump must be sustained by a countercurrent of cations (e.g. Na<sup>+</sup>, Ca<sup>2+</sup>) from the phagosome to the cytosol<sup>32</sup>. The ion channels that modulate this crucial electrical activity during phagosome maturation remain undefined. Ultimately, fusion of the phagosome with lysosomes forms an especially acidic organelle called phagolysosome, wherein, the acid-optimized lysosomal degradative enzymes complete the task of fully processing the engulfed cargo in a timely manner<sup>61</sup>. Interestingly, the uptake of non-opsonized apoptotic cells results in a significantly faster rate of phagosome maturation, when compared to Fc-receptor mediated engulfment of opsonized dead cells<sup>188</sup>. This observation supports the notion that mechanisms and kinetics of phagosome maturation may vary significantly between different types of phagocytosis, and these differences may have major implications on what constitutes non-inflammatory clearance of dead cells, versus a mechanism that activates an immune response to an antibody-labeled immunogenic cargo. Thus, the control and timing of phagosome maturation represents a crucial checkpoint at the crossroads of inflammation and tissue homeostasis. The components and signals that regulate phagosome maturation remain poorly defined, but there is considerable evidence indicating that Ca<sup>2+</sup>-signaling plays a significant role in membrane fusion events involved in phagosome maturation<sup>189,190</sup>.

The overall role of Ca<sup>2+</sup>-signaling in phagocytosis has been studied primarily in Fc-receptor mediated phagocytosis of opsonized cargo. Key molecular components of phagocytosis, including certain phospholipases (involved in membrane remodeling), gelsolins (necessary for cytoskeletal rearrangements) and synaptotagmins (crucial for membrane fusion), are activated by Ca<sup>2+</sup>-triggered mechanisms. Elevations in cytosolic Ca<sup>2+</sup> have long been observed to occur during phagocytosis<sup>191-194</sup>, but the underlying molecular machinery has not been defined. During Fc-

receptor mediated phagocytosis of opsonized targets, FcR-mediated activation of PLC $\gamma$  produces the potent second messenger IP3<sup>195</sup>. In turn, the activation of IP3-receptors, which are Ca<sup>2+</sup>-conducting ion channels on the endoplasmic reticulum (ER) membrane, releases the ER-stored Ca<sup>2+</sup>, and it is likely that subsequent store-operated Ca<sup>2+</sup>-entry (SOCE) through the Orai channels on the cell surface also contributes to the Ca<sup>2+</sup>-elevations seen during Fc-receptor mediated phagocytosis. Interestingly, the deletion of *Stim1* and *Stim2*, essential components of SOCE, fails to disrupt Fc-receptor mediated phagocytosis in macrophages<sup>57</sup>. Pertinently, deletion of STIM1 in dendritic cells impairs the fusion of phagosomes to lysosomes, but not the preceding phagosome acidification<sup>60</sup>. Thus, ER Ca<sup>2+</sup> plays an important role during FcR-mediated phagocytosis, but other sources of Ca<sup>2+</sup>, such as those from the phagosome itself<sup>196</sup> or the lysosome<sup>95</sup>, can also regulate phagosome maturation. In contrast to Fc-receptor mediated phagocytosis, it is not clear whether Ca<sup>2+</sup>-elevations occur during mammalian efferocytosis and whether Ca<sup>2+</sup>-signaling is required for efferocytosis. Genetic studies in *C. elegans*<sup>197,198</sup> and *D. melanogaster*<sup>199,200</sup> do suggest an important but undefined role for Ca<sup>2+</sup> signaling in efferocytosis. Even if efferocytosis is conjectured to require Ca<sup>2+</sup>-signaling, the specific ion channels, the molecular conduits that mediate these spatiotemporal Ca<sup>2+</sup>-signals have not been identified. Since ion channels are appealing molecular targets for pharmacological intervention, identification of ion channels that regulate efferocytosis in general and phagosome maturation in particular will advance this field toward clinical fruition.

In this study, we demonstrate that Ca<sup>2+</sup>-signaling is dispensable for the engulfment of non-opsonized apoptotic cells but is absolutely necessary for the subsequent phagosome maturation – as defined by phagosome acidification. Macrophages express a variety of Ca<sup>2+</sup> permeable channels that could potentially drive the Ca<sup>2+</sup>-signaling necessary for membrane-fusion events that facilitate acidification of the nascent phagosome and induce the formation of the phagolysosome. Using an siRNA screening approach, we identified the ion channel TRPM7 as a

vital component of phagosome acidification. TRPM7 is comprised of a  $\text{Ca}^{2+}$ -conducting channel (non-selective, also conducts  $\text{Na}^+$ ,  $\text{Zn}^{2+}$ , and  $\text{Mg}^{2+}$ ) and a serine-threonine kinase domain. Recently, we showed that TRPM7 also mediates  $\text{Ca}^{2+}$ -signaling triggered by CD14/TLR4 stimulation by LPS<sup>23</sup>. To define the function of TRPM7 in phagosome maturation, we used mouse lines that express genetically-encoded  $\text{Ca}^{2+}$  indicator GCaMP6s in myeloid cells and measured the  $\text{Ca}^{2+}$ -elevations associated with efferocytosis in *Trpm7*<sup>+/+</sup> and *Trpm7*<sup>-/-</sup> macrophages. We show that during efferocytosis,  $\text{Ca}^{2+}$ -elevations peak prior to phagosome acidification and are localized strikingly around the phagosome. Furthermore, TRPM7 is essential for phagosome-proximal elevations in  $\text{Ca}^{2+}$ , which promote phagosome acidification and maturation. We also show that TRPM7 is activated by low pH, and thus provides the cationic counter-current necessary for sustained acidification of the phagosome. The main thrust and significance of this study is that we have identified a novel TRPM7-mediated  $\text{Ca}^{2+}$ -signaling module necessary for phagosome maturation during apoptotic cell clearance.

## RESULTS

### Rapid, localized cytosolic Ca<sup>2+</sup> elevations are required for phagosome acidification during efferocytosis

To study phagocytosis of apoptotic cells, we stained apoptotic cells with dyes of varying sensitivity to pH<sup>201</sup> (**Fig 20A**). UV-induced apoptosis yielded a cellular “cargo” population that was largely “early apoptotic” (Annexin V+, 7AAD -) (**Fig. 21A and 21B**) and apoptotic cargo was co-stained with fluorescent dyes CellTrace Violet and CypHer5E. CypHer5E-stained cells display a linear, inversely proportional increase in fluorescence with pH (lowering pH increases CypHer5E fluorescence), while the CellTrace Violet fluorescence is stable across a broader range of pH, but quenched at extremely acidic pH (**Fig. 21C and 21D**). This orthogonal response to pH allows simultaneous measurement of cargo engulfment (CellTrace Violet) and acidification (CypHer5E) during phagocytosis. Using flow cytometry, we validated this method by verifying that Bafilomycin A1 (inhibitor of V-ATPase) prevented phagosome acidification without impairing the initial engulfment or binding by bone-marrow-derived macrophages (BMDMs) (**Fig 21E and 21F**). As an additional experimental control, we also pre-treated BMDMs with Cytochalasin D (inhibitor of actin polymerization) to prevent engulfment of apoptotic cells. Together, these reagents established a robust approach to quantify engulfment and phagosome maturation simultaneously.

We then tested the role of Ca<sup>2+</sup> signaling in macrophage efferocytosis. BMDMs were loaded with either BAPTA-AM or EGTA-AM prior to incubation with labeled apoptotic cells. This experimental design takes advantage of the fact that although BAPTA and EGTA have similar affinities of Ca<sup>2+</sup>, they exhibit very different kinetics of Ca<sup>2+</sup>-binding<sup>202</sup>. BAPTA, being a ‘fast’ Ca<sup>2+</sup> chelator, prevents cytosolic Ca<sup>2+</sup>-elevations so efficiently that even local Ca<sup>2+</sup>-elevations at the mouth of the Ca<sup>2+</sup>-conducting channel are prevented. In contrast, the slow chelation of Ca<sup>2+</sup> by EGTA prevents global Ca<sup>2+</sup>-elevations but allow local Ca<sup>2+</sup>-elevations or Ca<sup>2+</sup> ‘puffs’<sup>203</sup>. We found that BAPTA-AM-loaded BMDMs fail to acidify the phagosomes (90.3% decrease compared to

vehicle-treated BMDMs). Interestingly, EGTA-AM loaded macrophages show a relatively modest effect in acidification (only 48.5% decrease when compared to vehicle-treated BMDMs) (**Fig 20B and 20C**). In BMDMs that associated with cargo, neither chelator decreased engulfment (**Fig 21G**), and in fact, BAPTA-AM-loaded BMDMs appear to display increased association/engulfment of the cargo - likely because the BMDMs accumulate the labelled cargo when phagosome maturation is blocked completely. These observations indicate that 'fast' chelation of  $\text{Ca}^{2+}$  by BAPTA-AM, which chelates all cytosolic  $\text{Ca}^{2+}$  changes, completely inhibits phagosome acidification. In contrast, EGTA-AM, which cannot chelate rapid, localized  $\text{Ca}^{2+}$  'puffs' efficiently, has a relatively minor effect on phagosome acidification.

Although  $\text{Ca}^{2+}$ -elevations have been measured during Fc-receptor mediated phagocytosis, the spatiotemporal response of  $\text{Ca}^{2+}$ -elevations during efferocytosis (non-opsinized target) are not known. Macrophages pump out small molecule  $\text{Ca}^{2+}$  indicator dyes such as Fluo-4-AM or Fura-2-AM, and thus require the concomitant use of broad-spectrum pump blockers such as Probenecid. However, because of their nonspecific effects on pumps, ion channels, and transporters, such blockers of dye efflux are unsuitable for the study of phagosome maturation. Thus, to carry out these studies, we generated mice that express GCaMP6s in myeloid cells (*GCaMP6s<sup>CX3CR1 Cre</sup>*; herein, "WT GCaMP6s"). Using live-cell fluorescence microscopy, we monitored GCaMP6s-expressing BMDMs during phagocytosis of apoptotic cells (Supplemental Movie during oral presentation - data not shown). These BMDMs show clear cytosolic  $\text{Ca}^{2+}$  oscillations (~1 every 49s) upon 'sensing' of apoptotic cargo and during initial stages of engulfment (**Fig 20D**). However, as the cargo is steadily acidified, the macrophages display a concomitant and sustained rise in cytosolic  $\text{Ca}^{2+}$  that correlates with phagosome acidification (**Fig 20E and 20F**). Together, these results demonstrate that cytosolic  $\text{Ca}^{2+}$ -elevations occur during efferocytosis and local  $\text{Ca}^{2+}$ -signaling is necessary for phagosome

maturation. The dichotomy of BAPTA-AM and EGTA-AM results strongly suggest that  $\text{Ca}^{2+}$ -signals necessary for phagosome maturation are local and proximal to the phagosome.

### **Identification of novel $\text{Ca}^{2+}$ channel regulators of phagosome acidification**

Since Phospholipase C is activated during efferocytosis<sup>180,204</sup>, cytosolic  $\text{Ca}^{2+}$  elevations may involve SOCE through the Orai channels. However, recent studies have reported that macrophages deficient in *Stim1* and *Stim2*, crucial components of SOCE machinery, have no defects in phagocytosis<sup>57</sup> and furthermore, those experiments did not use apoptotic cell cargo. Using publicly available (Immunological Genome Project<sup>205</sup>) and in-house (data not shown) gene expression studies, we identified 14  $\text{Ca}^{2+}$ -conducting ion channels that are highly expressed in macrophages (**Fig 22A**) and devised siRNA-based knockdown protocols to effectively deplete (~80% reduction) the mRNA of each of these ion channels in primary BMDMs (**Fig 20G** and **Fig 22B**). We also tested an siRNA double-knockdown of *Stim1* and *Stim2*, which are required for SOCE. Then, using flow cytometry, we measured the acidification of engulfed apoptotic Jurkat cells after 90 min of phagocytosis by BMDMs depleted of each of these ion channels (**Fig 22C**).

We converted acidification (CypHer5E MFI) to z-scores relative to control scrambled siRNA (siScramble)-treated BMDMs. The z-scores for each siRNA-targeted gene sample was then plotted in relation to the average gene expression level across 4 macrophage subsets (ImmGen Project) (**Fig 20H**). Consistent with recent observations<sup>57</sup>, double-knockdown of *Stim1* and *Stim2*, did not substantially inhibit phagosome acidification. Through this analysis, we identified ion channels that regulate phagosome acidification positively and negatively, and multiple ion channels appear to be necessary for maturation (likely with overlapping functions). These are the subject of independent ongoing studies. However, when considering ion channel candidates in the top quartile for both gene expression and z-score, only *Trpm7* emerged as a candidate channel (in red **Fig 20H**), as knockdown of *Trpm7* results in a 53% decrease in acidification relative to siScramble-treated BMDMs (**Fig 20I**). As expected, Bafilomycin A1,

BAPTA-AM, and Cytochalasin D, inhibited cargo acidification (at least 60% decrease relative to vehicle-treated BMDMs) (**Fig 22D**). Interestingly, ionomycin, a  $\text{Ca}^{2+}$  ionophore, negatively influenced phagosome acidification, suggesting that a sustained, global influx of  $\text{Ca}^{2+}$  is likely detrimental to phagosome maturation. Thus, we identified TRPM7 as a major candidate to regulate phagosomal acidification in BMDMs.

### **TRPM7 regulates phagosomal acidification during macrophage efferocytosis**

To test the hypothesis that TRPM7 regulates phagosome acidification, we derived BMDMs from mice wherein *Trpm7* is deleted in myeloid cells [*Trpm7<sup>fl/fl</sup>* (*LysM Cre*)] – generated previously by us<sup>23</sup>. Here, these *Trpm7*-deficient BMDMs (“KO BMDMs”) are compared to BMDMs derived from *Trpm7<sup>fl/fl</sup>* mice (“WT BMDMs”). We used LysoTracker dye to fluorescently label the acidic compartments during efferocytosis – this dye labels acidic cellular compartments, including lysosomes, but is especially useful for the detection of the highly acidic and large phagolysosomes formed during efferocytosis. Labelled apoptotic cells were added to LysoTracker-stained BMDMs for 90 min and fixed prior to confocal microscopy. No gross differences in lysosomal numbers were observed between WT and KO BMDMs, prior to efferocytosis (**Fig 23A**). However, after 90 mins of efferocytosis, the KO BMDMs show a striking defect in the formation of large, highly acidic phagolysosomes when compared to WT BMDMs (**Fig 23A** and **23B**). We also used flow cytometry to measure engulfment and phagosome acidification in a large population of cells. Based on the analysis of CellTrace Violet and CypHer5E fluorescence, we see no significant differences in cargo uptake between WT and KO BMDMs over the course of 90 min of phagocytosis. However, *Trpm7*-deficient BMDMs had a significant decrease in acidification compared to WT BMDMs (**Fig 23C** and **23D**) and the defect was similar to Bafilomycin A1-treated cells. These results clearly indicate the TRPM7 regulates phagosome acidification during phagocytosis, but *Trpm7<sup>-/-</sup>* macrophages do not show a general defect in engulfment. Next, we

tested whether deletion of *Trpm7* from myeloid cells impairs the degradation of apoptotic cells *in vivo*.

### **Myeloid cells require TRPM7 for phagosome maturation of apoptotic cells in an *in vivo* model of efferocytosis.**

To measure the phagocytic and degradative capacity of myeloid cells in the peritoneal cavity, we utilized Jurkat cells that stably express GFP (“Jurkat-GFP”) and are labeled with CypHer5E. After UV-induced apoptosis, apoptotic Jurkat-GFP cells retain GFP fluorescence for 90+ min when cultured alone and show no spontaneous increase in CypHer5E fluorescence (**Fig. 25A**). As expected, when apoptotic Jurkat-GFP are engulfed by BMDMs *ex vivo*, their GFP fluorescence is diminished with time of engulfment and there is a concomitant rise in the acidification, as measured by CypHer5E MFI, demonstrating that loss of GFP fluorescence can be used as an indicator of cargo digestion by macrophages. Thus, by injecting co-stained Jurkat-GFP cells intraperitoneally, we used this method for an *in vivo* model of apoptotic cell clearance permitting simultaneous measurement of engulfment (CellTrace Violet), acidification (CypHer5E), and cargo degradation (GFP) (schematized in **Fig. 24A**).

We first characterized the proportion of peritoneal macrophages in TRPM7 WT and KO, as difference in this population could account for experimental variability. There were no significant differences in the proportion or number of CD11b+ peritoneal cells or macrophages (F4/80+, CD11c-) between *Trpm7<sup>fl/fl</sup>* and *Trpm7<sup>fl/fl</sup>LysM Cre* mice (**Fig 25B** and **25C**). Approximately 50% of peritoneal cells were myeloid cells and 95% of these cells were peritoneal macrophages. These results indicate that any differences in phagocytosis are due to qualitative differences between WT and *Trpm7<sup>-/-</sup>* myeloid cells – not differences in numbers of myeloid cells. Apoptotic Jurkat-GFP cells (4x10<sup>6</sup> total cells), labelled with CypHer5E and CellTrace Violet, were injected into the peritoneal cavity of mice and after 90 min, peritoneal cells were collected by lavage and analyzed by flow cytometry. The gating strategy used for flow cytometric analysis is

shown in **Fig 25D**. There were no differences in the percentage of cargo-associated phagocytes between *Trpm7<sup>fl/fl</sup>* and *Trpm7<sup>fl/fl</sup> LysM Cre* mice (**Fig 24B**). In the peritoneum of *Trpm7<sup>fl/fl</sup> LysM Cre* mice, the *Trpm7<sup>-/-</sup>* macrophages failed to acidify their phagosomes (low CypHer5E MFI) and degrade their cargo (high GFP MFI) (**Fig 24C**). This is especially striking when visualized as a ratio of acidification and degradation (**Fig 24D**). These results clearly demonstrate that TRPM7 is required for phagosome maturation and suggest that TRPM7 also regulates the phagolysosomal digestion of the apoptotic cell cargo during efferocytosis. Since GFP fluorescence is also sensitive to pH, these results do not allow us to conclude definitely that TRPM7 also regulates the formation of phagolysosome. To test that hypothesis, we used a direct assay of phagolysosomal proteolytic activity.

### **TRPM7 regulates the fusion of phagosome and lysosomes.**

The fusion of lysosomes with the phagosome is the penultimate stage of cargo degradation. Although acquisition of lysosomal markers on the phagosome may indicate close proximity of the organelles, direct measurement of phagolysosomal proteolytic activity is the optimal readout of the phagosome-lysosome fusion<sup>206</sup>. To test the hypothesis that TRPM7 regulates phagolysosome formation, we utilized an assay that measures the proteolytic activity of phagolysosome during phagocytosis. Fluorescent latex beads were conjugated to fluorescent DQ-Green BSA<sup>207</sup>. The fluorescence of this BODIPY dye conjugate is quenched when BSA is heavily labeled with the dye and resistant to physiological changes in pH. Upon hydrolysis of DQ Green-BSA by phagolysosomal proteases, the quenching is relieved producing green fluorescence. Thus, in contrast to GFP-Jurkats where the loss of fluorescence could also be accounted by sensitivity of GFP to pH, this assay reports proteolytic activity in the phagolysosome by gain of fluorescence signal (**Fig 26A**). WT and KO BMDMs were incubated with DQ-Green labelled beads, and the uptake (by intrinsic fluorescence) and fluorescence of DQ-green BSA were measured by flow cytometry at varying time points. As expected, Bafilomycin pre-treatment had a profound

decrease in phagolysosomal proteolytic activity (65% reduction relative to vehicle-treated WT BMDMs) (**Fig 26B**). No gross differences were observed between WT and KO BMDMs for cargo uptake (both >90% cargo+ by 30 minutes) nor gross amount of cargo engulfed (**Fig 26C**). However, phagolysosomal proteolysis, as shown by DQ-Green fluorescence, was decreased significantly in KO BMDMs at 30, 60, and 90 min (47, 33.5, and 24.3% decrease respectively, relative to WT) after incubation with the beads (**Fig 26D**). Although statistically significant, we do not consider the 3% average difference in cargo engulfment to be a salient defect because it likely arises as an effect secondary to primary defect in phagosome maturation. These results indicate that *Trpm7*-deficient BMDMs have decreased phago-lysosome fusion during phagocytosis. Collectively, these results clearly demonstrate that TRPM7 is required for phagosome maturation and provides evidence that TRPM7 regulates phagolysosome formation during efferocytosis.

### **TRPM7 associates with the nascent phagosome**

TRPM7 has been shown to be present on the macrophage plasma membrane<sup>23</sup>, but it has also been reported in the membrane of small intracellular vesicles in other cell types<sup>112,208</sup>. We tested whether TRPM7 is found in the membrane of the nascent phagosome, either by being internalized from the cell membrane or by recruitment of vesicles to the membrane. We transfected FLAG-TRPM7 into RAW 264.7 cells, a murine macrophage cell line and examined its subcellular location during efferocytosis using immunofluorescence-labeling and ImageStream flow-cytometry imaging. This method enables highly quantitative measurements of colocalization based on similarity scores of two labels (**Fig 27A**). Ectopic expression of GFP was used as a negative control, as it should be expressed throughout the cytosol and not specifically associate with the phagosome. As expected, CellTrace-labeled apoptotic cells engulfed by GFP-expressing RAW 264.7 cells displayed low colocalization with GFP (-0.15 mean similarity score) (**Fig 27B**). In contrast, FLAG-TRPM7 exhibited co-localization with the engulfed cargo after 60 min of phagocytosis (0.35 mean similarity score). Interestingly, neither treatment with Cytochalasin D

nor Bafilomycin A1 significantly altered cargo colocalization with TRPM7, suggesting that TRPM7 is localized near the contact site of the cargo itself. However, this approach does not definitively show that TRPM7 is present on the phagosome, and additional evidence using confocal microscopy or biochemical purifications of phagosomes would provide better evidence for whether TRPM7 may be localized to the phagosome. These results indicate that TRPM7 is not excluded from the nascent phagosome, likely through inclusion at the plasma membrane.

### **TRPM7 channel activity is essential for phagosome maturation**

The activity of TRPM7 incorporated in the phagosomal membrane may be regulated by changes in the membrane phospholipids<sup>123</sup> or the initial acidification of the phagosome. To test whether FTY720, a TRPM7 channel blocker<sup>147</sup>, could also inhibit phagosome maturation, BMDMs were pre-treated with FTY720 (5  $\mu$ M) 15 min prior to the addition of apoptotic cell cargo, and the inhibitor remained in the media for the duration of the assay (**Fig 26A**). There was a relatively modest decrease in engulfment at 30 min in FTY720-treated BMDMs compared to media alone, but no difference was observed at later time points (**Fig 27C and Fig 28B**). However, FTY720 decreased phagosomal acidification significantly, resulting in at least a 40% decrease in acidification across all time points (**Fig 27C**). Although the role of kinase activity of TRPM7 in phagosome maturation cannot be ruled out, the sensitivity of phagosome maturation to the TRPM7 channel blocker (FTY720) argues that the channel activity plays an important role in the regulation of phagosome maturation.

Activation of TRPM7 by PIP2 hydrolysis<sup>123</sup>, or another unknown mechanism, may be key to triggering TRPM7-mediated  $\text{Ca}^{2+}$ -influx. Additionally, after the initial acidification, a sustained monovalent cationic current through TRPM7 may play an important role in the maintenance of phagosomal pH. The pH-dependent activation of a monovalent  $I_{\text{TRPM7}}$  has been reported earlier<sup>209</sup> in 293T cells using whole-cell configuration (WCC). This electrophysiology configuration results

in a drastic dialysis of intracellular components and is highly disruptive to the cytoskeletal and intracellular structures that may be important for channel regulation. Indeed, regulation of TRPM7 is very difficult to study in WCC because  $I_{\text{TRPM7}}$  begins to “run up” toward maximal whole cell currents immediately after “break in” – a term used to describe the membrane rupture required for electrical access to the cell in WCC. Here, we tested whether macrophage-resident TRPM7 is activated by low pH in a perforated-patch configuration (PPC) – a technique which uses pore-forming compounds to induce small ion-permeable pores in the membrane patch acquired by the recording pipette-electrode. Thus, as illustrated in **Fig. 27D**, perforated-patch configuration permits *in situ* recordings of channel activity without extensive disruption of intracellular signalling<sup>123</sup>.

When BMDMs are recorded in PPC,  $I_{\text{TRPM7}}$  is robustly activated by low pH (pH = 4.0), eliciting a characteristic outwardly-rectifying  $I_{\text{TRPM7}}$  (**Fig. 27E**), which is readily blocked by a TRPM7 channel blocker (5  $\mu\text{M}$  FTY720). A switch to pH 4.0 yields a 2-fold and 8-fold increase in inward (at -100mV) and outward (+100mV) current densities, respectively.  $I_{\text{TRPM7}}$  was induced almost immediately (<2s) upon switch to pH 4.0. Next, we tested if TRPM7 can also be activated by pH 6.5 and pH 5.5. Using PPC we recorded  $I_{\text{TRPM7}}$  in WT and *Trpm7*<sup>-/-</sup> macrophages. These results clearly show that in WT cells, pH 5.5, but not pH 6.5, activates  $I_{\text{TRPM7}}$  (**Fig. 27F**). Unsurprisingly, but importantly, the veracity of the recorded  $I_{\text{TRPM7}}$  is evident by the fact that *Trpm7*<sup>-/-</sup> macrophages do not register any increase in current at pH 5.5 (**Fig. 27G**). These recordings indicate that in addition to  $\text{Ca}^{2+}$ -influx from the phagosomes, TRPM7 contributes robustly to a monovalent current from the phagosome during phagosome maturation. The implications of this observation are discussed later in this chapter.

## **TRPM7 mediates peri-phagosomal elevations in cytosolic Ca<sup>2+</sup> during efferocytosis.**

Given that TRPM7 mediates macrophage Ca<sup>2+</sup> signaling in response to immunomodulatory cues<sup>23</sup> and the evidence herein that TRPM7 regulates phagosome maturation, we tested the role of TRPM7 in Ca<sup>2+</sup> signaling during efferocytosis. We hypothesized that TRPM7 may mediate Ca<sup>2+</sup> elevations during macrophage phagocytosis, likely proximal to the phagosome. To investigate the role of TRPM7 in Ca<sup>2+</sup> signaling, we generated GCaMP6s-expressing mouse strains with (*Trpm7<sup>fl/fl</sup>GCaMP6s<sup>CX3CR1 Cre</sup>*; herein, “KO GCaMP6s”) and without deletion of *Trpm7* (*WT GCaMP6s*) (**Fig 29A**). To validate GCaMP6s function, we tested Ca<sup>2+</sup> responses in WT and KO GCaMP6s BMDMs to ATP, an important ‘find-me’ signal released by apoptotic cells<sup>210</sup>. At low concentrations used in this experiment, ATP signals through Gq-coupled P2Y receptors and mediates SOCE, without activating P2X7 ion channels present on macrophages – these require upwards of 0.5 mM ATP for activation. In the presence of 2 mM Ca<sup>2+</sup> outside, both WT and KO GCaMP6s BMDMs responded rapidly to ATP- $\gamma$ -S, a non-hydrolyzable analog of ATP, with a 5-fold increase in mean GCaMP6s fluorescence relative to baseline Ca<sup>2+</sup> levels (**Fig 29B**). ATP-triggered Ca<sup>2+</sup> elevations decayed slowly, likely due to SOCE, and maintained increased cytosolic Ca<sup>2+</sup> levels relative to baseline, until the addition of ionomycin to elicit the maximal Ca<sup>2+</sup> response. In 0 mM extracellular Ca<sup>2+</sup>, the release of intracellular stored Ca<sup>2+</sup> from the ER was comparable in amplitude to the SOCE seen in 2 mM Ca<sup>2+</sup>, but unsurprisingly, it was unable to sustain [Ca<sup>2+</sup>]<sub>i</sub> at levels appreciably higher than the baseline and decayed to baseline in 45 seconds. Addition of 2 mM extracellular Ca<sup>2+</sup> and ionomycin revealed maximal Ca<sup>2+</sup> elevations that were comparable to those in 2 mM extracellular Ca<sup>2+</sup>. Importantly, ATP-induced Ca<sup>2+</sup> elevations in both WT and KO GCaMP6s BMDMs were nearly identical. These results demonstrate the Ca<sup>2+</sup>-signaling in response to ATP, an important “find me” signal during efferocytosis is completely normal in *Trpm7<sup>-/-</sup>* macrophages.

Using WT and KO GCaMP6s BMDMs, we measured  $[Ca^{2+}]_i$  during phagocytosis using confocal microscopy. WT and KO GCaMP6s BMDMs were incubated with 4  $\mu$ m carboxylated beads and imaged via confocal microscopy. Both WT and KO GCaMP6s BMDMs readily associated with the beads, and by 10 min, had started to form nascent phagosomes (**Fig 29C**). In both WT and KO phagocytes, we observed modest elevations in cytosolic  $Ca^{2+}$  levels during phagocytosis. However, WT BMDMs displayed striking elevations in  $Ca^{2+}$ , proximal to the phagosome (**Fig 29D and 29E**). In contrast, KO BMDMs displayed spatially abnormal elevations in cytosolic  $Ca^{2+}$  which were distributed throughout the cell. We then measured  $[Ca^{2+}]_i$  during efferocytosis of fluorescently-labelled apoptotic cells. To evaluate subcellular changes in free cytosolic  $Ca^{2+}$ , GCaMP6s fluorescent intensity was measured in specific regions of interest (ROI) located in the cytoplasm and proximal to the phagocytic cargo (within 100 nm); baseline  $Ca^{2+}$  levels were measured in BMDMs that were not associated with cargo (**Fig 30A-C**). Efferocytosis initiated generalized  $[Ca^{2+}]_i$  elevations independently of TRPM7 (**Fig 29F**), but in WT GCaMP6s BMDMs, phagosome-proximal  $Ca^{2+}$  was significantly upregulated during phagocytosis, peaking at 2.6-fold above cytosolic  $Ca^{2+}$  levels between 30 and 40 minutes after the initiation of phagocytosis. These periphagosomal  $Ca^{2+}$  elevations were maintained for several minutes. In contrast, in KO GCaMP6s macrophages, the phagosome-proximal  $Ca^{2+}$  showed relatively minor elevations above cytosolic  $Ca^{2+}$  levels (average elevation of 1.1-fold increase relative to cytosolic  $Ca^{2+}$ ) (**Fig 30D**). These data indicate that TRPM7 mediates phagosome-proximal elevations in  $Ca^{2+}$  during phagocytosis in macrophages.

## DISCUSSION

This study advances our mechanistic understanding of efferocytosis by identifying TRPM7 as a crucial  $Ca^{2+}$ -conducting ion channel controlling phagosome maturation. We show that spatiotemporal regulation of  $Ca^{2+}$ -signaling is essential for subsequent phagosome maturation

and digestion of the engulfed cargo in the phagolysosomes. In this context, through an unbiased screen, we have identified a novel TRPM7-mediated  $\text{Ca}^{2+}$ -signaling pathway that controls phagosome maturation, but not engulfment. However, this screen design (high cargo load, prolonged engulfment period) may mask the effect of channels that could regulate engulfment, and not maturation. Absence of TRPM7 seriously compromises phagosome maturation and *Trpm7*<sup>-/-</sup> macrophages fail to digest the engulfed apoptotic cells normally. Historically, the study of intracellular  $\text{Ca}^{2+}$ -dynamics in phagocytosing macrophages has been challenging because myeloid cells are particularly efficient at pumping out small molecule  $\text{Ca}^{2+}$ -indicators and the use of broad spectrum pump-blockers such as Probenecid interferes with a variety of ion channels and transporters. We have circumvented that technical hurdle by generating mouse lines that express GCaMP6s in myeloid cells. We show that the TRPM7 channel mediates  $\text{Ca}^{2+}$  elevations proximal to the phagosome during phagocytosis, and we propose that these elevations control  $\text{Ca}^{2+}$ -dependent membrane fusion events, such as recruitment of vesicles and phago-lysosome fusion.

In addition to  $\text{Ca}^{2+}$ -signaling, TRPM7-mediated monovalent discharge from the phagosome to the cytosol may be a biophysically significant process for the generation and maintenance of low phagosomal pH. This is concordant with the fact that counterion conductance of cations is necessary to sustain the  $\text{H}^+$  pumping activity of the V-ATPase complex<sup>33</sup>. As the nascent phagosome forms, it is rapidly acidified by the activity of Hv1 and V-ATPase complex, which facilitate movement of  $\text{H}^+$  into the lumen of the nascent phagosome. The electrogenic activity of these complexes, along with build-up of  $\text{H}^+$ , generates a significant membrane potential across the phagosomal membrane, which is deleterious to V-ATPase function (and thereby, phagosome maturation)<sup>32</sup>. To mitigate this, cation efflux (and perhaps,  $\text{Cl}^-$  influx) is required to sustain continued phagosomal acidification<sup>33</sup>. However, the identity of the channel(s) that mediate this cation efflux necessary to sustain phagosome maturation is unknown. Using perforated patch

electrophysiology configuration, which retains the structural integrity of the intracellular protein complexes, we show that TRPM7 channel activity is highly sensitive to pH and propose that the TRPM7 incorporated into the nascent phagosome may exhibit sustained activity after initial acidification is successful. Thus, TRPM7 is well-positioned to serve as the major channel to facilitate the countercation current that is essential to phagosome maturation.

Our study has focused exclusively on the role of TRPM7 during efferocytosis, and future studies will investigate whether TRPM7 is also a crucial component of phagosome maturation in other forms of apoptosis – especially, FcR mediated phagocytosis of antibody-opsonized cargo. The siRNA screen revealed additional ion channels that regulate phagosome maturation during efferocytosis, and independent studies are ongoing to test their role in phagosome maturation. Much of the previous work on phagocytosis-associated  $\text{Ca}^{2+}$ -signaling has been carried out in the context of FcR-mediated phagocytosis, which triggers a robust SOCE response. Similarly, ATP-mediated activation of P2Y receptors is a potent “find me” signal for apoptotic cells<sup>210,211</sup>. Our expectation was that SOCE, likely initiated by Gq-coupled P2Y receptors in response to purinergic signals would play a major role in engulfment or phagosome maturation during efferocytosis. Surprisingly, the disruption of SOCE apparatus through the simultaneous depletion of *Stim1* and *Stim2* fails to have a major negative impact on phagosome acidification, and efferocytosis appears to proceed normally. It should be noted that the deletion of *Stim1* and *Stim2* does not prevent the release of ER-stored  $\text{Ca}^{2+}$ , so our observations do not challenge the importance of  $\text{Ca}^{2+}$ -release from the ER during phagocytosis<sup>212,213</sup>. Indeed, even in *Trpm7*<sup>-/-</sup> macrophages, we see substantial  $\text{Ca}^{2+}$  elevations in the cytosol during efferocytosis, and we speculate that these are largely mediated by the release of stored  $\text{Ca}^{2+}$ . The deletion of *Trpm7* does not affect the ATP-triggered release of ER-stored  $\text{Ca}^{2+}$  or the subsequent SOCE. Therefore, it is possible that TRPM7-mediated peri-phagosomal  $\text{Ca}^{2+}$ -signaling and ER-mediated global  $\text{Ca}^{2+}$ -signaling cooperate to orchestrate the  $\text{Ca}^{2+}$ -signaling processes during phagocytosis. An interesting

implication of this is that different kinds of phagocytosis may show varying degrees of reliance on different modes of  $\text{Ca}^{2+}$ -signals – with efferocytosis more reliant on TRPM7 and FcR-mediated phagocytosis of opsonized targets more reliant on SOCE.

TRPM7 resides in the macrophage cell membrane where it conducts monovalent and divalent cations, including  $\text{Ca}^{2+}$  and  $\text{Zn}^{2+}$ . It is also present in small intracellular vesicles enriched in  $\text{Zn}^{2+}$ <sup>112</sup>. This argues for selective activation of the phagosomal TRPM7 to control local periphagosomal  $\text{Ca}^{2+}$ . Indeed, *Trpm7*-deficient macrophages fail to elevate periphagosomal  $\text{Ca}^{2+}$  suggesting that TRPM7 discharges  $\text{Ca}^{2+}$  from the phagosome into the cytosol. The related observation that TRPM7 colocalizes with the phagosome during efferocytosis supports this model. The incorporation of TRPM7 into the phagosome is most likely to occur by inclusion of TRPM7 in the internalized plasma membrane, but we cannot rule out additional or alternative recruitment of vesicular TRPM7 by fusion to the nascent phagosome. Likewise, a model where TRPM7 is part of the recycling endosome trafficking system is also possible (similar to TRPML1<sup>95</sup>). In this model, vesicular or plasma membrane-localized TRPM7 is incorporated into the nascent phagosome, promotes early stages of maturation and acidification, then is removed and recycled to the plasma membrane during focal exocytosis to promote continued phagocytosis.

Phagosomal  $\text{Ca}^{2+}$  efflux has been reported previously in neutrophils<sup>196</sup> and postulated by others<sup>190</sup>. Precise measurements of phagosomal  $\text{Ca}^{2+}$  concentrations face major technical hurdles because of the relative sensitivity of  $\text{Ca}^{2+}$ -indicators to pH. We speculate that in addition to the extracellular  $\text{Ca}^{2+}$  internalized during phagocytosis, at least during efferocytosis, the  $\text{Ca}^{2+}$ -stores of the engulfed apoptotic cells will contribute significantly to the phagosomal  $\text{Ca}^{2+}$  concentration. In the later stages of phagosome maturation, the presence of certain lysosomal channels, such as TRPML1 in the lysosomes<sup>95</sup>, may also promote the  $\text{Ca}^{2+}$  signaling essential for the final fusion of the lysosomes to the phagosome.

Rapid changes in the phospholipid content of the nascent phagosome are likely to activate TRPM7. Elegant studies of FcR-mediated apoptosis have revealed that the activation of PLC $\gamma$  at the phagosome rapidly depletes 4,5-PIP<sub>2</sub> in the phagosomal membrane. The hydrolysis of PIP<sub>2</sub> activates TRPM7<sup>123</sup>, and in our model, the resulting Ca<sup>2+</sup>-flux from the phagosome to the cytosol promotes maturation. Other undefined mechanisms in the nascent phagosome may also activate TRPM7-mediated Ca<sup>2+</sup>-signaling and promote maturation. Initial acidification of the phagosome to pH ~5.5, which can occur minutes after engulfment<sup>214</sup>, would then sustain TRPM7 activity, resulting in a large monovalent discharge from the phagosome to counter the V-ATPase-mediated injection of H<sup>+</sup> into the phagosome. Thus, pH-dependent activation of TRPM7 mediates a cationic countercurrent necessary for maintaining the proton-pumping activity of the V-ATPase in the maturing phagosome. The unavailability of highly selective Na<sup>+</sup> dyes prevents the subcellular visualization of this cationic countercurrent during phagosome maturation.

This study focused on the role of TRPM7 channel, but whether TRPM7 kinase contributes meaningfully to phagosome maturation remains unknown. TRPM7 kinase may regulate actomyosin by phosphorylating the Myosin II Heavy Chain (MIIHC) and it can also phosphorylate Annexin A1, a modulator of membrane curvature. The TRPM7 kinase may also regulate the recruitment of other proteins associated with degradation of apoptotic cell cargo<sup>215</sup>. The proteolytic cleavage of TRPM7 is known to activate the channel and liberate a fully functional kinase domain that is untethered to membrane-resident channel<sup>113,118</sup>. It is not known whether such cleavage occurs during efferocytosis.

In addition to the outstanding cell biological questions outlined above, an important goal of our future studies is to define the implications of abnormal phagosome maturation in the context of innate immunity, tissue homeostasis and wound repair. A hallmark of efferocytosis is that the clearance of apoptotic cells and debris occurs in a non-inflammatory manner. However, in the absence of TRPM7, the cell autonomous response to the abnormal digestion of the apoptotic cell

cargo could be very different – these studies are likely to reveal profound insights that are of significance to many age-related diseases where the control of inflammation and tissue regeneration is of salience.

## FIGURES: Chapter 3

**Figure 20. Ca<sup>2+</sup> signaling requirements of phagosome acidification and identification of the ion channel TRPM7 as a regulator of phagosome acidification.**

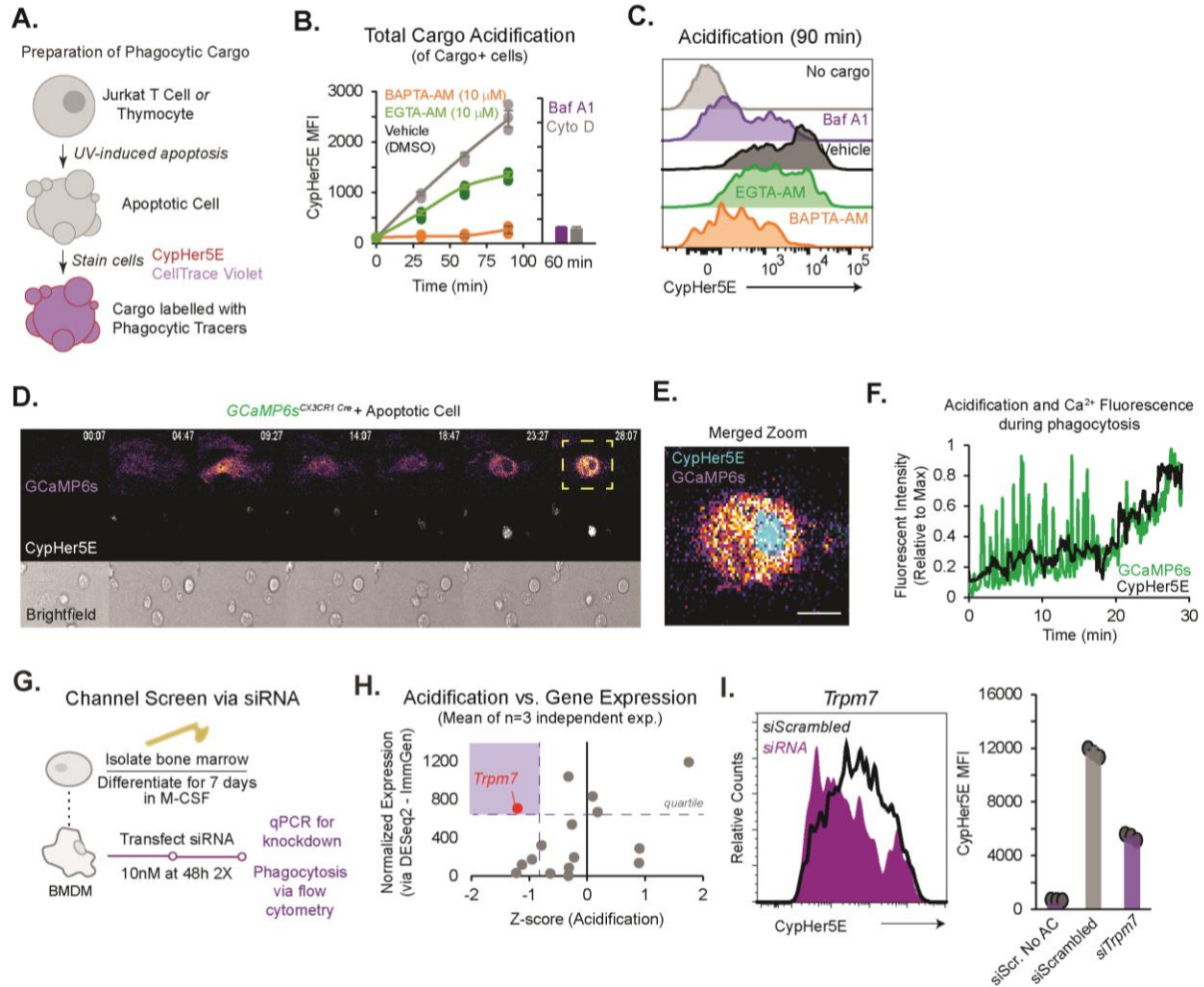


**Figure 20. Ca<sup>2+</sup> signaling requirements of phagosome acidification and identification of the ion channel TRPM7 as a regulator of phagosome acidification.**

(A) Preparation of apoptotic cell cargo is schematized. UV-irradiated apoptotic cells are stained with pH-insensitive (CellTrace Violet) and pH-sensitive (CypHer5E) dyes to measure cargo association and acidification, respectively. Apoptotic cells are then offered to macrophages by centrifugation, and unengulfed cells are removed by trypsinization and washes in Ca<sup>2+</sup>-free saline.

(B) Flow cytometry based measurement of acidification of phagosomes after engulfment of apoptotic cell cargo by BMDMs loaded with vehicle (DMSO), BAPTA-AM or EGTA-AM (both 10 μM, 30 min). Engulfing CD11b+ BMDMs containing labelled cargo (CellTrace Violet) were gated and analyzed for acidification (CypHer5E fluorescence). Bafilomycin A1 (BafA1; 500 nM) and Cytochalasin D (Cyto D; 1 μM) treated cells were used as negative controls. Data points indicate independent samples; bar charts represent mean value (Error bars = SD).  $p < 0.001$  for all statistical comparisons.

(C) Representative histograms showing phagosome acidification after 90 min of phagocytosis. Data are representative of triplicate samples described in Fig 2B.

(D) [Ca<sup>2+</sup>]<sub>i</sub> dynamics in GCaMP6s-expressing BMDMs during phagocytosis of apoptotic Jurkat cells. GCaMP6s (top image; Fire LUT), CypHer5E fluorescence (middle; grey), and brightfield (bottom image; grey) were acquired using wide-field microscopy (1 frame/7 s). Region of interest (ROI) shown in yellow box is magnified in *Panel E*.

(E) ROI outlined in *Panel D* is shown as a merged image of GCaMP6s (Fire LUT) and CypHer5E (Cyan) fluorescence, 28 min after the addition of apoptotic cells to BMDMs. Scale bar is 10 μm.

(F) Quantification GCaMP6s (green trace) and CypHer5E (black trace) fluorescence intensity over time. Measurements are from data depicted in *Panel D* over time.

(G) Schematic showing the siRNA knockdown of candidate calcium channels in BMDMs.

(H) Scatter plot showing the relationship between macrophage gene expression and relative effect on phagosomal acidification, depicted as mean Z-scores (n=3) from siRNA channel screen; target genes are depicted by single point; derivation of Z-scores is described in *Methods*. Gene expression value is average expression level across 4 macrophage subsets (ImmGen). Grey box denotes quartile for highest gene expression and the most negative effect on the z-score of acidification.

(I) *Left panel* shows overlaid histograms of acidification (CypHer5E fluorescence) in the *Trpm7* knockdown (*siTrpm7*, purple) and control (*siScrambled*, black) cells. *Right panel* shows Mean CypHer5E mean fluorescent intensity (MFI) of CypHer5E. The bar graphs depict mean values and error bars reflect SD (n=3).

**Figure 21. Validation of flow cytometry-based assay for phagocytosis.**

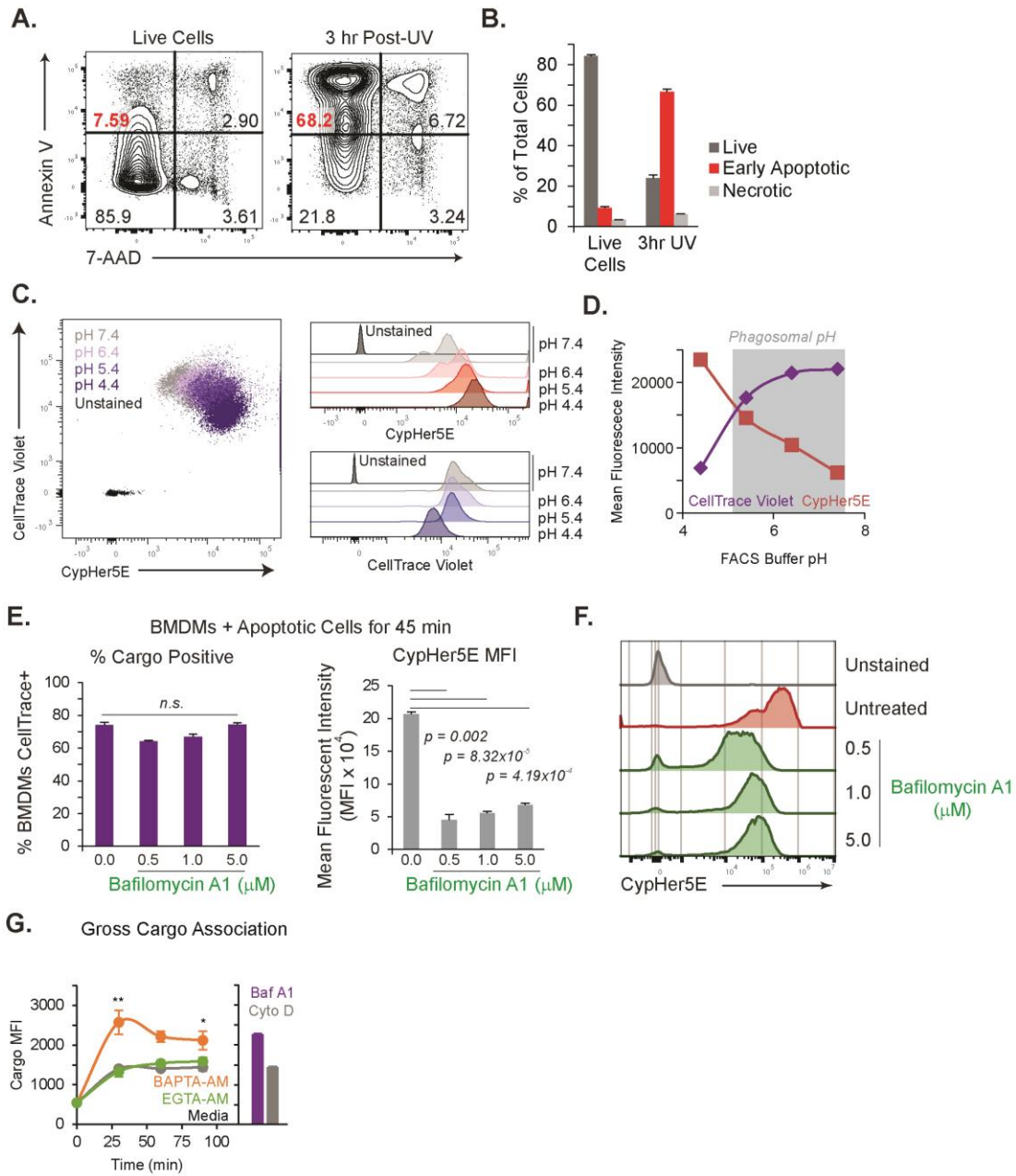


**Figure 21. Validation of flow cytometry-based assay for phagocytosis.**

(A) Live-dead staining of Jurkat cells after UV-induced apoptosis using flow cytometry. Pulse of UV-irradiation generated an increase in “early apoptotic cells” (Annexin V+, 7AAD-) 3 hr post-UV and the total cell population was used as apoptotic cell cargo in phagocytosis assays. Experiment by ZF.

(B) Mean percentage of cells gated as early apoptotic (Annexin V+, 7AAD-), live (Annexin V-, 7AAD-) or necrotic (Annexin V+, 7AAD+). Error bars represent SEM (n=3). Experiment by ZF.

(C) Flow cytometry based measurement of dye fluorescence in response to varying pH. *Left:* Overlaid cytographs of CypHer5E and CellTrace Violet-labelled apoptotic cells resuspended in buffers of indicated pH. *Right:* Histograms of CypHer5E (top) and CellTrace Violet (bottom) MFI in response to varying pH buffers.

(D) Relative mean fluorescence intensities (MFI) of CellTrace Violet and CypHer5E from analysis shown in *Panel C*. The gray shaded region denotes the pH range (5.0 - 7.5) most relevant to phagosome maturation.

(E) Phagocytosis of apoptotic cells in response to an inhibitor of phagosome acidification. Bafilomycin A1 was added as indicated for 15 min prior to addition of AC cargo. *Left:* Engulfing BMDMs measured by CellTrace+ cells. *Right:* Acidification in engulfing BMDMs with or without Bafilomycin A1 pre-treatment.

(F) Representative histograms of CypHer5E MFI of engulfing BMDMs shown in *Panel E*.

(G) Flow cytometry based measurement of gross association with apoptotic cell cargo (Thymocytes) by BMDMs (T:B, 5:1) over time. Engulfing CD11b+ BMDMs containing labelled cargo (CellTrace Violet) were gated and analyzed for mean fluorescence intensity (MFI) of the cargo label. Prior to collection, BMDMs were washed 3X in PBS and detached with 0.05% trypsin to remove unengulfed cargo from on the cell surface.

**Figure 22. Experimental controls and validation of siRNA channel screen.**

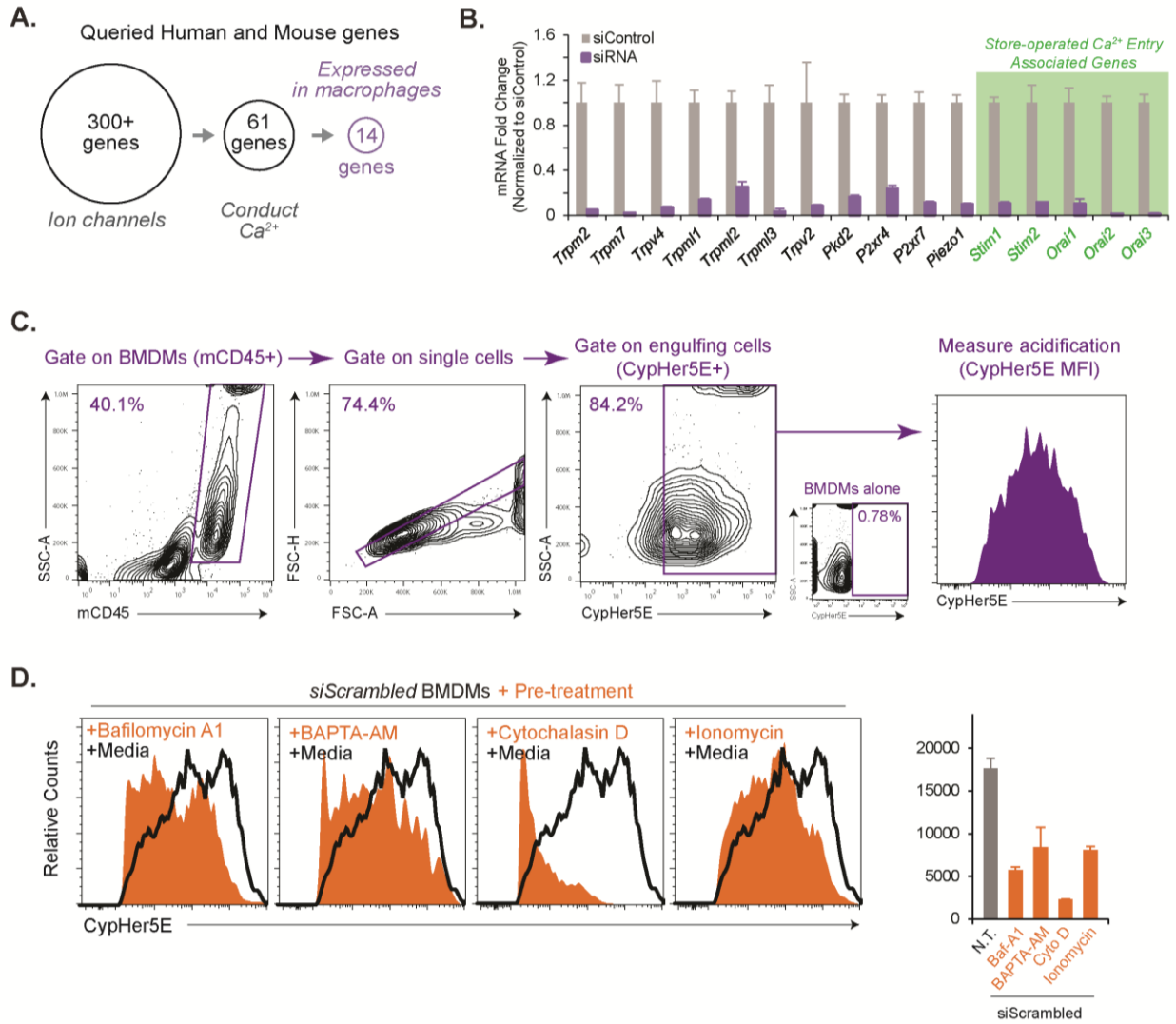


**Figure 22. Experimental controls and validation of siRNA channel screen.**

(A) Schematic of candidate  $\text{Ca}^{2+}$  channel genes. Relative gene expression levels used for candidate selection were determined by data available in the ImmGen RNAseq Database.

(B) Gene expression analysis (qPCR) of candidate genes. Knockdown was assessed by measuring expression relative to control (siScramble-treated) BMDMs. The method is schematized in Figure 20A and detailed in Methods. Experiment by TKD.

(C) Flow cytometry gating strategy used in Figure 20H and 20I.

(D) Representative data of control samples from siRNA channel screen. *Left:* Histograms of samples pre-treated with indicated controls (orange) compared to culture media alone. *Right:* Mean CypHer5E MFI values with error bars reflecting SD ( $n=3$ ). BMDMs were pre-treated for 15 min with media alone, Bafilomycin A1 (50 nM), Cytochalasin D (100 nM), or BAPTA-AM (10  $\mu\text{M}$ ); ionomycin (1  $\mu\text{M}$ ) was added simultaneously with AC cargo.

**Figure 23. TRPM7 is required for acidification of apoptotic cells during efferocytosis**

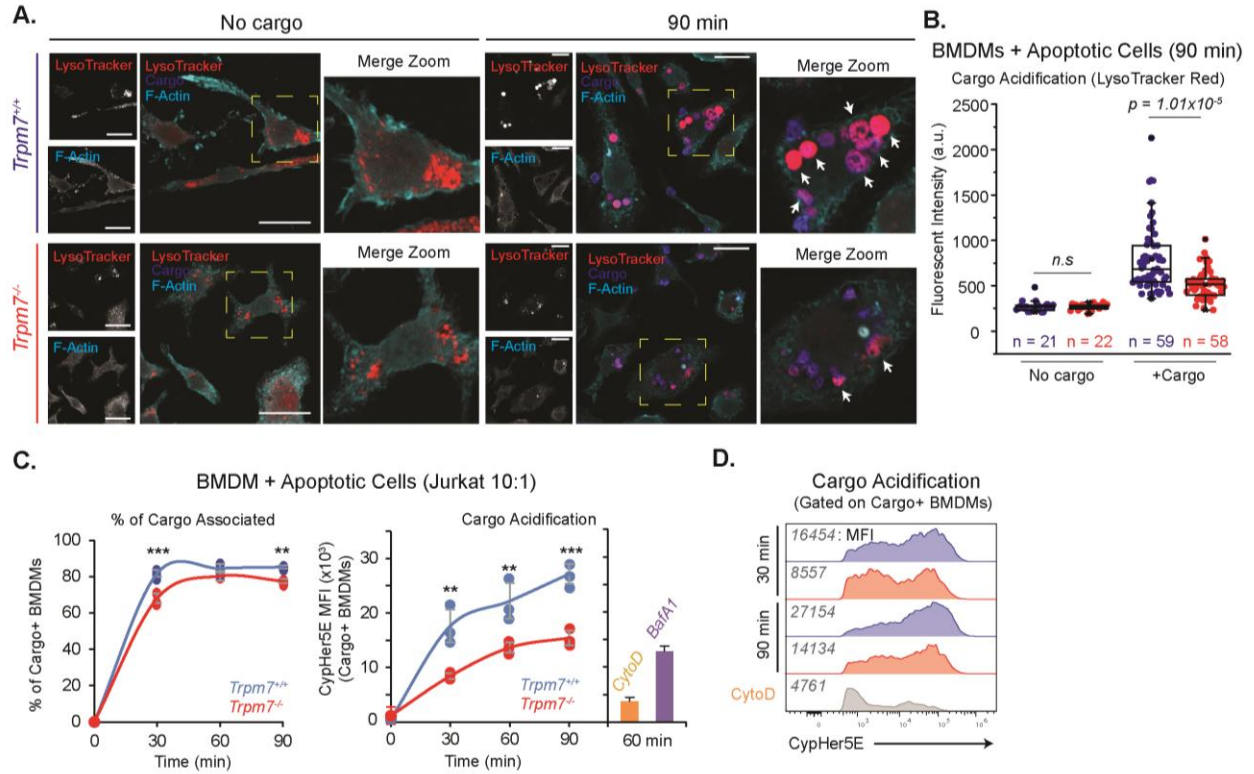


**Figure 23. TRPM7 is required for acidification of apoptotic cells during efferocytosis**

(A) Confocal immunofluorescence microscopy of BMDMs with or without addition of apoptotic cells as cargo for phagocytosis. Apoptotic cells were labelled with CellTrace Violet (Cargo-blue) and live BMDMs were stained with LysoTracker (red) prior to PFA-fixation and then phalloidin stained (cyan) after fixation. Single-channel images of LysoTracker and F-actin (phalloidin) are shown with merged pseudocolored image. Yellow dotted box indicates zoomed ROI of adjacent image and arrows indicate phagolysosomes. Single optical sections (0.45  $\mu\text{m}$ ) are shown. Scale bar = 20  $\mu\text{m}$ . Representative images are from 3 independent experiments.

(B) Quantification of LysoTracker fluorescent intensity, as shown in *Panel A*. Data points represent intensity measurement for single phagocyte; n values for each condition are included in the figure. The parameters included in the box charts are described in the methods.

(C) Flow cytometry-based measurement of phagocytosis of apoptotic Jurkat cell cargo by BMDMs (J:B = 10:1) over time. Cargo were stained with CellTrace Violet and CypHer5E prior to adding to BMDMs at level indicated in figure. Engulfing BMDMs were gated for anti-mCD45 antibody staining prior to the measurement of CellTrace Violet and CypHer5E staining. Control samples with Cytochalasin D (1  $\mu\text{M}$ ) and Bafilomycin A1 (500 nM) were pre-treated 15 min prior to the addition of AC cargo. Data points represent n=3 independent samples, and the data are representative of 3 independent experiments.

(D) Representative histograms of data in *Panel C*. Mean fluorescent intensity values are as indicated on figure panel. Representative of n=3 independent samples.

**Figure 24. Degradation of apoptotic cell cargo by peritoneal macrophages requires TRPM7**

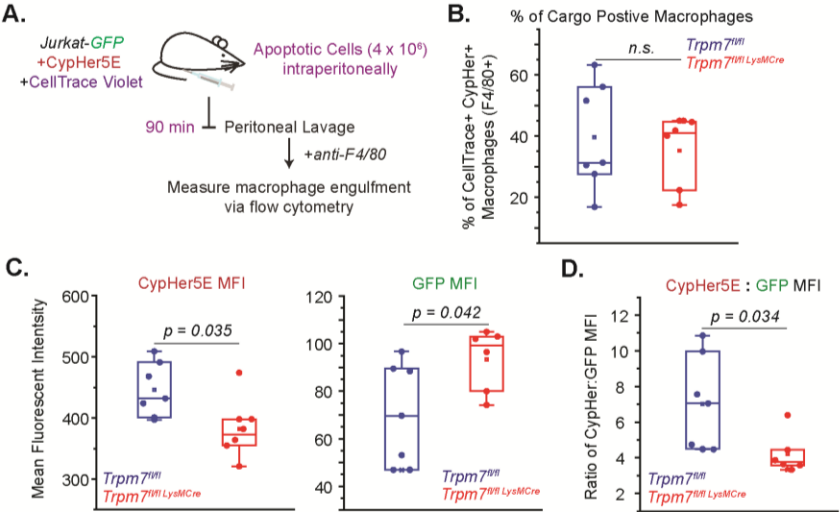


**Figure 24. Degradation of apoptotic cell cargo by peritoneal macrophages requires TRPM7**

(A) The experimental design to measure apoptotic cell clearance *in vivo* is schematized. Experiments supported by MES.

(B) Quantification of engulfing peritoneal macrophages (F4/80+) in *Trpm7<sup>fl/fl</sup>* (n=8) and *Trpm7<sup>fl/fl</sup> LysM Cre* (n=7) mice during clearance of apoptotic Jurkat-GFP cells. Dots represent individual mice and box charts demonstrate sample distribution. The box charts are described in the methods.

(C) MFI of CypHer5E, which measures cargo acidification (left) and GFP, which is stably-expressed in Jurkat-GFP cells (right). See also Figure 25 for gating strategy.

(D) Quantification of cargo degradation by WT and KO peritoneal macrophages as depicted by the ratio of CypHer5E MFI to GFP MFI in Cargo+ peritoneal macrophages.

**Figure 25. Experimental controls for *in vivo* peritoneal cell clearance**

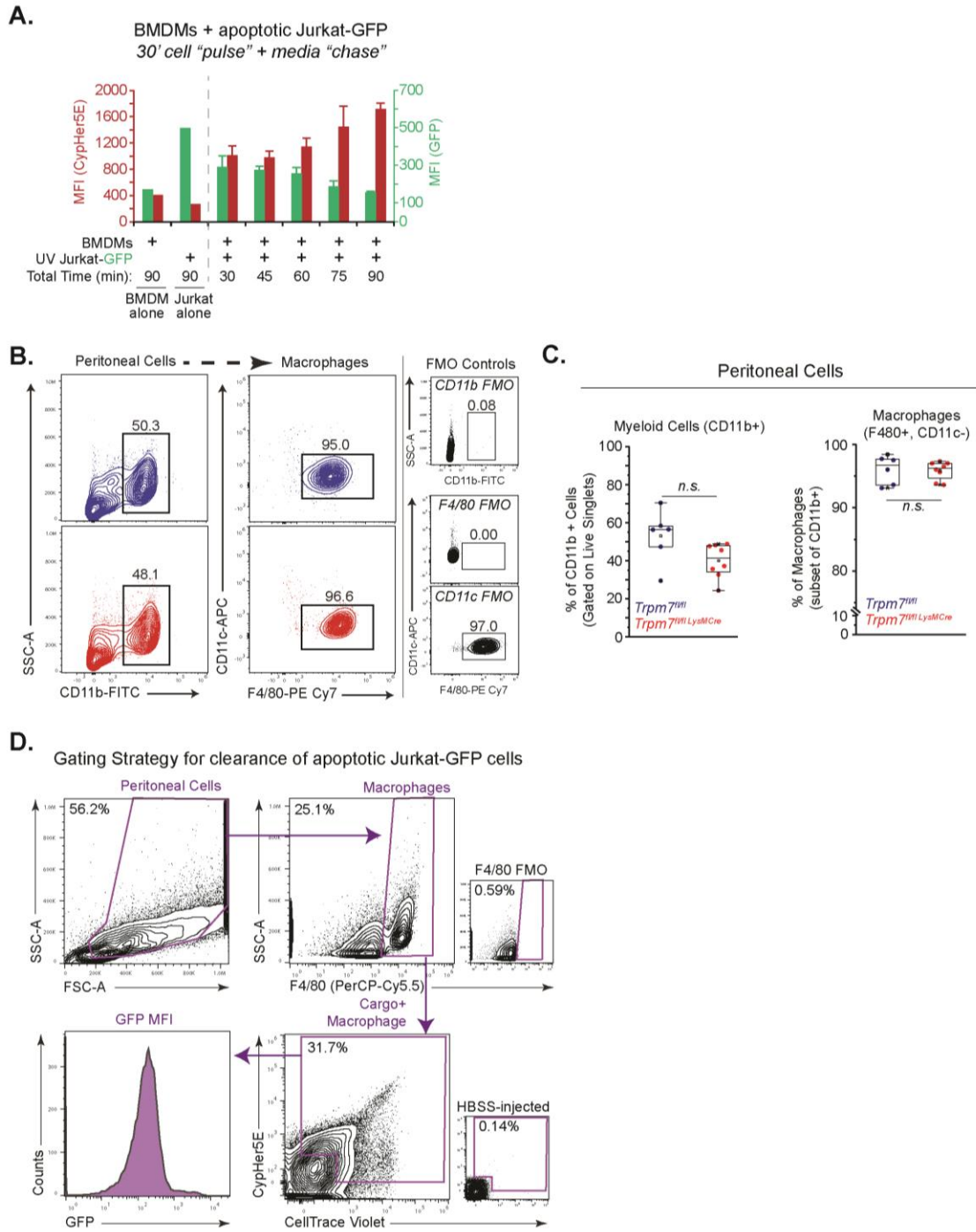


**Figure 25. Experimental controls for *in vivo* peritoneal cell clearance**

(A) Flow cytometry based quantification of degradation of triple-labelled, apoptotic Jurkat-GFP cells by BMDMs *ex vivo*. MFI of CypHer5E (acidification, red scale and bars), and GFP (cargo protein, green scale and bars) is shown for each condition. Bar charts represent mean of n=3 independent samples; error bars are SD.

(B) Representative cytographs depicting peritoneal cells and macrophage populations from *Trpm7<sup>fl/fl</sup>* and *Trpm7<sup>fl/fl</sup> LysM Cre* mice. Fluorescence minus one (FMO) controls are shown on the right. The data are representative of n=6 individual mice. Experiment by TKD.

(C) Quantification of CD11b+ and macrophage populations depicted in *Panel a*. Experiment by TKD.

(D) Flow cytometry gating strategy used in Figure panels 24A-D.

**Figure 26. TRPM7 regulates phago-lysosome fusion in macrophages**

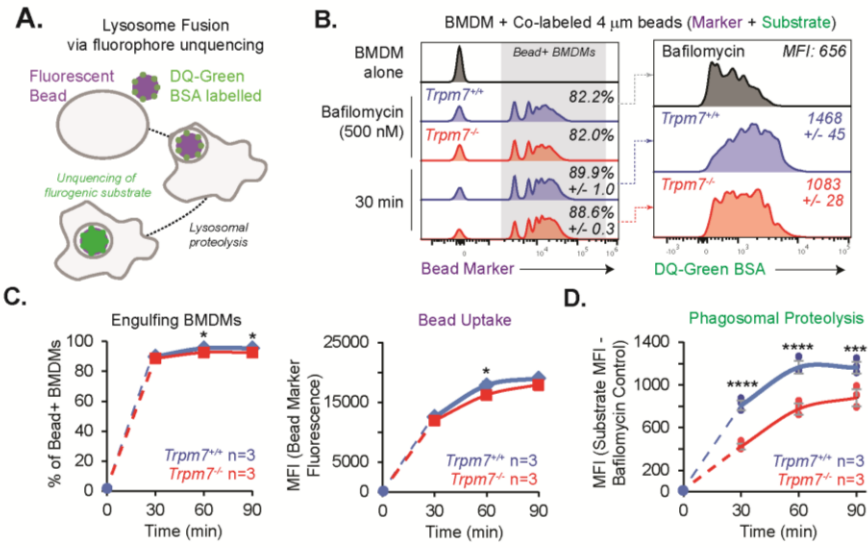


## Figure 26. TRPM7 regulates phago-lysosome fusion in macrophages

(A) Schematic of phagosomal proteolysis assay. Fluorescent beads were conjugated to DQ green-BSA and then offered to BMDMs as cargo for phagocytosis. In bead-containing macrophages, lysosomal proteolytic activity was measured, as reflected by increased DQ-Green BSA fluorescence due to proteolytic unquenching of the fluorophore.

(B) Flow cytometry-based measurement of proteolytic activity during phagocytosis of latex beads. DQ-green BSA-labelled fluorescent beads (4  $\mu\text{m}$ ) were incubated with WT and KO BMDMs for indicated time points. *Left*: Representative histograms of Bead+ BMDMs. *Right*: Measurement of DQ-green MFI in Bead+ BMDMs. Data representative of 2 independent experiments.

(C) Quantification of the assay shown in Panel b. DQ-green BSA MFI is shown as change from Bafilomycin A1 pre-treated BMDMs (negative control) and gated on Bead+ BMDMs.

(D) Quantification of bead uptake by *Trpm7<sup>+/+</sup>* and *Trpm7<sup>-/-</sup>* BMDMs. *Left*: Percentage of Bead+ BMDMs over time. *Right*: Quantification of gross bead uptake measured by Bead MFI of Bead+ BMDMs. Data points are mean of n=3 independent samples and individual points are plotted in *Panel D*. Error bars = SEM.

**Figure 27. TRPM7 associates with the nascent phagosome and is activated by acidic pH.**

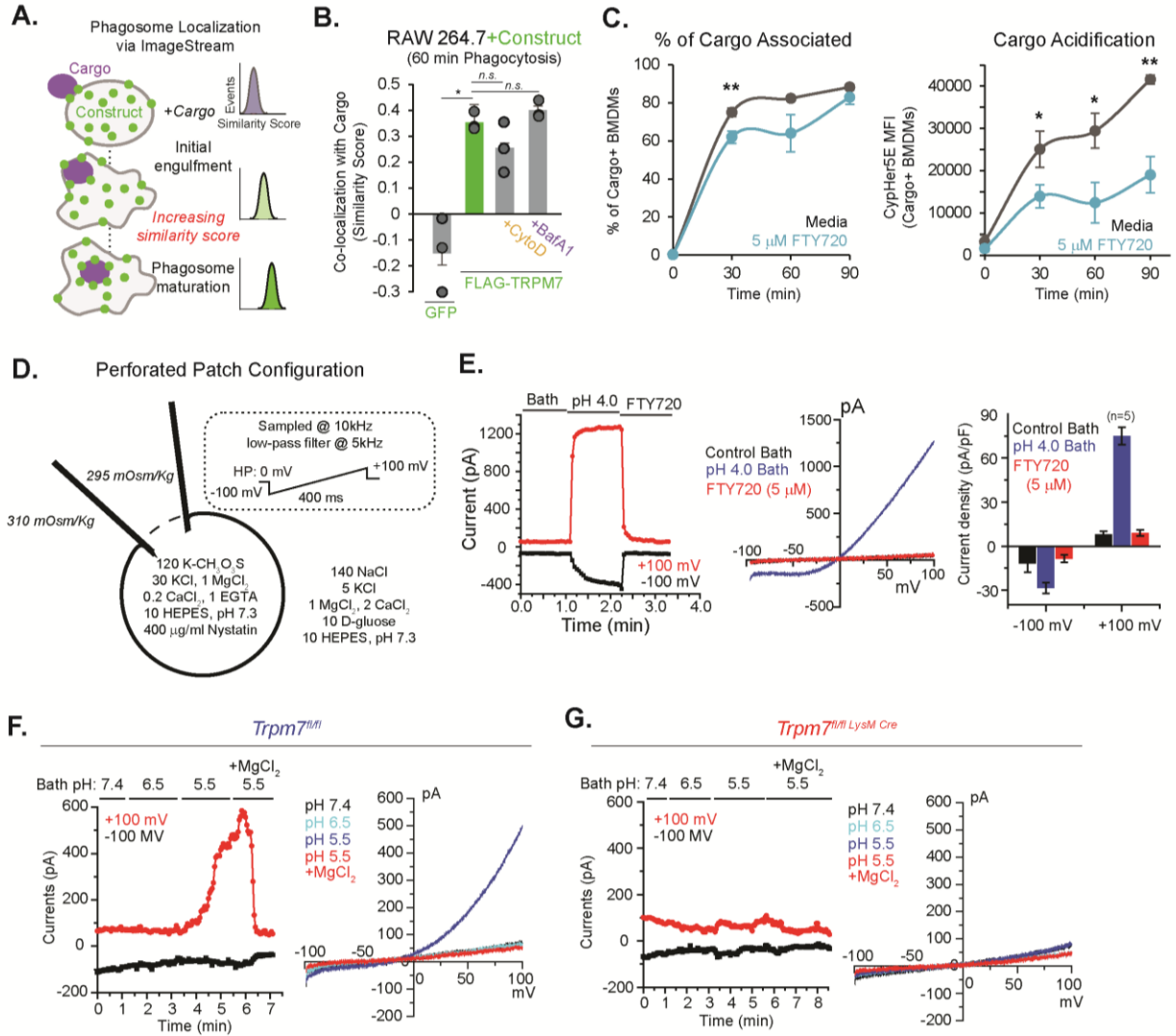


**Figure 27. TRPM7 associates with the nascent phagosome and is activated by acidic pH.**

(A) ImageStream based analysis of protein localization in RAW 264.7 cells during phagocytosis of apoptotic cells is schematized. Similarity score measures co-localization of expression construct with CellTrace Violet-labelled cargo, and the score increases with increased co-localization.

(B) ImageStream-based measurement of TRPM7 localization with phagocytosed apoptotic cells in fixed RAW 264.7 cells. Either FLAG-TRPM7 or GFP was transfected 16 hr prior to incubation with apoptotic cells. For controls, the cells were subjected to 15 min pre-treatment with Cytochalasin D (Cyto D; 1  $\mu$ M) or Bafilomycin A1 (BafA1; 500 nM). After phagocytosis, the RAW 264.7 cells were fixed and immunostained for FLAG immunopeptide. Fluorescence of GFP and anti-FLAG was measured via ImageStream flow cytometry. Bar charts represent mean of n=3 independent samples and the individual data points are overlaid; error bars are SEM. Representative results of two independent experiments are shown.

(C) Flow cytometry-based measurement of phagocytosis in BMDMs treated with media or FTY720 (5  $\mu$ M) during phagocytosis of apoptotic Jurkat cells (J:B = 10:1). *Left panel* shows cargo association with BMDMs (CellTrace Violet+ CypHer5E+). *Right panel* shows acidification of engulfed cargo (Cypher5E MFI). Data points are mean of n=3 independent samples; error bars are SD. Results are typical of 2 independent experiments.

(D) Schematic of perforated patch configuration used for electrophysiology.

(E) Perforated-patch electrophysiology of  $I_{TRPM7}$  in BMDMs in response to extracellular pH. *Left:* Time-current relationship of  $I_{TRPM7}$  activation and block by FTY-720. *Middle:* Representative I-V relationship of  $I_{TRPM7}$  as revealed in the perforated patch recording. **Right:** Quantification of current densities at -100 mV (inward current) and +100 mV (outward current). Experiment by SKM.

(F) pH-dependent activation of  $I_{TRPM7}$  in WT BMDMs using perforated-patch electrophysiology. *Left:* Time-current relationship of  $I_{TRPM7}$  activation and block by 10 mM  $MgCl_2$ . *Right:* Representative I-V relationship of perforated-patch clamp  $I_{TRPM7}$  current in response to varying bath conditions. Experiment by SKM.

(G) pH-dependent activation of  $I_{TRPM7}$  in KO BMDMs using perforated-patch electrophysiology. Left and Right panels are as described in *Panel F*. Experiment by SKM.

Figure 28. Flow cytometry gating strategy for phagocytosis by FTY720-treated BMDMs

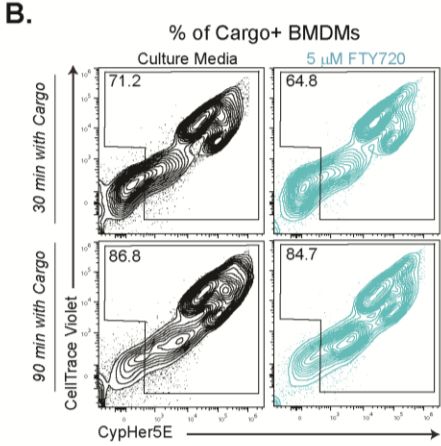
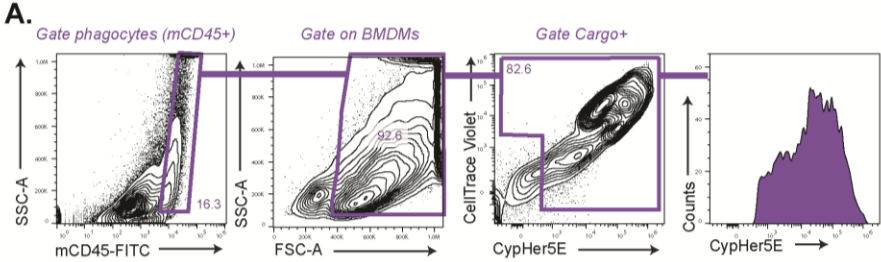


**Figure 28. Flow cytometry gating strategy for phagocytosis by FTY720-treated BMDMs**

**a.** Flow cytometry gating strategy shown in Figure 27E.

**b.** Representative cytographs of cargo-association (CellTrace Violet+) and acidification (CypHer5E) quantified in Figure 27G.

**Figure 29. Phagocytosis of apoptotic cells triggers phagosome-proximal elevations in  $Ca^{2+}$  that are dependent on TRPM7**

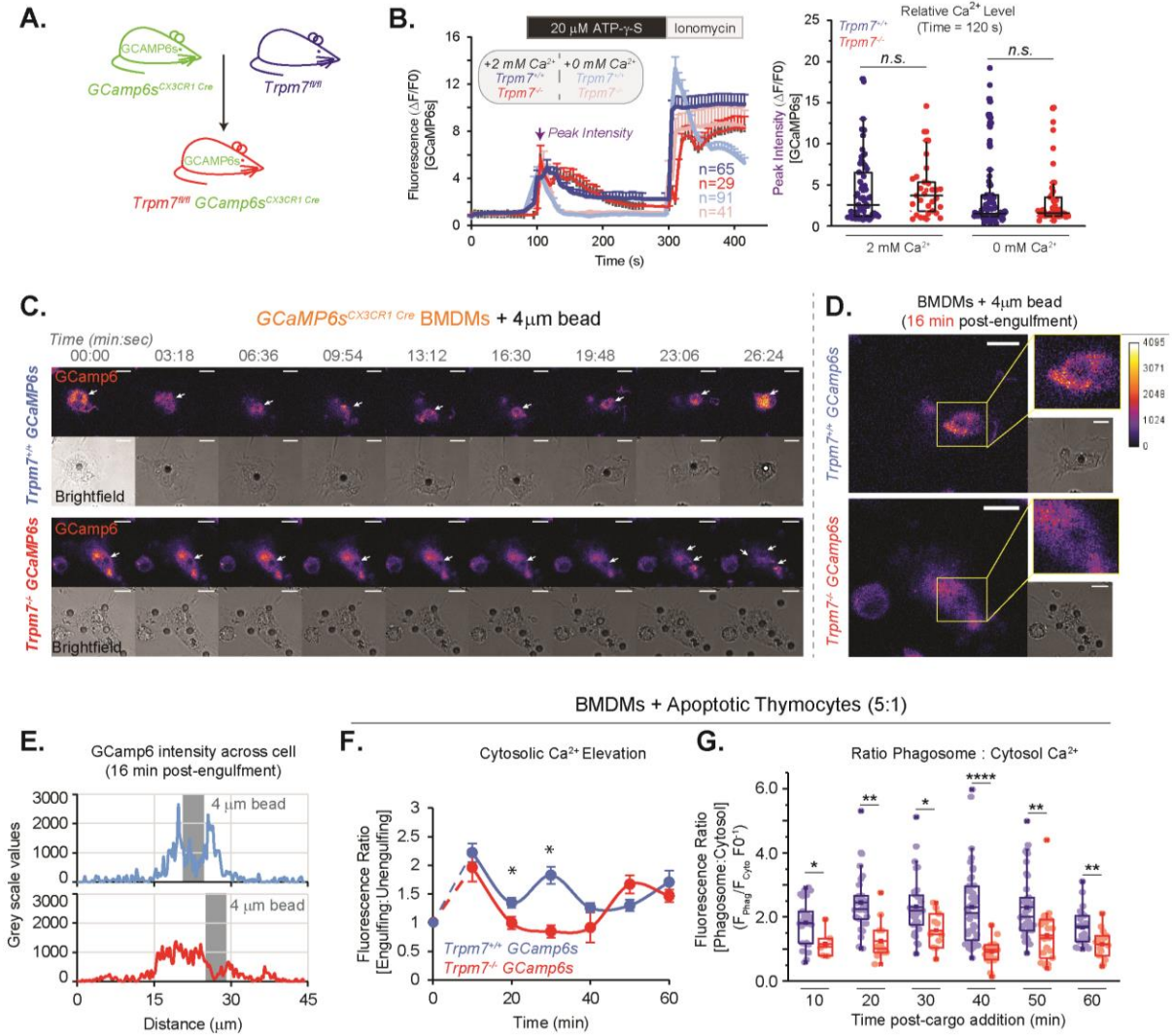


**Figure 29. Phagocytosis of apoptotic cells triggers phagosome-proximal elevations in  $\text{Ca}^{2+}$  that are dependent on TRPM7.**

(A) Generation of TRPM7 WT and KO GCaMP6s-expressing mouse strains is schematized.

(B) Relative changes in  $[\text{Ca}^{2+}]_i$ , as depicted by GcaMP6s fluorescence, in response to ATP over time in GCaMP6s-expressing BMDMs. Cells were treated with 20  $\mu\text{M}$  ATP- $\gamma$ -S for 3 min in bath solution containing either 0 or 2 mM  $\text{Ca}^{2+}$ , as indicated. Ionomycin (2  $\mu\text{M}$ ) was added as a positive control. *Left*: Mean GCaMP6s intensity over time (n values shown in the figure); error bars represent SEM. *Right*: Quantification of peak GcaMP6s fluorescence intensities after ATP- $\gamma$ -S addition, at the time point indicated by an arrow in the *Left panel*; Each data point in the box chart reflects a cell. The mean value is depicted by a solid horizontal line across the box.

(C) Changes in  $[\text{Ca}^{2+}]_i$  during phagocytosis in GCaMP6s-expressing WT (top) and KO BMDMs (bottom) during phagocytosis of 4  $\mu\text{m}$  carboxylated beads. Arrow indicates bead-containing phagosome. GCaMP6s fluorescence (top image; Fire LUT) and brightfield (bottom image; grey) were acquired via confocal microscopy and single optical section (0.5  $\mu\text{m}$ ) is shown. Scale bar is 10  $\mu\text{m}$ .

(D) Peri-phagosomal  $[\text{Ca}^{2+}]_i$  in WT and KO BMDMs is shown as a magnified image from *Panel A*, 16 min post-engulfment. GCaMP6s-fluorescence (fire) and brightfield (grey) are shown with ROI highlighted (yellow box). Relative scale of GCaMP6s intensity is show on the right. Scale bar is 10  $\mu\text{m}$ .

(E) Measurement of  $[\text{Ca}^{2+}]_i$  derived from a line scan analysis from cells depicted in Panel B. Fluorescent intensity of GCaMP6s was measured across the length of the cell through the indicated phagosome in a single x-y plane line trace. Bead location indicated by grey column.

(F) Relative changes in cytosolic  $[\text{Ca}^{2+}]_i$  in WT and KO BMDMs during phagocytosis of apoptotic cells. Changes in fluorescence of GCaMP6s represent changes in cytosolic  $\text{Ca}^{2+}$ . Data points were collected at indicated time points and measure the MFI in cargo-containing BMDMs relative to the fluorescence of non-engulfing BMDMs in the same field of view. Data points depict mean values; error bars reflect SEM (n > 20 cells).

(G) Relative changes in phagosome-proximal cytosolic  $[\text{Ca}^{2+}]_i$  during phagocytosis in WT and KO BMDMs. Data was measured from the same experiments shown in Panel F. Fluorescence ratio reflects fluorescence intensity in an ROI proximal to phagosome relative to the cytosol ROI. Analysis is described in Supplemental Figure 27A-C. Data points in the box chart represent individual phagosomes and the mean value is depicted as a horizontal line across the box.

**Figure 30. Analysis of phagosome-proximal Ca<sup>2+</sup> measurements**

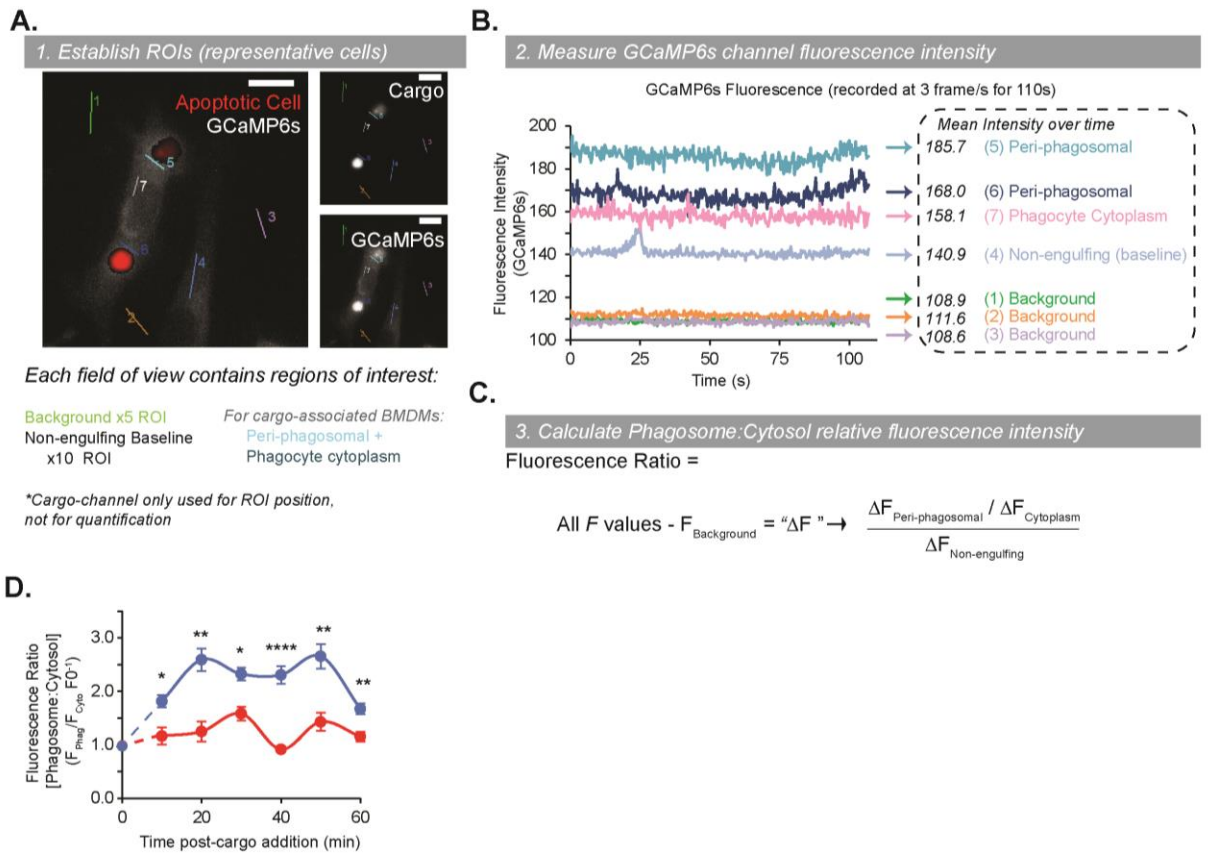


### Figure 30. Analysis of phagosome-proximal $\text{Ca}^{2+}$ measurements

(A) Data analysis for Figure 29F and 29G is schematized. Fluorescence was measured via wide-field microscopy and representative cells and ROIs are illustrated for analysis shown in *Panels b* and *c*. Live cells were imaged at 37°C every 300 ms for ~2 min. Merged image of GCaMP6s (grey) and apoptotic cell cargo (red) is shown. Each field of view used for analysis contained 5 background and 10 baseline (non-engulfing cells) ROIs; each phagosome included a phagosome-proximal and cytosolic ROI.

(B) Representative fluorescence intensities measured from the linear ROIs shown in Panel a. Mean fluorescence values for the ROI across the measured time course are shown on the right.

(C) Formula for the calculation of fluorescence intensity ratio of Phagosomal:Cytosolic  $\text{Ca}^{2+}$  during phagocytosis.

(D) Mean fluorescence ratio of changes in phagosome-proximal [ $\text{Ca}^{2+}$ ] over time in WT and KO BMDMs. Data is same data set depicted in Figure 29G, but without the overlay of individual data points. Error bars reflect SEM ( $n > 20$  cells).

## TABLES: Chapter 3

**Table 3.** Key Resources Table – Chapter 3

Reagent	Company	Catalog #
<i>Chemical Compounds</i>		
BAPTA-AM	Thermo Fisher	B6769
EGTA-AM	Thermo Fisher	E1219
FTY720	Cayman Chemical	402615-91-2
ATP-γ-S	Tocris	4080
Ionomycin	Cayman Chemical	56092-82-1
Bafilomycin A1	Cayman Chemical	88899-55-2
Cytochalasin D	Tocris	1233
Nystatin	Fisher BioReagents	BP2949-5
<i>Phagocytosis Assay Reagents</i>		
4μm FluoSpheres - Red fluorescent	Thermo Fisher	F8858
4μm polystyrene carboxylate-modified beads	Bangs Laboratories	PC05004
DQ-Green BSA	Thermo Fisher	D12050
CypHer5E	GE Healthcare	PA15405
CellTrace Violet	Thermo Fisher	C34557
<i>Antibody Reagents</i>		
Anti-F4/80 PE-Cy7 (Clone: BM8)	Thermo Fisher	25-4801-82
Anti-CD11b FITC (Clone: M1/70)	BD Pharmingen	557396
Anti-CD11c APC (Clone: N418)	Biolegend	117310
Anti-CD45 FITC (Clone: 30-F11)	Thermo Fisher	11-0451-82
TruStain FcX anti-mouse CD16/32 antibody	Biolegend	101320
OneComp eBeads	Thermo Fisher	01-1111-42
AnnexinV-7AAD Viability Staining Kit	BD Pharmingen	559763
CD11b-Alexa fluor 488	Thermo Fisher	53-0112-80
Anti-DYKDDDDK Epitope Tag (FLAG)	Thermo Fisher	MA1-91878
Alexa fluor 488 Donkey Anti-mouse AffiniPure IgG	Jackson ImmunoResearch Laboratories	715-545-150
<i>Other reagents</i>		
RPMI1640	Thermo Fisher	11875-093
Fetal Bovine Serum	RMBio	FBS-BBT
DMEM	Thermo Fisher	11965-092
HBSS	Thermo Fisher	14175-095
0.05% trypsin-EDTA	Thermo Fisher	25300-054
Paraformaldehyde	Alfa Aesar	43368
DMSO	Sigma	67-68-5
LysoTracker Red	Thermo Fisher	L7528
Phalloidin (CF488A)	Biotium	42
TAMRA-SE	Thermo Fisher	C1171
TransIT-X2 transfection reagent	Mirus	MIR 6003
Lipofectamine 3000	Thermo Fisher	L3000015

**Table 4.** Primer Sequences for Ca<sup>2+</sup> Channel Gene Expression Analysis

Target (mouse)	F/R	Sequence (5' to 3')
<i>Mcoln1</i>	F R	CCA GTG TCA TGC GTT TCT GC CGA GCG GAA CTT CAC ATG GT
<i>Mcoln2</i>	F R	CAC AGC CGC TTT TCC GC AGA CGC CAT CGC AGA TCC TT
<i>Mcoln3</i>	F R	TCC ACA GAC TTC TGA CGG TG TCC ACT GTG AGC CTT GTT GT
<i>Orai1</i>	F R	GAT GAG CCT CAA CGA GCA CT CCA TCG CTA CCA TGG CGA A
<i>Orai2</i>	F R	ACA GTC AGG CCT GGT CC TGG TGG TTA GAC GTG ACG AG
<i>Orai3</i>	F R	GCT ACC TGG ACC TTA TGG GG TGG CCA CCA TGG CGA AG
<i>Piezo1</i>	F R	TAA GAA TAT GCT GTC GCT CCT GTC AGG CTG AAG AGC TGG ATG ACC
<i>Pkd2</i>	F R	TCT GGA TGT TGT GAT TGT CGT G TGA AGA GCT TAA TCC AGA CCA A
<i>P2xr7</i>	F R	GTC CCC GGC TAC AAC TTC AG TTC CTC CAG TGC CGA AAA CC
<i>P2xr4</i>	F R	CAG CAG TGG AAT TGG GAC TGG ACC AAG AGG GTG AAG TTT TCT G
<i>Stim1</i>	F R	AGG AGA TTG TGT CGC CCT TG GGG TCA AAT CCC TCT GAG ATC C
<i>Stim2</i>	F R	CAC CTG CAC AGA GAA GAT AAG C ACT GCT ATC CTG GGG AGT GTT
<i>Trpm2</i>	F R	GGA TGA CCC AAG GAA CAC AGA CAT GAG TGT GCA GGT TCT CTT
<i>Trpm7</i>	F R	AGC AGT ATT CCA ATG ATT TTG GC TCA TAG CCA TCG TTT CAT CCT GT
<i>Trpv2</i>	F R	GTT TGA CCG TGA CCG ACT CT GAG CCT TCT GTG TAT GCC GA
<i>Trpv4</i>	F R	TCC TGA GGC CGA GAA GTA CA ACC ACT CTC ATC TCC AGG GG

**Table 5.** siRNA Sequences from Ca<sup>2+</sup> Channel Screen (SMARTpool siRNA – Dharmacon)

Cat. Identifier	Gene (mouse)	Target Sequences (SIGENOME siRNA)			
		1	2	3	4
94178	<i>Mcoln1</i>	GAACACC AUUGCCUUC CGA	UGAGAUCC CUGAUUGUJAC	CUGAUCAC AUUUAGCAAUA	CCUGAUACU ACCUGAGUA
68279	<i>Mcoln2</i>	GAGAGAU ACCGGACUGUUA	GGACGUCGAC GCUUUUUGU	GACCAGUACCAC GAGAAGUU	AGAAUACG AUUACCUUCGA
171166	<i>Mcoln3</i>	CCAAGAGU CUCACAAAGCUA	GACUUUACG CUGACUAUAA	ACGAAACAAU UAAGCACUA	GGUGUACAU UAUGAUCAU
109305	<i>Orai1</i>	GCACCUGU UUGCCCUCAUG	GGCCCAAGC UCUAUCUUAAG	CACC AAGCCUCCCGCUGAA	ACAUCCGAGG CUGGAGCAA
269717	<i>Orai2</i>	GGGCAUGG AUUACCGAGAC	UGGAACUCC GUACAGUCUA	GGCC CACCACC CGUGAUAUC	GUUGAA GCCGUGAAGCAACA
269999	<i>Orai3</i>	GUAGACU GUCCCUUAUGUU	GGCGC UACCUAGACCUUAU	UGGAGAAC GAUICAUUGAAUA	CUUGGGGAC UAGUGUUUAU
18438	<i>P2rx4</i>	GUCCAGAG AUUCCUGAUUA	AUUAAGU AUUGGGAAGACUA	UCAAGUC GUUCAUUUAUA	GCUCAUCC GCAGCCGUAAA
18439	<i>P2rx7</i>	GGAAAAGAG CUGUUAUCAG	UAGCAGAGG UGACGGAGAA	UACAUUAAGC UUUUGCUUUGG	GGALUCCAGAG CACGAAUUA
234839	<i>Plezo1</i>	CCACC AACCUUAUCAGUGA	GGCC AAGACUGUCCUGGGGA	GAAAUAC AACCAUCUAAAC	CAACGGCC AUUCUUCUCA
18764	<i>Pknox2</i>	GGAAUUUG UCUGAUGUUGU	UACGGGAGC UGUGACUUA	CAAGAUUG AUUGCCGUGAUU	CGUACAGUGG AAGCGGGUUA
20866	<i>Stim1</i>	GCACC GAACUUGGAAAGUA	CGAAACAU CCUAUAGCUGA	GUGAUGAGU UC UAAGGGA	GUCCAGUACU ACACAAUCUA
116873	<i>Stim2</i>	GCACAUUA ACUUGUAGGAAU	CAUCAGAA GUCACAAUUG	GAUGAAA GACUUAAGAGAU	GGACGGAU GC GAUCUGGUG
28240	<i>Tpm2</i>	GAACAGCG CUUAAGCCUAUG	GGACUAA GCUGGAAAAAGUU	GGAGUUGG GAUCCAAAAAGAA	GCACUGGCC UGUJAGCAAGA
58800	<i>Tpm7</i>	GCAGAAA GCUUGUJAGAA	GAUUAUUG GC UUGUUAUG	GGACAGAGU UUCAUUUGUA	GAAAGAAC CUAGUGCUGUA
63873	<i>Tpv4</i>	GGAGAAA GGUUGUGGAGAA	GGACUGGC UCUCUUCUUGU	GACGUGAGG UGACAGAUUA	UCAAAA GACUUGUUCACGAA
22368	<i>Tpv2</i>	GGCUGAAC CUUGCUUAUAUA	GGGCAGG CAUCACUUGGUUA	UGACUGG ACUUGCUJAGAGUA	GAAGUAAA ACUGGGCUGCAU

## METHODS

### Mouse Strains

Male and female mice aged 7 to 14 weeks were used for all experiments. *Trpm7<sup>fl/fl</sup>* and *Trpm7<sup>fl/fl</sup>* (*LysM cre*) mice were generated as described previously. *Trpm7<sup>fl/fl</sup>* (*CX3CR1 Cre*) mice were generated through crossing *Trpm7<sup>fl/fl</sup>* mice to B6J.B6N(Cg)-Cx3cr1tm1.1(cre)Jung/J (Jackson Laboratories; 025524) to subsequently generate *Trpm7<sup>fl/fl</sup>* and *Trpm7<sup>fl/fl</sup>* (*CX3CR1 Cre*) mice on a mixed background. GCamp6s-expressing strains were generated crossing established mouse strains with the B6;129S-Gt(ROSA)26Sortm96.1(CAG-GCaMP6s)Hze/J mice, which contain a LoxP-flanked STOP codon. Deletion of *Trpm7* was confirmed via quantitative real-time PCR analysis and patch-clamp electrophysiology.

### Cell Culture

Bone marrow-derived macrophages were isolated and cultured as previously described<sup>152</sup>. In brief, bone marrow was extracted from murine femur and tibia via centrifugation. Bone marrow was then lysed in ACK Lysis buffer and plated on petri dishes in BMDM Media (RPMI 1640 + 10% FBS + 20% L929-conditioned media). Cells were differentiated for 7 days and the media was refreshed afterwards every 3 days. For experiments, BMDMs were used between day 7 to 14 post-differentiation. For cultured cell lines, Jurkat (Clone E6-1 (ATCC® TIB-152™)) and RAW 264.7(ATCC® TIB-71™) cells were cultured and maintained according to the vendor's instructions. Jurkat-GFP cells were a gift from Dr. Kodi Ravichandran (University of Virginia) and maintained in T75 culture flasks (RPMI+10% FBS) at 0.1 to 2.0 x 10<sup>6</sup> cells/ml.

### Preparation of apoptotic cells

Thymocytes were freshly isolated prior to experimentation. Briefly, mice were euthanized, the thymus was removed, and cells were dissociated through a 40  $\mu\text{m}$  cell strainer in PBS. Thymocytes were collected via centrifugation (1650 rpm for 5 min), resuspended in ACK lysis buffer for 5 min at RT, pelleted via centrifugation, and resuspended in HBSS. In experiments using Jurkat cells, cultured Jurkat cells were collected via centrifugation and resuspended in HBSS. Cell suspensions were added to petri dishes, which were irradiated with 150000  $\mu\text{J}$  of UV light (UV Stratalinker 1800). Cells were incubated for 3 hr at 37°C and 5% CO<sub>2</sub>. After 3 hrs, apoptotic cells were pelleted by centrifugation (1800 rpm for 5 min) and resuspended in HBSS. Cells were stained with indicated fluorescent dyes for 30 min at 37°C. For flow cytometry, where indicated, cells were stained with CypHer5E NHS Ester (GE Healthcare; PA15405) and CellTrace Violet (Thermo Fisher; C34557), each at 1  $\mu\text{M}$ . Apoptotic cells were washed 3X in culture media (containing 10% FBS) and destained by incubating in media for 30 min at 37°C. Apoptosis was confirmed by Annexin V-7AAD viability staining (BD Biosciences; Cat# 559763) and measured via flow cytometry. Cells were pelleted and resuspended in culture media for counting “total” numbers of cells via trypan blue exclusion. Apoptotic cells were added to macrophages at ratio indicated in figures and legends.

### **Measurement of Phagocytosis by Flow Cytometry**

Macrophages were plated on 24-well non-coated tissue culture plates at a density of  $0.1 \times 10^6$  cells/well overnight prior to experimentation. Apoptotic cells were prepared as described above; beads were washed 3X in culture media prior to experimentation. For pharmacological treatments, macrophages were incubated with drug at the indicated concentration for 30 min prior to addition of cargo in serum-free media and added with cargo in culture media. After addition of cargo, plates were then centrifuged at 750 rpm for 1 min, rotated, and centrifuged for an additional 1 min to synchronize phagocyte-cargo contact. Plates were incubated at 37°C and 5% CO<sub>2</sub> for indicated time points. At the end of the experiment, cells were washed 3X with cold PBS and

incubated with 0.05% trypsin-EDTA for 5 min to remove unengulfed cargo and detach macrophages. Cold culture media was added to inhibit trypsin activity and cell suspensions were then collected (1500 rpm for 5 min), washed 1X with PBS, and resuspended in FACS Buffer. With Jurkat cargo, mCD45-FITC (Clone: 30-F11; 0.5  $\mu$ g/ml) was used to further discriminate macrophages from cargo; with thymocytes, CD11b-Alexa fluor 488 (Thermo Fisher; Cat# 53-0112-80; 0.5  $\mu$ g/ml). Instrument voltages and gating was established based on unstained macrophages, unstained cargo, and single-stained fluorescent controls (with 0.01% HCl added for CypHer5E positive control). Gating strategy is described in Supplemental Figures. Measurements were acquired using the Attune NxT (Thermo Fisher) and analyzed using FlowJo (BD Biosciences).

### **Ca<sup>2+</sup> Channel Screen using siRNA**

On day 7 post-isolation, BMDMs were collected and aliquoted into individual cell suspensions for each siRNA tested. BMDMs were resuspended in OPTIMEM with appropriate SMARTpool siRNA (Dharmacon) and Lipofectamine 3000 (ThermoFisher; L3000015), according to the manufacturer's instructions. Cells were plated at  $0.5 \times 10^6$  cells/mL in 6-well non-treated culture plates for 48 hrs. After 48 hrs, cells were washed 3X with HBSS and detached using 0.05% trypsin. Cells were then counted via trypan blue exclusion and normalized to  $0.3 \times 10^6$  cells/tube/siRNA. Cells were resuspended in siRNA-containing transfection media, as described above, and plated at  $0.1 \times 10^6$  cells/well on 24-well non-treated culture plates in culture media for 48 hours. On the day of the experiment, cells were washed 1X with PBS and resuspended in culture media. Gene knockdown was confirmed via quantitative real-time PCR as previously described<sup>23</sup>. Z-scores were calculated as the difference between CypHer MFI of *siScramble*-treated cells from target gene divided by standard deviation of the data set; z-scores across the experiment were then averaged and plotted as shown.

## Perforated-Patch Clamp Electrophysiology

TRPM7 currents ( $I_{\text{TRPM7}}$ ) were measured using perforated-patch configuration using similar methods described previously<sup>123</sup> and depicted in Figure 5C. The extracellular bath solution contained (in mM): 140 NaCl, 5 KCl, 1 MgCl<sub>2</sub>, 2 CaCl<sub>2</sub>, 10 HEPES, 10 Glucose (adjusted to pH 7.3 with osmolality 280 mOsm/kg). The pipette solution contained (in mM): 120 K-methanesulfonate, 30 KCl, 1 MgCl<sub>2</sub>, 0.2 CaCl<sub>2</sub>, 1 EGTA, 10 HEPES (adjusted to pH 7.3 with osmolality 273 mOsm/kg). A final concentration of 400  $\mu\text{g/ml}$  Nystatin was used to establish membrane perforation and prepared by adding 16  $\mu\text{l}$  of Nystatin dissolved in DMSO to 1 ml of pipette solution; this was prepared fresh for each experiment. BMDMs were freshly-plated prior to analysis. MgCl<sub>2</sub> (10 mM) or FTY720 (5  $\mu\text{M}$ ) was added to the external solution to inhibit  $I_{\text{TRPM7}}$ . For recordings, a ramp from -100 mV to +100 mV over 400 ms was used, with a holding potential of 0 mV; signals were low-pass filtered at 5 kHz and sampled at 10 kHz. All electrophysiology recordings were conducted at RT with an Axopatch 200B amplifier (Molecular Devices, Sunnyvale, CA).

## Immunocytochemistry

Cells were plated overnight on coverslips prior to experiments. Following experimentation, coverslips were washed 3X in PBS to remove media and unbound apoptotic cells. For LysoTracker Red staining, cells were stained in PBS with LysoTracker Red (250 nM) at RT for 15 min. Coverslips were fixed in 4% PFA (in PBS) for 30 min at room temperature (RT). Coverslips were washed 3X in wash buffer (PBS with 0.05% Tween-20), blocked at RT for 1 hr in blocking buffer (5% donkey serum, 1% BSA, 0.1% fish gelatin, 0.1% Triton X-100, and 0.05% Tween-20 in PBS), and incubated with primary antibody diluted in blocking buffer overnight at 4°C. Coverslips were washed 3X in wash buffer and incubated at RT with the appropriate secondary antibody in blocking buffer for 90 min, followed by 3X wash in wash buffer. If stained for F-actin,

coverslips were stained with a fluorophore-conjugated phalloidin in wash buffer for 15 min at RT and washed 1X with wash buffer. Coverslips were then mounted on glass slides (ProLong Gold Antifade; ThermoFisher #P36930), allowed to cure overnight, and imaged within 48 hours. Confocal microscopy was performed on an Olympus Fluoview FV1000. Data were acquired with Olympus Fluoview (Ver 4.1a) and analyzed using ImageJ.

### **Ca<sup>2+</sup> Imaging during Phagocytosis**

GCaMP6s-expressing BMDMs were plated on coverslips overnight prior to imaging. Coverslips were washed 1X in culture media. For apoptotic cell cargo, cells were stained with 2.5  $\mu$ M TAMRA-SE or 1  $\mu$ M CypHer5E (in RPMI 1640) for 30 min at RT followed by 3X wash in RPMI 1640+10% FBS to remove unbound dye and placed in imaging media (RPMI 1640 without phenol red + 20 mM HEPES). For phagocytosis of latex beads, 4  $\mu$ m carboxylated beads were washed in FBS followed by PBS prior imaging. Phagocytic cargo was added at a ratio specified in figures and legends for 10 min at RT to promote association with BMDMs, but minimize engulfment. Coverslips were washed 1X in imaging media and placed in the imaging chamber. Coverslips were imaged at 37°C +/- 1°C. Wide-field microscopy was performed Zeiss Axio Observer microscope using a Pinkle filter set (Semrock; GFP/dsRed 2X-A-000) and Lambda DG4 Illuminator. Fluorescence was excited using a DG4 Illuminator (Sutter Instruments, Canada) and detected using an ORCA-Flash 4.0 V2 CMOS camera (Hamamatsu). Data was acquired using SlideBook software (3i) and analyzed using Origin Pro and Microsoft Excel. Microscopy was performed on the Leica SP5 confocal microscope with excitation from 'White light' and 488 nm argon lasers using Leica Applicate Suite Software (Leica) and analyzed using ImageJ. For measurements in Figure 6, data analysis was performed as described in Supplemental Figure 5.

### **Expression of TRPM7 Constructs**

FLAG-TRPM7 construct was developed as previously described<sup>113</sup>. Prior to transfection, RAW 264.7 cells were plated at  $0.2 \times 10^6$  cells/well in 12-well plate. FLAG-TRPM7 or GFP was transfected into RAW 264.7 cells using TransIT-X2 transfection reagent according to the manufacturer's protocol at 1  $\mu\text{g}$  of plasmid/well (0.1  $\mu\text{g}$  plasmid/well for GFP). Transfected RAW 264.7 cells were cultured for 24 hours prior to experimentation, which is describe in figures and legends. ImageStream data was acquired using the Amnis ImageStream (EMD Millipore) flow cytometer and analyzed using INSPIRE analysis software according to the manufacturer's guidelines (Amnis-EMD Millipore).

### **In vivo measurement of phagocytosis**

Male and female mice were injected intraperitoneally with 200  $\mu\text{l}$  HBSS or  $4 \times 10^6$  apoptotic cells resuspended in HBSS. Apoptotic Jurkat-GFP cells were prepared as described herein for Jurkat cells. After 90 min, mice were euthanized and peritoneal lavage was performed as described previously. Recovered cells were pelleted, resuspended in ACK lysis buffer for 5 min (red blood cell lysis), washed 1X in cold PBS, and stained for flow cytometry. For peritoneal phenotyping, cells were stained with TruStain FcX anti-mouse CD16/32 (5  $\mu\text{g}/\text{ml}$ ; Biolegend; #101320) for 10 min at 4°C prior to addition of the fluorophore-conjugated antibody cocktail for 30 min. As shown, antibodies used for staining were anti-mouse CD11b FITC (Clone: M1/70), F4/80 PE-Cy7 (Clone: BM8), and CD11c APC (Clone: N418). Cells were then washed 2X in FACS Buffer (0.5% BSA, 2 mM EGTA) prior to analysis. All experiments included single stain controls using OneComp eBeads (Thermo Fisher; #01-1111-42) to determine appropriate compensation values and fluorescence minus one controls with cells for gating. Flow cytometry measurements were performed on the Attune NxT Flow Cytometer (Thermo Fisher) and analysis performed in FlowJo Software (v10; FlowJo, LLC BD). Gating strategies are show in supplemental figures, and additional reagent information is in Supplemental Table 1.

## **Generation of DQ Green BSA Reporter Beads**

DQ Green BSA reporter beads were prepared according to as described previously, with minor modifications<sup>207</sup>. In brief,  $5 \times 10^7$  4  $\mu\text{m}$  beads were washed 3 times in 1 mL of PBS (2000g for 2 min) and vortexed to disperse into 'single-bead' suspension in PBS (pH 7.2). Freshly-prepared solution of cyanamide (crosslinker) was added to a final concentration of 25 mg/ml and incubated for 15 min with agitation. Beads were then washed twice in coupling buffer (0.1 M Na-borate in sterile H<sub>2</sub>O; pH 8.0 with NaOH) and resuspended in 1 mg/ml DQ Green BSA in coupling buffer for 12h at 4°C. Beads were then washed twice in 250 mM glycine (in PBS; pH 7.2) followed by two washes in PBS. Beads were washed in complete media prior to experimentation.

## **Ca<sup>2+</sup> Imaging with ATP stimulation**

GCaMP6s-expressing BMDMs were plated on #1 coverslips overnight prior to imaging. Cells were imaged in Ringer Solution ([in mM] 155 NaCl, 4.5 KCl, 2 CaCl<sub>2</sub>, 1 MgCl<sub>2</sub>, 5 HEPES, 10 glucose, pH 7.4) or in Ca<sup>2+</sup>-free Ringer Solution (155 NaCl, 4.5 KCl, 5 EGTA, 1 MgCl<sub>2</sub>, 5 HEPES, 10 glucose, pH 7.4) at RT. Measurements were performed with perfusion of bath solution with or without ATP- $\gamma$ -S (20  $\mu\text{M}$ ) using a gravity feed system and ionomycin (2  $\mu\text{M}$ ). Fluorescence was excited using a DG4 Illuminator (Sutter Instruments, Canada) and detected using an ORCA-Flash 4.0 V2 CMOS camera (Hamamatsu) using SlideBook 6 software (3i).

## **Statistics**

All data were analyzed using GraphPad Prism 8.0 (GraphPad Software), Origin Pro 9.1.0 (Origin Lab), or Excel (Microsoft) software. Data are presented as individual data points of independent samples or means with error bars as indicated in figures legends. Bar charts and line graphs were plotted in Excel; dot plots, GraphPad Prism; box charts, Origin Pro. Statistical box charts contain boxes and whisker bars, which denote the 25-75 and 1-99 percentile range, respectively, with individual data points overlaid; median value is denoted by a horizontal line and mean by a

rectangle. Normality was tested graphically (QQ plots) or D'Agostino-Pearson normality tests. Data that passed normality and variance tests were analyzed by *t* tests for 2 groups and ANOVA for >2 groups using two-tailed tests; Bonferroni post-hoc correction for multiple comparisons was applied where appropriate. Mann-Whitney test was used for non-parametric data with 2 groups. Sample sizes are indicated in figures and legends, and *p* values less than 0.05 were considered statistically significant (\* denotes  $p < 0.05$ ; \*\*,  $p < 0.01$ ; \*\*\*,  $p < 0.001$ ; \*\*\*\*,  $p < 0.0001$ ).

## CHAPTER 4: DISCUSSION AND FUTURE DIRECTIONS

Although TRPM7 is highly expressed in the immune system, the role of TRPM7 in innate immunity was unknown. This thesis and supporting work<sup>23,152</sup> describes two functions of TRPM7 in macrophages: identifying the role of TRPM7 in LPS-induced macrophage activation and during efferocytosis. In response to LPS, TRPM7 channel mediates cytosolic Ca<sup>2+</sup> elevations that are essential for TLR4 endocytosis and inflammatory cytokine production (Chapter 2; Graphical Abstract - Figure 4). During phagocytosis of apoptotic cells, phagosome maturation is regulated by TRPM7, which promotes acidification of the phagosome by modulating phagosome-proximal Ca<sup>2+</sup> levels (Chapter 3; Graphical Abstract - Figure 19). In this chapter, I will address some outstanding questions and future directions of inquiry that were not discussed in the preceding chapters.

The studies described herein position TRPM7 as a crucial regulator of major macrophage processes: cytokine production and phagocytosis. In both cases, we uncovered a role for TRPM7 *channel* to modulate the electrical activity necessary to enhance signal transduction at specialized membrane domains to execute complex cellular functions. Both LPS signal transduction and efferocytosis require initiation by immunological receptors, recruitment of co-receptors, activation of phospholipases, remodeling of lipid domains (i.e. phosphoinositide modification – discussed below), and Ca<sup>2+</sup> signaling to facilitate the formation of specialized endosomes and activate distinct immunological programs. The context of our observations (LPS activation and efferocytosis) could be canonically described as a role in pro- and anti-inflammatory processes; however, this categorization focuses on the immunological output, not the underlying cell biology. Although these contexts yield different immunological consequences, they are shaped by the specific cellular receptors that initiate the inflammatory programs (i.e. TLR4 for LPS; Tim4 [amongst many others<sup>184,216</sup>] for efferocytosis), these cellular programs, which are fundamental to

innate immunity, rely on overlapping cell biology, suggesting that TRPM7 may help 'fine tune' their signal transduction towards the appropriate immunological activation.

Our observations do not definitively identify a unifying activation mechanism for TRPM7, but four major unifying mechanisms are possible in both paradigms: cleavage of TRPM7 (which potentiates  $I_{TRPM7}$ ), direct interaction with co-receptors essential for immuno-signal transduction<sup>216</sup>, activation by acidic pH, modulation by membrane phospholipids (discussed in detail below). Future studies should examine whether cleavage of TRPM7 or direct interaction with key co-receptors (i.e. CD14) may be occurring in these contexts. Likewise, there is an unclear biophysical and structural basis for how immunological co-receptors might directly interact with and regulate ion channel activity, although this has been proposed for other ion channels during LPS signaling<sup>217</sup>. Future studies using overexpression systems should provide preliminary evidence of TRPM7-receptor interactions. Regardless, it is clear that TRPM7 channel functions to amplify signal transduction in macrophages, particularly at sites of specialized endosome formation. To this end, many early endosomes are modestly acidified, and TLR-containing endosomes may be included<sup>218</sup>. This creates the possibility that TRPM7 channel activity may be augmented by modest acidification of TLR4 containing endosomes (which are destined for lysosomal degradation<sup>219</sup>), thereby unifying a "pH-induced activation" model for TRPM7. However, the precise composition of TLR4-CD14 endosomes and the presence of TRPM7 within them remains unclear.

In this work, an underlying theme of inflammatory signal transduction, phagocytosis, and regulation of ion channels is the dynamic modification of phosphoinositol lipids. These lipids help act as 'flags' in the membrane, facilitating clustering of receptors, binding of signaling adaptors, and modulating ion channels juxtaposed to them in the membrane<sup>220</sup>. The seven phosphoinositides mark distinct membrane domains to directly modulate membrane-resident proteins (such as ion channels) and allow reversible recruitment of cytosolic proteins. In particular,

PI(4,5)P<sub>2</sub> (generally referred to as “PIP<sub>2</sub>”, but distinct from PI(3,5)P<sub>2</sub>) denotes sites of membrane endo- and exocytosis and regulates organization of cell surface receptors<sup>220</sup>. Clapham and colleagues have speculated that PIP<sub>2</sub> could be a candidate master regulator of TRP channels<sup>9</sup>. For instance, TLR4 complexes form on the membrane (through its adaptor TIRAP) at PIP<sub>2</sub>-rich sites<sup>24</sup>, and PIP<sub>2</sub> is rapidly consumed from the nascent phagosome during phagosome maturation<sup>186</sup>. TRPM7 is modulated by PIP<sub>2</sub>, and activated by PLC-associated signaling<sup>115,123</sup>. Although whole-cell patch clamp electrophysiology recordings have demonstrated that addition of PLC agonists can inactivate TRPM7 channel<sup>115</sup>, these findings are likely misleading. Whole-cell configuration requires a complete disruption of the cellular membrane during ‘break-in’, allowing an electrophysiologist to impose the contents of one’s pipette solution on the cell, and for TRPM7, this results in maximal current at break-in. In contrast, perforated patch configuration (PPC), which uses a low-dose of a pore-forming compound in the pipette to permeabilize the membrane to the pipette solution, provides a much milder diffusion of the electrophysiological solution into the cell. Using perforated patch,  $I_{\text{TRPM7}}$  is clearly induced by PLC agonists, and likely represents a better approach to evaluating the channel properties of TRPM7<sup>123</sup>. Likewise, using this approach, we have measured an increase in  $I_{\text{TRPM7}}$  in response to LPS, and this current was absent from *Trpm7*-deficient BMDMs (S. Mendu, unpublished data). This approach enables future studies to directly test whether PIP<sub>2</sub> or other stimuli activate TRPM7 in response to LPS.

Likewise, organization of PIP<sub>2</sub> in the membrane, which is regulated by membrane potential, may have major consequences for immunological signal transduction. Seminal research from Hancock and colleagues<sup>89</sup> identified that membrane depolarization redistributed phosphatidylserine and PIP<sub>2</sub> in the plasma membrane. Membrane depolarization resulted in “nanoclustering” of PIP<sub>2</sub> in the plasma membrane of neurons, which amplified K-RAS signaling (determined by measurement of phospho-ERK). A ~50% increase in P-ERK was evident with only a 30 mV depolarization, which is comparable to the membrane depolarization observed in

macrophages stimulated with ATP and other immunomodulatory molecules<sup>31</sup>. This effect on K-RAS signaling was demonstrated to modulate cellular proliferation and proposed to serve a major mechanism to modulate the “gain” of cellular signaling pathways<sup>89</sup>.

In the context of this work, small perturbations in resting membrane potential remain an unexplored aspect of immunological signal transduction, as opening of non-selective cation channels (i.e. TRPM7) is expected to depolarize the cell membrane. Cells have many ways to establish and maintain  $V_m$  at the plasma membrane<sup>1</sup>, and given the number of potential compensatory mechanisms, it is unlikely that TRPM7 play a major role in determining *resting*  $V_m$ . However, LPS-induced activation of TRPM7 would acutely depolarize the cell, and modulation of PIP2 clustering could significantly impact formation of the Myddosome subsequent LPS signal transduction<sup>132</sup>. Whether TRPM7 is required for Myddosome formation is unknown, but this question could be central to unraveling the activation mechanism of TRPM7 in response to LPS. Assuming the ‘depolarization modulates PIP2’ phenomena translates to innate immune cells, whether TRPM7 is ‘gated’ by PIP2 in this context could be suggested by whether 1) membrane depolarization modulates Myddosome formation (likely if it is highly-dependent on PIP2 clustering), and whether 2) TRPM7 is required for Myddosome formation. If Myddosome formation requires PIP2 but not TRPM7, TRPM7 may be activated coincidentally with Myddosome formation (perhaps by PIP2 clustering). Alternatively, if TRPM7 regulates Myddosome formation, it could suggest that TRPM7-triggered membrane depolarization is necessary for PIP2 clustering and Myddosome formation, and therefore, TRPM7 is gated by another mechanism.

In the case of phagosome maturation, TRPM7 is likely gated by a non-PIP2-dependent mechanism: acidic pH. Nascent phagosomes are depleted of PIP2 prior to sealing of the phagosomal membrane (<30 min), and *Trpm7*-deficient macrophages do not begin to exhibit defects in phagocytosis until after engulfment of apoptotic cells is complete (~30+ min). Within minutes of phagosomal closure, V-ATPases begin to rapidly acidify the phagosome below pH 6,

and this requires a counteraction efflux from the phagosome<sup>32,33</sup> – our work proposes that TRPM7 mediates this necessary electrical activity. TRPM7 is robustly activated at physiological membrane potentials in response to acidic pH, with an estimated EC<sub>50</sub> around pH 5 to 5.5<sup>137</sup>. In the context of the proposed model, this work does not directly demonstrate that phagosomal TRPM7 is activated by pH, as electrophysiology recordings were conducted at the plasma membrane in macrophages. Strong evidence for this model could be shown through electrophysiological recordings of intact phagosomes<sup>95</sup>, although this procedure is technically challenging. However, generation of cell lines expressing variants of TRPM7 could be used to resolve how TRPM7 may contribute to phagosome maturation. With mutations in the TRPM7 pore domain, TRPM7-variant E1047Q renders the channel impermeable to Ca<sup>2+</sup> and Mg<sup>2+</sup> and abolishes pH-sensitivity, and E1052Q largely retains pH-sensitivity but not divalent cation permeability<sup>121</sup>. A compelling electrophysiological case could be made for TRPM7's role in modulating V<sub>m</sub> of other “organelles”, such as the phagosome (Chapter 3), which require rapid and robust acidification<sup>214</sup>. Thus, discrete activation of TRPM7 channel (as discussed elsewhere), particularly on the membrane of organelle-specific microdomains, could be an emerging theme of cellular regulation by TRPM7. Future studies employing these constructs would provide substantial mechanistic insight into the role of TRPM7 in phagocytosis.

This work, with continued investigation into the underlying mechanisms, provides strong evidence to validate TRPM7 as a tractable pharmacological target for inflammatory disease. To complement these future studies, a more robust validation of TRPM7's role in innate immunity is required *in vivo* to further advance its prospective as an immunological drug target. Evidence from our research (S. Mendu; not described herein) suggests that mice with *Trpm7*-deficient T cells (*Trpm7*<sup>fl/fl</sup> Lck Cre) contain elevated numbers of immunosuppressive T regulatory cells - these mice are protected from inflammatory damage in a model of hepatic inflammatory insult, but how they respond to an infection challenge also remains unknown. In relation to this dissertation, although

LPS challenge is a convenient model to examine animal responses to a TLR4 ligand, animal models with a *bona fide* pathogen are required for a more complete picture for the requirement of TRPM7 in host defense. For instance, during infection with a virulent gram negative pathogen (such as *S. typhimurium*), a *Trpm7*-deficient animal may effectively combat the pathogen with a decreased inflammatory burden or it may succumb to the infection challenge due to an inability to mount an effective immune response. However, if targeting TRPM7 is largely immunosuppressive, it could reveal an effective application for transplant therapy or treatment of lymphoma cancers, where inhibiting immune cell function is paramount. These supporting animal studies will help define an effective context for TRPM7 as an immunological drug target. Thus, a small molecular inhibitor for TRPM7 may be effective in prevention of autoimmune conditions with a major pro-inflammatory component (such as rheumatoid arthritis), but may leave the host susceptible to infection.

Although this work identifies key functional roles for TRPM7 in macrophages and previous electrophysiological studies provided a basic characterization of TRPM7 channel properties, the natural, physiological ligands for TRPM7 remain mysterious. Using a combination of GCaMP-expressing and *Trpm7*-deficient cells, future work has the exciting opportunity to discover novel TRPM7 agonists and inhibitors in well-designed compound screens. Given TRPM7's intersection in immunological 'sensory' transduction, bioactive lipids, such as arachidonic acid and its biochemical products (the eicosanoids), may be strong candidates to modulate TRPM7. Arachidonic acid has been described as an agonist of TRPV4<sup>90</sup>, but not tested on TRPM7 channel function. Advancing research in "eicosadomics" continues to reveal new bioactive lipids and their varied mechanisms of signaling, including eicosanoid class switching (transformation from a pro- to anti-inflammatory compound), transcellular biosynthesis (pro-lipid produced by one cell is converted to a bioactive form by another cell), and conversion by soluble phospholipases<sup>17</sup>. Although the role of these immunomodulatory lipids has long been studied in biology, they present

an exciting opportunity as candidate ligands of TRP channels and TRPM7. Likewise, TRPM7 may be activated indirectly by a variety of immunomodulatory molecules. Increased understanding of TRPM7 pharmacology may provide significant advances to understanding the broader biological role for TRPM7.

For instance, electrophysiological studies show that TRPM7 is inhibited by FTY720 (fingolimod) and sphingosine, but not sphingosine-1-phosphate<sup>147</sup>. The immunological and physiological significance of sphingosine-lipids is clear<sup>221</sup>, but their cellular role and effect on ion channel function is poorly defined (in contrast to phosphoinositols). Sphingosine is thought to be regulated by an 'inside-out' mechanism: sphingosine is phosphorylated by sphingosine kinases to form sphingosine-1-phosphate (S1P), S1P is exported out of the cell, where signals in a paracrine and autocrine manner prior to reuse in synthesis of ceramides and sphingolipids<sup>221</sup>. FTY720 is a pro-drug that is phosphorylated by sphingosine kinases to create an S1P mimetic that acts as an S1P receptor antagonist<sup>148</sup>. Treatment of macrophages with FTY720 yields profound inhibition of inflammatory signaling and phagosome maturation, but the effective concentration ( $IC_{50} \sim 2 \mu M$ )<sup>23</sup> is 1000-fold higher than its effect on S1PRs ( $IC_{50} < 2 \text{ nM}$ ) and consistent with inhibitory concentrations for TRPM7 channel<sup>147</sup>. Many of the potent inhibitory effects of FTY720 on macrophages *ex vivo* occur in addition to blockade of TRPM7 channel, especially given the robust expression of sphingosine kinases and S1PRs (which are GPCRs) in myeloid cells. Two possibilities exist (and it is likely a combination of both): 1) FTY720/sphingosine modulate additional channels that may serve supporting or partially redundant functions of TRPM7, or 2) TRPM7 uniquely sits at the intersection of immunological and sphingosine signaling in myeloid cells.

This work has identified novel roles for TRPM7 and  $Ca^{2+}$  signaling in macrophages. However, TRPM7 may also be central regulator for another signaling ion:  $Zn^{2+}$ . It is an essential element in cell biology (see the zinc-finger proteins), and the electrochemical driving force for  $Zn^{2+}$

is significant (10  $\mu\text{M}$   $\text{Zn}^{2+}$  outside versus 10 nM in cytosol). However, due to the lack of highly-specific tool compounds, fluorescent indicators, and genetically-encoded sensors, our understanding of the precise role of  $\text{Zn}^{2+}$  in immunity is in its nascent stages<sup>222</sup>. In response to LPS, macrophages and DCs require  $\text{Zn}^{2+}$  for efficient TLR signal transduction and upregulation of antigen presentation machinery<sup>223,224</sup>. However, the molecular conduits of  $\text{Zn}^{2+}$  in these contexts are poorly defined. TRPM7 has been proposed to help form unique  $\text{Zn}^{2+}$ -rich organelles in HEK cells, which may be important sensors of oxidative stress and regulate cellular pools of  $\text{Zn}^{2+}$ <sup>112</sup>. However, the biology role for these organelles and whether they are observable in other cell types remains to be seen.

Although this work identifies TRPM7 as a major regulator of LPS signal transduction and phagosome maturation in macrophages, it does not exclude the possibility that other ion channels play a contributing role. Of note, *Trpm2*-deficient macrophages exhibit phenotypes of high similarity to *Trpm7*-deficient macrophages in our studies, particularly in the case of LPS-mediated responses<sup>104,106</sup>. Studies examining the pharmacological sensitivity of LPS signaling observed that the signal transduction is decreased in the presence of 2-APB, which modulates various ion channels. 2-APB blocks both TRPM2 and TRPM7, which are exceptional amongst TRP channels in this regard<sup>83</sup>. TRPM2 is also a reputed 'chanzyme', with its enzymatic domain modulating channel activity through sensing of  $\text{NAD}^+$ - related metabolite ADPR. TRPM7 kinase has been proposed by others to modulate TRPM7 channel activity<sup>113,119</sup>, but the precise mechanism is unclear. A recent study identified a novel kinase that serves as sensor of bacterial metabolites<sup>225</sup> – this kinase (alpha kinase 1) is highly homologous to TRPM7 kinase, perhaps setting the stage for a regulatory mechanism for TRPM7 channel that is analogous to TRPM2. TRPM7 or TRPM2-dependent metabolite sensing could influence immunity remains unknown. Thus, examining potential interactions between TRPM7 and TRPM2 may reveal novel regulatory mechanisms for ion channels in immunity.

TRPM7 has been implicated in membrane fusion and endocytic events in a variety of cell types and signaling contexts<sup>113,208</sup>. Generally, deletion or inhibition of TRPM7 results in defects in membrane fusion and endocytosis<sup>23,113,226</sup>. Could TRPM7 be a “master regulator” of vesicular trafficking? In the context of other ion channels, TRPM7 *channel* is not uniquely modulated by membrane remodeling or endocytic events<sup>1,18</sup>. However, perhaps the most distinguishing feature of TRPM7 is its serine-threonine *kinase* domain. Although the biological role for the kinase domain is poorly understood, it associates with multiple proteins involved in membrane remodeling. TRPM7 kinase has also been proposed as a key sensor of second messengers<sup>227</sup>, which cue the kinase to impose regulatory activity on the channel itself. Likewise, cleavage of TRPM7 kinase is a unique regulatory feature of the protein<sup>113</sup>. Working in tandem, the kinase may support localization and activation of TRPM7 channel, which in response to the relevant physiological ligand, could help traffic TRPM7 to provide ‘targeted’ electrical activity at pertinent cellular domains. Ultimately, coordination of TRPM7 channel and kinase activities could provide a significant and highly specific ‘enzymatic leverage’ for cellular signaling.

However, to test these (and other) hypotheses, characterizing the subcellular localization of TRPM7 must be resolved. Overexpression studies or use of ‘knock-in’ cell lines derived from cancer cells are useful tools to suggest where TRPM7 may be generally localized within cells. However, these studies do not sufficiently characterize the subcellular endosomes that TRPM7 may localize to or account for the unique morphological characteristics of certain cell types, such as formation of pseudopods or highly-secretory cells. Development of TRPM7 antibodies or generation of loop-inserted immune-epitope tags is essential to defining TRPM7 localization. In the case of the latter, even formation of a functional channel domain risks disrupting key residues for TRPM7 tetramerization, loops involved in ‘gating’ the channel, or protein trafficking. In summary, TRPM7 plays a key ‘sensory’ role in macrophages, and an abundance of exciting opportunities to understand the biological purpose of TRPM7 lie ahead.

## **APPENDIX A: MEASUREMENT OF TLR4 AND CD14 RECEPTOR**

### **ENDOCYTOSIS USING FLOW CYTOMETRY**

#### **Disclaimer:**

The contents of this chapter (text and figures) appear as published in *Bio-protocols*. Minor modifications to the manuscript contents have been made for increased clarity. All work presented herein was performed by myself (Michael Schappe). This work was published with the following citation: Schappe, M. and Desai, B. "Measurement of TLR4 and CD14 Endocytosis Using Flow Cytometry." *Bio-protocols*, 8(14) Jul 2018, DOI: [10.21769/BioProtoc.2926](https://doi.org/10.21769/BioProtoc.2926). All figures and experiments were prepared and performed by MSS.

## Abstract

After recognizing extracellular bacterial lipopolysaccharide (LPS), the toll-like receptor 4 (TLR4)-CD14 signaling complex initiates two distinct signaling pathways—one from the plasma membrane and the other from the signaling endosomes<sup>133</sup>. Understanding the early stages of TLR4 signal transduction therefore requires a robust and quantitative method to measure LPS-triggered TLR4 and CD14 receptor endocytosis, one of the earliest events of LPS detection. Here, we describe a flow cytometry-based method that we used recently to study the role of the ion channel TRPM7 in TLR4 endocytosis<sup>23</sup>. The assay relies on stimulating the cells with LPS and measuring the cell surface levels of TLR4 (or CD14) at various time points using flow cytometry. Although we detail the method specifically for TLR4 and CD14 from murine bone marrow-derived macrophages, it can be readily adapted to evaluate receptor endocytosis in a variety of other signaling contexts.

## Background

Innate immune cells, including macrophages and dendritic cells, employ a variety of pattern recognition receptors (PRRs) to survey their environments for danger- and pathogen-associated molecular patterns. Trafficking and signaling of PRRs from various subcellular compartments enables wider immune surveillance and has emerged as an important design principle of innate immunity<sup>127</sup>. The detection of the bacterial endotoxin LPS is highly dependent on TLR4 and its co-receptor CD14. The endocytosis of the TLR4 complex requires CD14 and is essential for LPS-induced macrophage activation (Zanoni *et al.*, 2011; Tan *et al.*, 2015). Endocytosis of TLR4 is essential to activate secondary signaling complexes at the newly-formed 'signaling endosome,' which promotes interferon regulatory factor 3-dependent transcription through the signaling adaptor TIR-domain containing adapter-inducing interferon- $\beta$  (TRIF)<sup>133</sup>. TLR4 endocytosis has been observed in macrophages, dendritic cells, and epithelial cells<sup>228</sup>. Understanding the underlying mechanisms of this critical step in macrophage activation requires a robust and quantitative method to measure LPS-triggered TLR4 endocytosis. Here, we describe a version of a flow cytometry-based method that was initially reported by Kagan and colleagues<sup>133</sup>, and used by others, to monitor TLR4 endocytosis. We have used the method recently to study the role of transient receptor potential melastatin-like 7 (TRPM7), an ion channel, in TLR4 endocytosis<sup>23</sup>. The experimental logic of this method relies on measuring the loss of TLR4 and CD14 staining at the cell surface after LPS treatment. We stain LPS-treated cells with an anti-TLR4 (or anti-CD14) fluorophore-conjugated antibody without permeabilization. The fluorescence intensity acquired using flow cytometry reports the relative quantity of receptor resident in the plasma membrane (**Figure 31**). Although specific for TLR4 and CD14, the assay can be readily adapted to evaluate receptor endocytosis in a variety of other signaling contexts.

# Materials and Reagents

## A. Materials

1. Pipette tips
2. 5 ml round, disposable round-bottom tube (FACS Tube) (Corning, Falcon®, catalog number: [352052](#))
3. Aluminum foil (Genesee Scientific, catalog number: [88-101](#))
4. 0.2 µm bottle filter (Thermo Fisher Scientific, Nalgene™, catalog number: [566-0020](#))
5. 6-well non-treated culture plates (Corning, catalog number: [3736](#))
6. Sterile cell scrapers (Fisher Scientific, Fisherbrand™, catalog number: [08-100-240](#))
7. Sterile individually packaged serological pipette (10 ml) (Greiner Bio One International, catalog number: [607160](#))
8. Sterile individually packaged serological pipette (5 ml) (Greiner Bio One International, catalog number: [606160](#))
9. 1.7 ml microfuge Eppendorf tubes (Genesee Scientific, Olympus Plastics, catalog number: [24-281](#))
10. Nunc™ TripleFlask™ Treated Cell Culture Flasks (Thermo Fisher Scientific, catalog number: [132867](#))
11. Falcon® 50 ml Conical Centrifuge Tube (Corning, catalog number: [352098](#))

## B. Cell line

1. L-929 cells (ATCC, catalog number: [CCL-1](#))

## C. Reagents

1. LPS EB-Ultrapure (lipopolysaccharide from *E. coli* O111:B4, InvivoGen, catalog number: [tlrl-3pelps](#))
2. PBS (Thermo Fisher Scientific, Gibco™, catalog number: [10010023](#))
3. Mouse TruStain fcX™ (anti-CD16/32) (BioLegend, catalog number: [101320](#))

4. TLR4 [anti-mouse CD284] (PE) (clone: SA15-21; isotype: Rat IgG2a,  $\kappa$ ) (BioLegend, catalog number: [145404](#))
5. CD14 [anti-mouse] (APC) (clone: Sa2-8; isotype: Rat IgG2a,  $\kappa$ ) (Thermo Fisher Scientific, eBioscience™, catalog number: [17-0141-81](#))
6. RPMI 1640 (Thermo Fisher Scientific, Gibco™, catalog number: [11875093](#))
7. Fetal bovine serum (heat-inactivated), certified, USA origin (Thermo Fisher Scientific, Gibco™, catalog number: [10082147](#))
8. Trypan blue (Thermo Fisher Scientific, Gibco™, catalog number: [15250061](#))
9. HBSS, no calcium, no magnesium (Thermo Fisher Scientific, Gibco™, catalog number: [14170112](#))
10. BSA (Bovine serum albumin) (Roche Molecular Systems, catalog number: 3116956001)
11. DMEM, high glucose (Thermo Fisher Scientific, Gibco™, catalog number: [11965092](#))
12. BMDM Media (see Recipes)
13. Culture Media (see Recipes)
14. Treatment Media (see Recipes)
15. FACS Buffer (see Recipes)
16. L929-conditioned media (see Recipes)

## Equipment

1. TC20 Automated cell counter (Bio-Rad Laboratories, catalog number: [1450102](#))
2. Pipet-aid Pipette Controller (Drummond Scientific, catalog number: [4-000-101](#))
3. 4 °C Cold Room
4. 4 °C Benchtop centrifuge
5. 37 °C Cell Culture Incubator with CO<sub>2</sub> control
6. Sterile cell culture hood
7. Flow Cytometer (BD, model: [FACSCanto™ II](#), or equivalent)

## Software

1. GraphPad Prism 7 (Graph Pad Software; La Jolla, CA USA)

## Procedure

1. Day 0, Cell culture
  - a. Collect cultured bone marrow-derived macrophages (BMDMs) by gentle scraping. Disperse the cells into a single-cell suspension by repeatedly running the pipetted cell suspension along the test tube walls. Centrifuge cells (400 x g, 5 min, 23 °C), aspirate supernatant, and resuspend cell pellet in BMDM media. Count live cells via trypan blue exclusion assay.
  - b. Plate  $0.5 \times 10^6$  cells/well in a 6-well, non-treated, tissue culture plate. Culture the cells overnight in 2 ml/well of BMDM media. After 16 h of incubation (37 °C, 5% CO<sub>2</sub>), cells should be adherent and ready for the experiment.
2. Day 1, Preparation before LPS stimulation
  - a. Prepare Culture and Treatment Media as described in Recipes. Warm the LPS-containing treatment media to 37 °C prior to use.
  - b. Chill sterile PBS, 1.5 ml Eppendorf tubes, and FACS buffer to 4 °C, prior to use. After LPS treatment, the cells will be collected using these solutions and tubes.
3. Day 1, LPS stimulation of cells
  - a. Aspirate BMDM media and wash 3 x with 3 ml of HBSS (room temperature) to remove dead cells and debris from each well. Add HBSS down the wall of the culture well and gently swirl plate to wash.

- b. Gently add 2 ml of Culture Media to wells labeled “Unstained BMDMs” and “ $t = 0$  min/Untreated” treatment groups.
  - c. Gently add 2 ml of Treatment Media to each well by pipetting the media along the side of the wells. Gently swirl the plate to ensure that the media is evenly distributed in the wells.
  - d. Incubate at 37 °C for desired time points. Repeat Steps 3a to 3c as necessary for remaining LPS-treatment groups. Stagger the LPS treatment such that all samples are harvested at the same time.
4. Day 1, Cell collection and antibody staining
- Note: All reagents should be cold and the procedure should be performed at 4 °C (cold room).*
- a. Transfer plates treated in Step 3 to 4 °C for 5 min prior to collection – this is required to arrest endocytosis.
  - b. Aspirate media from each well. Wash 2 x each with 2 ml of sterile, pre-chilled PBS.
  - c. Add 1 ml of sterile, pre-chilled PBS to each well. Gently scrape to detach cells and pipette-mix to disperse the cells into a single cell suspension.
  - d. Transfer the cell suspension to 1.5 ml Eppendorf tubes and centrifuge (400 x g, 5 min) to pellet the cells.
  - e. After aspirating and discarding the supernatant, resuspend the cell pellet in 50 µl of cold FACS Buffer premixed with TruStain fcX™ antibody (1 µg/ml), for 10 min.
  - f. Add 50 µl of the 2x-concentrate of antibody (anti-TLR4 or anti-CD14; see **Table 4**) in FACS Buffer to the cell suspension. Add 50 µl of FACS Buffer to “Unstained BMDMs” samples.
  - g. Pipette gently to mix and stain for 20 min in the dark.

- h. Add 1 ml of FACS Buffer, collect cells by centrifugation (400 x g, 5 min) and aspirate supernatant to remove excess antibody.
- i. Resuspend the cell pellet in 200 µl of FACS Buffer and transfer the cell suspension to FACS tubes. Keep samples on ice and in the dark (e.g., cover with aluminum foil) prior to measurement by flow cytometry.
- j. Analyze samples via flow cytometry within 1 h.

## Data analysis

1. Flow cytometry analysis
  - a. For flow cytometry analysis, collect > 100,000 events for each sample.
  - b. For analysis, the events are gated on FSC-A and SSC-A bivariate cytographs; the low FSC-SSC events comprising of dead cells and cellular debris are excluded from analysis. Cells are then gated on FSC-A and FSC-H to gate on single cells.
  - c. These cells can then be visualized for the intensity of the antibody stain as a histogram. Fluorescent intensity of the antibody stain on the gated population is recorded as the geometric mean of the cell population, or mean fluorescent intensity (MFI).
2. Data analysis for the measurement of TLR4 and CD14 Endocytosis
  - a. For data analysis, the MFI of “Unstained cells” can be used for background subtraction from all samples [“Background Subtracted MFI”]. Divide the “background subtracted MFI” value for a given time point by the “Unstimulated [t = 0 min]” sample; “t = 0 min” value should be 1.00. Repeat this for all subsequent experimental samples to determine “Relative % of surface expression” relative to the “Unstimulated [t = 0 min]” sample. All sample values reflect the ratio of MFI from stimulated to unstimulated cells at desired time points.

- b. We convert the “Relative % of surface expression” value to a percentage; Thus, the “Untreated” or “Time = 0 min” sample should equal ‘100% percentage of surface expression’. One expects to see a steady reduction in this value at various time points after LPS stimulation.
  - c. Since MFI values are sensitive to variations in flow cytometry calibrations, we recommend that data analysis be confined to each independent experiment and each condition run in technical triplicate. “Percentage of surface expression” should be reproducible across independent experiments and therefore amenable to statistical analysis of multiple experiments. Results from a typical experiment are shown in **Figure 32**. The original data presentation and additional information are available in our manuscript, which originally utilized the protocol described herein [PubMed](#).
3. For experimental and statistical analysis, we use GraphPad Prism. To compare two experimental groups, we use a Student’s *t*-test. For comparison of three or more data groups, other statistical analysis, such as a one-way ANOVA, are necessary.

## Notes

1. The murine macrophage RAW 264.7 cell line also exhibits characteristic TLR4 endocytosis – it can be used to establish the method and for experiments.
2. Although non-treated culture plates may permit detachment with trypsin, the enzymatic detachment may alter macrophage epitope expression at the plasma membrane.
3. Performing “Procedure” Step 4 in a walk-in 4 °C cold room greatly improves the quality of data. Although chilling materials and reagents on ice may be convenient, variations in

temperature between the ice, samples, and ambient laboratory air may inadvertently warm samples above 4 °C, thereby permitting endocytosis to proceed.

4. Although procedural steps after “Procedure” Step 3d are not performed under sterile conditions, using sterile reagents minimizes inadvertent contamination with ligands that may promote TLR4 or CD14 endocytosis.
5. Although spectrally non-overlapping fluorophores are available, we advise staining with a single anti-TLR4 or CD14 antibody for each experiment.
6. With careful spectral consideration, fluorescent live/dead dyes can be included in this assay to enrich for live cell populations. If the experimenter includes these dyes, we advise that only spectrally-compatible nucleic acid binding dyes, which can rapidly label dead cells during the final suspension be used. Some viability dyes and staining methods (such as “live/dead fixable dyes” or Annexin V-based staining kits) require additional staining steps that may compromise the time and temperature-sensitivity of this assay.
7. Titration of antibodies, including new batches of the same antibody clone, is essential. Although recommendations are provided in Table 1, improper staining will limit signal-to-noise ratio (SNR) in the assay and lower data quality in terms of sensitivity and consistency.
8. Avoid sample groups larger than 24 samples to minimize sample processing time prior to flow cytometry analysis.
9. The majority of our data were collected on the BD FACSCanto II flow cytometer.

## Recipes

1. BMDM Media
  - a. RPMI 1640 + 10% FBS + 20% L929-conditioned media

- b. Store at 4 °C for up to 1 month
- 2. Culture Media
  - a. RPMI 1640 + 10% FBS
  - b. Store at 4 °C for up to 1 month
- 3. Treatment Media
  - a. RPMI 1640 + 10% FBS + 1 µg/ml LPS
  - b. Prepare fresh for each experiment
- 4. FACS Buffer
  - a. PBS + 1% BSA
  - b. Sterile filter buffer through 0.22 µm filter prior to use
  - c. Store at 4 °C for up to 1 week
- 5. L929-conditioned Media

*Note: Generated from the culture of L-929 cells (available from ATCC). Cells are passaged according to the vendor's instructions and cultured in DMEM, high glucose + 10% FBS.*

- a. To generate L929-conditioned media, add 150 ml of DMEM, high glucose + 10% FBS to a T-150 TripleFlask. Add  $0.72 \times 10^6$  L-929 cells and carefully mix by equilibrating the media volume at the hole in the corner of the flask. Culture for 7 days at 37 °C, 5% CO<sub>2</sub>
- b. On Day 7, collect media, sterile filter through a 0.22 µm filter into a flask, and store at -20 °C ["Week 1 media"]; add 150 ml of DMEM, high glucose + 10% FBS to TripleFlask to replace collected media
- c. On Day 14, collect media from the flask and sterile filter through a 0.22 µm filter ["Week 2 media"]. Thaw Week 1 media at 23 °C
- d. Combine Week 1 and Week 2 media and aliquot into 50 ml tubes. L929-conditioned media is stored at -20 °C for up to 6 months

## **Acknowledgments**

We would like to thank Dr. Jonathan Kagan (Boston Children's Hospital) and colleagues whose protocol (cited herein) we adapted for our research. We also would like to thank members of the Desai laboratory for their assistance in editing this manuscript. We also thank the UVA Flow Cytometry Core and Carter Immunology Center Flow Cytometry Core. We appreciate our funding that supported this work: grants GM108989 (BND) and 5T32GM007055-41 (MSS) from the National Institutes of Health.

**FIGURES:** Appendix A

**Figure 31. Schematic of TLR4 and CD14 endocytosis protocol**

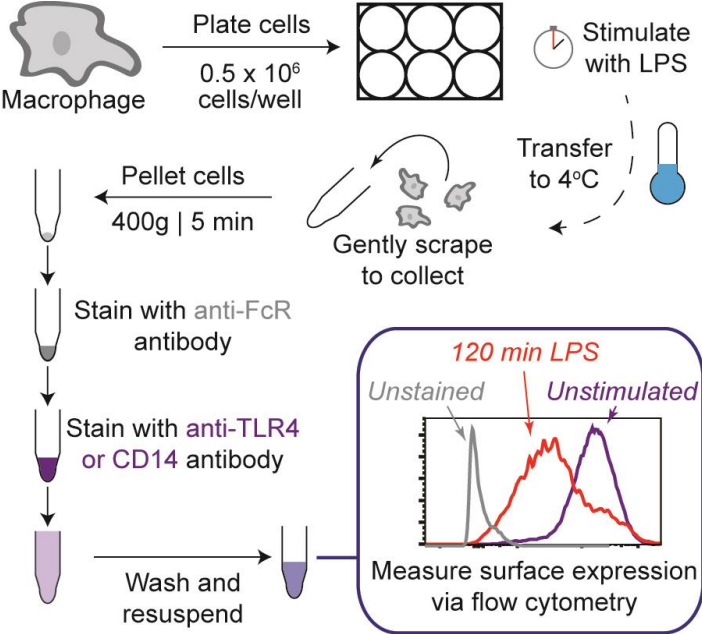


**Figure 31. Schematic of TLR4 and CD14 endocytosis protocol.**

Experimental workflow described in protocol “Procedure”.

**Figure 32. TLR4 and CD14 receptor endocytosis data analysis and suggested presentation.**

**A.**

Relative percentage of surface receptor at given timepoint  $x$  :

$$\text{TLR4 or CD14 receptor endocytosis} : \frac{\text{MFI}_{x \text{ time}} - \text{MFI}_{\text{Unstained}}}{\text{MFI}_{0 \text{ min}} - \text{MFI}_{\text{Unstained}}} \times 100\%$$

**B.**

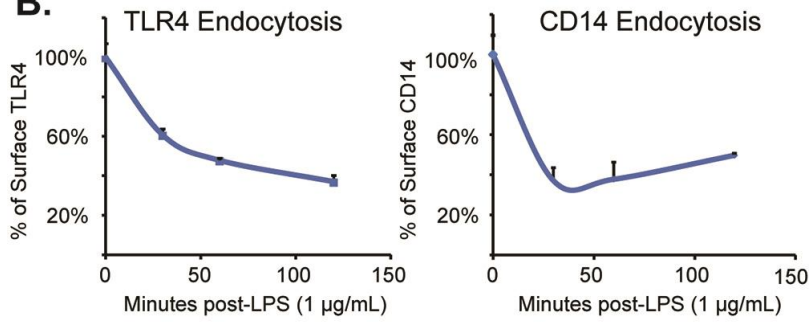


**Figure 32. TLR4 and CD14 receptor endocytosis data analysis and suggested presentation.**

A. “Data analysis” calculation described as a formula.

B. Characteristic TLR4 and CD14 endocytosis measured over time in bone-marrow derived macrophages. Data was modified from its original presentation in Schappe *et al.*, 2018 with author permission.

**Table 6. Antibodies used for measuring TLR4 and CD14 endocytosis**

<b>Antibody</b>	<b>Clone</b>	<b>Suggested Final Concentration</b>	<b>Notes</b>
Anti-TLR4	SA15-21 (anti-mouse)	0.2 µg/ml	Recognizes TLR4 independent of LPS-receptor complex formation
Anti-CD14	Sa2-8 (anti-mouse)	0.4 µg/ml	Recognizes CD14

## RESULTING PUBLICATIONS

**Schappe, M\***. and Desai, B. Measurement of TLR4 and CD14 Endocytosis Using Flow Cytometry. *Bio-protocols*, 8(14) Jul 2018. DOI: [10.21769/BioProtoc.2926](https://doi.org/10.21769/BioProtoc.2926)

\*Corresponding author

**Schappe, M.**, Sztejn, K., Stremaska, M., Mendu, S., Downs, T., Seegren, P. Mahoney, M., Dixit, S., Krupa, J., Stipes, E., Rogers, J., Adamson, S., Leitinger, N., Desai, B. Chanzyme TRPM7 mediates Ca<sup>2+</sup> influx necessary for LPS-induced TLR4 endocytosis and macrophage activation. *Immunity*, 48(1):59-74e5, Jan 2018.  
DOI:[10.1016/j.immuni.2017.11.026](https://doi.org/10.1016/j.immuni.2017.11.026)

\*Featured commentary by F. Granucci (*Immunity*, 2018)

\*Ted W. Rall Award for Outstanding Publication in Pharmacology (UVA, 2018)

**Schappe, M.**, Downs, T., Mendu, S., Flegal, Z., Stipes, E., Stremaska, M., Seegren, P., Desai, B. "Efferocytosis requires periphagosomal Ca<sup>2+</sup> signaling and TRPM7-mediated electrical activity." (Under review - *eLife*).

**Schappe, M.** and Desai, B. Ion channels and regulation of innate immunity. (Manuscript in preparation)

## ADDITIONAL PUBLICATIONS

Serbulea, V., Upchurch, C., **Schappe, M.**, Voigt, P., DeWeese, D., Desai, B., Meher, A., Leitinger, N. Macrophage phenotype and bioenergetics are controlled by oxidized phospholipids identified in lean and obese adipose tissue. *Proceedings of the National Academy of Sciences*, June 2018. DOI: [10.1073/pnas.1800544115](https://doi.org/10.1073/pnas.1800544115)

Chiu, Y., **Schappe, M.**, Desai, B., Bayliss, D. Revisiting multimodal activation and channel properties of Pannexin 1. *The Journal of General Physiology*, 150(1):19-39, Jan 2018. DOI: [10.1085/jgp.201711888](https://doi.org/10.1085/jgp.201711888)

Weaver, J., Arandjelovic, S., Brown, G., Mendu, S., **Schappe, M.**, Buckley, M., Chiu, Y., Shu, S., Kim, J., Chung, J., Krupa, J., Jevtovic-Todorovic, V., Desai, B., Ravichandran, K., Bayliss, D. Hematopoietic pannexin 1 function is critical for neuropathic pain. *Scientific Reports*, 7:42550, Feb 2017. DOI: [10.1038/srep42550](https://doi.org/10.1038/srep42550)

Mendu, S., **Schappe, M.**, Moser, E., Krupa, J., Rogers, J., Stipes, E., Parker, C., Braciale, T., Desai, B. Chanzyme TRPM7 controls thymic development of Treg cells by regulating STAT5 activation. (Under Review - *Science Signaling*)

## REFERENCES

- 1 Feske, S., Wulff, H. & Skolnik, E. Y. Ion channels in innate and adaptive immunity. *Annu Rev Immunol* **33**, 291-353, doi:10.1146/annurev-immunol-032414-112212 (2015).
- 2 Janssen, W. J., Bratton, D. L., Jakubzick, C. V. & Henson, P. M. Myeloid Cell Turnover and Clearance. *Microbiology spectrum* **4**, 10.1128/microbiolspec.MCHD-0005-2015, doi:10.1128/microbiolspec.MCHD-0005-2015 (2016).
- 3 Ginhoux, F. & Jung, S. Monocytes and macrophages: developmental pathways and tissue homeostasis. *Nature reviews. Immunology* **14**, 392-404, doi:10.1038/nri3671 (2014).
- 4 Gouaux, E. & Mackinnon, R. Principles of selective ion transport in channels and pumps. *Science* **310**, 1461-1465, doi:10.1126/science.1113666 (2005).
- 5 The International Transporter, C. *et al.* Membrane transporters in drug development. *Nature Reviews Drug Discovery* **9**, 215, doi:10.1038/nrd3028 (2010).
- 6 Lin, L., Yee, S. W., Kim, R. B. & Giacomini, K. M. SLC transporters as therapeutic targets: emerging opportunities. *Nature Reviews Drug Discovery* **14**, 543, doi:10.1038/nrd4626 (2015).
- 7 Verkman, A. S., Anderson, M. O. & Papadopoulos, M. C. Aquaporins: important but elusive drug targets. *Nature Reviews Drug Discovery* **13**, 259, doi:10.1038/nrd4226 (2014).
- 8 Prakiya, M. & Lewis, R. S. Separation and characterization of currents through store-operated CRAC channels and Mg<sup>2+</sup>-inhibited cation (MIC) channels. *The Journal of General Physiology* **119**, 487-508 (2002).
- 9 Clapham, D. E. TRP channels as cellular sensors. *Nature* **426**, 517-524, doi:10.1038/nature02196 (2003).

- 10 Naccache, P. H., Showell, H. J., Becker, E. L. & Sha'afi, R. I. Involvement of membrane calcium in the response of rabbit neutrophils to chemotactic factors as evidenced by the fluorescence of chlorotetracycline. *The Journal of cell biology* **83**, 179-186 (1979).
- 11 Pope, S. D. & Medzhitov, R. Emerging Principles of Gene Expression Programs and Their Regulation. *Molecular cell* **71**, 389-397, doi:10.1016/j.molcel.2018.07.017 (2018).
- 12 Underhill, D. M. & Goodridge, H. S. Information processing during phagocytosis. *Nature reviews. Immunology* **12**, 492-502, doi:10.1038/nri3244 (2012).
- 13 Kieser, K. J. & Kagan, J. C. Multi-receptor detection of individual bacterial products by the innate immune system. *Nature reviews. Immunology* **17**, 376-390, doi:10.1038/nri.2017.25 (2017).
- 14 Vig, M. & Kinet, J. P. Calcium signaling in immune cells. *Nature immunology* **10**, 21-27, doi:10.1038/ni.f.220 (2009).
- 15 Serezani, C. H., Ballinger, M. N., Aronoff, D. M. & Peters-Golden, M. Cyclic AMP: master regulator of innate immune cell function. *American journal of respiratory cell and molecular biology* **39**, 127-132, doi:10.1165/rcmb.2008-0091TR (2008).
- 16 Bridgeman, A. *et al.* Viruses transfer the antiviral second messenger cGAMP between cells. *Science* **349**, 1228-1232, doi:10.1126/science.aab3632 (2015).
- 17 Dennis, E. A. & Norris, P. C. Eicosanoid storm in infection and inflammation. *Nature Reviews Immunology* **15**, 511, doi:10.1038/nri3859 (2015).
- 18 Ramsey, I. S., Delling, M. & Clapham, D. E. An introduction to TRP channels. *Annual review of physiology* **68**, 619-647, doi:10.1146/annurev.physiol.68.040204.100431 (2006).
- 19 Voets, T., Talavera, K., Owsianik, G. & Nilius, B. Sensing with TRP channels. *Nature Chemical Biology* **1**, 85, doi:10.1038/nchembio0705-85 (2005).

- 20 Dolmetsch, R. E., Xu, K. & Lewis, R. S. Calcium oscillations increase the efficiency and specificity of gene expression. *Nature* **392**, 933-936, doi:10.1038/31960 (1998).
- 21 Dolmetsch, R. E., Lewis, R. S., Goodnow, C. C. & Healy, J. I. Differential activation of transcription factors induced by Ca<sup>2+</sup> response amplitude and duration. *Nature* **386**, 855-858, doi:10.1038/386855a0 (1997).
- 22 Altman, A. & Kong, K.-F. Protein Kinase C Enzymes in the Hematopoietic and Immune Systems. *Annual Review of Immunology* **34**, 511-538, doi:10.1146/annurev-immunol-041015-055347 (2016).
- 23 Schappe, M. S. *et al.* Chanzyme TRPM7 Mediates the Ca<sup>(2+)</sup> Influx Essential for Lipopolysaccharide-Induced Toll-Like Receptor 4 Endocytosis and Macrophage Activation. *Immunity* **48**, 59-74.e55, doi:10.1016/j.immuni.2017.11.026 (2018).
- 24 Kagan, J. C. & Medzhitov, R. Phosphoinositide-mediated adaptor recruitment controls Toll-like receptor signaling. *Cell* **125**, 943-955, doi:10.1016/j.cell.2006.03.047 (2006).
- 25 Zanoni, I. *et al.* CD14 controls the LPS-induced endocytosis of Toll-like receptor 4. *Cell* **147**, 868-880, doi:10.1016/j.cell.2011.09.051 (2011).
- 26 Chiang, C. Y., Veckman, V., Limmer, K. & David, M. Phospholipase C $\gamma$ -2 and intracellular calcium are required for lipopolysaccharide-induced Toll-like receptor 4 (TLR4) endocytosis and interferon regulatory factor 3 (IRF3) activation. *The Journal of biological chemistry* **287**, 3704-3709, doi:10.1074/jbc.C111.328559 (2012).
- 27 Gallin, E. K., Wiederhold, M. L., Lipsky, P. E. & Rosenthal, A. S. Spontaneous and induced membrane hyperpolarizations in macrophages. *J Cell Physiol* **86 Suppl 2**, 653-661 (1975).
- 28 Miles, P. R., Bowman, L. & Castranova, V. Transmembrane potential changes during phagocytosis in rat alveolar macrophages. *J Cell Physiol* **106**, 109-117, doi:10.1002/jcp.1041060112 (1981).

- 29 Kitagawa, S. *et al.* Functional maturation of membrane potential changes and superoxide-producing capacity during differentiation of human granulocytes. *The Journal of clinical investigation* **73**, 1062-1071, doi:10.1172/jci111291 (1984).
- 30 Ypey, D. L. & Clapham, D. E. Development of a delayed outward-rectifying K<sup>+</sup> conductance in cultured mouse peritoneal macrophages. *Proceedings of the National Academy of Sciences of the United States of America* **81**, 3083-3087 (1984).
- 31 Buisman, H. P. *et al.* Extracellular ATP induces a large nonselective conductance in macrophage plasma membranes. *Proceedings of the National Academy of Sciences of the United States of America* **85**, 7988-7992 (1988).
- 32 Steinberg, B. E., Touret, N., Vargas-Caballero, M. & Grinstein, S. In situ measurement of the electrical potential across the phagosomal membrane using FRET and its contribution to the proton-motive force. *Proceedings of the National Academy of Sciences of the United States of America* **104**, 9523-9528, doi:10.1073/pnas.0700783104 (2007).
- 33 Steinberg, B. E. *et al.* A cation counterflux supports lysosomal acidification. *The Journal of cell biology* **189**, 1171-1186, doi:10.1083/jcb.200911083 (2010).
- 34 Black, Joel A. & Waxman, Stephen G. Noncanonical Roles of Voltage-Gated Sodium Channels. *Neuron* **80**, 280-291, doi:<https://doi.org/10.1016/j.neuron.2013.09.012> (2013).
- 35 Grinstein, S., Clarke, C. A., Dupre, A. & Rothstein, A. Volume-induced increase of anion permeability in human lymphocytes. *The Journal of General Physiology* **80**, 801-823, doi:10.1085/jgp.80.6.801 (1982).
- 36 Voss, F. K. *et al.* Identification of LRRC8 Heteromers as an Essential Component of the Volume-Regulated Anion Channel VRAC. *Science* **344**, 634-638, doi:10.1126/science.1252826 (2014).

- 37 Pedersen, S. F., Klausen, T. K. & Nilius, B. The identification of a volume-regulated anion channel: an amazing Odyssey. *Acta Physiol (Oxf)* **213**, 868-881, doi:10.1111/apha.12450 (2015).
- 38 Sawada, A. *et al.* A congenital mutation of the novel gene LRRC8 causes agammaglobulinemia in humans. *The Journal of clinical investigation* **112**, 1707-1713, doi:10.1172/JCI18937 (2003).
- 39 Behe, P. *et al.* The LRRC8A Mediated "Swell Activated" Chloride Conductance Is Dispensable for Vacuolar Homeostasis in Neutrophils. *Frontiers in pharmacology* **8**, 262-262, doi:10.3389/fphar.2017.00262 (2017).
- 40 Kubo, Y., Baldwin, T. J., Jan, Y. N. & Jan, L. Y. Primary structure and functional expression of a mouse inward rectifier potassium channel. *Nature* **362**, 127-133, doi:10.1038/362127a0 (1993).
- 41 Vicente, R. *et al.* Differential voltage-dependent K<sup>+</sup> channel responses during proliferation and activation in macrophages. *The Journal of biological chemistry* **278**, 46307-46320, doi:10.1074/jbc.M304388200 (2003).
- 42 Hanley, P. J. *et al.* Extracellular ATP induces oscillations of intracellular Ca<sup>2+</sup> and membrane potential and promotes transcription of IL-6 in macrophages. *Proceedings of the National Academy of Sciences of the United States of America* **101**, 9479-9484, doi:10.1073/pnas.0400733101 (2004).
- 43 Toyama, K. *et al.* The intermediate-conductance calcium-activated potassium channel KCa3.1 contributes to atherogenesis in mice and humans. *The Journal of clinical investigation* **118**, 3025-3037, doi:10.1172/jci30836 (2008).
- 44 Guo, J. *et al.* Structures of the calcium-activated, non-selective cation channel TRPM4. *Nature* **552**, 205-209, doi:10.1038/nature24997 (2017).

- 45 Serafini, N. *et al.* The TRPM4 channel controls monocyte and macrophage, but not neutrophil, function for survival in sepsis. *Journal of immunology* **189**, 3689-3699, doi:10.4049/jimmunol.1102969 (2012).
- 46 Barbet, G. *et al.* The calcium-activated nonselective cation channel TRPM4 is essential for the migration but not the maturation of dendritic cells. *Nature immunology* **9**, 1148-1156, doi:10.1038/ni.1648 (2008).
- 47 Miller, D. J. Sydney Ringer; physiological saline, calcium and the contraction of the heart. *The Journal of physiology* **555**, 585-587, doi:10.1113/jphysiol.2004.060731 (2004).
- 48 Clapham, D. E. Calcium signaling. *Cell* **131**, 1047-1058, doi:10.1016/j.cell.2007.11.028 (2007).
- 49 Wuytack, F., Raeymaekers, L. & Missiaen, L. Molecular physiology of the SERCA and SPCA pumps. *Cell Calcium* **32**, 279-305 (2002).
- 50 Efremov, R. G., Leitner, A., Aebersold, R. & Raunser, S. Architecture and conformational switch mechanism of the ryanodine receptor. *Nature* **517**, 39-43, doi:10.1038/nature13916 (2015).
- 51 Stolk, M., Leon-Ponte, M., Merrill, M., Ahern, G. P. & O'Connell, P. J. IP3Rs are sufficient for dendritic cell Ca<sup>2+</sup> signaling in the absence of RyR1. *Journal of leukocyte biology* **80**, 651-658, doi:10.1189/jlb.1205739 (2006).
- 52 Kushnir, A., Betzenhauser, M. J. & Marks, A. R. Ryanodine receptor studies using genetically engineered mice. *FEBS letters* **584**, 1956-1965, doi:10.1016/j.febslet.2010.03.005 (2010).
- 53 Prakriya, M. *et al.* Orai1 is an essential pore subunit of the CRAC channel. *Nature* **443**, 230-233, doi:10.1038/nature05122 (2006).
- 54 Bagur, R. & Hajnoczky, G. Intracellular Ca<sup>2+</sup> Sensing: Its Role in Calcium Homeostasis and Signaling. *Molecular cell* **66**, 780-788, doi:10.1016/j.molcel.2017.05.028 (2017).

- 55 Park, C. Y. *et al.* STIM1 Clusters and Activates CRAC Channels via Direct Binding of a Cytosolic Domain to Orai1. *Cell* **136**, 876-890, doi:<https://doi.org/10.1016/j.cell.2009.02.014> (2009).
- 56 Feske, S. *et al.* A mutation in Orai1 causes immune deficiency by abrogating CRAC channel function. *Nature* **441**, 179-185, doi:10.1038/nature04702 (2006).
- 57 Vaeth, M. *et al.* Ca<sup>2+</sup> Signaling but Not Store-Operated Ca<sup>2+</sup> Entry Is Required for the Function of Macrophages and Dendritic Cells. *Journal of immunology* **195**, 1202-1217, doi:10.4049/jimmunol.1403013 (2015).
- 58 Braun, A. *et al.* STIM1 is essential for Fcγ receptor activation and autoimmune inflammation. *Blood* **113**, 1097-1104, doi:10.1182/blood-2008-05-158477 (2009).
- 59 Nunes, P. *et al.* STIM1 juxtaposes ER to phagosomes, generating Ca<sup>2+</sup> hotspots that boost phagocytosis. *Current biology : CB* **22**, 1990-1997, doi:10.1016/j.cub.2012.08.049 (2012).
- 60 Nunes-Hasler, P. *et al.* STIM1 promotes migration, phagosomal maturation and antigen cross-presentation in dendritic cells. *Nature communications* **8**, 1852, doi:10.1038/s41467-017-01600-6 (2017).
- 61 Kinchen, J. M. & Ravichandran, K. S. Phagosome maturation: going through the acid test. *Nature reviews. Molecular cell biology* **9**, 781-795, doi:10.1038/nrm2515 (2008).
- 62 Cardenas, C. *et al.* Essential regulation of cell bioenergetics by constitutive InsP3 receptor Ca<sup>2+</sup> transfer to mitochondria. *Cell* **142**, 270-283, doi:10.1016/j.cell.2010.06.007 (2010).
- 63 Demaurex, N. & Nunes, P. The role of STIM and ORAI proteins in phagocytic immune cells. *American Journal of Physiology-Cell Physiology* **310**, C496-C508, doi:10.1152/ajpcell.00360.2015 (2016).

- 64 Qureshi, O. S., Paramasivam, A., Yu, J. C. & Murrell-Lagnado, R. D. Regulation of P2X4 receptors by lysosomal targeting, glycan protection and exocytosis. *Journal of cell science* **120**, 3838-3849, doi:10.1242/jcs.010348 (2007).
- 65 Yamamoto, K. *et al.* Impaired flow-dependent control of vascular tone and remodeling in P2X4-deficient mice. *Nature medicine* **12**, 133-137, doi:10.1038/nm1338 (2006).
- 66 Csoka, B. *et al.* Macrophage P2X4 receptors augment bacterial killing and protect against sepsis. *JCI insight* **3**, doi:10.1172/jci.insight.99431 (2018).
- 67 Di Virgilio, F., Dal Ben, D., Sarti, A. C., Giuliani, A. L. & Falzoni, S. The P2X7 Receptor in Infection and Inflammation. *Immunity* **47**, 15-31, doi:10.1016/j.immuni.2017.06.020 (2017).
- 68 Pippel, A. *et al.* Localization of the gate and selectivity filter of the full-length P2X7 receptor. *Proceedings of the National Academy of Sciences* **114**, E2156-E2165, doi:10.1073/pnas.1610414114 (2017).
- 69 Harkat, M. *et al.* On the permeation of large organic cations through the pore of ATP-gated P2X receptors. *Proceedings of the National Academy of Sciences* **114**, E3786-E3795, doi:10.1073/pnas.1701379114 (2017).
- 70 Karasawa, A., Michalski, K., Mikhelzon, P. & Kawate, T. The P2X7 receptor forms a dye-permeable pore independent of its intracellular domain but dependent on membrane lipid composition. *eLife* **6**, doi:10.7554/eLife.31186 (2017).
- 71 Muñoz-Planillo, R. *et al.* K<sup>+</sup> Efflux Is the Common Trigger of NLRP3 Inflammasome Activation by Bacterial Toxins and Particulate Matter. *Immunity* **38**, 1142-1153, doi:<https://doi.org/10.1016/j.immuni.2013.05.016> (2013).
- 72 Karmakar, M., Katsnelson, M. A., Dubyak, G. R. & Pearlman, E. Neutrophil P2X7 receptors mediate NLRP3 inflammasome-dependent IL-1 $\beta$  secretion in response to ATP. *Nature communications* **7**, 10555, doi:10.1038/ncomms10555 (2016).

- 73 Solle, M. *et al.* Altered cytokine production in mice lacking P2X(7) receptors. *The Journal of biological chemistry* **276**, 125-132, doi:10.1074/jbc.M006781200 (2001).
- 74 Coste, B. *et al.* Piezo1 and Piezo2 are essential components of distinct mechanically activated cation channels. *Science* **330**, 55-60, doi:10.1126/science.1193270 (2010).
- 75 Coste, B. *et al.* Piezo proteins are pore-forming subunits of mechanically activated channels. *Nature* **483**, 176, doi:10.1038/nature10812 (2012).
- 76 Murthy, S. E., Dubin, A. E. & Patapoutian, A. Piezos thrive under pressure: mechanically activated ion channels in health and disease. *Nature reviews. Molecular cell biology* **18**, 771-783, doi:10.1038/nrm.2017.92 (2017).
- 77 Jiang, D., Zhao, L. & Clapham, D. E. Genome-Wide RNAi Screen Identifies Letm1 as a Mitochondrial Ca<sup>2+</sup>/H<sup>+</sup> Antiporter. *Science* **326**, 144-147, doi:10.1126/science.1175145 (2009).
- 78 Kirichok, Y., Krapivinsky, G. & Clapham, D. E. The mitochondrial calcium uniporter is a highly selective ion channel. *Nature* **427**, 360, doi:10.1038/nature02246 (2004).
- 79 Baughman, J. M. *et al.* Integrative genomics identifies MCU as an essential component of the mitochondrial calcium uniporter. *Nature* **476**, 341, doi:10.1038/nature10234 (2011).
- 80 Denton, R. M. Regulation of mitochondrial dehydrogenases by calcium ions. *Biochimica et Biophysica Acta (BBA) - Bioenergetics* **1787**, 1309-1316, doi:<https://doi.org/10.1016/j.bbabi.2009.01.005> (2009).
- 81 Kamer, K. J. & Mootha, V. K. The molecular era of the mitochondrial calcium uniporter. *Nature reviews. Molecular cell biology* **16**, 545-553, doi:10.1038/nrm4039 (2015).
- 82 Zhang, X., Hu, M., Yang, Y. & Xu, H. Organellar TRP channels. *Nat Struct Mol Biol* **25**, 1009-1018, doi:10.1038/s41594-018-0148-z (2018).

- 83 Nilius, B. & Szallasi, A. Transient receptor potential channels as drug targets: from the science of basic research to the art of medicine. *Pharmacological reviews* **66**, 676-814, doi:10.1124/pr.113.008268 (2014).
- 84 Bautista, D. M. *et al.* The menthol receptor TRPM8 is the principal detector of environmental cold. *Nature* **448**, 204, doi:10.1038/nature05910 (2007).
- 85 Ferguson, S. S. G. Evolving Concepts in G Protein-Coupled Receptor Endocytosis: The Role in Receptor Desensitization and Signaling. *Pharmacological reviews* **53**, 1-24 (2001).
- 86 Neeper, M. P. *et al.* Activation Properties of Heterologously Expressed Mammalian TRPV2: EVIDENCE FOR SPECIES DEPENDENCE. *Journal of Biological Chemistry* **282**, 15894-15902, doi:10.1074/jbc.M608287200 (2007).
- 87 Szollosi, A. G. *et al.* Transient receptor potential vanilloid-2 mediates the effects of transient heat shock on endocytosis of human monocyte-derived dendritic cells. *FEBS letters* **587**, 1440-1445, doi:10.1016/j.febslet.2013.03.027 (2013).
- 88 Link, T. M. *et al.* TRPV2 has a pivotal role in macrophage particle binding and phagocytosis. *Nature immunology* **11**, 232-239, doi:10.1038/ni.1842 (2010).
- 89 Zhou, Y. *et al.* SIGNAL TRANSDUCTION. Membrane potential modulates plasma membrane phospholipid dynamics and K-Ras signaling. *Science* **349**, 873-876, doi:10.1126/science.aaa5619 (2015).
- 90 Watanabe, H. *et al.* Anandamide and arachidonic acid use epoxyeicosatrienoic acids to activate TRPV4 channels. *Nature* **424**, 434, doi:10.1038/nature01807 (2003).
- 91 Luo, J. *et al.* Transient receptor potential vanilloid 4-expressing macrophages and keratinocytes contribute differentially to allergic and nonallergic chronic itch. *The Journal of allergy and clinical immunology* **141**, 608-619.e607, doi:10.1016/j.jaci.2017.05.051 (2018).

- 92 Dong, X. P. *et al.* PI(3,5)P(2) controls membrane trafficking by direct activation of mucolipin Ca<sup>2+</sup> release channels in the endolysosome. *Nature communications* **1**, 38, doi:10.1038/ncomms1037 (2010).
- 93 Shen, D. *et al.* Lipid storage disorders block lysosomal trafficking by inhibiting a TRP channel and lysosomal calcium release. *Nature communications* **3**, 731, doi:10.1038/ncomms1735 (2012).
- 94 Bargal, R. *et al.* Identification of the gene causing mucopolipidosis type IV. *Nature Genetics* **26**, 118, doi:10.1038/79095 (2000).
- 95 Samie, M. *et al.* A TRP channel in the lysosome regulates large particle phagocytosis via focal exocytosis. *Developmental cell* **26**, 511-524, doi:10.1016/j.devcel.2013.08.003 (2013).
- 96 Dayam, R. M., Saric, A., Shilliday, R. E. & Botelho, R. J. The Phosphoinositide-Gated Lysosomal Ca<sup>2+</sup> Channel, TRPML1, Is Required for Phagosome Maturation. *Traffic* **16**, 1010-1026, doi:10.1111/tra.12303 (2015).
- 97 Bretou, M. *et al.* Lysosome signaling controls the migration of dendritic cells. *Science immunology* **2**, doi:10.1126/sciimmunol.aak9573 (2017).
- 98 Sun, L., Hua, Y., Vergarajauregui, S., Diab, H. I. & Puertollano, R. Novel Role of TRPML2 in the Regulation of the Innate Immune Response. *Journal of immunology* **195**, 4922-4932, doi:10.4049/jimmunol.1500163 (2015).
- 99 Plesch, E. *et al.* Selective agonist of TRPML2 reveals direct role in chemokine release from innate immune cells. *eLife* **7**, doi:10.7554/eLife.39720 (2018).
- 100 Perraud, A.-L. *et al.* ADP-ribose gating of the calcium-permeable LTRPC2 channel revealed by Nudix motif homology. *Nature* **411**, 595, doi:10.1038/35079100 (2001).

- 101 Shen, B. W., Perraud, A.-L., Scharenberg, A. & Stoddard, B. L. The Crystal Structure and Mutational Analysis of Human NUDT9. *Journal of Molecular Biology* **332**, 385-398, doi:[https://doi.org/10.1016/S0022-2836\(03\)00954-9](https://doi.org/10.1016/S0022-2836(03)00954-9) (2003).
- 102 Iordanov, I., Mihályi, C., Tóth, B. & Csanády, L. The proposed channel-enzyme transient receptor potential melastatin 2 does not possess ADP ribose hydrolase activity. *eLife* **5**, e17600, doi:10.7554/eLife.17600 (2016).
- 103 Yamamoto, S. *et al.* TRPM2-mediated Ca<sup>2+</sup> influx induces chemokine production in monocytes that aggravates inflammatory neutrophil infiltration. *Nature medicine* **14**, 738-747, doi:[http://www.nature.com/nm/journal/v14/n7/supinfo/nm1758\\_S1.html](http://www.nature.com/nm/journal/v14/n7/supinfo/nm1758_S1.html) (2008).
- 104 Di, A. *et al.* The redox-sensitive cation channel TRPM2 modulates phagocyte ROS production and inflammation. *Nature immunology* **13**, 29-34, doi:10.1038/ni.2171 (2012).
- 105 Knowles, H., Li, Y. & Perraud, A. L. The TRPM2 ion channel, an oxidative stress and metabolic sensor regulating innate immunity and inflammation. *Immunol Res* **55**, 241-248, doi:10.1007/s12026-012-8373-8 (2013).
- 106 Wehrhahn, J., Kraft, R., Harteneck, C. & Hauschildt, S. Transient receptor potential melastatin 2 is required for lipopolysaccharide-induced cytokine production in human monocytes. *Journal of immunology* **184**, 2386-2393, doi:10.4049/jimmunol.0902474 (2010).
- 107 Di, A., Kiya, T., Gong, H., Gao, X. & Malik, A. B. Role of the phagosomal redox-sensitive TRP channel TRPM2 in regulating bactericidal activity of macrophages. *Journal of cell science* **130**, 735-744, doi:10.1242/jcs.196014 (2017).
- 108 Rah, S. Y., Kwak, J. Y., Chung, Y. J. & Kim, U. H. ADP-ribose/TRPM2-mediated Ca<sup>2+</sup> signaling is essential for cytolytic degranulation and antitumor activity of natural killer cells. *Scientific reports* **5**, 9482, doi:10.1038/srep09482 (2015).
- 109 Tripathi, J. K. *et al.* Oxidant sensor cation channel TRPM2 activates neutrophil extracellular trap formation by autophagy and plays a protective role in pneumoseptic

- Klebsiella pneumoniae* infection. *The Journal of Immunology* **200**, 117.121-117.121 (2018).
- 110 Duan, J. *et al.* Structure of the mammalian TRPM7, a magnesium channel required during embryonic development. *Proceedings of the National Academy of Sciences of the United States of America* **115**, E8201-E8210, doi:10.1073/pnas.1810719115 (2018).
- 111 Jin, J. *et al.* Deletion of Trpm7 disrupts embryonic development and thymopoiesis without altering Mg<sup>2+</sup> homeostasis. *Science* **322**, 756-760, doi:10.1126/science.1163493 (2008).
- 112 Abiria, S. A. *et al.* TRPM7 senses oxidative stress to release Zn<sup>2+</sup> from unique intracellular vesicles. *Proceedings of the National Academy of Sciences of the United States of America* **114**, E6079-E6088, doi:10.1073/pnas.1707380114 (2017).
- 113 Desai, B. N. *et al.* Cleavage of TRPM7 releases the kinase domain from the ion channel and regulates its participation in Fas-induced apoptosis. *Developmental cell* **22**, 1149-1162, doi:10.1016/j.devcel.2012.04.006 (2012).
- 114 Deason-Towne, F., Perraud, A. L. & Schmitz, C. Identification of Ser/Thr phosphorylation sites in the C2-domain of phospholipase C gamma2 (PLCgamma2) using TRPM7-kinase. *Cellular signalling* **24**, 2070-2075, doi:10.1016/j.cellsig.2012.06.015 (2012).
- 115 Runnels, L. W., Yue, L. & Clapham, D. E. The TRPM7 channel is inactivated by PIP(2) hydrolysis. *Nature cell biology* **4**, 329-336, doi:10.1038/ncb781 (2002).
- 116 Dorovkov, M. V. & Ryazanov, A. G. Phosphorylation of annexin I by TRPM7 channel-kinase. *The Journal of biological chemistry* **279**, 50643-50646, doi:10.1074/jbc.C400441200 (2004).
- 117 Clark, K. *et al.* TRPM7 Regulates Myosin IIA Filament Stability and Protein Localization by Heavy Chain Phosphorylation. *Journal of Molecular Biology* **378**, 790-803, doi:<http://dx.doi.org/10.1016/j.jmb.2008.02.057> (2008).

- 118 Krapivinsky, G., Krapivinsky, L., Manasian, Y. & Clapham, D. E. The TRPM7 channel is cleaved to release a chromatin-modifying kinase. *Cell* **157**, 1061-1072, doi:10.1016/j.cell.2014.03.046 (2014).
- 119 Kaitsuka, T. *et al.* Inactivation of TRPM7 kinase activity does not impair its channel function in mice. *Scientific reports* **4**, 5718, doi:10.1038/srep05718 (2014).
- 120 Zierler, S. *et al.* TRPM7 kinase activity regulates murine mast cell degranulation. *J Physiol* **594**, 2957-2970, doi:10.1113/JP271564 (2016).
- 121 Li, M. *et al.* Molecular determinants of Mg<sup>2+</sup> and Ca<sup>2+</sup> permeability and pH sensitivity in TRPM6 and TRPM7. *The Journal of biological chemistry* **282**, 25817-25830, doi:10.1074/jbc.M608972200 (2007).
- 122 Runnels, L. W., Yue, L. & Clapham, D. E. The TRPM7 channel is inactivated by PIP2 hydrolysis. *Nature cell biology* **4**, 329-336 (2002).
- 123 Langeslag, M., Clark, K., Moolenaar, W. H., van Leeuwen, F. N. & Jalink, K. Activation of TRPM7 Channels by Phospholipase C-coupled Receptor Agonists. *Journal of Biological Chemistry* **282**, 232-239, doi:10.1074/jbc.M605300200 (2007).
- 124 Nadler, M. J. *et al.* TRPC7 is a Mg<sup>2+</sup>-ATP-regulated divalent cation channel required for cell viability. *Nature* **411**, 590-595, doi:10.1038/35079092 (2001).
- 125 Aarts, M. *et al.* A key role for TRPM7 channels in anoxic neuronal death. *Cell* **115**, 863-877 (2003).
- 126 Iwasaki, A. & Medzhitov, R. Control of adaptive immunity by the innate immune system. *Nature immunology* **16**, 343-353, doi:10.1038/ni.3123 (2015).
- 127 Brubaker, S. W., Bonham, K. S., Zanoni, I. & Kagan, J. C. Innate immune pattern recognition: a cell biological perspective. *Annu Rev Immunol* **33**, 257-290, doi:10.1146/annurev-immunol-032414-112240 (2015).

- 128 Gay, N. J., Symmons, M. F., Gangloff, M. & Bryant, C. E. Assembly and localization of Toll-like receptor signalling complexes. *Nature reviews. Immunology* **14**, 546-558, doi:10.1038/nri3713 (2014).
- 129 O'Neill, L. A. J. & Bowie, A. G. The family of five: TIR-domain-containing adaptors in Toll-like receptor signalling. *Nature reviews. Immunology* **7**, 353-364 (2007).
- 130 Barton, G. M. & Kagan, J. C. A cell biological view of Toll-like receptor function: regulation through compartmentalization. *Nature reviews. Immunology* **9**, 535-542, doi:10.1038/nri2587 (2009).
- 131 Poltorak, A. *et al.* Defective LPS signaling in C3H/HeJ and C57BL/10ScCr Mice; mutations in Tlr4 gene. *Science* **282**, 2085-2088 (1998).
- 132 Tan, Y., Zanoni, I., Cullen, Thomas W., Goodman, Andrew L. & Kagan, Jonathan C. Mechanisms of Toll-like Receptor 4 Endocytosis Reveal a Common Immune-Evasion Strategy Used by Pathogenic and Commensal Bacteria. *Immunity* **43**, 909-922, doi:<http://dx.doi.org/10.1016/j.immuni.2015.10.008> (2015).
- 133 Kagan, J. C. *et al.* TRAM couples endocytosis of Toll-like receptor 4 to the induction of interferon-beta. *Nature immunology* **9**, 361-368, doi:10.1038/ni1569 (2008).
- 134 Nelson, D. E. *et al.* Oscillations in NF-kappaB signaling control the dynamics of gene expression. *Science* **306**, 704-708, doi:10.1126/science.1099962 (2004).
- 135 Afonina, I. S., Muller, C., Martin, S. J. & Beyaert, R. Proteolytic Processing of Interleukin-1 Family Cytokines: Variations on a Common Theme. *Immunity* **42**, 991-1004, doi:10.1016/j.immuni.2015.06.003 (2015).
- 136 Brough, D. *et al.* Ca<sup>2+</sup> Stores and Ca<sup>2+</sup> Entry Differentially Contribute to the Release of IL-1 and IL-1 from Murine Macrophages. *The Journal of Immunology* **170**, 3029-3036, doi:10.4049/jimmunol.170.6.3029 (2003).
- 137 Jiang, J., Li, M. & Yue, L. Potentiation of TRPM7 Inward Currents by Protons. *J Gen Physiol* **126**, 137-150, doi:10.1085/jgp.200409185 (2005).

- 138 Moran, M. M., McAlexander, M. A., Biro, T. & Szallasi, A. Transient receptor potential channels as therapeutic targets. *Nature reviews. Drug discovery* **10**, 601-620, doi:10.1038/nrd3456 (2011).
- 139 Geissman, F. *et al.* Development of monocytes, macrophages, and dendritic cells. *Science* **327**, 656 (2010).
- 140 Krishnamoorthy, M. *et al.* The ion channel TRPM7 is required for B cell lymphopoiesis. *Science signaling* **11**, doi:10.1126/scisignal.aan2693 (2018).
- 141 Medzhitov, R. & Horng, T. Transcriptional control of the inflammatory response. *Nature reviews. Immunology* **9**, 692-703 (2009).
- 142 Garlanda, C., Dinarello, C. A. & Mantovani, A. The interleukin-1 family: back to the future. *Immunity* **39**, 1003-1018, doi:10.1016/j.immuni.2013.11.010 (2013).
- 143 Broz, P. & Dixit, V. M. Inflammasomes: mechanism of assembly, regulation and signalling. *Nature reviews. Immunology* **16**, 407-420, doi:10.1038/nri.2016.58 (2016).
- 144 Murakami, T. *et al.* Critical role for calcium mobilization in activation of the NLRP3 inflammasome. *Proceedings of the National Academy of Sciences of the United States of America* **109**, 11282-11287, doi:10.1073/pnas.1117765109 (2012).
- 145 Rada, B., Park, J. J., Sil, P., Geiszt, M. & Leto, T. L. NLRP3 inflammasome activation and interleukin-1 $\beta$  release in macrophages require calcium but are independent of calcium-activated NADPH oxidases. *Inflammation Research* **63**, 821-830, doi:10.1007/s00011-014-0756-y (2014).
- 146 Perregaux, D. & Gabel, C. A. Interleukin-1 beta maturation and release in response to ATP and nigericin. Evidence that potassium depletion mediated by these agents is a necessary and common feature of their activity. *The Journal of biological chemistry* **269**, 15195-15203 (1994).

- 147 Qin, X. *et al.* Sphingosine and FTY720 are potent inhibitors of the transient receptor potential melastatin 7 (TRPM7) channels. *British journal of pharmacology* **168**, 1294-1312, doi:10.1111/bph.12012 (2013).
- 148 Brinkmann, V. *et al.* The immune modulator FTY720 targets sphingosine 1-phosphate receptors. *The Journal of biological chemistry* **277**, 21453-21457, doi:10.1074/jbc.C200176200 (2002).
- 149 Rosadini, C. V. & Kagan, J. C. Early innate immune responses to bacterial LPS. *Current opinion in immunology* **44**, 14-19, doi:10.1016/j.coi.2016.10.005 (2016).
- 150 Yamamoto, M. *et al.* TRAM is specifically involved in the Toll-like receptor 4-mediated MyD88-independent signaling pathway. *Nature immunology* **4**, 1144-1150, doi:10.1038/ni986 (2003).
- 151 Yamamoto, M. *et al.* Role of adaptor TRIF in the MyD88-independent toll-like receptor signaling pathway. *Science* **301**, 640-643, doi:10.1126/science.1087262 (2003).
- 152 Schappe, M. S. & Desai, B. N. Measurement of TLR4 and CD14 Receptor Endocytosis Using Flow Cytometry. *Bio-protocol* **8**, doi:10.21769/BioProtoc.2926 (2018).
- 153 Akashi, S. *et al.* Cutting edge: cell surface expression and lipopolysaccharide signaling via the toll-like receptor 4-MD-2 complex on mouse peritoneal macrophages. *Journal of immunology* **164**, 3471-3475 (2000).
- 154 Akashi, S. *et al.* Lipopolysaccharide interaction with cell surface Toll-like receptor 4-MD-2: higher affinity than that with MD-2 or CD14. *The Journal of experimental medicine* **198**, 1035-1042, doi:10.1084/jem.20031076 (2003).
- 155 Vallabhapurapu, S. & Karin, M. Regulation and function of NF-kappaB transcription factors in the immune system. *Annu Rev Immunol* **27**, 693-733, doi:10.1146/annurev.immunol.021908.132641 (2009).
- 156 Zhong, H., SuYang, H., Erdjument-Bromage, H., Tempst, P. & Ghosh, S. The Transcriptional Activity of NF-kB Is Regulated by the Ikb-Associated PKAc Subunit

- through a Cyclic AMP–Independent Mechanism. *Cell* **89**, 413-424, doi:[http://dx.doi.org/10.1016/S0092-8674\(00\)80222-6](http://dx.doi.org/10.1016/S0092-8674(00)80222-6) (1997).
- 157 Yang, F., Tang, E., Guan, K. & Wang, C. Y. IKK Plays an Essential Role in the Phosphorylation of RelA/p65 on Serine 536 Induced by Lipopolysaccharide. *The Journal of Immunology* **170**, 5630-5635, doi:10.4049/jimmunol.170.11.5630 (2003).
- 158 Lin, R., Mamane, Y. & Hiscott, J. Structural and functional analysis of interferon regulatory factor 3: localization of the transactivation and autoinhibitory domains. *Mol Cell Biol* **19**, 2465-2474 (1999).
- 159 Kawai, T., Adachi, O., Ogawa, T., Takeda, K. & Akira, S. Unresponsiveness of MyD88-deficient mice to endotoxin. *Immunity* **11**, 115-122 (1999).
- 160 Macia, E. *et al.* Dynasore, a cell-permeable inhibitor of dynamin. *Developmental cell* **10**, 839-850, doi:10.1016/j.devcel.2006.04.002 (2006).
- 161 Kirchhausen, T., Macia, E. & Pelish, H. E. Use of Dynasore, the Small Molecule Inhibitor of Dynamin, in the Regulation of Endocytosis. **438**, 77-93, doi:10.1016/s0076-6879(07)38006-3 (2008).
- 162 Maguire, O., Collins, C., O'Loughlin, K., Miecznikowski, J. & Minderman, H. Quantifying nuclear p65 as a parameter for NF-kappaB activation: Correlation between ImageStream cytometry, microscopy, and Western blot. *Cytometry. Part A : the journal of the International Society for Analytical Cytology* **79**, 461-469, doi:10.1002/cyto.a.21068 (2011).
- 163 Liu, X. *et al.* T Cell Receptor-induced Nuclear Factor kappaB (NF-kappaB) Signaling and Transcriptional Activation Are Regulated by STIM1- and Orai1-mediated Calcium Entry. *The Journal of biological chemistry* **291**, 8440-8452, doi:10.1074/jbc.M115.713008 (2016).

- 164 Letari, O., Nicosia, S., Chiavaroli, C., Vacher, P. & Schlegel, W. Activation by bacterial lipopolysaccharide causes changes in the cytosolic free calcium concentration in single peritoneal macrophages. *Journal of immunology* **147**, 980-983 (1991).
- 165 Li, M., Jiang, J. & Yue, L. Functional characterization of homo- and heteromeric channel kinases TRPM6 and TRPM7. *The Journal of general physiology* **127**, 525-537, doi:10.1085/jgp.200609502 (2006).
- 166 Maruyama, T., Kanaji, T., Nakade, S., Kanno, T. & Mikoshiba, K. 2-APB, 2-Aminoethoxydiphenyl Borate, a Membrane-Penetrable Modulator of Ins(1,4,5)P<sub>3</sub>-Induced Ca<sup>2+</sup> Release. *The Journal of Biochemistry* **122**, 498-505, doi:10.1093/oxfordjournals.jbchem.a021780 (1997).
- 167 Prakriya, M. & Lewis, R. S. Potentiation and inhibition of Ca<sup>2+</sup> release-activated Ca<sup>2+</sup> channels by 2-aminoethoxydiphenyl borate (2-APB) occurs independently of IP<sub>3</sub> receptors. *The Journal of Physiology* **536**, 3-19, doi:10.1111/j.1469-7793.2001.t01-1-00003.x (2001).
- 168 Lemonnier, L., Prevarskaya, N., Mazurier, J., Shuba, Y. & Skryma, R. 2-APB inhibits volume-regulated anion channels independently from intracellular calcium signaling modulation. *FEBS letters* **556**, 121-126, doi:10.1016/S0014-5793(03)01387-5 (2004).
- 169 Rittirsch, D., Flierl, M. A. & Ward, P. A. Harmful molecular mechanisms in sepsis. *Nature reviews. Immunology* **8**, 776-787, doi:10.1038/nri2402 (2008).
- 170 Kadl, A., Pontiller, J., Exner, M. & Leitinger, N. Single bolus injection of bilirubin improves the clinical outcome in a mouse model of endotoxemia. *Shock (Augusta, Ga.)* **28**, 582-588, doi:10.1097/shk.0b013e31804d41dd (2007).
- 171 Santoni, G. *et al.* The role of transient receptor potential vanilloid type-2 ion channels in innate and adaptive immune responses. *Frontiers in immunology* **4**, 34, doi:10.3389/fimmu.2013.00034 (2013).

- 172 Tauseef, M. *et al.* TLR4 activation of TRPC6-dependent calcium signaling mediates endotoxin-induced lung vascular permeability and inflammation. *The Journal of experimental medicine* **209**, 1953-1968, doi:10.1084/jem.20111355 (2012).
- 173 Desai, B. N. & Leitinger, N. Purinergic and calcium signaling in macrophage function and plasticity. *Frontiers in immunology* **5**, 580, doi:10.3389/fimmu.2014.00580 (2014).
- 174 Schilling, T., Miralles, F. & Eder, C. TRPM7 regulates proliferation and polarisation of macrophages. *Journal of cell science* **127**, 4561-4566, doi:10.1242/jcs.151068 (2014).
- 175 Shi, J. *et al.* Inflammatory caspases are innate immune receptors for intracellular LPS. *Nature* **514**, 187-192, doi:10.1038/nature13683 (2014).
- 176 Clausen, B. E., Burkhardt, C., Reith, W., Renkawitz, R. & Forster, I. Conditional gene targeting in macrophages and granulocytes using LysMcre mice. *Transgenic research* **8**, 265-277 (1999).
- 177 Schmittgen, T. D. & Livak, K. J. Analyzing real-time PCR data by the comparative CT method. *Nat. Protocols* **3**, 1101-1108 (2008).
- 178 Helmchen, F. Calibration of fluorescent calcium indicators. *Cold Spring Harbor protocols* **2011**, 923-930, doi:10.1101/pdb.top120 (2011).
- 179 Henson, P. M. Cell Removal: Efferocytosis. *Annual review of cell and developmental biology* **33**, 127-144, doi:10.1146/annurev-cellbio-111315-125315 (2017).
- 180 Arandjelovic, S. & Ravichandran, K. S. Phagocytosis of apoptotic cells in homeostasis. *Nature immunology* **16**, 907-917, doi:10.1038/ni.3253 (2015).
- 181 Houde, M. *et al.* Phagosomes are competent organelles for antigen cross-presentation. *Nature* **425**, 402-406, doi:10.1038/nature01912 (2003).
- 182 Flannagan, R. S., Jaumouille, V. & Grinstein, S. The cell biology of phagocytosis. *Annu Rev Pathol* **7**, 61-98, doi:10.1146/annurev-pathol-011811-132445 (2012).

- 183 Pauwels, A. M., Trost, M., Beyaert, R. & Hoffmann, E. Patterns, Receptors, and Signals: Regulation of Phagosome Maturation. *Trends Immunol* **38**, 407-422, doi:10.1016/j.it.2017.03.006 (2017).
- 184 Jaumouille, V. & Grinstein, S. Molecular Mechanisms of Phagosome Formation. *Microbiology spectrum* **4**, doi:10.1128/microbiolspec.MCHD-0013-2015 (2016).
- 185 Levin, R., Grinstein, S. & Canton, J. The life cycle of phagosomes: formation, maturation, and resolution. *Immunological reviews* **273**, 156-179, doi:10.1111/imr.12439 (2016).
- 186 Botelho, R. J. *et al.* Localized biphasic changes in phosphatidylinositol-4,5-bisphosphate at sites of phagocytosis. *The Journal of cell biology* **151**, 1353-1368 (2000).
- 187 Cotter, K., Stransky, L., McGuire, C. & Forgac, M. Recent Insights into the Structure, Regulation, and Function of the V-ATPases. *Trends Biochem Sci* **40**, 611-622, doi:10.1016/j.tibs.2015.08.005 (2015).
- 188 Erwig, L. P. *et al.* Differential regulation of phagosome maturation in macrophages and dendritic cells mediated by Rho GTPases and ezrin-radixin-moesin (ERM) proteins. *Proceedings of the National Academy of Sciences of the United States of America* **103**, 12825-12830, doi:10.1073/pnas.0605331103 (2006).
- 189 Czubener, C. *et al.* Ca<sup>2+</sup> and synaptotagmin VII-dependent delivery of lysosomal membrane to nascent phagosomes. *The Journal of cell biology* **174**, 997-1007, doi:10.1083/jcb.200605004 (2006).
- 190 Nunes, P. & Demarex, N. The role of calcium signaling in phagocytosis. *Journal of leukocyte biology* **88**, 57-68, doi:10.1189/jlb.0110028 (2010).
- 191 Sawyer, D. W., Sullivan, J. A. & Mandell, G. L. Intracellular free calcium localization in neutrophils during phagocytosis. *Science* **230**, 663-666 (1985).

- 192 Kruskal, B. A. Cytosolic free calcium increases before and oscillates during frustrated phagocytosis in macrophages. *The Journal of cell biology* **105**, 2685-2693, doi:10.1083/jcb.105.6.2685 (1987).
- 193 Jaconi, M. E. *et al.* Cytosolic free calcium elevation mediates the phagosome-lysosome fusion during phagocytosis in human neutrophils. *The Journal of cell biology* **110**, 1555-1564 (1990).
- 194 Marks, P. W. & Maxfield, F. R. Local and global changes in cytosolic free calcium in neutrophils during chemotaxis and phagocytosis. *Cell Calcium* **11**, 181-190 (1990).
- 195 Guilliams, M., Bruhns, P., Saeys, Y., Hammad, H. & Lambrecht, B. N. The function of Fcγ receptors in dendritic cells and macrophages. *Nature Reviews Immunology* **14**, 94, doi:10.1038/nri3582 (2014).
- 196 Lundqvist-Gustafsson, H., Gustafsson, M. & Dahlgren, C. Dynamic Ca<sup>2+</sup> changes in neutrophil phagosomes A source for intracellular Ca<sup>2+</sup> during phagolysosome formation? *Cell Calcium* **27**, 353-362, doi:10.1054/ceca.2000.0130 (2000).
- 197 Kinchen, J. M. *et al.* A pathway for phagosome maturation during engulfment of apoptotic cells. *Nature cell biology* **10**, 556-566, doi:10.1038/ncb1718 (2008).
- 198 Gronski, M. A., Kinchen, J. M., Juncadella, I. J., Franc, N. C. & Ravichandran, K. S. An essential role for calcium flux in phagocytes for apoptotic cell engulfment and the anti-inflammatory response. *Cell death and differentiation* **16**, 1323-1331, doi:10.1038/cdd.2009.55 (2009).
- 199 Cuttell, L. *et al.* Undertaker, a Drosophila Junctophilin, links Draper-mediated phagocytosis and calcium homeostasis. *Cell* **135**, 524-534, doi:10.1016/j.cell.2008.08.033 (2008).

- 200 Weavers, H., Evans, I. R., Martin, P. & Wood, W. Corpse Engulfment Generates a Molecular Memory that Primes the Macrophage Inflammatory Response. *Cell* **165**, 1658-1671, doi:10.1016/j.cell.2016.04.049 (2016).
- 201 Han, C. Z. *et al.* Macrophages redirect phagocytosis by non-professional phagocytes and influence inflammation. *Nature* **539**, 570, doi:10.1038/nature20141 (2016).
- 202 Tsien, R. Y. New calcium indicators and buffers with high selectivity against magnesium and protons: design, synthesis, and properties of prototype structures. *Biochemistry* **19**, 2396-2404 (1980).
- 203 Smith, I. F. & Parker, I. Imaging the quantal substructure of single IP3R channel activity during Ca<sup>2+</sup> puffs in intact mammalian cells. *Proceedings of the National Academy of Sciences of the United States of America* **106**, 6404-6409, doi:10.1073/pnas.0810799106 (2009).
- 204 Todt, J. C., Hu, B. & Curtis, J. L. The receptor tyrosine kinase MerTK activates phospholipase C gamma2 during recognition of apoptotic thymocytes by murine macrophages. *Journal of leukocyte biology* **75**, 705-713, doi:10.1189/jlb.0903439 (2004).
- 205 Heng, T. S. & Painter, M. W. The Immunological Genome Project: networks of gene expression in immune cells. *Nature immunology* **9**, 1091-1094, doi:10.1038/ni1008-1091 (2008).
- 206 Russell, D. G., VanderVen, B. C., Glennie, S., Mwandumba, H. C. & Heyderman, R. The macrophage mashes on its phagosome: dynamic assays of phagosome function. *Nature reviews. Immunology* **9**, 594-600, doi:10.1038/nri2591 (2009).
- 207 Podinovskaia, M. *et al.* Dynamic quantitative assays of phagosomal function. *Current protocols in immunology / edited by John E. Coligan ... [et al.]* **102**, Unit 14 34, doi:10.1002/0471142735.im1434s102 (2013).

- 208 Krapivinsky, G., Mochida, S., Krapivinsky, L., Cibulsky, S. M. & Clapham, David E. The TRPM7 Ion Channel Functions in Cholinergic Synaptic Vesicles and Affects Transmitter Release. *Neuron* **52**, 485-496, doi:<http://dx.doi.org/10.1016/j.neuron.2006.09.033> (2006).
- 209 Jiang, J., Li, M. & Yue, L. Potentiation of TRPM7 inward currents by protons. *The Journal of General Physiology* **126**, 137-150, doi:10.1085/jgp.200409185 (2004).
- 210 Medina, C. B. & Ravichandran, K. S. Do not let death do us part: 'find-me' signals in communication between dying cells and the phagocytes. *Cell death and differentiation* **23**, 979-989, doi:10.1038/cdd.2016.13 (2016).
- 211 Elliott, M. R. *et al.* Nucleotides released by apoptotic cells act as a find-me signal to promote phagocytic clearance. *Nature* **461**, 282-286, doi:10.1038/nature08296 (2009).
- 212 Demaurex, N. & Nunes, P. The role of STIM and ORAI proteins in phagocytic immune cells. *American journal of physiology. Cell physiology* **310**, C496-508, doi:10.1152/ajpcell.00360.2015 (2016).
- 213 Wang, Y. *et al.* Mitochondrial Fission Promotes the Continued Clearance of Apoptotic Cells by Macrophages. *Cell* **171**, 331-345 e322, doi:10.1016/j.cell.2017.08.041 (2017).
- 214 Lukacs, G. L., Rotstein, O. D. & Grinstein, S. Determinants of the phagosomal pH in macrophages. In situ assessment of vacuolar H<sup>+</sup>-ATPase activity, counterion conductance, and H<sup>+</sup> "leak". *The Journal of biological chemistry* **266**, 24540-24548 (1991).
- 215 Martinez, J. *et al.* Microtubule-associated protein 1 light chain 3 alpha (LC3)-associated phagocytosis is required for the efficient clearance of dead cells. *Proceedings of the National Academy of Sciences of the United States of America* **108**, 17396-17401, doi:10.1073/pnas.1113421108 (2011).
- 216 Canton, J., Neculai, D. & Grinstein, S. Scavenger receptors in homeostasis and immunity. *Nature reviews. Immunology* **13**, 621-634, doi:10.1038/nri3515 (2013).

- 217 Dagvadorj, J. *et al.* Lipopolysaccharide Induces Alveolar Macrophage Necrosis via CD14 and the P2X7 Receptor Leading to Interleukin-1 $\alpha$  Release. *Immunity* **42**, 640-653, doi:<https://doi.org/10.1016/j.immuni.2015.03.007> (2015).
- 218 Blasius, A. L. & Beutler, B. Intracellular Toll-like Receptors. *Immunity* **32**, 305-315, doi:<https://doi.org/10.1016/j.immuni.2010.03.012> (2010).
- 219 Husebye, H. *et al.* Endocytic pathways regulates toll-like receptor 4 signaling and link innate and adaptive immunity. *EMBO* **25**, 683-692, doi:10.1038/ (2006).
- 220 Schink, K. O., Tan, K. W. & Stenmark, H. Phosphoinositides in Control of Membrane Dynamics. *Annual review of cell and developmental biology* **32**, 143-171, doi:10.1146/annurev-cellbio-111315-125349 (2016).
- 221 Spiegel, S. & Milstien, S. The outs and the ins of sphingosine-1-phosphate in immunity. *Nature reviews. Immunology* **11**, 403-415, doi:10.1038/nri2974 (2011).
- 222 Vinkenborg, J. L. *et al.* Genetically encoded FRET sensors to monitor intracellular Zn<sup>2+</sup> homeostasis. *Nature methods* **6**, 737-740, doi:10.1038/nmeth.1368 (2009).
- 223 Kitamura, H. *et al.* Toll-like receptor-mediated regulation of zinc homeostasis influences dendritic cell function. *Nature immunology* **7**, 971-977, doi:10.1038/ni1373 (2006).
- 224 Wan, Y., Petris, M. J. & Peck, S. C. Separation of zinc-dependent and zinc-independent events during early LPS-stimulated TLR4 signaling in macrophage cells. *FEBS letters* **588**, 2928-2935, doi:10.1016/j.febslet.2014.05.043 (2014).
- 225 Zhou, P. *et al.* Alpha-kinase 1 is a cytosolic innate immune receptor for bacterial ADP-heptose. *Nature* **561**, 122-126, doi:10.1038/s41586-018-0433-3 (2018).
- 226 Brauchi, S., Krapivinsky, G., Krapivinsky, L. & Clapham, D. E. TRPM7 facilitates cholinergic vesicle fusion with the plasma membrane. *Proceedings of the National Academy of Sciences of the United States of America* **105**, 8304-8308, doi:10.1073/pnas.0800881105 (2008).

- 227 Takezawa, R. *et al.* Receptor-mediated regulation of the TRPM7 channel through its endogenous protein kinase domain. *Proceedings of the National Academy of Sciences of the United States of America* **101**, 6009-6014, doi:10.1073/pnas.0307565101 (2004).
- 228 Roy, S., Karmakar, M. & Pearlman, E. CD14 Mediates Toll-like Receptor 4 (TLR4) Endocytosis and Spleen Tyrosine Kinase (Syk) and Interferon Regulatory Transcription Factor 3 (IRF3) Activation in Epithelial Cells and Impairs Neutrophil Infiltration and *Pseudomonas aeruginosa* Killing in Vivo. *Journal of Biological Chemistry* **289**, 1174-1182, doi:10.1074/jbc.M113.523167 (2014).